Influence of Substrate Properties on Bonding Mechanism of Cold Sprayed Titanium Dioxide Coating

(コールドスプレー酸化チタン皮膜の接合メカニズムにおける基材特性の影響)

SEPTEMBER, 2021

DOCTOR OF PHILOSOPHY (Engineering)

NOOR IRINAH BINTI OMAR

ノー・イリナ・ビンティー・オーマー

TOYOHASHI UNIVERSITY OF TECHNOLOGY

Abstract

Current attention has focused on the preparation of thick ceramic coating using nanostructured materials as feedstock materials using thermal spray process. Cold spray method has appeared as a promising process to form ceramic nanostructured coating without significantly changing the microstructure of the initial feedstock materials due to its low processing temperature. However, deposition of ceramic powders by cold spray is not easy due to brittle characteristics of the material. Moreover, the bonding mechanism on how the ceramic coating was formed on the substrate is still unclear as cold spray process requires plastic deformation of particles upon the impact onto the substrate and it only apply for metal materials. On top of, the adhesion strength of pure TiO_2 coating is low, thus, hindering the adoption of this new technology breakthrough into the society.

Therefore, in this study, focused have been made on the substrate properties which were annealing throughout of the study. The relationship between coating adhesion strength and annealing substrate properties on soft and hard metals substrate were investigated to identify the factors that influence bonding mechanism involved. The following results which obtained by this study were summarized here:

1. Apparent affect of surface roughness was not recognized in the present study both on soft and hard metals substrate.
2. The annealing process contributed to the induced ductility of soft metals substrate especially when annealed at a recrystallization temperature of 400°C. The soft metals substrate hardness was reduced as a result, and it became softer. When the high-velocity cold sprayed TiO_2 particle impacted the soft metals substrate surface with thick oxide film, plastic deformation of the substrate is present but some of the oxide layer remained as shown by the TEM results,

which prevented metallurgical bonding from occurring in between the TiO_2 coating and soft metals substrate. The primary bonding mechanism of TiO_2 particle and soft metal substrate is metallurgical bonding which required free oxide surface.

3. The primary bonding mechanism of TiO_2 particle and stainless steel substrate is inter-oxide bonding, which is provided by a chemical reaction of TiO_2-OH^-, where OH^- is provided by chromium oxide, Cr_2O_3, which is thermodynamically preferred in SUS304. Only certain substrate oxide compositions on certain materials, such as stainless steel, have chemically induced inter-oxide bonding. Other oxide compositions of the substrate, such as Fe_2O_3 on structural steel must be removed in order for TiO_2-substrate to form a bond.

Table of contents

TABLE OF CONTENTS

List of Figure

List of Table

Nomeclature

A - Cross sectional area of the nozzle

A^* - Cross sectional area of the throat of the nozzle

γ - Ratio of specific heats

M_a - Mach number

M_{ae} - Mach number at the exit of the nozzle

T - Gas temperature

P - Gas pressure

ρ - Gas density

T_0 - Stagnation temperature

P_0 - Stagnation pressure

ρ_0 - Stagnation density

R - Universal gas constant

M_w - Molecular weight of the gas

M_p - Mass of the particle

ρ_p - Density of the particle

V_p - Velocity of the particle

V_{cr} - Critical velocity of the particle

A_p - cross sectional area of the particle

C_D - Coefficient of drag

t - Time

a - speed of sound

1 Introduction

1.1 Surface engineering

Surface engineering involves design and modification of the surface of the substrate to provide specific engineering advantages like improved wear resistance, corrosion resistance, oxidation resistance, electronic properties and etc. The surface can be modified using metallurgical, mechanical or chemical methods or by applying a layer of metallic or non-metallic coating using PVD, CVD, plating and spraying.

1.1.1 Thermal spraying

Thermal spraying is a generic term for applying metallic and non-metallic coatings in which the molten or semi-molten particles are deposited onto a substrate [1]. In thermal spraying, the particles are heated and accelerated towards a substrate onto which a coating is formed. The combination of high particle temperature and high particle velocity results in forming a deformed splat on the substrate. Deposition of successive splats causes a coating thickness from a few microns to few millimeter to be built up on the substrate. Thermal spray processes can be grouped into three broad categories: flame spray, electric arc spray and plasma arc spray [1]. Different energy sources (i.e flame, electric arc and plasma) are used to melt the coating materials in powder, wire or rod form and propel them towards the substrate. The key advantage of thermal spraying is that material or composites which partially melt without decomposing can be sprayed. Flame spray includes low velocity powder flame, wire flame and high velocity oxy-fuel (HVOF) methods where the gas temperature is relatively low. In rod flame, the coating material is aspirated into the

oxy-fuel stream, heated and carried by the flame towards the substrate [1]. In arc wire spray process, two consumable wire electrodes are fed into the gun. This creates an arc between them which melts the tip of the wire. The molten metal is then atomized by a gas stream and propelled towards the substrate. The velocity of the particles is around 100-200 m/s and the temperature is higher than flame spray processes [1]. However, in plasma spray process, the powder heating regions is from 2500˚C to 14000˚C, significantly above the melting point of any known material. Typically argon or argon-hydrogen mixture is heated by a dc arc to produce the plasma [1]. A range of materials including ceramics can be sprayed using plasma spray. In contrast to all thermal spray processes, cold spray is a material deposition technique where the particles are accelerated to a velocity of 300-1200 m/s with nitrogen or helium gas at a relatively low temperature of the gas, generally below the melting point of material and for metals such as titanium and copper temperatures in the range of 400-800 ˚C can be used.

1.1.2 Cold spraying

Cold spraying is a high strain-rate material deposition technique, in which powder particles (typically 10-40 μm in size) are accelerated to speed of between 300-1200 m/s and upon impact with a substrate or previously deposited particles, deform plastically and adhere [2-5]. The process is also referred to as cold gas dynamic spray because the process utilizes gas dynamic principle of helium or nitrogen as an accelerating gas. Deposition rates up to 14 kg/h have also been reported in the literature [1]. There are two types of cold spraying; high pressure cold spraying (HPCS) in which the working gas is nitrogen or helium at pressure above 1.5MPa, a flow rate of more than 2 m^3/min. In low pressure cold spraying (LPCS), the working gas is a compressed gas with pressure 0.5-1.0 MPa, flow rate 0.5-2 m^3/min [1].

In the cold spraying process, the gas and particle temperatures remain well below the melting temperature of the spray materials and therefore the particles are in solid state and formation of coatings occurs due to the kinetic energy of the particles on impact [2]. Unlike thermal spraying, where the particles are molten or semi molten, the deposition of particles in the solid state by cold spraying has various advantages. Some of the key advantages of cold spray are mentioned as follow [6].

- High deposition efficiency, values as high as 100% for titanium [7] and copper have been reported.
- Substrate preparation by grit-blasting is not required for ductile materials as the process can be viewed as combination of grit-blasting, spray coating and shot peening [6].
- Low porosity coating because of visco-plastic deformation of the particles during deposition [5]. Also the particles from the trailing edge of the moving plume sputter away any loosely bonded particles and shot-peen the underlaying layer to reduce porosity.
- Minimal thermal input to the substrate because of the absence of any high temperature jet to heat the substrate.
- Compressive residual stress in the coating because of plastic deformation in the solid state which enhances fatigue properties of the coating.

- Less oxidation and no grain growth due to a lack of heating of the powders compared with thermal spray.
- High thermal and electrical conductivity of coatings can be produced from metals like copper due to a low porosity and negligible oxide [8].
- High strength and hardness of the cold sprayed coatings compared to the bulk material because of the high degree of plastic deformation of the particles [9].

1.1.2.1 Gas dynamic principles in cold spraying

The key component of a cold spray process is a convergent-divergent nozzle (or de laval nozzle) which accelerates the gas supersonically and gives the particles their required velocity to deposit onto a substrate. In a de laval nozzle, there are two sections: a convergent section and a divergent section. The area of the nozzle between the convergent and divergent section is called the throat. Figure 1.1 shows the schematics of a de laval nozzle used in cold spraying. In a de laval nozzle the flow can be accelerated or decelerated by changing the flow areas [10-11]. The compressible nature of a gas allows the laval nozzle to operate. At the throat of the nozzle, the gas reaches sonic condition (M_a^2 =1). At the divergent section of the nozzle, the gas continues to accelerate to supersonic velocities. As the gas accelerates in the divergent section of the nozzle, the temperature and pressure decrease from their original stagnation values [10]. The particles accelerate as they pass along the nozzle gaining kinetic energy from the supersonic gas [12].

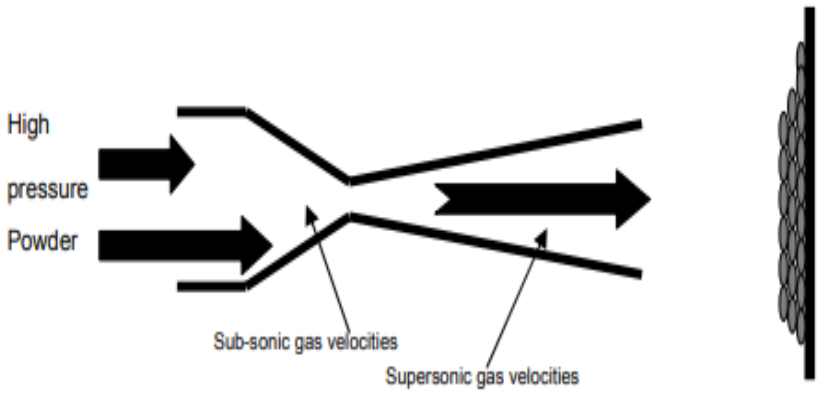

Figure 1.1 : Schematic of a cold gas dynamic spray de Laval nozzle [10-11].

1.1.2.2 Flow in a convergent-divergent nozzle

The key equations for compressible flow inside a de laval nozzle, it is assumed that the gas flow is isentropic (adiabatic and frictionless), one dimensional, a perfect gas with a constant specific heat and external forces (i.e gravitational effects) are negligible [10,12-13]. The following equation shows the relationship between change in area with the change in velocity of an isentropic fluid

$$\frac{dA}{dV} = \left({M_a}^2 - 1\right)\frac{A}{V} \qquad \text{equations 1.1}$$

Where A is the cross-sectional area, V is the velocity of the gas and M_a is Mach number. Because A and V are positive, it may be concluded from the equation that:

If M_a <1, the flow is subsonic, i.e, decreasing the area increases the velocity. The flow in the convergent section of the nozzle.

If M_a >1, the flow is supersonic, i.e, increasing the area increases the velocity. The flow in the divergent section of the nozzle.

If M_a = 1, then dA/dV = 0, has to be minimum, i.e., at the throat of the nozzle.

If it is assumed that the exit area of the nozzle is known and then the Mach number at the exit of the nozzle (M_{ae}) has the following relationship with the throat area (A_e*)

$$\left(\frac{A}{A_{e^*}}\right) = \frac{1}{m_a}\left[\frac{2}{\gamma+1}\left(1 + \frac{\gamma-1}{1}\,{M_{ae}}^2\right)\right]^{\frac{\gamma+1}{2(\gamma-1)}} \qquad \text{equations 1.2}$$

Where γ is the ratio of specific heat. When the exit Mach number is known, the other gas parameters can be obtained using the isentropic gas flow equations and have the following final form with stagnation conditions (o) where T is temperature, P is pressure and ρ is density.

$$T = \frac{T_0}{1 + \left(\frac{\gamma - 1}{2}\right) {M_a}^2} \qquad \text{equations 1.3}$$

$$P = \frac{P_0}{\left[1 + \left(\frac{\gamma - 1}{2}\right) {M_a}^2\right]^{\frac{\gamma}{\gamma - 1}}} \qquad \text{equations 1.4}$$

$$\rho = \frac{\rho_o}{\left[1 + \left(\frac{\gamma - 1}{2}\right) {M_a}^2\right]^{\frac{1}{\gamma - 1}}} \qquad \text{equations 1.5}$$

The velocity can be obtained using the following equation

$$V = M_a \sqrt{\gamma R T} \qquad \text{equations 1.6}$$

1.1.2.3 Particle acceleration model

In cold spraying, the adequacy of the cold spray process is determined by velocity of the particles not the gas stream. It is assumed that the two-phase flow (gas and particle) is dilute enough. The mass times the acceleration of the particle can be equated to the drag force of the particle [10,14] as follows

$$M_\rho \frac{dV_p}{dt} = M_P V_P \frac{dV_P}{dx} = \frac{C_D A_P \rho \left(V - V_p\right)^2}{2} \qquad \text{equations 1.7}$$

Where V_p is the particle velocity, A_p is the cross-sectional area of the particle, C_p is co-efficient of drag, m_p is mass of the particle, t is time and x is the axial distance travelled by the particle. The equation can be integrated if the gas velocity and density are held constant and the drag coefficient is assumed constant. After integration

$$\log\left(\frac{V - V_p}{V}\right) + \frac{V}{V - V_p} - 1 = \frac{C_D A_P \rho_x}{2M_\rho} \qquad \text{equations 1.8}$$

For low values of spray particle velocity compared to gas velocity, the equation can be simplified as follows [10]

$$V_p = \sqrt{\frac{C_D A_p \rho_x}{M_\rho}} \qquad \text{equations 1.9}$$

This relationship states that the spray particle velocity is proportional to square roof of the distance travelled over the particle diameter. It should be noted that the drag coefficient and gas density vary over the length of the nozzle [14-15]. In addition, it has been shown [16-18] that the particle velocity increases with the decrease of particle size and a particle of lower density under the same conditions will reach a higher velocity. However, this high velocity of smaller particles does not necessary contribute to deposition in cold spray due to plate shocks, external to the nozzle which will be explained in section 1.1.2.5.

1.1.2.4 Role of gas pressure and temperature

The velocity of the particles in cold spraying is affected by the type of gas used, gas pressure and gas temperature. In the previous section, we have seen how the gas properties depend on the Mach

number. However, Mach number is nothing but the ratio of the speed of an object in the medium to the speed of sound in that medium. The equation for speed of sound (a) is expressed as follows

where γ is the ratio of specific heats, R is the gas constant, T is the gas temperature, M_w is the molecular weight of the gas. The gas velocity will increase if a gas with lower molecular weight is used, such as helium or the gas temperature is increased as stated in equations 1.10;

$$a = \sqrt{(\gamma RT / M_w)} \qquad \text{equations 1.10}$$

Van Steenkiste et al. [19] reported that when the pressure downstream of the convergent divergent nozzle is equal to 52.8% of the pressure upstream, in the case of air, the throat of the nozzle is choked (sonic condition). Increase in pressure at upstream will not result in an increase in gas velocity through the throat of the nozzle as a result of this. However, increase in pressure will result in an increase in density, and mass flow rate is a function of density. The mass flow rate will increase linearly as a result of pressure increase while the gas velocity remains constant.

1.1.2.5 Effect of stand-off distance and bow shock

Interaction of particles with the substrates from a fluid mechanics point of view in the cold spraying has been subjected to much research [14,17,20-24]. Computational fluid dynamics (CFD) codes and Schlieren images were both used to study the gas and particle properties beyond the nozzle exit. Yin et al. [24] reported a complex wave structure at the nozzle exit which are composed of oblique shock due to overexpansion, expansion waves as a result of interaction with atmospheric boundaries and bow shock due to interaction with the substrate.

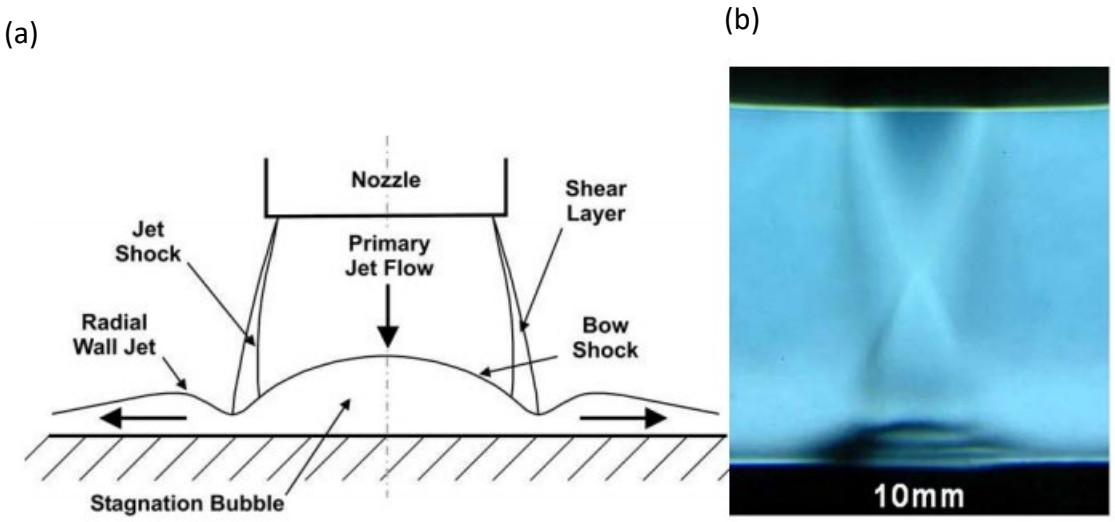

Figure 1.2: (a) Schematic diagram of the supersonic impingement zone at the substrate (b) Schlieren images of bow shock at 10 mm standoff distance from the nozzle [21].

Shockwaves occur as a result of the adjustment of a supersonic flow to downstream conditions; which in cold spraying is the substrate [21]. Figure 1.2 (a) shows the schematic diagram of the interaction zone between the substrate and the supersonic flow. When the gas molecules impact the substrate, there is a change in energy and momentum, and the pressure waves form a normal shock wave. The subsonic flow downstream of shock wave adjusts by taking the form of a radial jet of the primary jet flow. Since the substrate is perpendicular to the gas flow, the deflection angle is greater than maximum deflection angle for an oblique shock waves and as a result the shockwave is curved and detached- which is called a bow shock [21].

The pressure in the bow shock region is well confined which leads to a sharp increase of pressure and temperature in front of the substrate [24]. The bow shock formed at the interaction zone

reduces the velocity of the gas and that of the entrained particles. If the particles are too small and light, they might acquire a high velocity but may be decelerated in the bow shock zone [14,25].

In addition, as the standoff distance is increased, the free gas jet shows a continual reduction in velocity away from the nozzle and viscous effects of the gas periphery cause the gas velocity to decrease and eventually turn into a subsonic stream [21]. The gas velocity is highest at the center of the jet and can be imagined as a cone emanating from the nozzle exit. As the standoff distance is increased, the interaction area of this cone and substrate is decreased and the effect of bow shock is also decreased. With increasing standoff distance the bow shock disappears and deposition performance is increased. However, if the standoff is increased beyond an optimum distance the deposition efficiency is decreased due to a decrease of particle velocity [17].

1.2 Bonding mechanism of metal in cold spray

The mechanism of bonding in cold spraying is a matter of some debate. A number of hypotheses have been proposed concerning the mechanism by which bonding takes place in cold spraying.

1.2.1 Experimental investigations

1.2.1.1 Shear lip formation and cratering of substrates

Early observations of particle-substrate interactions in cold spraying showed shear lips formation at the interface of deposited particles and crater formation of the substrate from the rebounded particles. Papyrin et al [26] studied the interaction of individual aluminum particles with the copper substrate at different velocities to investigate the transition from rebound to adhesion of particles.

At a lower particle velocity there were individual craters formed by the particle impact and there were no deposited particles. With increasing the particle velocity, particles started adhering to the substrate. These experiments showed that beyond a threshold velocity of the particles, critical velocity, a transition from substrate erosion to deposition occurs. The jet type morphology of shear lips around the deposited copper particles onto copper substrate was reported by Assadi et al [2]. This jet type morphology was not noticed on the craters at the substrate left by non-adhering particles. Moreover, in a study of cold spraying of copper particle onto steel substrate, Dykhuizen et al [10] reported that the crater formation is dependent on the particle velocity, i.e with increasing the velocity the depth of the crater also increases.

1.2.1.2 Role of surface deformation and surface oxide

It has been proposed that the first layer of coating buildup, deposition of particles onto the substrate involves, substrate surface cratering and activation of the surface by removing any surface contamination [1,26,27-28]. Papyrin et al. argued that the first impinging particles increase the chemical activity of the surface by elevating the dislocation concentrations on the very top layer [28]. During the particle deformation phenomena, the oxide shells on the interacting surfaces are broken and clean surfaces are pressed together and thus bonded. It has also been proposed that the interfacial material jet produced from adiabatic shear instability phenomena helps in removing the oxide films from the surface and thus enable an intimate metal-to-metal contact to be established [2,5,27,29]. In addition, Grujicic et al. [3] argued that adhesion might also be a mechanism for particle bonding. Adhesion on the nano scale involves atomic interactions between the contacting

clean interface and high contact pressure to make the surface mutually conforming. The removal of surface oxide by a material jet produced by adiabatic shear instability can in principle, provide clean surface for adhesion between two mutually conforming regions.

Kang et al. [30] and Li et al. [31] studied the role of oxide content of the powder on critical velocity for deposition. It was argued that the critical velocity of material does not only depend on material properties but also on oxidation condition. It was found that increasing the oxide content of the copper powder from 0.02 wt.% to 0.38 wt.%, the critical velocity increased from 300 m /s to 610 m / s [31]. In addition, Kang et al. [30] studied the role of oxide content of aluminum feedstock powder on critical velocity. It was reported that increasing the oxide content of the same powder size distribution from 0.001 wt.% to 0.045 wt.% increased the critical velocity from 742 m / s to 867 m / s. It was suggested that the critical velocity also depended on the oxide scale thickness. The thicker the oxide scale is, the more energy is required to remove the oxide and less plastic deformation energy is dissipated into the particle. Moreover, an increase in oxide content resulted in a decrease in particle flatting ratio. It is believed that the adiabatic shear instability at the particle-substrate interface can disrupt the oxide film; however, some part of the oxide remains at the interface which hinders particle-substrate adhesion as shown by Figure 1.3.

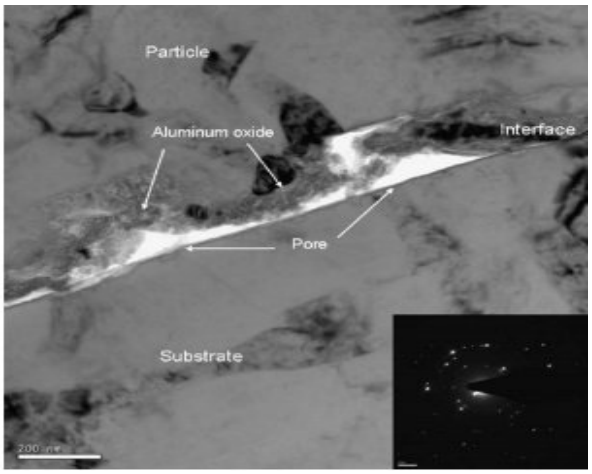

Figure 1.3: FE-TEM micrographs: bright field image of interface between aluminum powder and substrate showing aluminum oxide layer [30].

In recent years, a number of TEM investigations of the interface of cold sprayed copper particles onto aluminum substrates have been published [25-32]. In one study, it was argued that the bonding occurred between cold sprayed copper splats because of the two oxide films, which were on two separate particle surfaces, fused together to form one continuous layer. In addition, the particle surface could reach a very high temperature resulting in releasing of oxygen which could get trapped in the liquid film. At the copper particle-aluminum substrate interface a number of different phases including nano-crystallized phases and intermetallics were present within a thickness of ~20nm, except the bottom of the splat. The authors argued that the thickness of the intermediate phases suggest that diffusion occurred in a liquid state than in a solid state [24-34]. It was hypothesized that transient melting might act as a mechanism in Cu-Al interaction. King et al. [35] also reported melting of aluminum substrate at the crater wall where the copper particle slid past aluminum. It was suggested that adhesion was promoted from the solid material jetting and molten material jetting, which also contributed to mechanical interlocking [32].

1.2.1.3 Characterization of bond formation

Price et al. [12,36] proposed a method to characterize the bonding between aluminum and copper particles following deposition by cold spraying. A blended copper-aluminum powder was cold sprayed and subsequently heat treated at 400 °C to form a layer of intermetallic where the true metal-to-metal contact had occurred, Figure 1.4 shows the BSE image of a heat treated copper-aluminum cold sprayed deposit showing formation of intermetallic where the metal-to-metal bond had established. In other regions, metal-to-metal contact was inhibited by a thin layer of surface oxide film. It was reported that by increasing the particle in flight velocity, a greater degree of particle deformation and hence a greater metal-to-metal contact between particles was established.

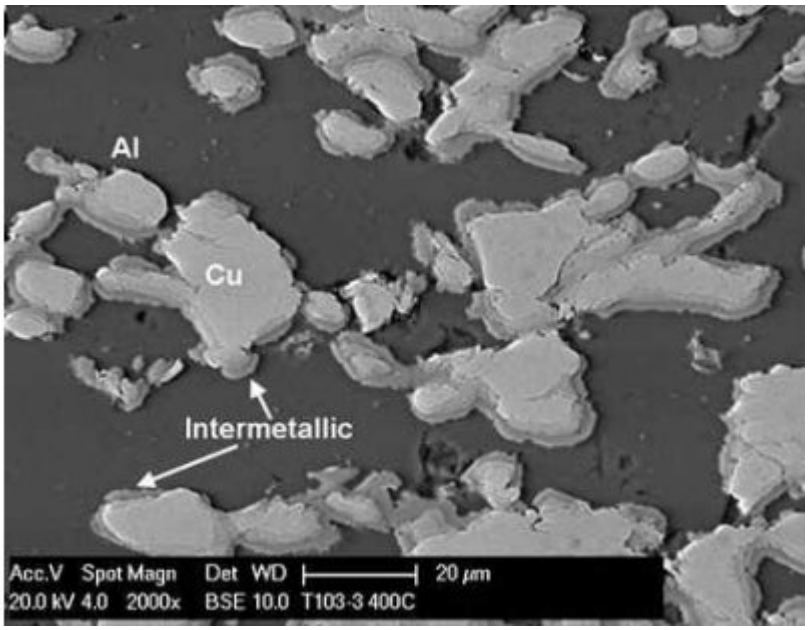

Figure 1.4: BSE image of heat-treated Cu-Al deposits showing intermetallic layers as an indicator of metal-to-metal bond formation [36].

1.2.1.4 Interfacial curvature and instability phenomena

The nano-micro scale mechanical material mixing at the cold sprayed coating substrate interface was observed by several researchers [37-40]. They attributed this mixing phenomenon to Kelvin-Helmholtz instability mechanism. In the kelvin- Helmholtz instability phenomenon, when tow fluids in contact are moving at different velocities parallel to each other, instability can occur (due to non-zero curvature of the interace) and one fluid flows around the other, a centrifugal force is generated. This centrifugal force might also promote amplification of the interfacial perturbation.

Champagne et al. [39] provided the following equation to estimate particle velocity required for interfacial material mixing

$$v_p = \left[(7.5 \times 10^4)\left(\frac{B'}{\rho_P}\right)\right]^{0.5} \qquad \text{equations 1.11}$$

Where v_p is the particle velocity, B′ is the Brinell hardness number of the substrate and ρ_P is the density of the coating material. This equation shows that the interfacial material mixing depends on substrate hardness and coating material density. This interfacial material may also be responsible for mechanical interlocking of the coating and substrate [38]. In addition, Klinkov et al. [38] proposed a mechanism called- "sticking'', the particle first sticks to the substrate due to Van Der Waals or electrostatic forces, and strong adhesion is only formed when incoming particles impact onto sticking particles.

1.2.1.5 Coating build up mechanisms

Van Steenkiste et al. [27] studied the formation of cold sprayed aluminum coating with a relatively large powder particles (>50 μm) and proposed a model to explain the coating build up process. The model was composed of four basic stages: in stage 1 the substrate surface is activated by substrate cratering and a first layer of coating is built up by fracturing the surface oxide layer, in stage 2 the particles deform and realign as a result of successive particle impact, in stage 3 metallic bond is formed which also result in a reduction of porosity and in the final stage the coating is further densified and work hardened. The four stage of coating build up is schematically shown in Figure 1.5.

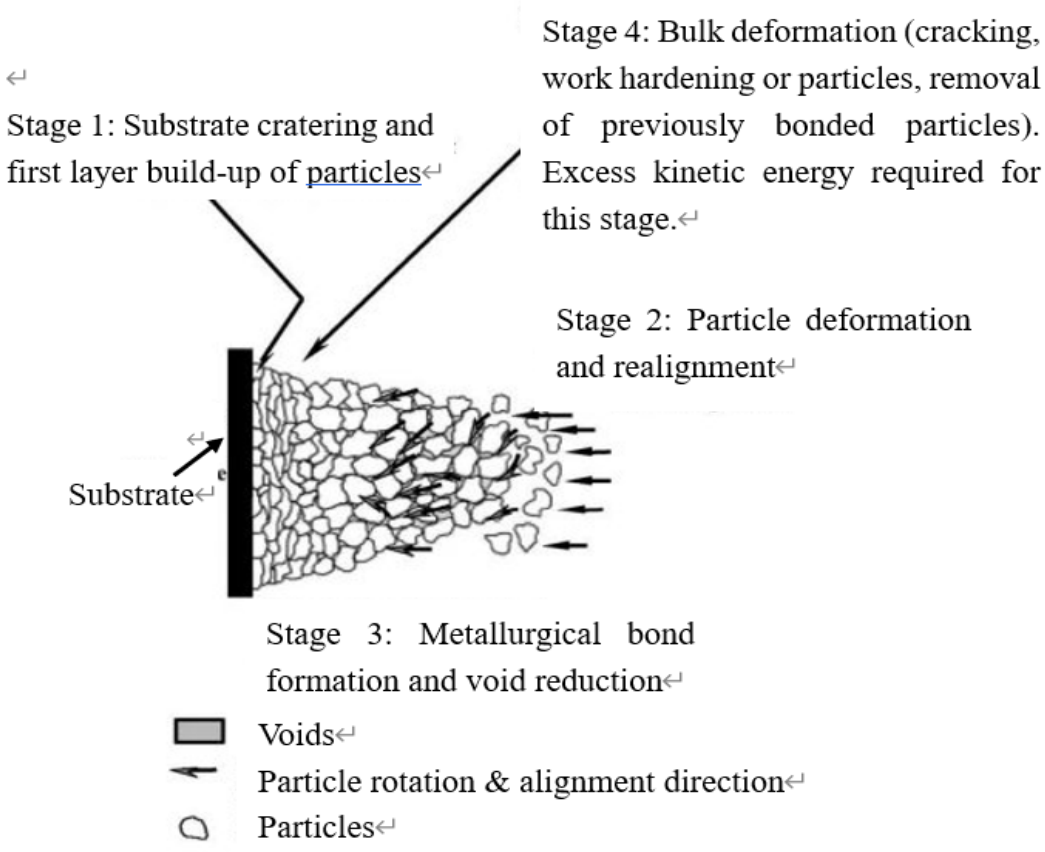

Figure 1.5: Stages in coating formation in kinetic spray process [27].

1.2.1.6 Role of substrate surface preparations

Marrocco et al. [41] explored the effect of different surface preparation techniques in controlling the bond strength of a cold sprayed titanium coating on Ti6Al4V. They proposed that grit-blasting of the Ti6Al4V substrate caused work hardening, which subsequently limited its deformation by impact of a titanium particle during cold spraying; it was argued that this restriction of substrate deformation resulted in less effective removal of surface oxide and thus led to lower bond strengths being observed. Wu et al. [42] studied an Al-Si coating, cold sprayed onto both polished and grit-blasted mild steel. Micro-pores and defects were found in the grit-blasted surface while an "intimate" interface was found following deposition onto a polished substrate; it was argued that the micro-pores on the grit-blasted surface resulted in lower bond strengths being observed. They also reported higher bond strengths with increasing particle incident velocity. In contrast to the work of Marrocco et al. [41] and Wu et al. [42] Makinen et al. [43] found higher bond strengths for a copper deposit cold sprayed onto a grit-blasted copper surface compared to that observed for deposition onto an as-received surface.

The effect of substrate surface preparation on the deposition efficiency of the process has also been assessed. Sakaki et al. [44] reported a slight increase in the deposition efficiency of cold spraying copper and titanium by increasing substrate surface roughness (grit-blasted substrate compared to polished substrate). Richer et al. [45] also reported an increase in deposition efficiency in spraying an aluminium alloy particle onto a coarser grit-blasted surface when compared to a finer grit-blasted surface. However, the substrate surface roughness has an effect only on the first few layers of coating deposited and the effect on deposition efficiency may be small, depending on the significance of the initiation stage of the coating in the total time for the development of the coating.

1.2.2 Bonding mechanisms

1.2.2.1 Metallic bonding

In cold spray, the particle or substrate or both materials will experience intensive plastic deformation due to the high-velocity impact. At the interfacial region, extremely localized deformation results in the occurrence of adiabatic shear instability, ASI and the consequent thermal softening. Metals therefore behave like a viscous flow to form the outward jet-like features [46-47]. The oxide film originally on the particle and substrate surfaces will be disrupted and removed in this process and a large area of fresh metals thus expose, which allow the intimate metal to metal contact. This process is roughly comparable to that in the explosive welding [48] or shock wave powder compaction [48], which has been considered as a pre-condition for the metallic bonding in cold spray [2-4].

1.2.2.2 Mechanical and metallurgical bonding

Mechanisms responsible for cold spray adhesion are related to the high plastic deformation and high strain rates of the powder particles during impact. Comprehensive computational analysis has been conducted to examine the bonding between the particles and the substrate [49,46]. The most extended theory to justify cold spray bonding is the adiabatic shear instability (ASI) mechanism, which is controlled by the plastic deformation of the particles with velocities above critical velocity (Vc). ASI occurs due to the combination of strain hardening during impact, attributed to the high plastic deformation developed on the powder particles, and softening induced by the heat released at the particle/substrate interface owing to high strain rate deformation during impact.

Bonding mechanisms have been experimentally and numerically studied. From an experimental point of view, the morphology of the impacted particles has been analyzed using scanning electron microscopy (SEM) [50,49,51,2,46]. Results show in figure 1.6 is the formation of a ring with a jet-type morphology around the impacted particle bonded to the substrate. In contrast, non-adhering particles leave a crater on the surface with no signs of jetting. The adhesion of the splats is controlled by the ductility of the powder and the substrate. When the ductility of the particle and the substrate are similar, both materials plastically deform. Deeper embedment is achieved using softer materials. If the powders are harder than the substrate, the powder particles will embed in the surface. Depending on the resistance of the substrate to embedment, the particles can be slightly or not at all deformed. Finally, if the powders are softer than the substrate, they will be mainly deformed and adhered to the surface.

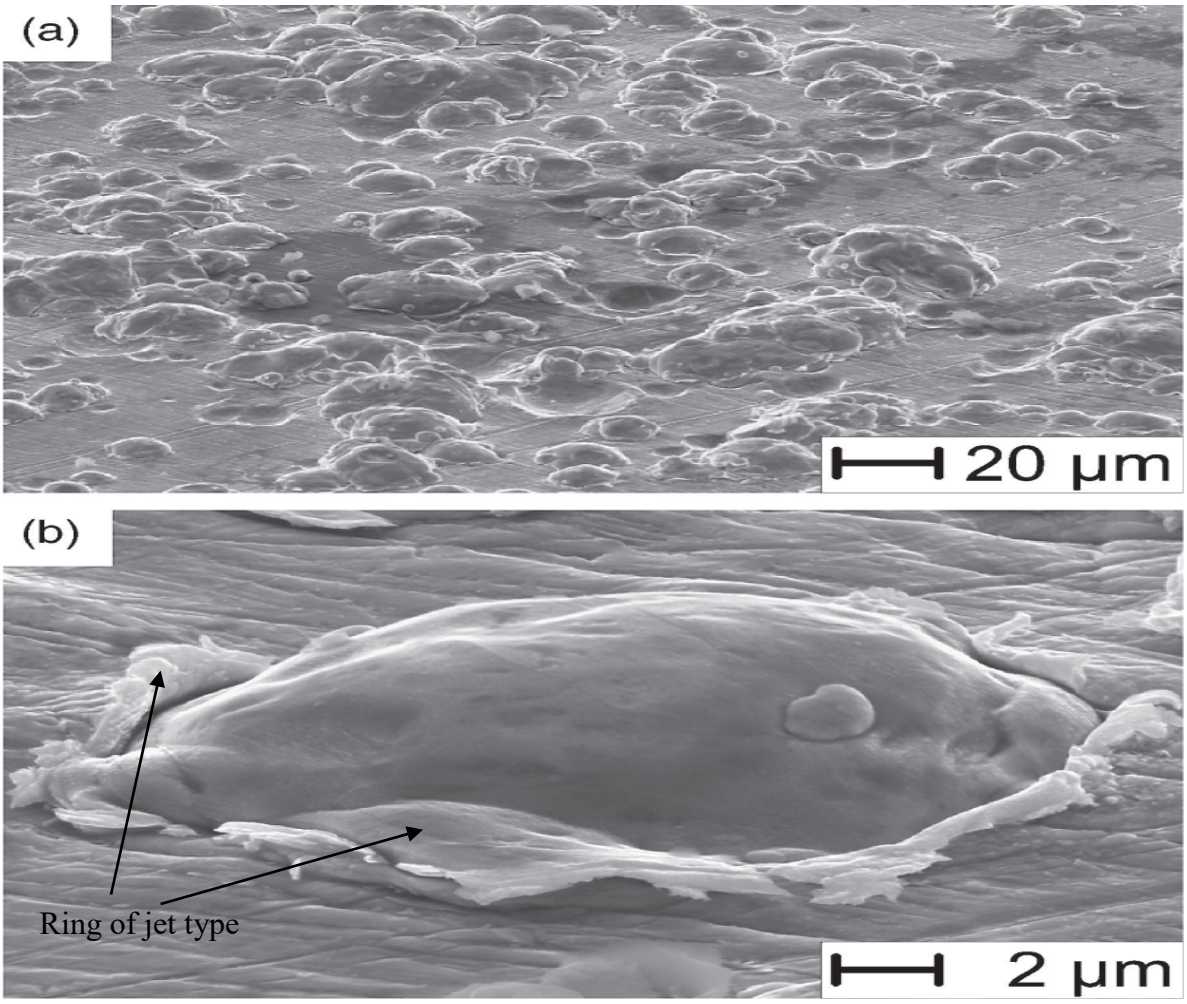

Figure 1.6: SEM images of the Cu particles cold-sprayed on a Cu substrate. (a) Overview. (b) Detailed view showing jet formation [2].

Plastic deformation occurs in a thin region close to the particle–substrate interface. Maximum plastic deformation is concentrated at the contact area border, where a jet of highly plastically deformed material is formed. These findings agree with the experimental observations and validate the idea that the ASI mechanism is responsible for cold spray bonding. Jetting occurs due to the extrusion of material from the interface. The onset of ASI at the particle–substrate interface is considered a key factor in promoting the adhesion of particles to the substrate during cold spray.

As mentioned above, two mechanisms compete. Owing to the high powder impact velocity, both the substrate and the particles plastically deform at very high strain rates, facilitating work hardening. With an increase in temperature, material softening occurs because of friction and dissipation mechanisms. Effective plastic deformation and temperature increase depend on the particle velocity and the initial particle temperature. Therefore, ASI takes place at a critical particle velocity, which is related to Vc [50,49,51,2,46,52–54]. The two mains internal micro mechanisms responsible for bonding are mechanical interlocking and metallurgical bonding, both of which can be activated by ASI [49,56-57]. Mechanical interlocking does not include any chemical reaction and involves mechanical trapping of particles by the substrate, resulting in a mutual geometric interlocking. In contrast, metallurgical bonding takes place via chemical reactions or atomic diffusion at the interface was considered as the main bonding mechanism [58-59], which can provide strong adhesion strength. The formation of intermetallic phase at the interface has been widely accepted as a sign of metallurgical bonding [60-61]. Alternatively, dimple-like features on the ductile fractured surface were also regarded as an evidence for metallurgical bonding. Currently, such dimple-like features on the inter-coating fractured surface have been widely reported, providing strong evidence of metallurgical bonding inside the coating [62-63].

1.2.2.3 Mechanical anchoring bonding

The actual mechanism by which the solid particles deform and bond during the cold-spray process is still not well understood. The most prevailing theory for cold-spray bonding postulates that, during impact, the solid particles undergo plastic deformation, disrupt thin (oxide) surface films and, in turn, achieve intimate conformal contact with the target surface. The intimate conformal contact combined with high contact pressures promotes bonding. This theory is supported by a number of experimental findings such as: (a) a wide range of ductile (metallic and polymeric) materials can be successfully cold-sprayed while non-ductile materials such as ceramics can be deposited only if they are co-cold-sprayed with a ductile (matrix) material; (b) the mean deposition particle velocity should exceed a minimum (material-dependent) critical velocity to achieve deposition which suggests that sufficient kinetic energy must be available to plastically deform the solid material and/or disrupt the surface film; and (c) the particle kinetic energy at impact is typically significantly lower than the energy required to melt the particle suggesting that the deposition mechanism is primarily, or perhaps entirely, a solid state process. The lack of melting is directly confirmed through micrographic examination of the cold-sprayed materials [64].

During the collision, the interfacial deformation was responsible for the bonding of the particle and the substrate. The degree of deformation can be used as a tool to classify the bonding mechanism into three natures. In general, the mechanical bonding can be an interfacial mixing [65-67], an embedment in the substrate [68-71] or anchoring of particles on the substrate surface [72-74]. Complex deformation makes the interfacial mixing possible. Within the Interfacial affected zone, the intermixing of the powder particles and the substrate occur at the vertices as shown in Figure 4a. The generation of bulk deposit/substrate intermixed by swirling kinematic is due to this

kind of specific morphology. Deposition of Cu/Al as particle/substrate is evidence of interface material mixing techniques. To produce interfacial mixing, substrate condition specification was presented by Champagne et al. [65] before the particle deposition can occur. The interfacial complex kinematics was not accounted for directly using this approach. However, the distinction from the contribution of an interlocking by embedment becomes tricky since a penetration of the particle in the substrate would create such a mechanical bonding. This mechanism of adhesion (mechanical embedment) has played a vital role in combinations of several materials as particle/substrate such as metallic/metallic [70], ceramic/metallic [69], oxide/polymer [74], as well as metallic/polymer [69,67,74]. An open surface that produces a metallic bonding through metallic powders partial embedment in the case of a non-similar combination of materials generates Metallic coating formation figure 1.7.

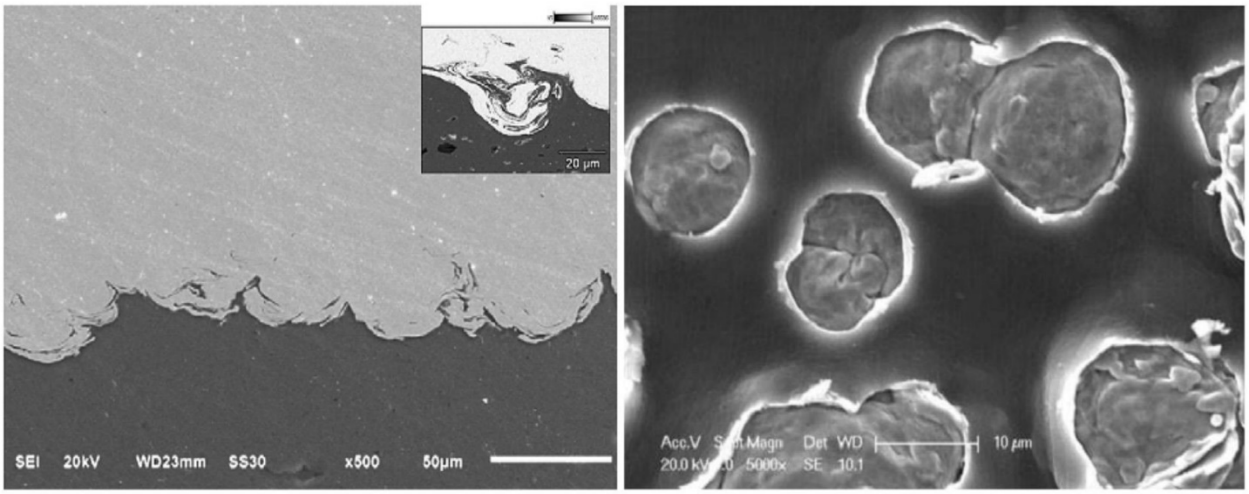

Figure 1.7: Intermixing of complex material at Cu powder particles and Al substrate interface during (a) Cold spraying of Cu/Al surface [76], and (b) embedment of Cu/Al surface [77].

Weak penetration at the bonding interface is enough to generate an interlocking between the substrate and the particle without significant penetration. Metallic/glass combination is a typical example of this phenomenon [78,73]. It has been discovered that metal powders can impact and adhere to the roughened or smooth surface of a glass substrate. This had made angular particles such as copper powders to be mechanically onto a smooth glass surface or silicon rough substrate surface [73]. Some investigations on this bonding phenomenon covered in the literature described the adhesion of metallic powders and non-metallic particles (ceramics) [78,73,79-80]. It is worth noting that the apparent adhesion at the interfacial bonding zone of particle/ substrate experiences a variation of mechanical anchoring. At the bonding interface, it can be depicted that continuity in the material structure is observed suggesting a mechanical anchoring of the deposit within the imperfect surface structure of the substrate [68,66]. This deposit/substrate mechanical accommodation was perfect for combining polymer particle and metallic substrate [80,82], metallic/ceramic [79], and metallic/polymer [68,78,74,83]. In the case of polymer/metal combination, complete adhesion can be achieved when the deposition is heat treated. The build-up coating on the metal substrate was facilitated by the layer of the melted polymer [82].

1.2.2.4 Chemical bonding

Few researchers have proposed chemical bonding as a bonding mechanism in the cold spray process especially ceramic cold spray like TiO_2 where a TiO_2 coating was produced from a recombination of broken up crystallite's links during the cold spray process, which was initiated by the porous structure of the agglomerated powders. They proposed that chemical bonding may allow thick coatings to be deposited by cold spray process. The agglomerated powder in nano-scale primary particles which also contains nano porosity were fractured, leaving an unstable surface with a dangling bonds structure. To reobtain a stable surface, the fractured particles decoupled and formed a surface with improved stability, which lead to bonding of the newly impacting particles and in turns building up of the coating [84].

Salim et al [84] prepared TiO_2 coatings of 400 μm and 150 μm on metal and tile respectively. It was observed that adhesion strength changed little with the change of spraying parameters. This indicated that mechanical interlocking was not the main bonding mechanism in this case, so was the substrates' shear instability. It was discovered that both the hardness and the oxidizability of the substrates affected adhesion strength of TiO_2 coatings. The adhesion strength of TiO_2 coatings could be improved by changing the surface chemistry of the substrates. It was proposed that the chemical or physical bonding mechanism was the main bonding mechanism of ceramic coating. TEM images proved the existence of chemical bonding between TiO_2 particles. By the way, preheating could increase the oxidizability of the substrate, thus deteriorating the adhesion strength of coatings. The result seems to be in agreement with the chemical bonding mechanism.

Gardon et al. [85] reported that the mechanism responsible for the deposition of TiO_2 on the stainless-steel substrate in the cold-spraying process is the chemical bonding between the particles and the substrate. They have shown that the previous layer of titanium sub-oxide prepares the substrate with the appropriate surface roughness needed for the deposition of the TiO_2 particle on substrate surface.

1.2.3 Influence of substrate hardness on bonding mechanisms

In cold spray, deformation of the substrate facilitates ASI and jet formation [86-87]. The formation of jets results in mechanical and metallurgical bonding at the interface. Soft substrates (e.g., Al, Cu) are susceptible to higher deformation than hard substrates (e.g., ceramics, steels), hence, results in a better adhesion strength [88-89]. Studies have been made to attain good adhesion strength for hard substrates, out of which, substrate pre-heating is the most common strategy. However, Singh et al. [89-90] found that electroplating of the SS 316 substrate with a softer material such as Ni improved the adhesion strength of cold spray Cu coatings. Furthermore, Perton et al. [91] applied laser heat treatment prior to CS to improve the adhesion strength by reducing the substrate hardness. Wang et al. [92] found that a hard steel substrate induced high deformation onto the striking Al particles, which improved the cohesive strength in the coating nearer to the substrate. However, hard particles (Al_2O_3) were embedded inside the soft Al substrate, which led to strong interfacial bonding. Therefore, it can be concluded that the substrate hardness influences the coating properties significantly in the vicinity of the interface. Wang et al. [93] found that softer substrates resulted in higher deposition efficiency, better cohesion strength, higher hardness and lower porosity; all of which were attributed to the higher impact temperature of the particle-substrate interface. The higher interfacial temperature facilitated metallurgical bonding that was identified from development of ~5 μm adiabatic shear bands along the interface.

The feedstock material has a significant influence on the deposition mechanism of the particles. Soft particles deform more severely than hard particles and result in better adhesion strength. Hard particles cause erosion of the substrate, while soft particles deform over the substrate without causing erosion [94]. Additionally, the hardness of the substrate also plays a significant role in the

adhesion mechanism. For instance, a soft-on-soft interface results in a better adhesion strength that is attributed to jet formation. A schematic of different particle substrate hardness combinations is represented in Figure 9 [95].

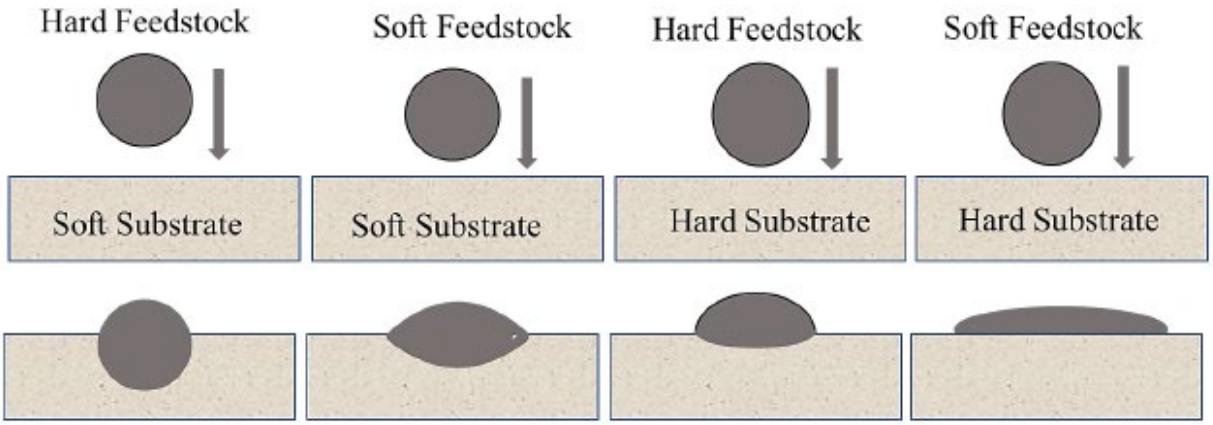

Figure 1.8: A schematic represents the impact behavior of different particle-substrate hardness combinations [95].

In the cold spray deposition process, the particle/substrate interaction can be classified into four impact cases according to the physical and mechanical properties of the processed materials: soft/soft, hard/hard, soft/hard, and hard/soft. In order to investigate the particle impact behaviour under the mentioned different impact conditions, Bae et al. [96,115-116] analysed four representative particle/substrate combinations, namely Al/Al (soft/soft), Ti/Ti (hard/hard), Al/mild steel (soft/hard), and Ti/Al (hard/soft). In the case of Al/Al, as shown in Figure 1.9(a), a relatively large deformation was observed as compared to the Ti/Ti case (Figure 1.9(b)), due to the lower strength of the processed material. Moreover, the Al/Al condition shows a wider high temperature region in the substrate than that of Ti/Ti owing mainly to its relatively high ductility, high thermal softening effect, and low strain hardening. As for the impact cases of dissimilar materials Al/mild steel and Ti/Al, Figure 1.9 (c and d), a different impact behaviour was observed with respect to the

previous cases. In particular, the initial kinetic energy of the particle is mostly dissipated into plastic deformation of the softer counterpart; therefore, a much higher temperature on the soft side is achieved. The simulation outcomes point out that the soft/hard case results in pronounced flattening of the softer particles with a slightly deformed substrate (Figure 1.9 (c)). On the other hand, in the hard/soft case the substrate experienced a significant deformation with a less deformed particle that deeply penetrated into the softer counterpart (Figure 1.9 (d)). In addition, relatively low critical velocities of 365m s−1 for Al/mild steel and 665m s−1 for Ti/Al were numerically found. It was also proved that at the interface between particles and substrate the temperatures can reach the melting point of the softer material in the dissimilar cases. The region at melting temperature can spread over a very large area on the soft side. A close view of this zone shows that the thicknesses of the 'thin-molten-layer' is greater for Ti/Al system, resulting in better/reliable metallurgical bonding.

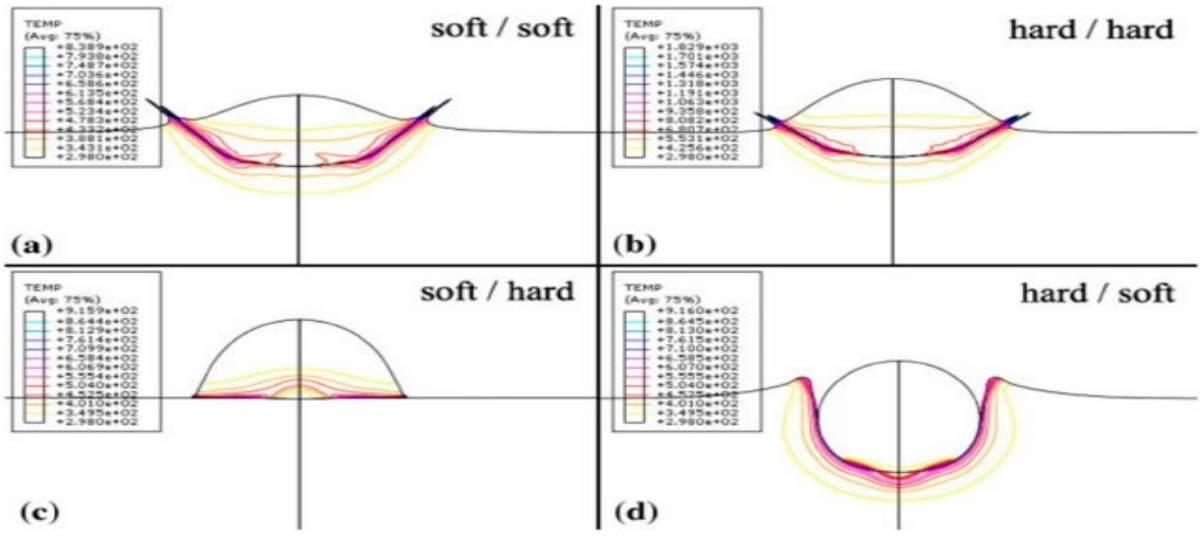

Figure 1.9: Impact process simulation for different material combination: (a) Al/Al (soft/soft), (b) Ti/Ti (hard/hard), (c) Al/mild steel (soft/hard), (d) Ti/Al (hard/soft) [96,115-116].

1.3 Cold spraying of titanium dioxide

1.3.1 Bonding mechanisms of titanium dioxide

It is well known that cold spraying ceramic materials can be difficult because cold spraying requires plastic deformation of the feedstock particles for adhesion to the substrate. The difficulty lies on difficult to plastically deform hard and brittle ceramic materials,such as TiO_2. However, previous studies reported the possibility of cold spraying thick pure TiO_2 but the bonding mechanism of cold sprayed TiO_2 is not fully understand [83].

Environmental pollution has drawn attention in the world today due to the need of safe and clean environment. Industrial activities and transportation are some examples that contribute to the unhealthy surroundings especially in the urban areas. The technologies recently use to reduce the pollution in our environment are by the applications of photocatalysts. TiO_2 have attracted much attention to be used as photocatalyst materials among the photocatalytically active materials due to its availability, low cost, chemical stability and nontoxic properties [12].

The drawback of the conventional thermal spray process to prepare TiO_2 coating is the irreversible phase transformation of TiO_2 structure from anatase to a less photocatalytic rutile phase at 500-600°C under normal conditions. Therefore, the alternative option is to prepare TiO_2 coating by cold spraying process.

1.3.2 Influence of titanium dioxide properties on bonding mechanism of titanium dioxide

Winnicki et al. used a low-pressure cold-spray system for cold-sprayed amorphous, anatase, and rutile TiO_2 powders with a particle size of 10–70 μm and similar shape, which were prepared by the sol-gel process. The 100 μm TiO_2 coatings were prepared on aluminum and the mechanism responsible for powder deposition was the mechanical interlocking of submicron powders with a local presence of agglomerates. They also indicate that the key parameter for the process seems to be the working gas temperature [97].

Hajipour et al. cold sprayed two types of TiO_2 powder; nanocrystal particles with a particle diameter of about 100 ± 15.3 nm and agglomerating ultra-fine particle with a diameter of about 80 ± 11 μm on aluminum substrate. The thickness of the coating is about 490 nm for nanocrystal particles and 15–20 μm for the agglomerating ultra-fine particle as shown by Figure 1.10 and 1.11. They indicated that for a brittle material such as TiO_2, the first layer is achieved by plastic deformation of the ductile metallic substrate when the particles are embedded into the substrate without any additional binding agent or calcination procedure. The coating/substrate interface is relatively rough when the particle hits the substrate at a high speed as shown by Figure 1.12-1.13. As a result, the titanium dioxide particles are embedded in the Al substrate. Roughness causes mechanical entanglement that might also play an important role in the buildup stage. They also conducted a coating bond strength testing by ultrasonic cleanout of 185 W for 1 min. The adhesion was assessed according to the spalling state of the coating. They identified that there was no spalling of the coating after 1 min [98].

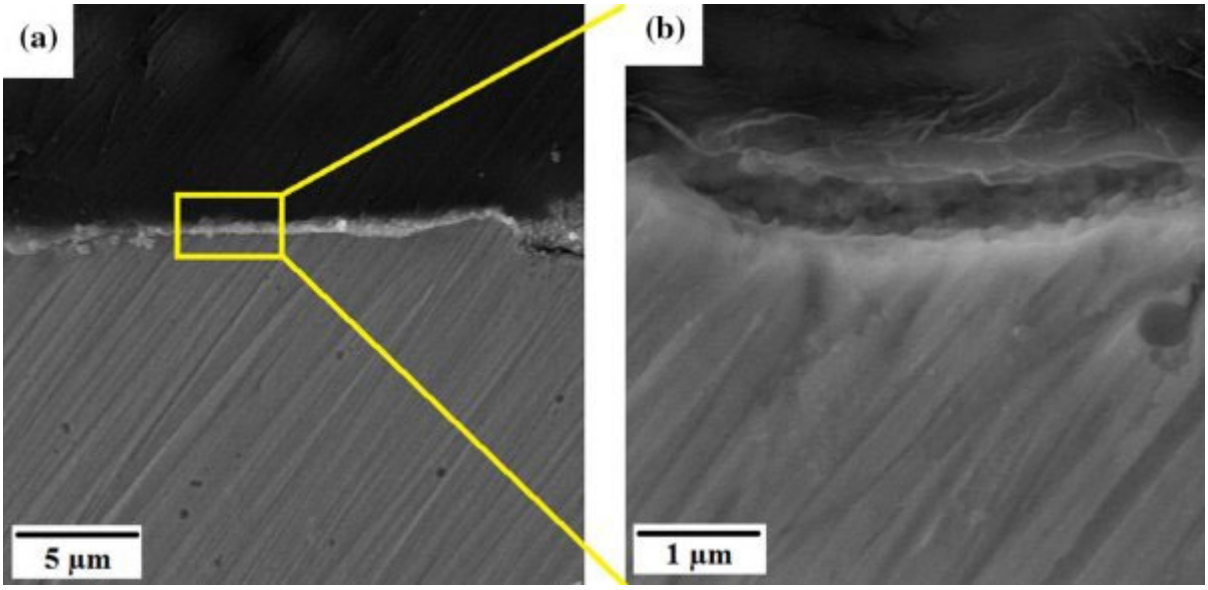

Figure 1.10: FESEM micrograph of the TiO_2 coating deposited with powder A: (a) cross-sectional image, (b) zoom up image [98].

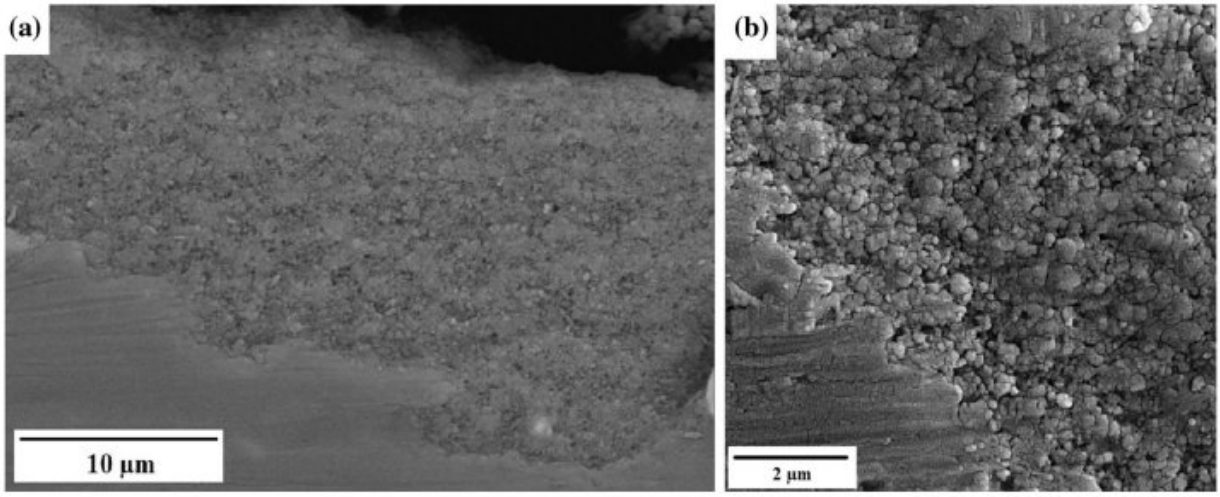

Figure 1.11: Interface the TiO_2 coating by powder B and Al substrate: (a) SEM images of cold-sprayed TiO_2 coating, (b) FESEM of interface [98].

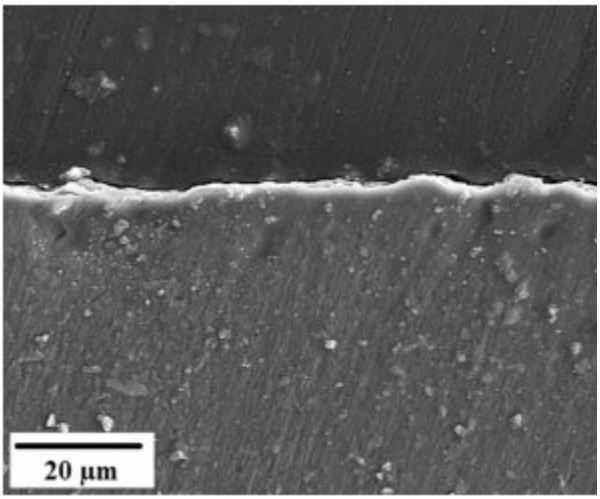

Figure 1.12: Surface roughness of the Al substrate before coating [98].

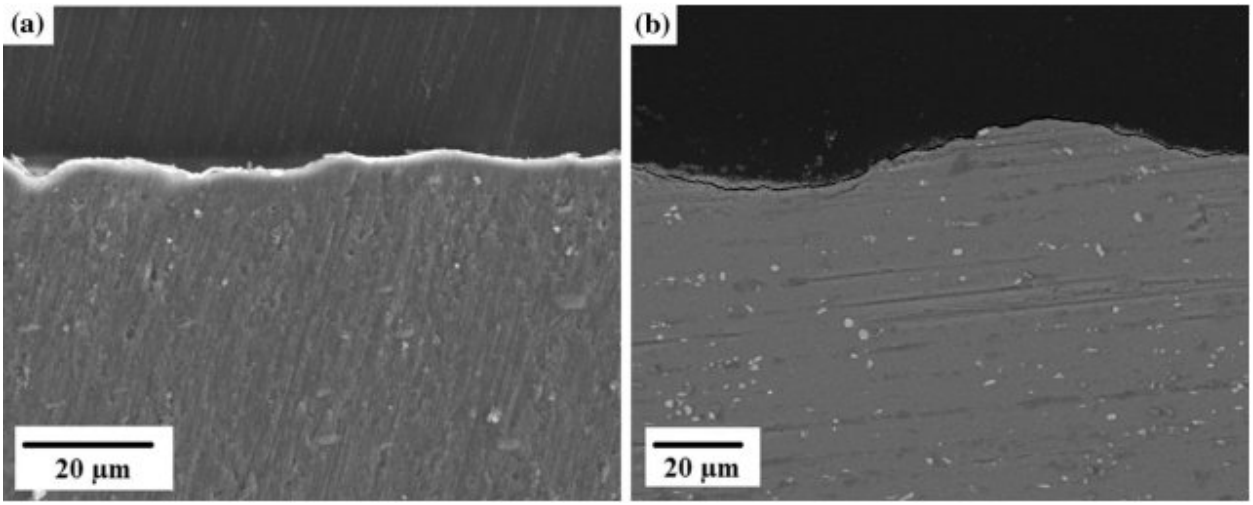

Figure 1.13: Surface roughness of the Al substrate after cold spray process with ; (a) powder A, (b) powder B [98].

Moreover, study by Yang et al. proposed that nanoporous TiO_2 film which about thickness of 10-15 μm was deposited by cold spray method using agglomerated TiO_2 powder with primary particle size of 200 nm and polyvinyl alcohol was used as a binder during the agglomeration as shown by Figure 1.14 [99]. They suggested that the sprayed TiO_2 powders was deformed under high transient impact pressure due to the polymeric binder that used during the agglomeration of TiO_2 nanoparticles, which lead to deformation that comparable to the deformation of metallic powders by cold spray process.

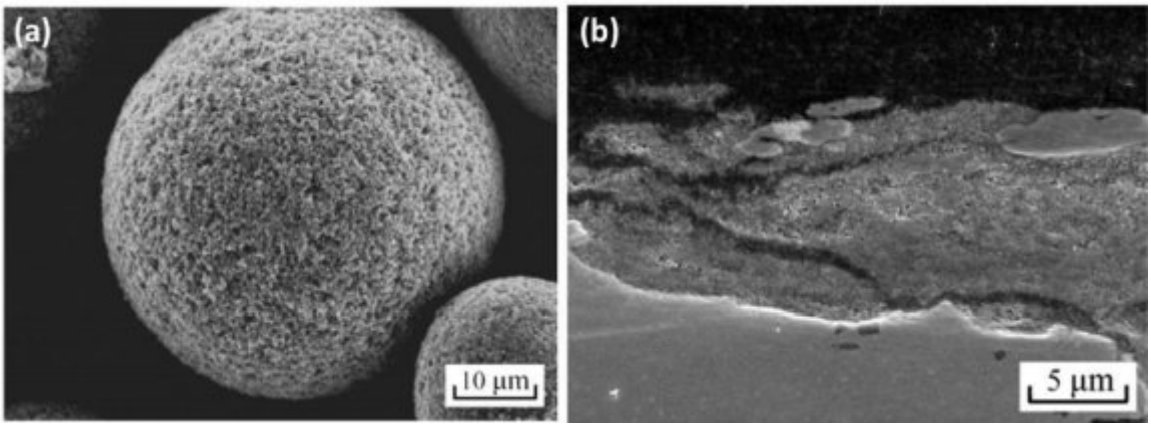

Figure 1.14: SEM image of (a) the spray TiO_2 powder agglomerated from nanoparticles using polymer binder and (b) the cross-section of TiO_2 coating deposited by cold spray process [99].

Later on, study conducted by Yamada et al. shows that process gas conditions, either using helium (He) or nitrogen (N_2) as the process gas is not the main factor to form TiO_2 coating using cold spray process as both type of the gas was possible to build up coating layer on the substrate [83]. They also reported that deposition efficiency of sprayed particles can be controlled by the temperature of the process gas as shown in Figure 1.15 and Figure 1.16 using He and N_2 gas at different temperatures, respectively.

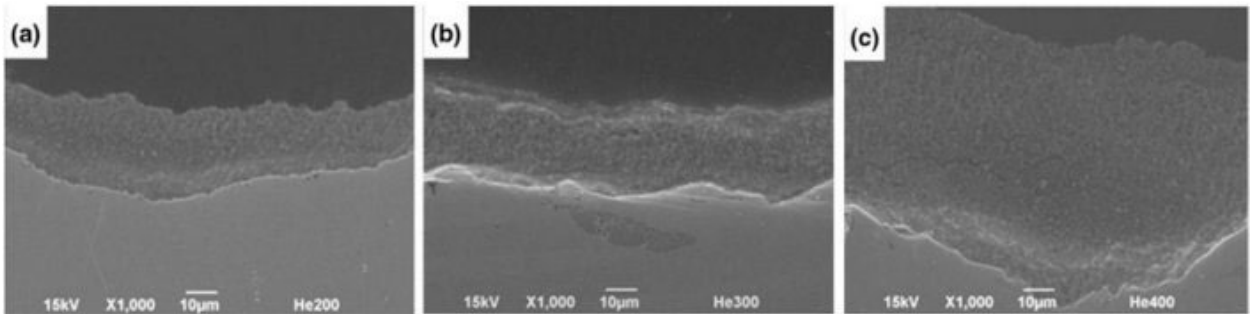

Figure 1.15: Cross section microstructure of coatings sprayed with He. Spraying with gas temperature of (a) 200 °C, (b) 300 °C, and (c) 400 °C [83].

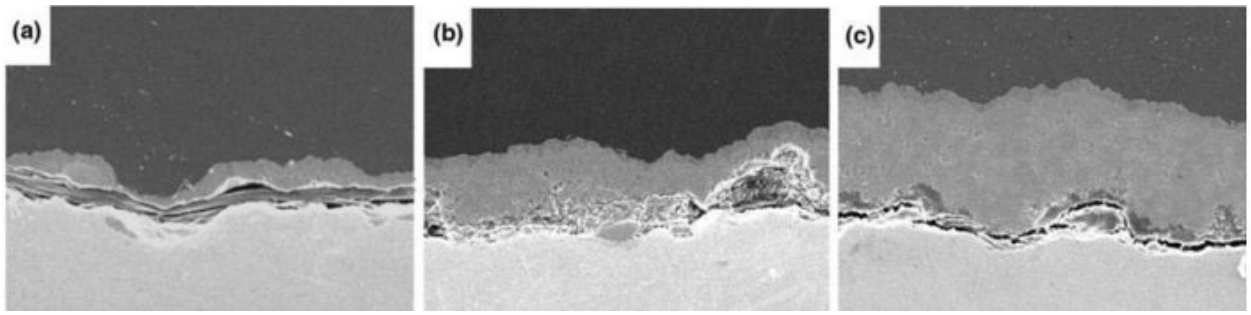

Figure 1.16: Cross section microstructure of coatings sprayed with N_2. Spraying with gas temperature of (a) 200 °C, (b) 300 °C, and (c) 400 °C [83].

The same authors also reported that a TiO_2 coating was produced from a recombination of broken up crystallite's links during the cold spray process, which was initiated by the porous structure of the agglomerated powders [100]. They proposed that chemical bonding may allow thick coatings to be deposited by cold spray process. The authors described that during the process, the agglomerated powder in nano-scale primary particles which also contains nanoporosity were fractured, leaving an unstable surface with a dangling bonds structure. In order to reobtain a stable

surface, the fractured particles decoupled and formed a surface with improved stability, which lead to bonding of the newly impacting particles and in turns building up of the coating (Figure 1.13-d). They did believe that starting feedstock materials play important role for the deposition of TiO_2 coating by cold spray process. Figure 1.17 shows the morphology of the feedstock powders that have been used to prepare TiO_2 coating.

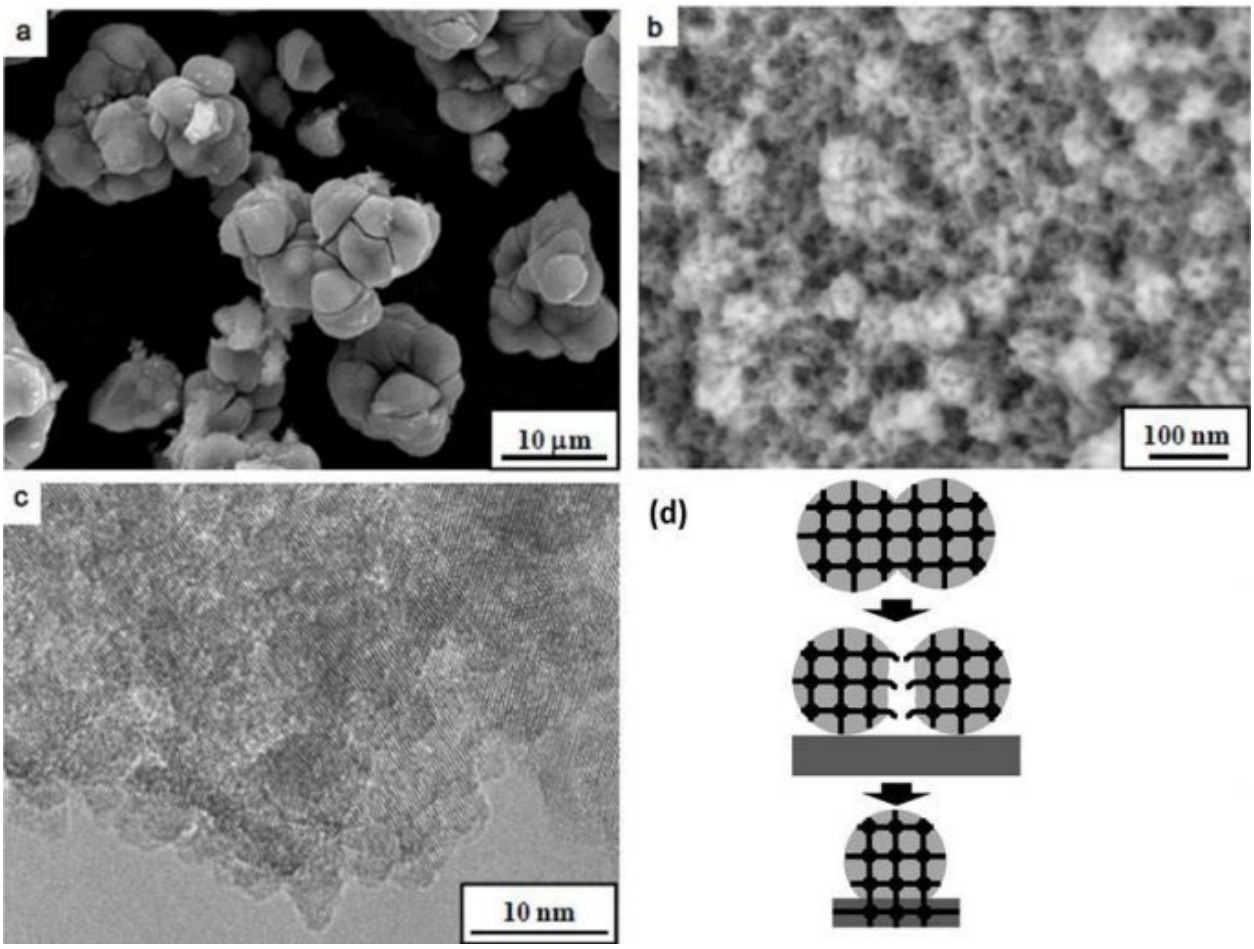

Figure 1.17: Morphology of TiO_2 feedstock powder; (a) SEM image, (b) FE-SEM image, (c) TEM image and schematic image of adhesion mechanism of cold-sprayed TiO_2 particle [83,100].

Toibah et al. have been successfully synthesized TiO_2 powders by a simple hydrolysis method without the addition of binder and/or inorganic salt. The method that has been employed successfully produced agglomerated anatase TiO_2 powders which were able to be used directly as feedstock powder for cold spray process. However, only as-synthesized TiO_2 and TiO_2 powders, that calcined at 200°C and 300°C showed the successful deposition of TiO_2 coating on the ceramic tile substrate by the cold spray method as shown by Figure 1.18. The calcined TiO_2 powders indicated a better crystallinity and thicker coating compared to the as-synthesized powder. A higher calcination temperature of 400°C do not only promotes grain growth and the crystallite size of the as-synthesized TiO_2 powders, but also reduces the porosity present in the agglomerated powder by densification of the particles. The presence of a certain amount of porosity in the ceramic feedstock powder is crucial in order to build up the coating during deposition [101].

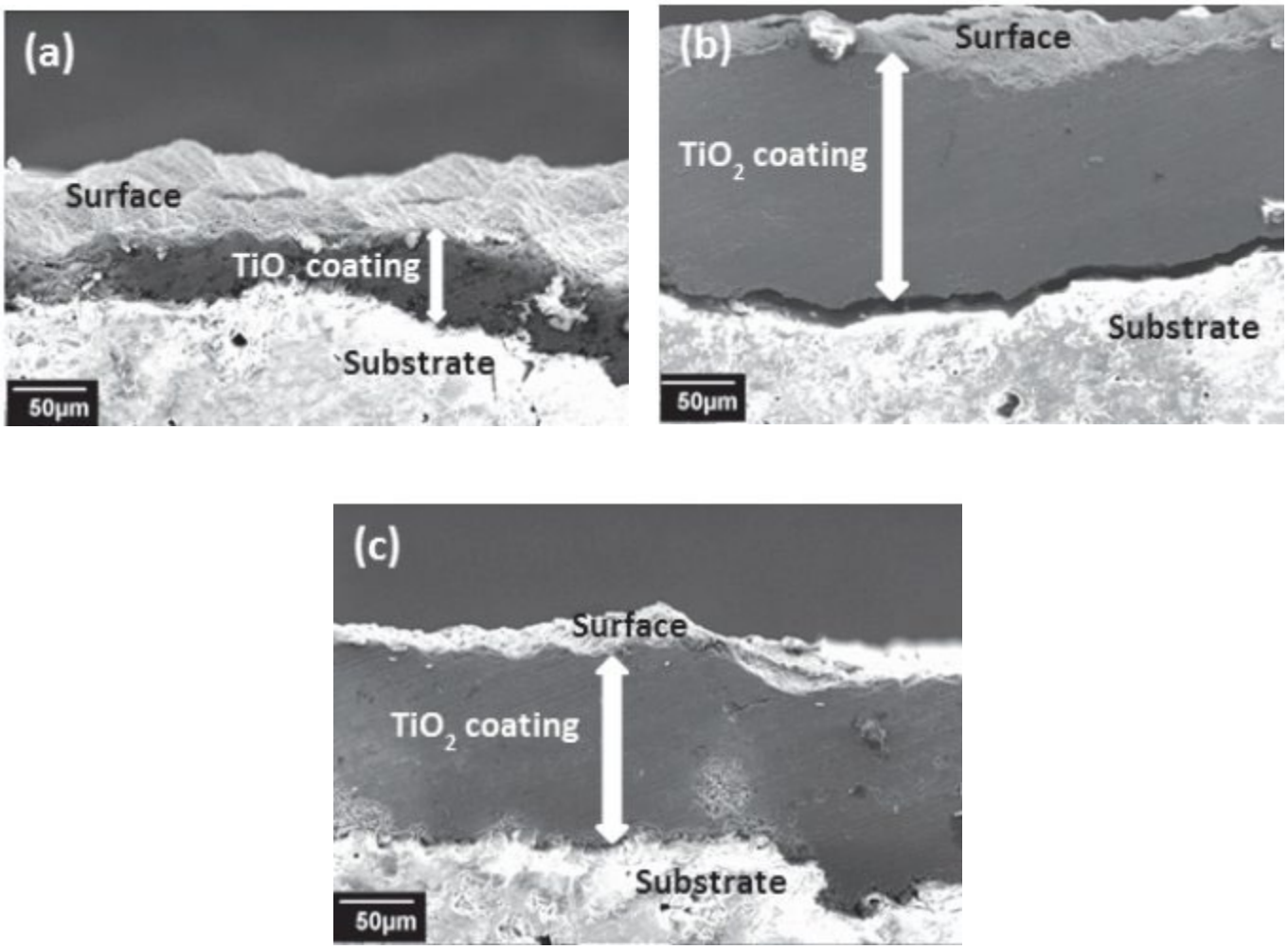

Figure 1.18: Cross-sectional view of the nanostructured TiO_2 coating deposited on a ceramic tile substrate by a CS process using: (a) as-synthesized powder (TiO_2-0), (b) TiO_2 powder calcined at 200°C (TiO_2-2), and (c) TiO_2 powder calcined at 300°C (TiO_2-3) [101].

1.3.3 Influence of substrate properties on bonding mechanism of titanium dioxide

Schmidt et al. used 0.1–10 μm of TiO_2 particles that were cold sprayed onto the flat polished surface of the titanium substrate. They identified that the plastic deformation of the substrate leads to a large continuous contact zone between the particles and the substrate and thus to durable bonding as shown by Figure 1.19. They also tested the bond strength of the coating by ultrasonic cleaning with a maximum intensity of 40.8 W/cm^2. No local changes in the number, positions, and volumes of the particles could be observed after the cleaning cycle, indicating that the bonding of all the TiO_2 particles to the substrate resists cleaning up to a maximum intensity of 40.8 W/cm^2 in the ultrasonic bath [102].

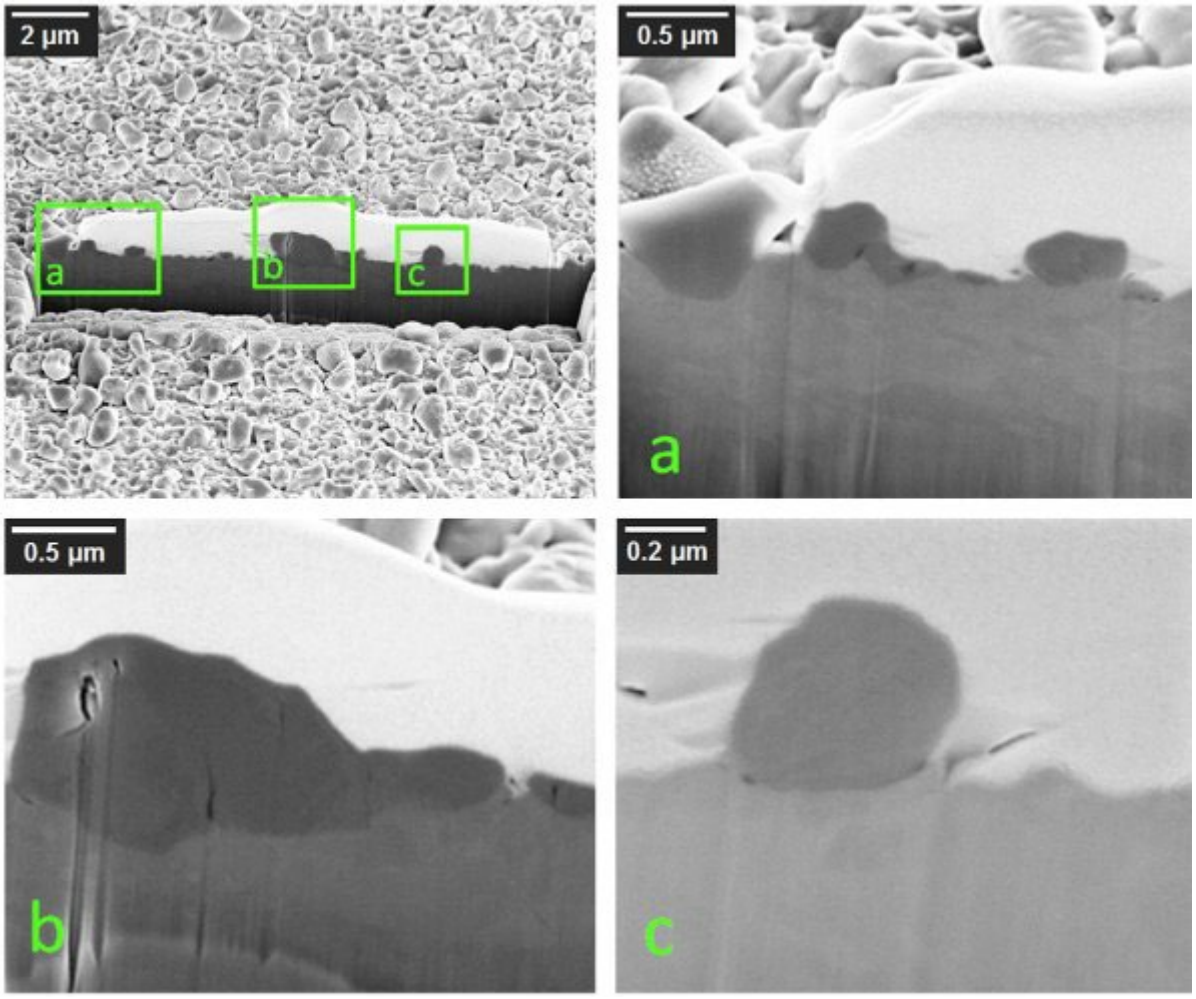

Figure 1.19: SEM images with a magnification of 20kX of the rectangular notch of about 17 µm x 2 µm size and a depth > 5 µm, prepared by FIB milling. The images show the bring protective platinum layer, the Ti substrate and some of the TiO_2 particles transected by the FIB milling (a) and (b) show details with magnification of 100kX and (c) shows a particle cut with a magnification of 200kX [102].

Kliemann et al. used 3–50 µm TiO_2 agglomerates formed from 5 to 15 nm of primary particles for continuous coating of steel, Cu, Ti, and $AlMg_3$ substrates as showed by Figure 1.20. They identified ductile substrates that allow shear instabilities to happen as the primary bonding mechanism between the particles and the substrate as shown by Figure 1.21 [103].

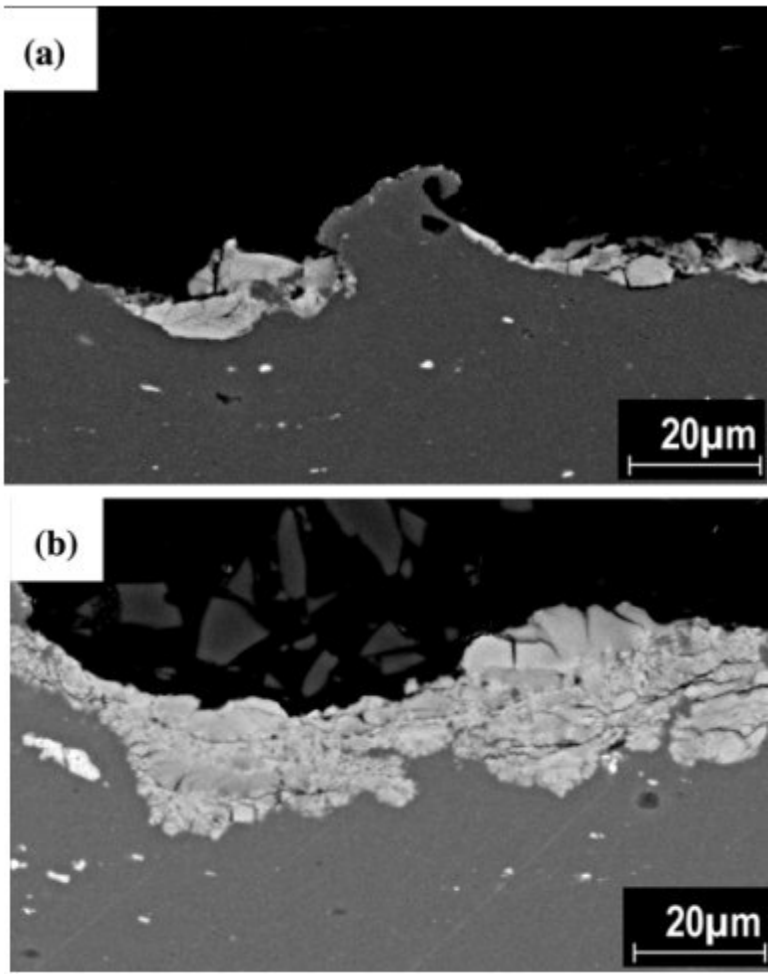

Figure 1.20: SEM images of cold-sprayed TiO_2 coatings on $AlMg_3$ substrate. (a) Sprayed as one pass with 800 ˚C process gas temperature and 40 bar pressure and (b) sprayed with 10 passes under the same process parameters [103].

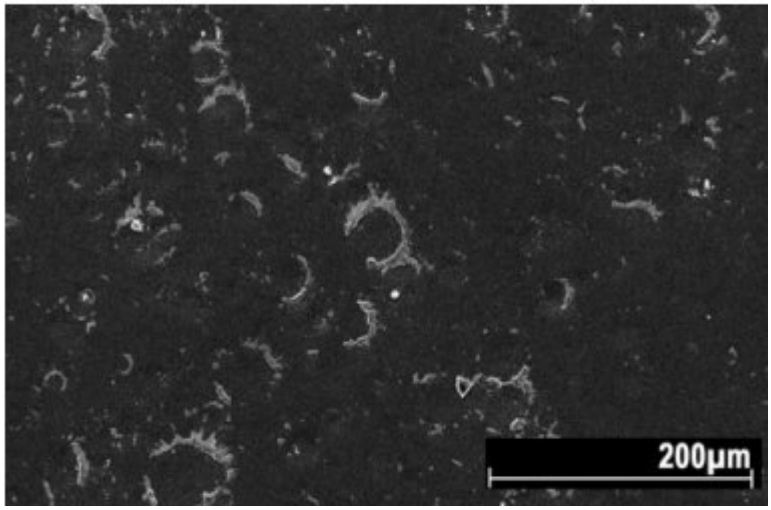

Figure 1.21: Top view morphology of several TiO_2 single particle impacts on stainless steel. The ring-like shape of the remaining TiO_2 is the dominant pattern in this case [103].

Gutzmann et al. obtained the impact morphology of single TiO_2 particles and studied the deposition of different particles on substrates with different temperatures. They showed that there were concentric rings on the impacted substrates such as the shear instability zone. The deposition of a single TiO_2 particle could be achieved only when the substrate temperature was above a certain value. The softer the substrate, the higher the deposition efficiency. It has been proposed that the preheating of the substrates could make them soft and facilitate the substrate shear instability, thus helping the deposit of the coating [104].

Gardon et al. [85] reported that the mechanism responsible for the deposition of TiO_2 on the stainless-steel substrate in the cold-spraying process is the chemical bonding between the particles and the substrate. They have shown that the previous layer of titanium sub-oxide prepares the substrate with the appropriate surface roughness needed for the deposition of the TiO_2 particle as shown by Figure 1.22. In addition, the composition of the substrate is also important for deposition

as it can provide chemical affinities during the particle interaction after impact. Substrate hardness may also ease the interaction between the particles and the substrate [86]. Proposed bonding mechanism of cold sprayed TiO_2- stainless steel showed by Figure 1.23.

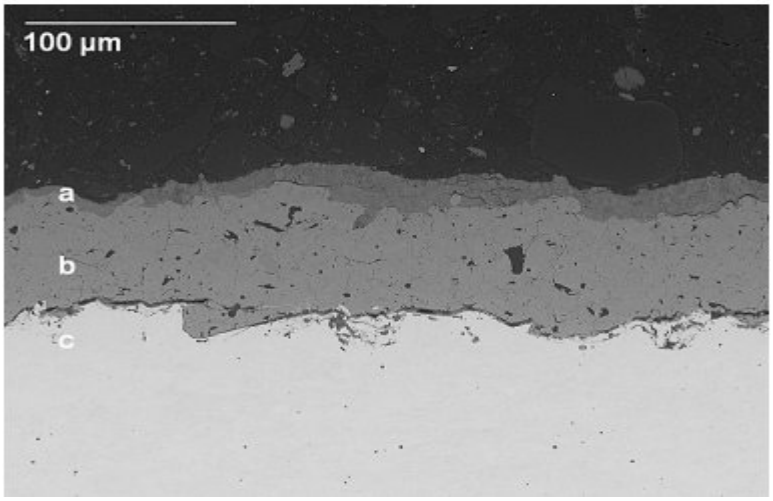

Figure 1.22: SEM micrograph of the CGS coating cross-sectional area (a) CGS nano-TiO_2 layer, (b) APS TiO_2-coating and (c) steel [85].

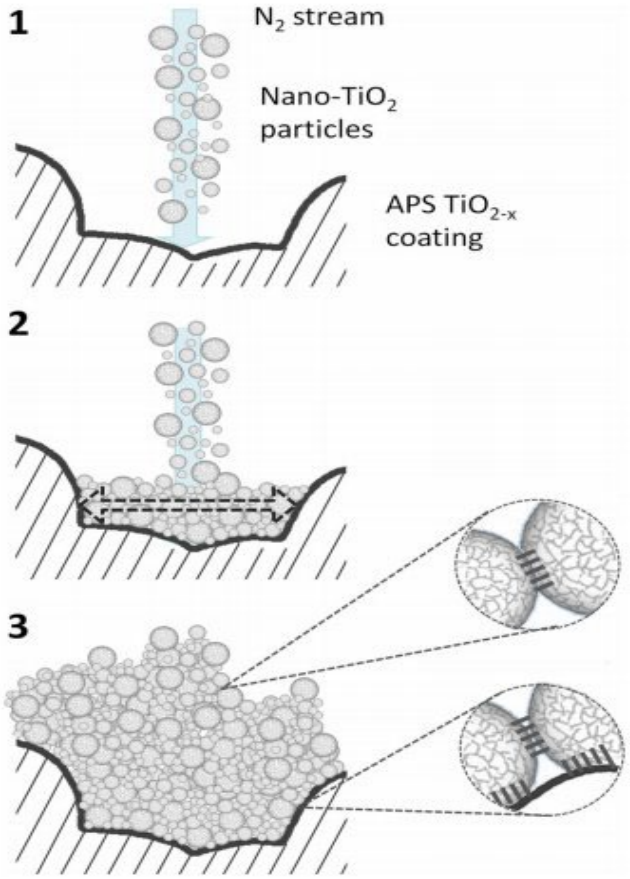

Figure 1.23: Possible mechanism of bonding between CGS nano-TiO_2 particles and APS TiO_{2-x} bond coat [85].

Clearly from the previous discussed studies conducted the results show that cold spray coating of TiO_2 is not easy to be obtained but it is not impossible and there is still considerable uncertainty concerning the bonding mechanism involved for pure TiO_2 powder with soft and hard substrates in order to increase coating adhesion strength.

1.4 Objectives

The adhesion strength of cold spray coatings with the substrate is not only based on mechanical interlocking. It is determined also by adiabatic shear instability, plastic deformation of the colliding materials and static recrystallization [105-109]. All these factors are attributable to substrate conditions such as hardness, material chemistry, surface roughness and temperature of the substrate. In cold spray, deformation of the substrate facilitates adiabatic shear instability and jet formation [87-88]. The formation of jets results in mechanical and metallurgical bonding at the interface. Soft substrates are susceptible to higher deformation than hard substrates, hence, results in a better adhesion strength [89-90]. Therefore, objective of this work to understand bonding mechanism for ceramic cold spray, pure TiO_2 powder on two cluster of materials, soft metals and hard metals, in order to increase coating adhesion strength. To accomplish this objective, 4 sub-objectives are addressed. This study embarks on the following objectives:

1. To prepare the substrates with hardness and oxide properties by heat treatment in electric furnace, air medium for varying annealing temperature. An annealing is a heat treatment that changes the physical and chemical properties of a material in order to improve its ductility and reduce its hardness, making it more workable.
2. To examine the effects of cold spray TiO_2 coating on soft and hard metals annealed substrates by tensile strength testing and cross-sectional microstructure by SEM.
3. To characterize the properties of annealed soft and hard metals substrate that influence bonding mechanism such as surface roughness, hardness, oxide thickness and oxide chemical composition by several methods such as Vickers hardness and XPS.

4. To investigate the mechanism of single particle bonding by wipe test on soft and hard metals substrates by FIB and TEM. Factors that contribute to the formation of the cold spray TiO_2 coating has been investigated based on the substrate properties of soft and hard metals. Mechanism of the deposition has been discussed based on the soft and hard metals substrate to form the TiO_2 coating by cold spray method.

1.5 Thesis organization

This thesis consists of 7 chapters, which include the introduction, experimental, 3 content chapters, the overall conclusion and also chapter on the contribution of this study to the research/academic and industrial field. Chapter 1 discusses brief idea, philosophy and the objectives of the study which lead to this research focus. This chapter also focuses on the review of main theories and describes previous works related to this research, including the material and process that chosen in this study to fabricate the coating in order to achieve the objectives of this study.

Chapter 2 presents the experimental process used to prepare the substrates for the cold spraying process. Generally, this chapter describes the substrate preparation method that can be used to study the substrate properties like surface roughness, hardness and substrate oxidation characteristic by annealing process. The characterization of the annealed substrates and coating also included in this chapter.

The bonding mechanism of cold sprayed titanium dioxide coating on soft metals substrate is discussed in Chapter 3. As a substrate, pure aluminum and pure copper were chosen and annealed before being cold sprayed with titanium dioxide powder. Surface roughness, hardness, oxide thickness, and oxide composition of soft metals were discussed in relation to the bonding mechanism involved. The bonding mechanism in cold sprayed TiO_2/soft metals substrate is metallurgical bonding, which requires oxide free on the substrate surface.

The bonding mechanism of cold sprayed titanium dioxide coating on hard metals substrate is discussed in Chapter 4. As a substrate, stainless steel and structural steel were chosen and annealed before being cold sprayed with titanium dioxide powder. Surface roughness, hardness, oxide

thickness and oxide composition of hard metals were discussed in relation to the bonding mechanism involved. The bonding mechanism in cold sprayed TiO_2/SUS304 substrate is chemical bonding by inter-oxide reaction of TiO_2-OH^-. Inter-oxide reaction occurs between hydroxyl, OH-, which originates from chromium oxide, Cr_2O_3, which is thermodynamically preferred in SUS304, and TiO_2, which has a high affinity to steel oxygen. In order to confirm the role of Cr_2O_3 in the bonding mechanism, a pure chromium substrate was also investigated in this chapter. Only certain substrates and oxides play a role in bonding, such as SUS304, whereas others, such as structural steel, require an oxide-free surface to form bonding between TiO_2/substrate surface.

Chapter 5 provides a summary of the bonding mechanism of cold sprayed titanium dioxide on soft and hard metals, as well as a comparison to the bonding mechanism of cold sprayed metallic material. Cold sprayed ceramic (TiO_2) on soft metals substrate demonstrated a similar tendency to metallurgical bonding in cold sprayed metallic materials. Cold sprayed ceramic (TiO_2) on hard metals substrate especially for SUS304, showed a chemical bonding involved.

General conclusions and recommendation of further work are summarized in chapter 7. Contribution of the study to the research / academic and industrial field have been discussed briefly in Chapter 8.

2 General Experimental Procedures

2.1 Introduction

Two specific interaction types exist in cold-spray deposition, which must be distinguished: first, particle-to-substrate interaction, necessary for the initial particle-formation layer, and pertinent to the strength of adhesion of the substrate's final coating; and second, the interaction between particles, related to the coating's accumulation and the deposit's cohesive strenth [110-111]. This indicates the substrate type's and surface conditions' strong influence in terms of the strength of the adhesion. Research that exemplifies the substrate material's impact on the properties of the coating in the process of cold spraying is provided in references [112-117]. Klinkov [38] reported that temperature influences the process of cold spray in different ways. First, with the temperature of stagnation increasing, the velocity of the process gas is increased and therefore also the velocity of impacts of the particles. Second, the elastic and plastic properties of materials depend on the temperature. The temperature of the materials can be changed both by using a higher gas temperature and by preheating the substrate. An increased temperature of the materials could enhance thermal softening which is important for the bonding mechanism proposed by Assadi et al. [118]. Furthermore, it is well known that chemical reactions and diffusion also strongly depend on the temperature. Chemical reactions and / or diffusion can support the adhesion between the particles and the surface.

This study to change substrate property in each material by annealing was conducted. The substrate preparation is very crucial to adhesion bonding of first layer cold sprayed TiO_2 coating and substrate surface. Figure 2.1 shows overview of substrate preparation and characterizations.

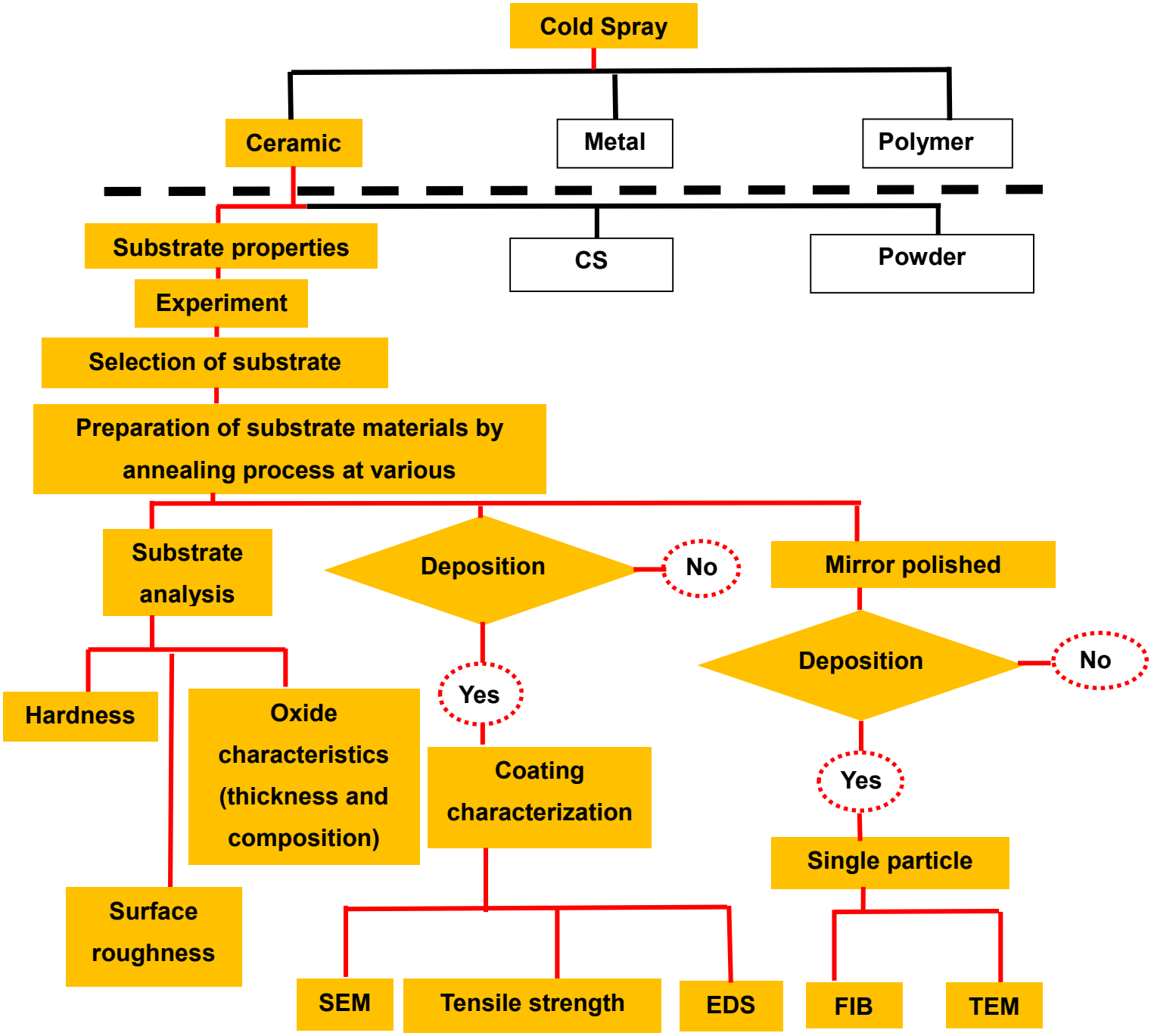

Figure 2.1 : Overview of substrate preparations and characterizations.

2.2 Substrate preparations

2.2.1 Material composition

Table 2.1 shows the chemical composition of the substrates used. This range of materials is used as a substrate to better understand the bonding mechanism. Over a decade, pure aluminum and pure copper have been extensively investigated in the cold spray area, and they have been used as fundamental to understand bonding mechanisms in this study. As a substrate, stainless steel and structural steel were used. The substrate was made of a hard material to eliminate the possibility of a substrate metal jet forming due to particle impact, to give better understanding of bonding mechanism involved.

Table 2.1: Materials chemical composition [wt%]

	Cu	P	Mn	Zn	Sn	Ni	Co	Zr	Ag
C1020	Bal	0.04	1.1	0.1	0.72	0.06	0.21	0.05	0.04
	Al	Fe	Si	Zn	Cu	Mn	Mg	Ti	Other
AA1050	Bal	0.40	0.25	0.05	0.05	0.05	0.05	0.05	0.03
	Fe	C	Mn	P	S	Si			
SS400	Bal	0.30	1.00	0.04	0.05	0.28			
	Fe	Cr	Ni	Mo	S	P	Mn	Si	C
SUS304	Bal	18	11	-	0.030	0.045	2.00	1.00	0.08

2.2.2 Blasting process

The surface of the substrate was blasted using an air blast device (Shinto Brater Co., Ltd., Myblast MY-30B) as a pretreatment substrate prior to the annealing process in an electric furnace. Fe-based projection material (SB Steel Grit GH-10, manufactured by Shinto Kogyo Co., Ltd.) was used in the blasting process and the projection pressure was 0.3 MPa and the projection time was 60 seconds.

2.2.3 Electric furnace annealing process

Substrates were annealed with an electric furnace at different temperatures respectively, referring to each material as shown in Table 2.2. The increment was 15˚C/5 minutes, and after a five-minute soaking, the substrates were cooled to room temperature in the furnace. The schematic diagram of the electric furnace and temperature increment are shown below in Figure 2.2 and 2.3.

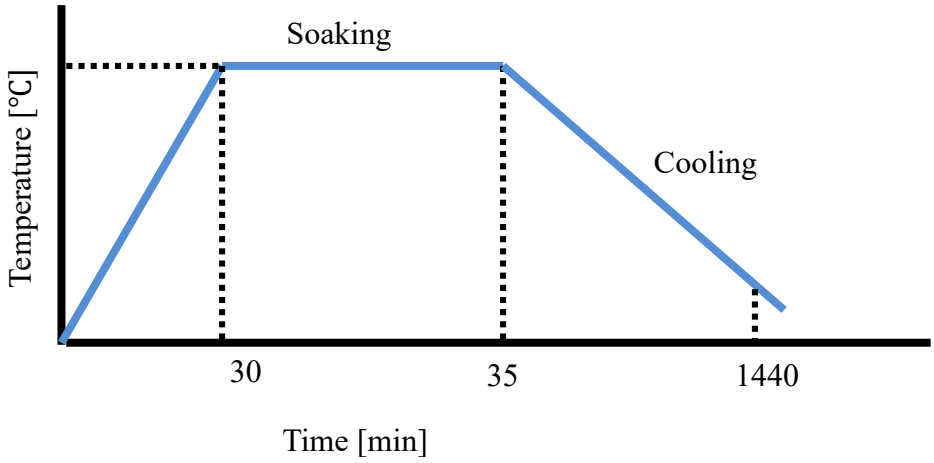

Figure 2.2: Schematic of annealing temperature increment process.

Table 2.2: Materials vs annealed temperatures

Materials	Annealed temperature
Pure copper, C1020	Room temperature, 100˚C, 200˚C, 300˚C and 400˚C.
Pure aluminum, Al 1050	Room temperature, 100˚C, 200˚C, 300˚C and 400˚C.
Structural steel, SS 400	Room temperature, 400˚C, 700˚C and 1000˚C.
Stainless steel, SUS 304	Room temperature, 400˚C, 700˚C and 1000˚C.
Pure Chromium	Room temperature, 400˚C, 700˚C and 1000˚C.

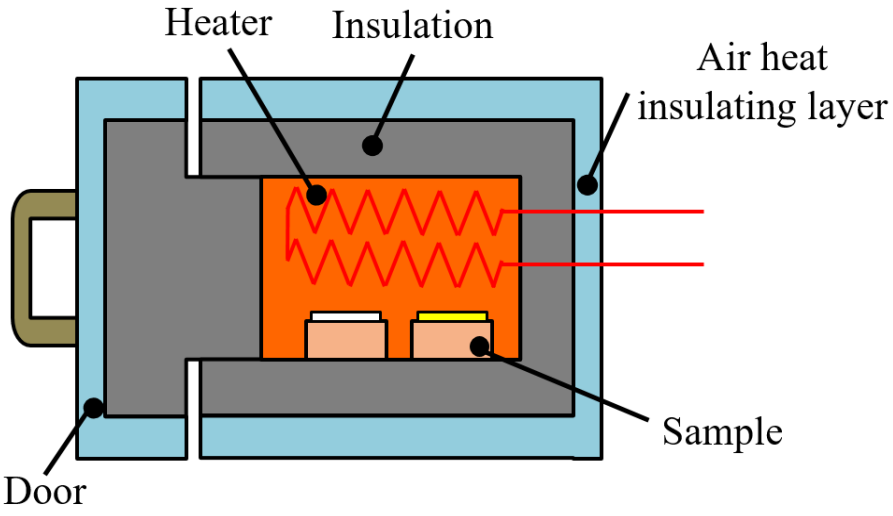

Figure 2.3: Schematic of electric furnace.

2.3 Properties of titanium dioxide powder

Agglomerated TiO_2 powder (TAYCA Corporation, WP0097) containing pure anatase crystalline structure with an average particle size of about 7.55 μm was used as the feedstock powder for the coating deposition. Figure 2.4 shows the morphology of the agglomerated powder particles.

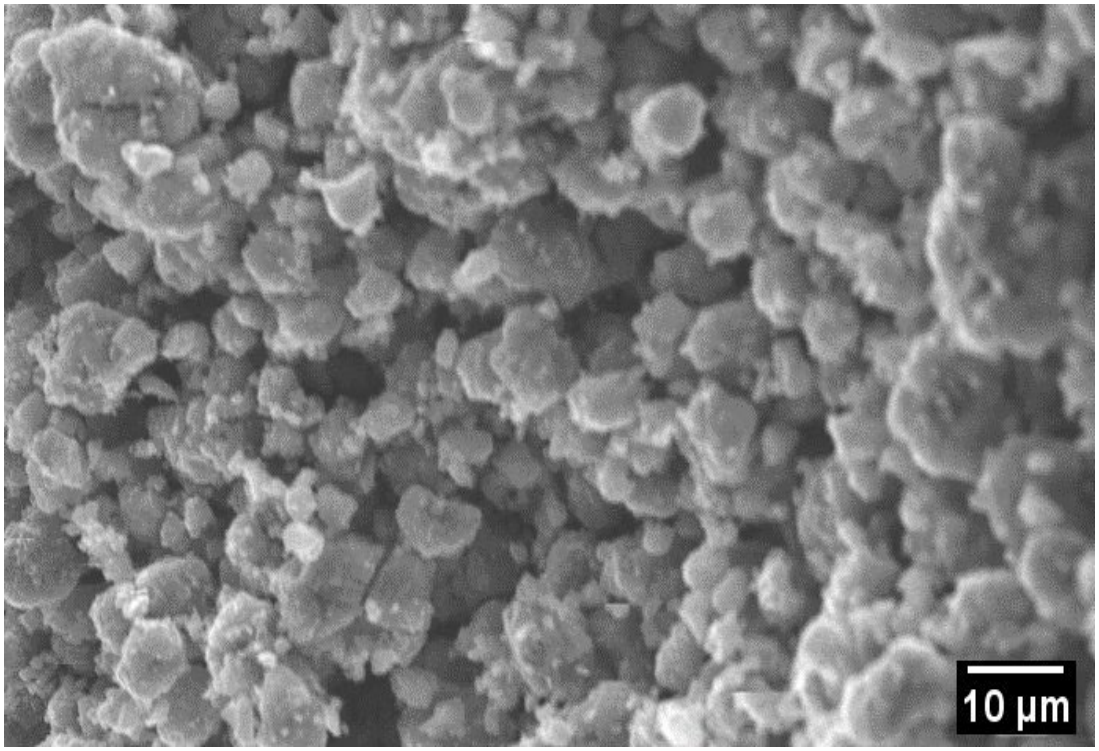

Figure 2.4: Morphology of titanium dioxide powder.

2.4 Overview of cold spray equipment

2.4.1 Cold spraying with the cold spray system

In this experiment, the coating was formed using a commercially available cold spray device (Cold Gas Technology, KINETIKS 4000). A schematic diagram of this system is shown in Figure 2.5 and its specifications are shown in Table 2.3. This equipment consists of a gas cylinder, a heater for gas heating, a nozzle, and a feedstock powder supply device. Commercially available nitrogen was used as a carrier gas for this experiment. In this equipment, the carrier gas supplied from the gas cylinder is heated by a gas heater, and supersonic speed is achieved at the De-Laval part of the nozzle. At the same time, the feedstock powder is injected into the pressurized carrier gas from the axial direction of the nozzle. The particles in the feedstock powder are accelerated by the carrier gas and are finally projected onto the substrate to form a coating. A custom-made De-Laval nozzle (Cold Gas Technology, 24TC) was used as a nozzle. The cross-sectional shape of the nozzle is shown in Figure 2.6. This nozzle has a tapered and wide shape with a throat diameter of 3 mm. It was used because it has a long expansion part and is advantageous for particle acceleration. The carrier gas temperature and pressure used as process conditions were the temperature and pressure at the nozzle inlet. Therefore, the actual temperature of the carrier gas downstream of the nozzle is lower than the set carrier gas temperature.

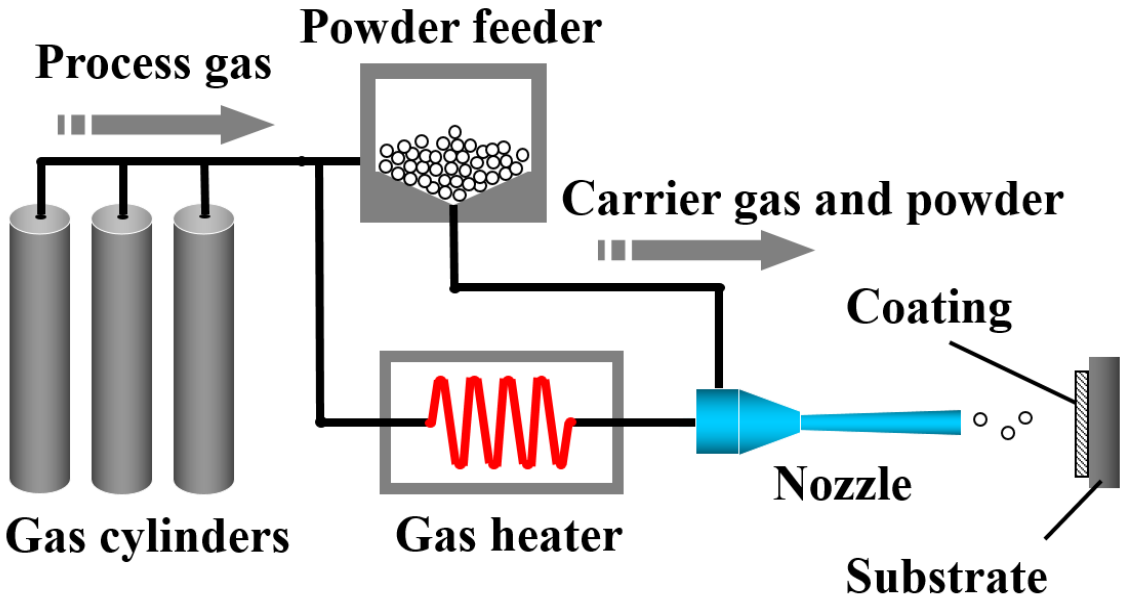

Figure 2.5: Schematic diagram of cold spray system.

Table 2.3: Specifications of cold spray system.

Model Number	Kinetics 4000
Process Gas	N_2
Maximum Process Gas Temperature [°C]	800
Maximum Process Gas Pressure [MPa]	4.0

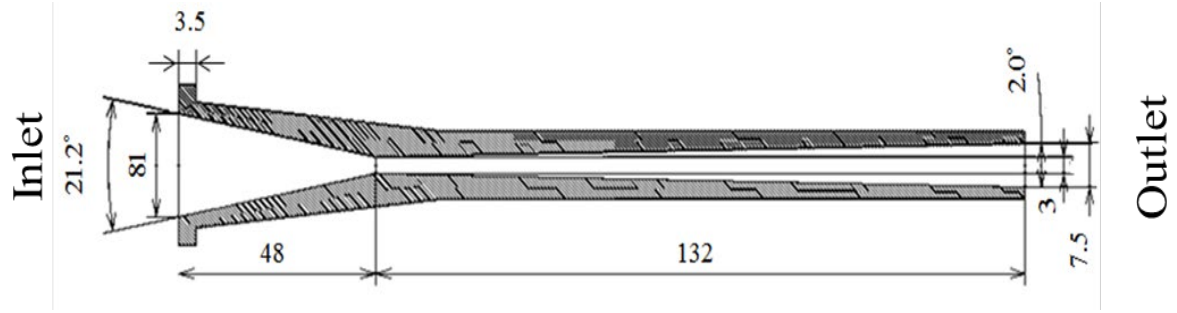

Figure 2.6: Cross sectional shape of nozzle.

2.4.2 Cold spray deposition conditions

Coating experiment was conducted to evaluate the adhesion strength of annealed substrates. A schematic diagram of the coating experiment is shown in Figure. 2.7 and the experimental conditions are shown in Table 2.4. The substrate was fixed using a jig, and the coating was formed by controlling the nozzle fixed to the tip of a 6-axis robot arm (M-710iC, manufactured by FANUC).

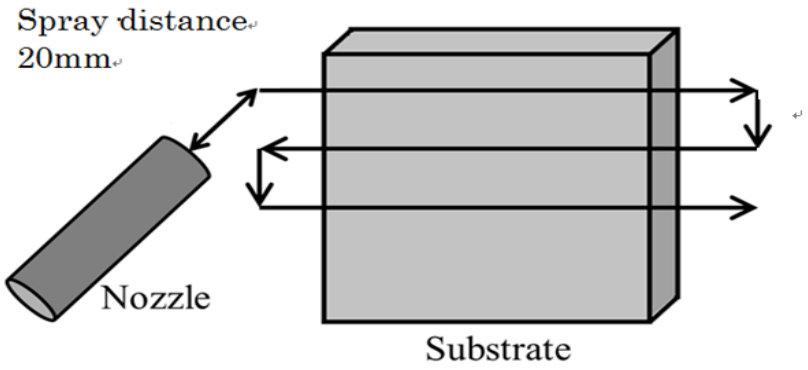

Figure 2.7: Schematic diagram of coating experiment.

Table 2.4: Coating experiment conditions

Process gas pressure [MPa]	3.0
Process gas temperature [˚C]	500˚C
Powder	TiO_2 (Agglomerated, ϕ7.55μm)
Powder supply system	High pressure feeder system
Substrate	Al 1050, C1020, SS 400, SUS 304 and Pure Cr
Traverse speed [mm/s]	10
Traverse pitch [mm]	2.0
Spray distance [mm]	20

2.5 Overview of characterization testing

2.5.1 Adhesion strength TiO_2 coating testing

In accordance with Japan Industrial Standard, JIS H 8402, specimens of dimensions of Ø 25 mm x 10 mm as shown by Figure 2.8, assessed the adhesion strength of the coating given as the fracture load value as measured by the universal testing machine (Auto graph AGS-J 10kN Shimadzu) and subsequently divided by the cylindrical coating area. The epoxy-based strong adhesive was used to bond the pin and coating (Huntsman Advanced Materials Company: Aralkyl Standard) as shown by Figure 2.9. The strength test was performed after the glue was cured for a period of 24 hours. For each substrate parameter, the tensile strength was repeated 5 times to obtain the average adhesion strength value.

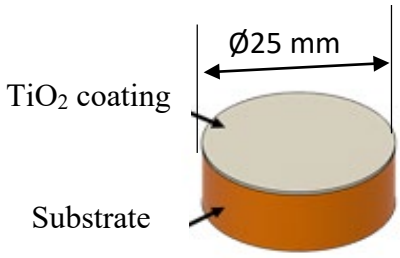

Figure 2.8: Specimen with TiO_2 coating.

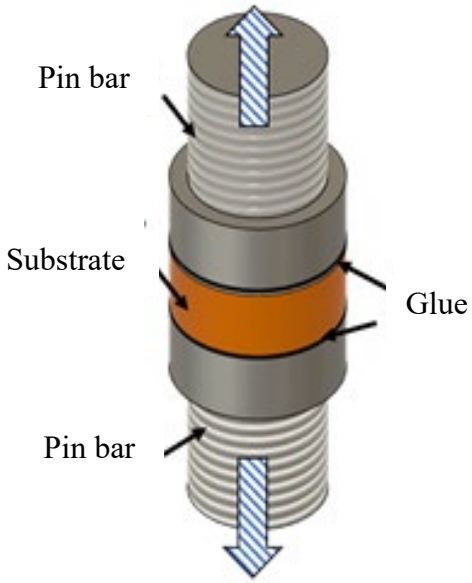

Figure 2.9: Sample preparation for tensile strength testing.

2.5.2 EDX on fracture coating

The FE-SEM & VP-SEM microscope (JSM-IT300LV, JEOL) was used to conduct EDX on fracture coating samples as shown by Figure 2.10.

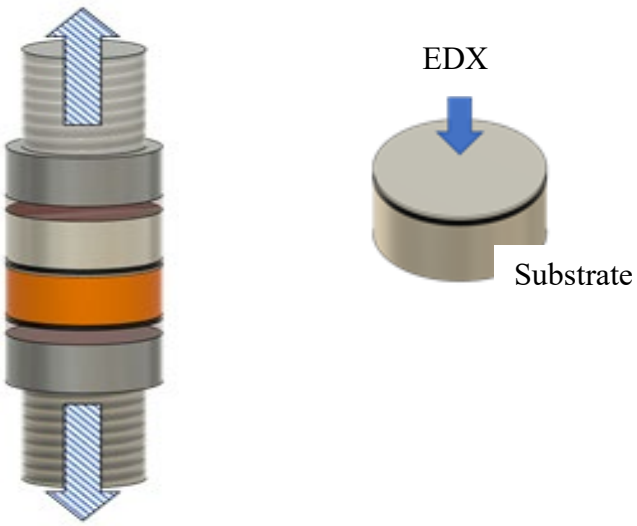

Figure 2.10: EDX on fracture coating

2.5.3 SEM cross-sectional observation

Scanning electron microscope (SEM: JSM-6390, JEOL) was used to observe cross-sectional microstructures of the coating. The observation sample of the TiO_2 coating was prepared by embedding the 25mm x 10mmx 5mm sample into a hardenable resin. The hardened sample in hardened resin was grinded with silica papers to a #3000 grit size and was finally polished with 1μm and 0.3μm alumina suspension.

2.5.4 Substrate surface roughness testing

To investigate the oxide roughness in nanoscale, atomic force microscopy (NanoWizard 3, Bruker) is conducted on annealed substrate surface by areal analysis at scanning area of 5μm.

2.5.5 Substrate Vicker's hardness testing

To investigate the relationship between substrate`s surface hardness after oxidation and adhesion strength, substrate`s hardness was measured using micro-Vickers hardness tester (HMV-G, Shimadzu). The measurement showed a hardness of HV 0.1 and the test load on the cross section was 980.07 [mN]. The final micro-hardness value was the average of 5 tests taken at approximately the same points for each substrate.

2.5.6 Oxide composition of substrate evaluation by X-ray photoelectron spectroscopy, XPS

X-ray photoelectron spectroscopy (XPS) is a versatile surface analysis technique used for compositional and chemical state analyses. In this study, XPS analysis (PHI Quantera SXM-CI, ULVAC-PHI) using a monochromatic Al Kα source (15 mA, 10 kV) was performed. Wide and narrow scans (0–1000 eV) of Fe 2p, Cr 2p, Al 2p , Cu 2p and O1s for different annealed substrates were collected. The measured binding energies were then corrected with C 1s at 285.0 eV. When pre-sputtering to clean the surface was performed, the sample surface was reduced and the measurements were affected, so XPS analysis was performed without pre-sputtering. Table 2.5 shows the XPS analysis conditions for substrates oxide analysis.

Table 2.5: XPS parameters for substrate oxide layer analysis.

Measured regions	Fe 2p,	O 1s,
	Cr 2p,	Al 2p , Cu 2p
Measured X-ray output [W]	10	
Probe diameter [μm]	50	
Time per step [ms]	30	
Pass energy	140	
Cycle	30	

2.5.7 Wipe test

A CGT Kinetiks 4000 cold-spray system (Cold Gas Technology, Ampfing, Germany) with a custom-made suction nozzle was used to perform the wipe test and coating using TiO_2 powder onto the annealed substrates. The wipe test was conducted to study the deformation behavior of a single particle on this substrate. Prior to deposition, substrate was ground and polished until a mirror finish surface was obtained. The process gas temperature and pressure used were 500°C and 3 MPa, respectively. Nitrogen was used as the process gas. The distance between the exit of the nozzle and the substrate was fixed at 20 mm. The traverse speed of the process was 2000 mm/s. We change the traverse speed from 10 mm/s to 2000 mm/s due to the collection of particles and the prevention of the formation of full coating. Prior to spraying, the substrates were rinsed with acetone. A field emission SEM (FESEM) and focused ion beam (FIB) microscope (Helios Dual Beam 650, FEI) was used to investigate the single particle TiO_2 deposition onto mirror polish annealed substrate.

2.5.8 High resolution transmission electron microscopy, TEM

Thin membranes for transmission electron microscopy (TEM) observation were carefully made from deposited TiO_2 particles onto annealed mirrored polish substrate by focused ion beam (FIB) milling equipment (Helios Dual Beam 650, FEI). Without further sample preparation, electron-transparent membranes were made and investigated by field emission gun (FEG) electron microscopy (JEM-2100F, JEOL) with a scanning mode at an applied voltage of 200kV.

3 Bonding mechanism of cold sprayed TiO_2 coating on soft metals substrate

3.1 Introduction

Aluminum is the most commonly used material for cold spraying due to its availability and ductile properties [119-125]. The role of a stable oxide film of aluminum in bond formation in cold spraying, on the other hand, has been widely debated. It was argued that the oxide shell fracture is consistent with the coating formation threshold velocity. Aluminum coating was found to exhibit anistropic behavior in bond formation and particle deformation. Zhang et al. [123] investigated the effect of different substrates on bond formation in cold spraying of aluminum and concluded that metallic substrates harder than aluminum particles promoted deposition in general.

Over the last decade, the microstructure of cold sprayed copper coatings has been extensively studied using optical microscopes, scanning electron microscopes, focused ion beam (FIB) lift out, transmission electron microscopes, and a variety of other techniques [127-135,108,137-138]. The cold sprayed copper coating's microstructure is made up of highly deformed "pancake shaped" splats with near zero porosity as measured by electrochemical tests, making this face centred cubic (FCC) copper an ideal candidate for cold spraying [131].

The mechanism of bonding in cold spraying is still being debated. A set of hypotheses have been proposed regarding the mechanism of bonding in cold spraying. The bonding mechanism for metallic cold spray is believed to be the result of an adiabatic shear instability at the interface during impact, which occurs as a result of high strain rate deformation processes and produces a metal jet [138-141]. It is proposed that the formation of this metal jet results in the removal of the surface oxide layer, allowing true metal-to-metal contact to be established.

Numerical simulations of particle impact in cold spraying provide valuable information about the high strain rate deformation behavior of materials, but are unable to provide a clear indication of the conditions under which intimate metallic bonding is established. Prince et al. [142] proposed a method to characterize the inter particle bond formation in cold spraying is a blended of copper and aluminum particles was cold sprayed and subsequently annealed at 400ºC. It is known [143-144] that the formation of intermetallic phases during annealing of aluminum-copper diffusion couples indicates that the surface in contact are free of oxide layer and thus utilized the formation of such intermetallic between copper and aluminum particles within the coating as indicator of metal-to-metal bonding where surface oxide films had been removed during spraying.

Cold spraying can be used to metallize ceramics, in which aluminum (Al), titanium (Ti) and copper (Cu) coatings were used as the coating materials and alumina (Al_2O_3), aluminum nitride (AlN), silicon nitride (Si_3N_4), silicon carbide (SiC), magnesium fluoride (MgF_2), zirconate titanate (PZT) and zirconia (ZrO_2) were employed as the substrates [145]. Ko et al.[146] reported the amorphization and atomic intermixing phenomena at the interface of Cu/AlN and Al/ZrO_2 bonding couples. The authors attributed bonding between metal and ceramic to chemical adhesion. Wüstefeld et al.[147] reported local heteroepitaxial growth phenomena in the bonding couple of Al/AlN. Local heteroepitaxy between Al and AlN was attributed to the increase of the substrate temperature and the recrystallization or melting of Al coatings. However, the heteroepitaxial growth was not found for other ceramics. Drehmann et al.[148] attributed the bonding to mechanical interlocking in several bonding couples, e.g. Al/SiC, Al/Si_3N_4, Al/MgF_2. Kromer et al. [149] pre-treated rough surfaces on SiC and Al_2O_3 ceramics using laser surface texturing before cold spraying, which promoted mechanical anchoring between metal and ceramic. In addition, King et al.[150] reported that mechanical adhesion took place by penetrating aluminium into the

open pores on the smooth PZT substrates. Another interesting issue should be noted that the bonding strength of the metallic coatings on these ceramics did not present quite different no matter whether the heteroepitaxial growth phenomenon was reported or not.

In the case for cold spraying pure ceramic, a brittle ceramic would not go through plastic deformation but instead break. Several studies have shown the ability to fabricate a pure ceramic coating such as TiO_2 by cold spray process [83,100-101]. The objective of this chapter to investigate the interfacial bonding mechanism between cold sprayed TiO_2 coating with an aluminum and copper substrate in term of substrate properties; surface roughness, hardness, oxide thickness and oxide composition.

3.2 Preliminary study of substrate and titanium dioxide coating characterization on room temperature substrates

3.2.1 Substrate hardness testing for room temperature substrates

Figure 3.1 shows the substrate hardness of AA1050, C1020, SS400 and SUS304. AA1050 had the lowest substrate hardness at 45.36 Hv, followed by 103.2Hv for C1020 and for both hard steel, SS 400 was 175.0 Hv and SUS304 was 345.9 Hv. 1050 aluminum is work hardened by rolling to half hard. Work hardening involves modification of the structure due to plastic deformation. It increases the mechanical resistance and hardness but decreases ductility [119].

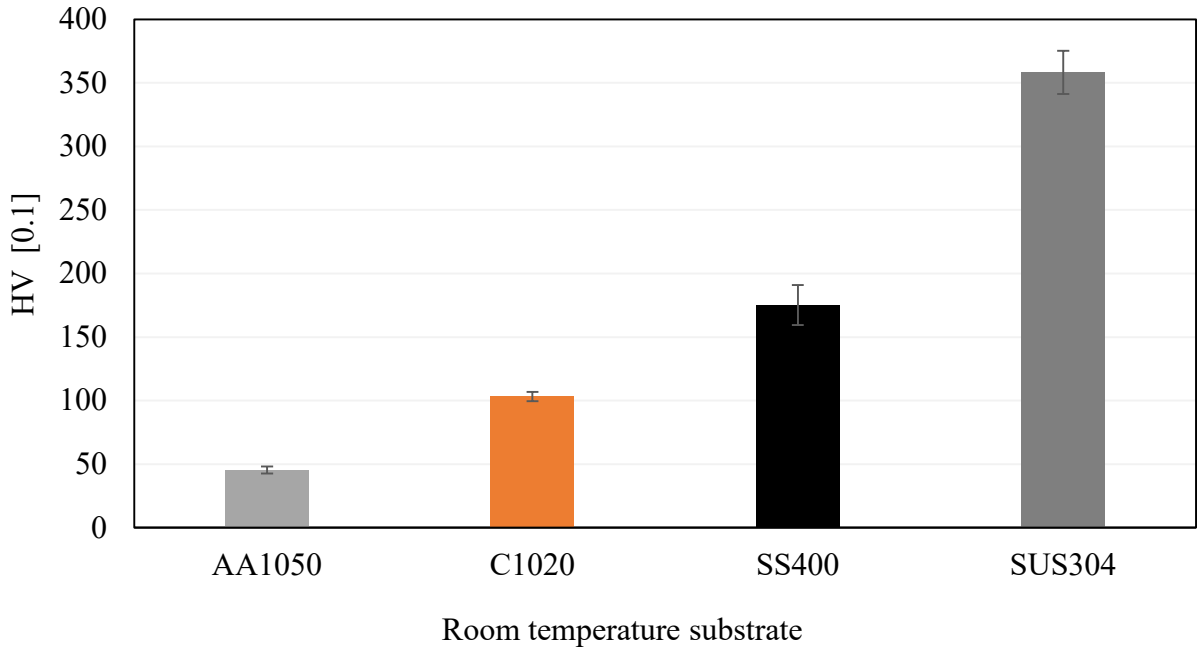

Figure 3.1: Room temperature substrate hardness for different type of materials.

3.2.2 Adhesion strength testing on room temperature substrates

Figure 3.2 shows the coating adhesion strength on different types of substrate. This figure showed highest coating adhesion strength is 3.88 MPa on pure aluminum and lowest is 0.36 MPa on stainless steel. Correlation between Figure 3.1 and coating adhesion strength indicate that, softer substrate gives highest coating adhesion strength at room temperature conditions. Therefore, we proceed to do annealing on substrates to change substrate property in each material and study the relationship with coating adhesion strength.

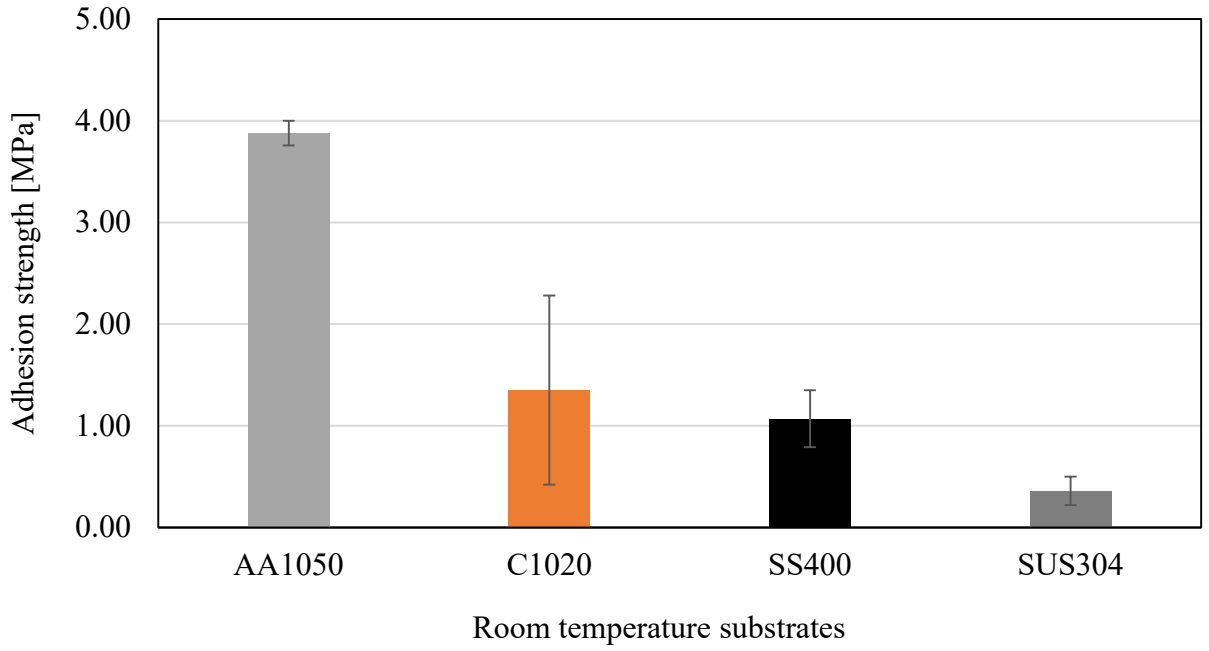

Figure 3.2: Coating adhesion strength on different types of substrate materials.

3.3 Substrate and titanium dioxide coating characterization on annealed substrates

3.3.1 Adhesion strength testing and fracture surface analysis on annealed soft metals substrate

Figure 3.3 shows the adhesion strength of the cold-sprayed TiO_2 coating on pure aluminum (AA 1050) and pure copper (C1020). The soft-annealed substrates showed a decreased trend of the adhesion strength cold-sprayed TiO_2 coatings as the annealed substrate temperature was increased from room temperature to 400°C, 3.88 to 2.05 MPa for AA1050 and 1.35 to 0.49 MPa (300ºC) for C1020. The coatings sprayed upon the pure copper substrate at 400°C; in the course of the specimen preparation automatically peeled off. Consequently, no coating succeeded at this temperature.

A recent study by Winnicki et al. cold sprayed pure amorphous and anatase TiO_2 powder on the ABS substrate with varying gas temperatures of 200 and 300ºC. The bond strength of the coating was tested using a tensile strength test machine and the highest value was 2 MPa for TiO_2 at 200 and 300ºC gas temperature [151].

Figure 3.4 and 3.5 shows the image of the fractured surface of substrate and TiO_2 coating after tensile strength test was conducted. This image confirms that the fracture was interfacial fracture of substrate and coating, thus, proving that strong cohesive bond between TiO_2 particles had been achieved during the coating formation process.

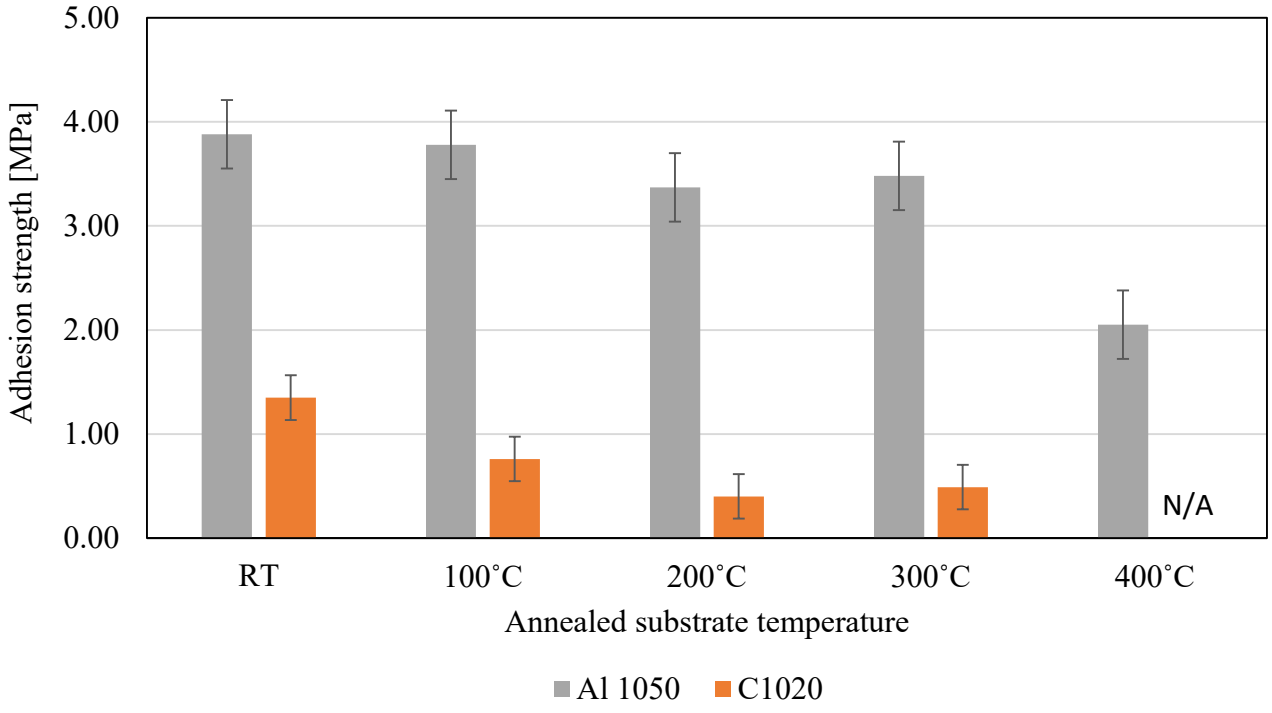

Figure 3.3: Adhesion strength of the TiO_2 coating on AA1050 and C1020 from room temperature to 400˚C annealed.

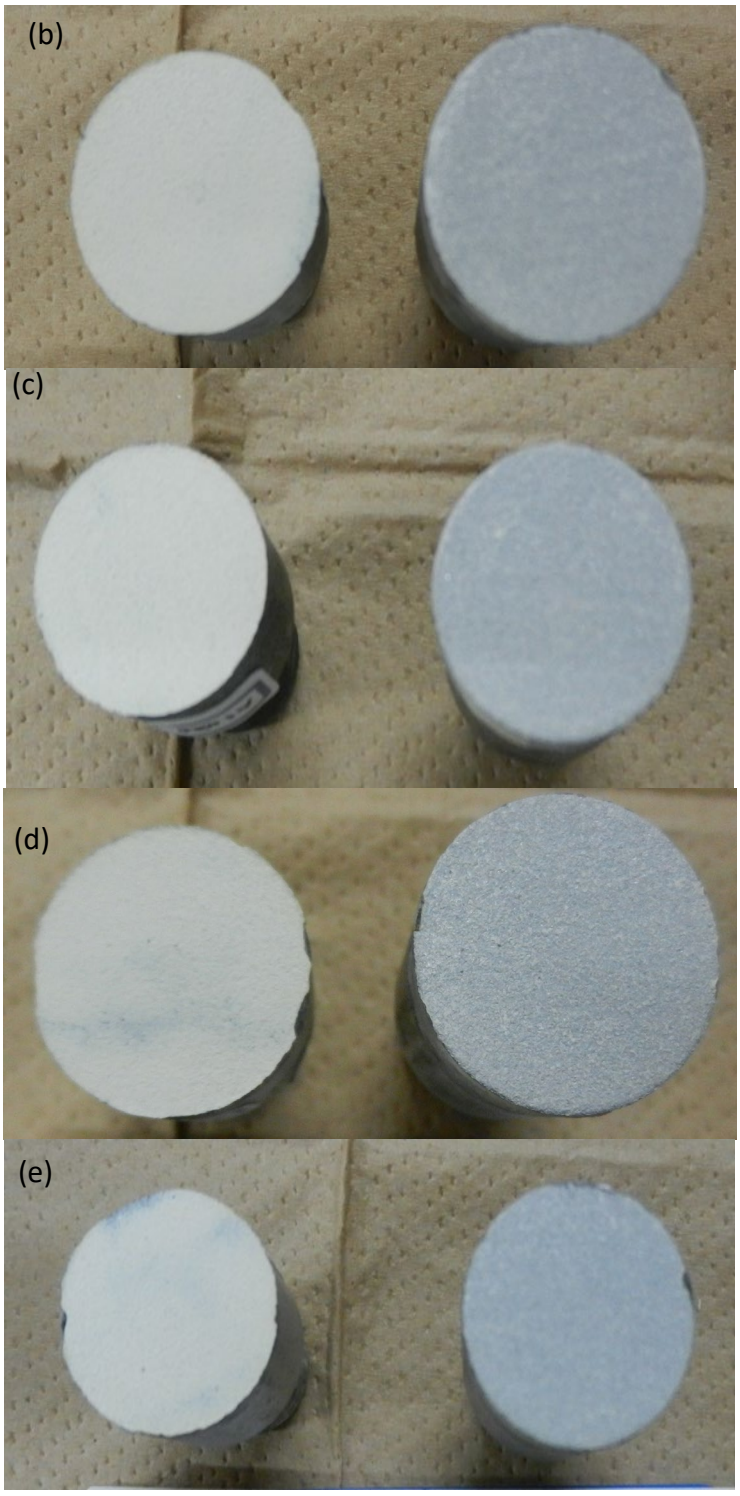

Figure 3.4: Fracture surface substrate and TiO_2 coating after tensile strength testing on AA1050. (a) Room temperature (b) annealed at 100°C (c) annealed at 200°C (d) annealed at 300°C and (e) annealed at 400°C.

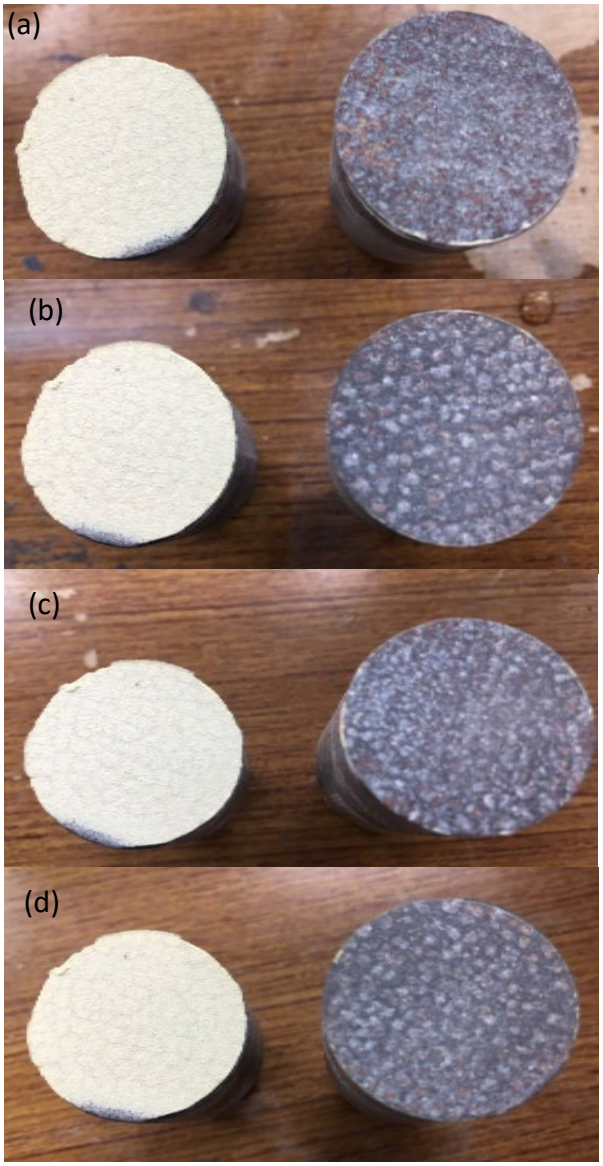

Figure 3.5: Fracture surface substrate and TiO_2 coating after tensile strength testing on C1020. (a) Room temperature (b) annealed at 100°C (c) annealed at 200°C and (d) annealed at 300°C.

EDS mappings as illustrated in Figure 3.6 showed that elements present are aluminum (Al), titanium (Ti), oxygen (O) and carbon (C) for fractured coating of titanium dioxide on annealed aluminum substrate. This EDS mapping showed that large part of aluminum substrate is embedded on TiO_2 coating.

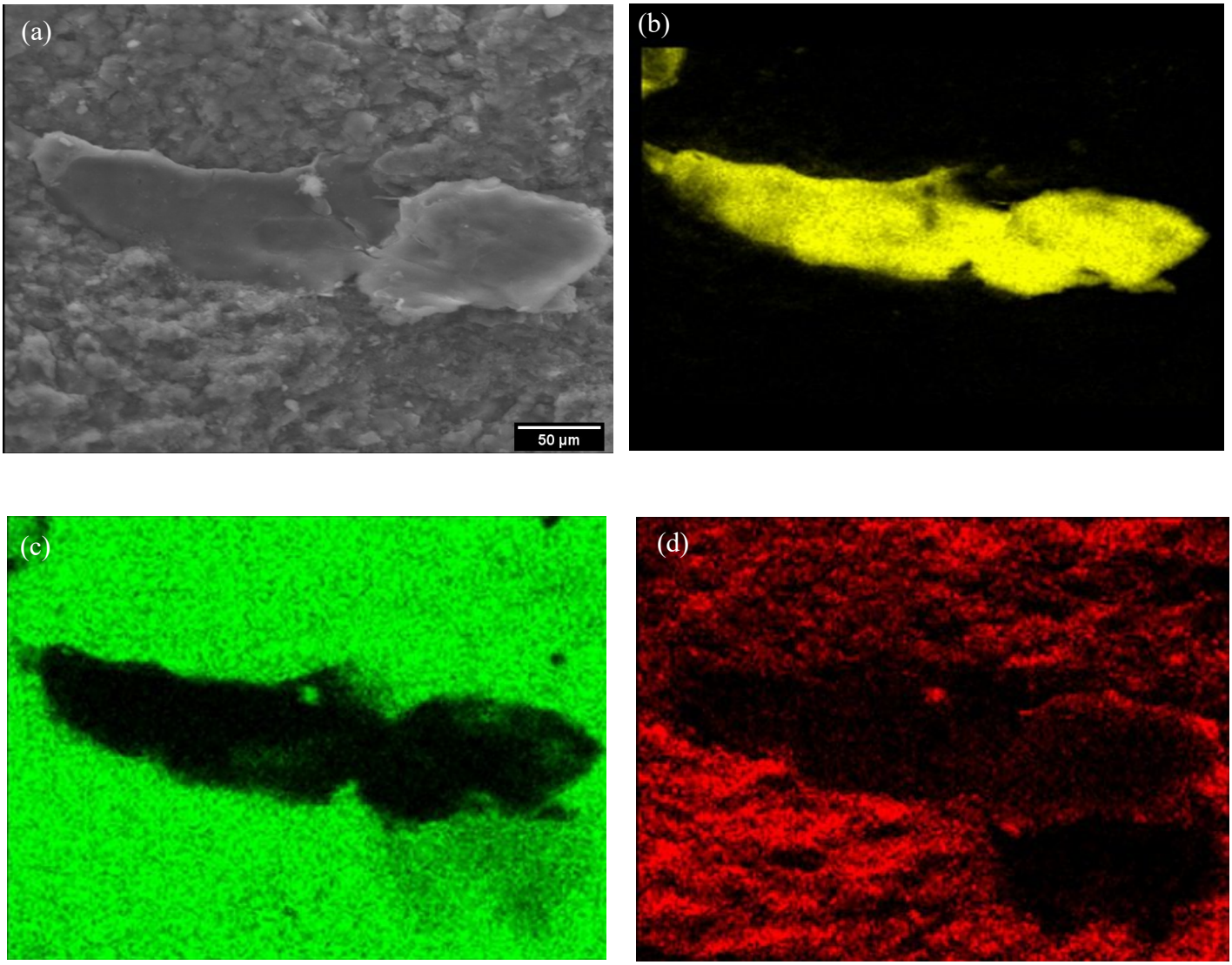

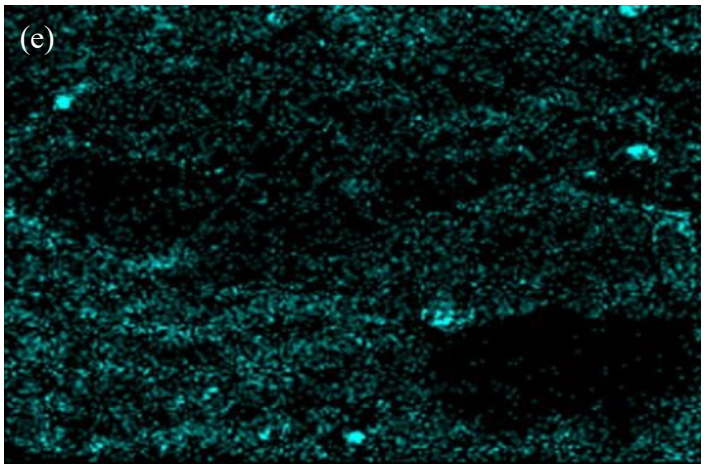

Figure 3.6: EDX on fracture coating (a) SEM image (b) Aluminum (c) Titanium (d) Oxygen (e) Carbon.

EDS mappings as illustrated in Figure 3.7 showed that elements present are copper (Cu), titanium (Ti), oxygen (O) and carbon (C) for fractured coating of titanium dioxide on annealed copper substrate. This EDS mapping showed that large part of copper substrate is embedded on TiO_2 coating.

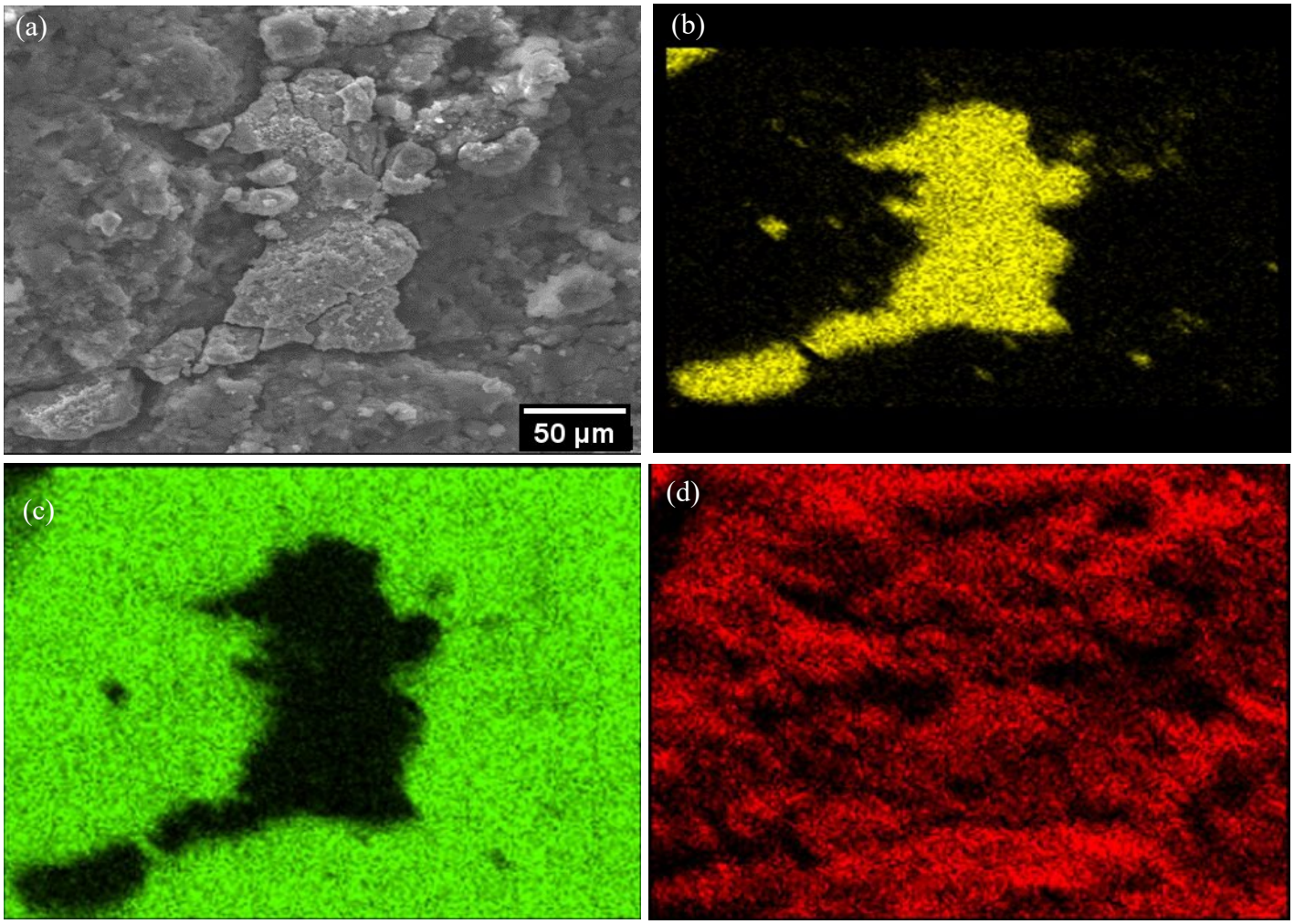

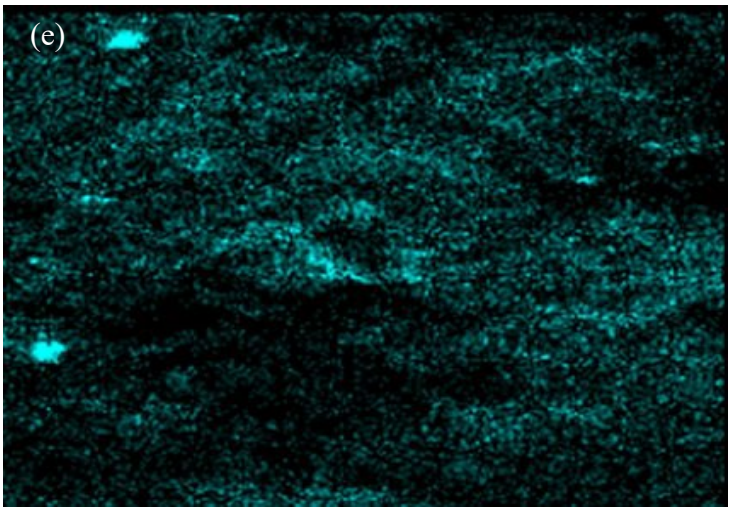

Figure 3.7: EDX on fracture coating (a) SEM image (b) Copper (c) Titanium (d) Oxygen (e) Carbon.

3.3.2 SEM microstructure cross-section on annealed substrates

Figure 3.8 and 3.9 shows the TiO_2 coating cross-sectional area on AA1050 for room temperature and 400ºC annealed substrates. Substrates at room temperature and 400°C were chosen for observation to clarify the interface adhesion between substrates which yielded the highest and lowest adhesion strength. Figure 3.8 **(**a) show that the TiO_2 coating adhered well on AA1050 room temperature but for 400ºC annealed, where crack is present between TiO_2 coating and substrate as indicated in Figure 3.8 **(**b). This conditions also occurs on C1020. Meanwhile, the interface area of substrates at 400℃ shows visibly cracks occur on AA1050 and C1020. This shows that the 400℃ annealing process has major impact on the interface adhesion between substrate and TiO_2 coating. To further understand this situation, annealed soft metal substrates properties will be further investigated.

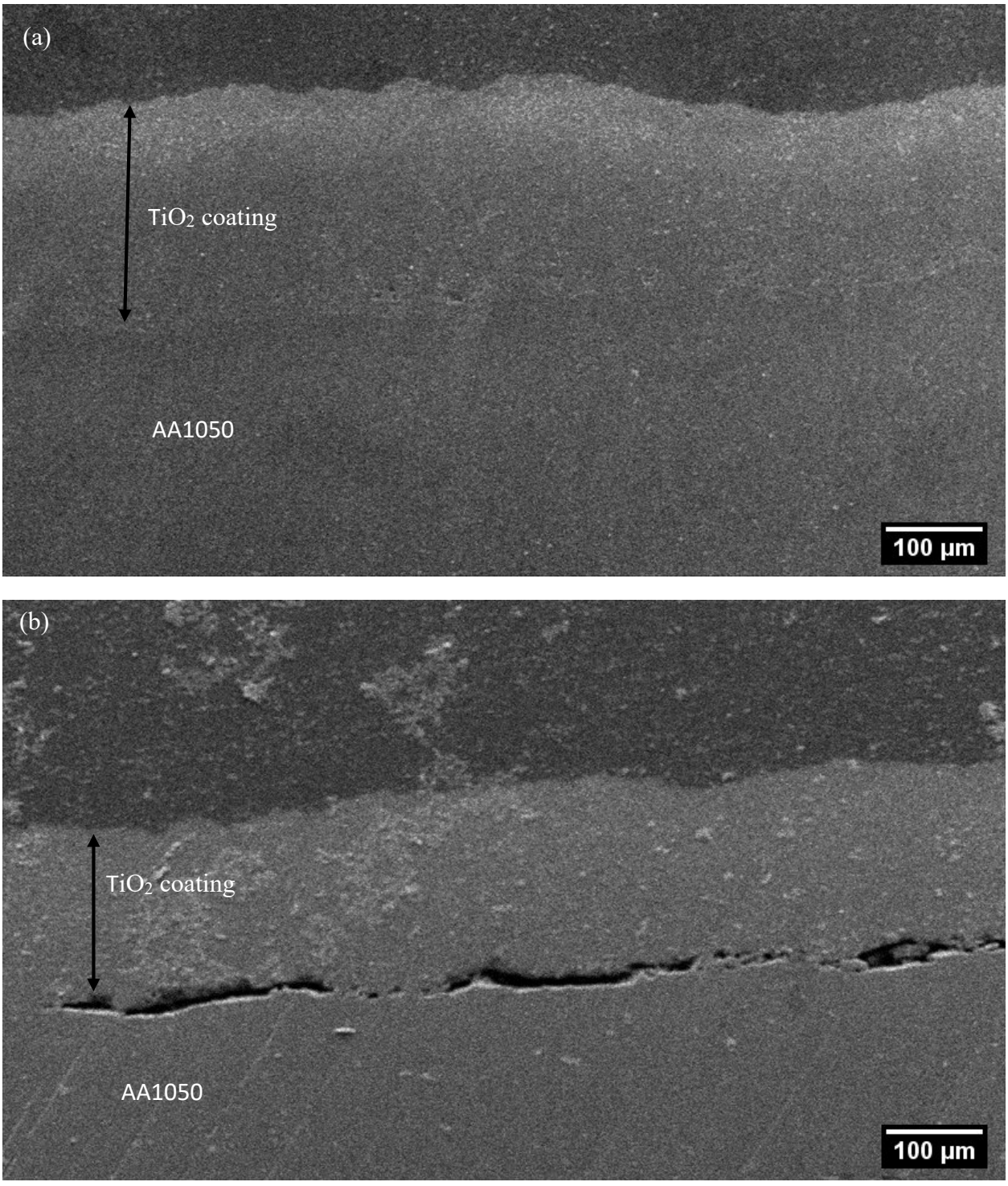

Figure 3.8: Cross-section microstructure of TiO_2 coatings on AA1050. (a) Room temperature and (b) 400°C annealed.

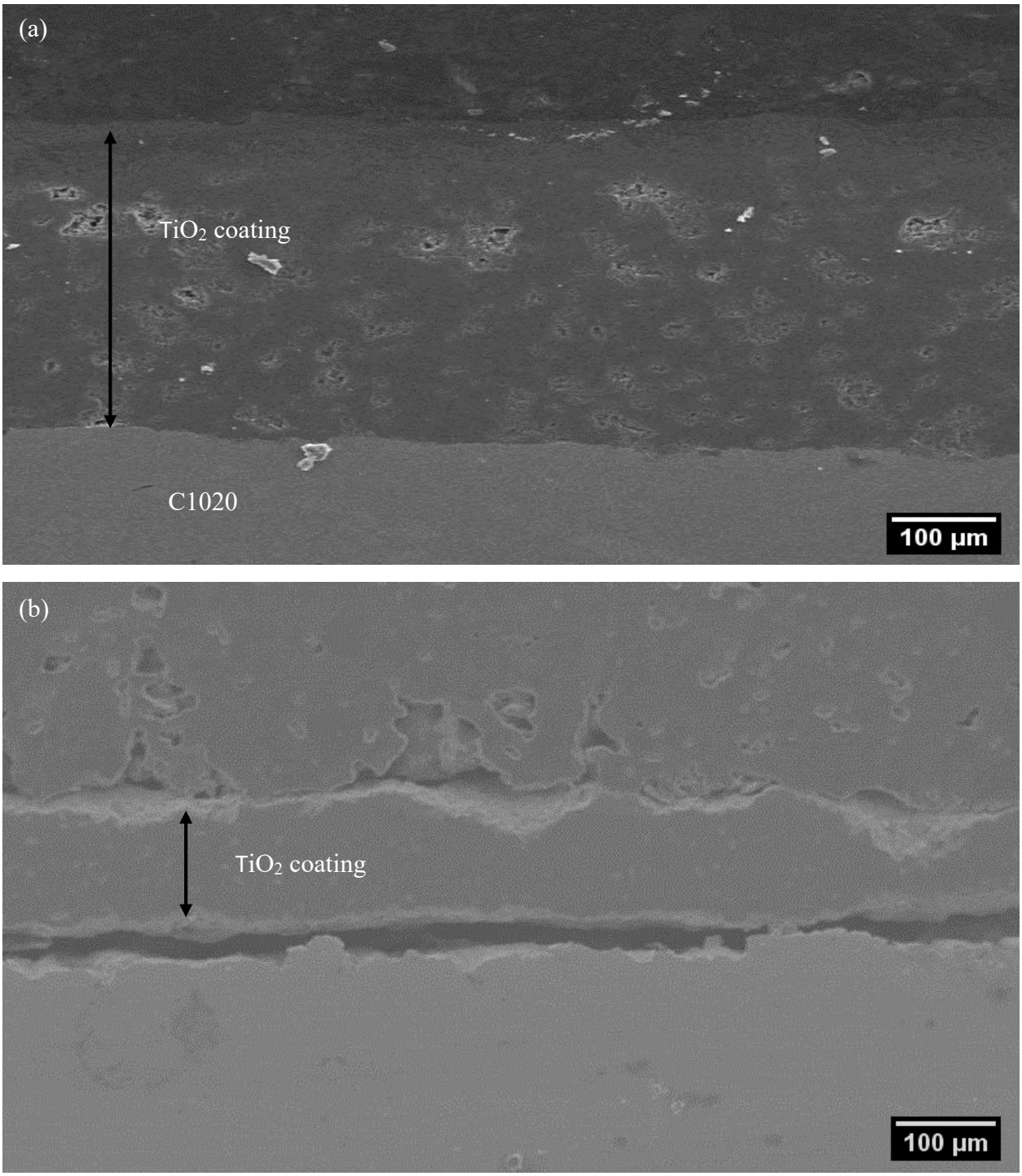

Figure 3.9: Cross-section microstructure of TiO_2 coatings on C1020. (a) Room temperature and (b) 400°C annealed.

3.3.3 Substrate surface roughness testing on annealed substrates

The annealing process made an oxide growth on the surface of the substrate. In order to understand the influence of oxide surface roughness, atomic force microscopy, AFM result of oxide surface roughness for room temperature and 400°C annealed AA1050 and C1020 shown in Figures 3.10 3.11, 3.12 and 3.13 below. The result shown an increase of oxide surface roughness from 20.56nm (RT) to 121.9nm (400˚C) as indicate by Table 3.1 and 3.2, respectively for AA1050, 13.89nm (RT) to 45.02nm (400˚C) as shows by Table 3.3 and 3.4, respectively for C1020. This clearly shows that oxide surface roughness has no significant effect on coating adhesion strength on annealed soft metal substrate. When our feedstock powder, agglomerated TiO_2 powder containing pure anatase crystalline structure with an average particle size of about 7.55 μm, is impacted on annealed soft metal substrates covered with oxide surface roughness in nanoscale, it has negligible surface roughness impact on coating deposition. Richer et al reported that the effect of using different grit sizes for the substrate preparation is limited to small changes in the deposition efficiency of only the first few layers of deposited material. The substrate surface roughness has no significant effect on the macrostructure and microstructure of the coating [152].

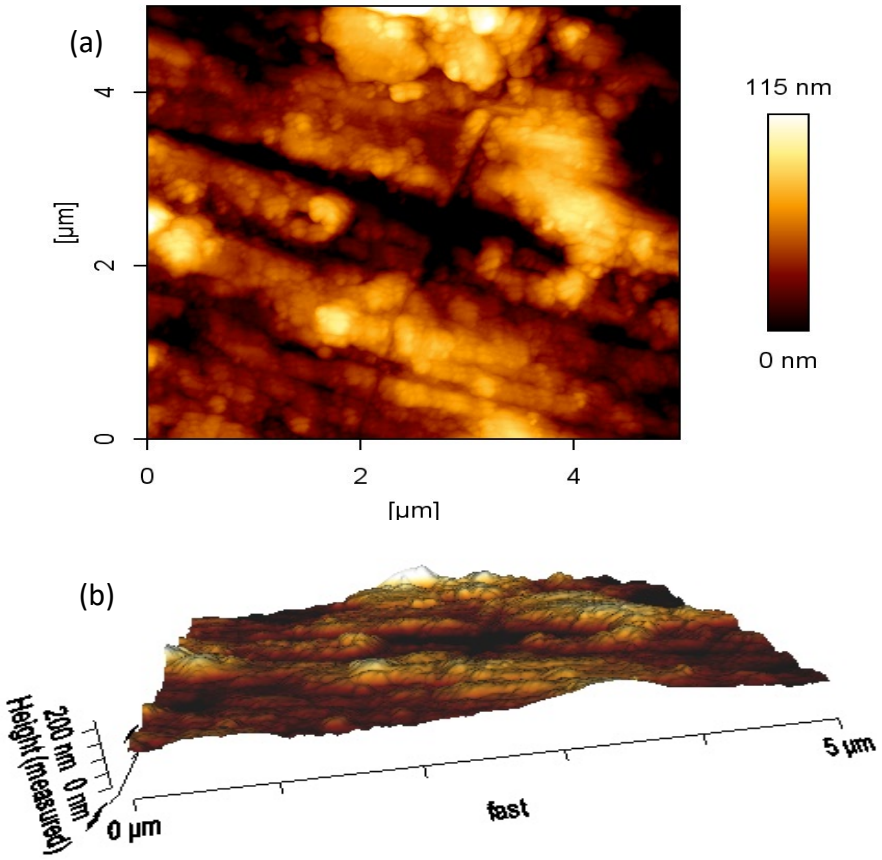

Figure 3.10: Oxide surface roughness for room temperature pure aluminum (a) 2D (b) 3D.

Table 3.1: Oxide surface roughness analysis for room temperature pure aluminum.

Physical size (µm)	5.000 x 5.000
Average value	-6.245×10^{-17}
Average roughness Ra (nm)	20.56
RMS roughness Rq (nm)	26.12

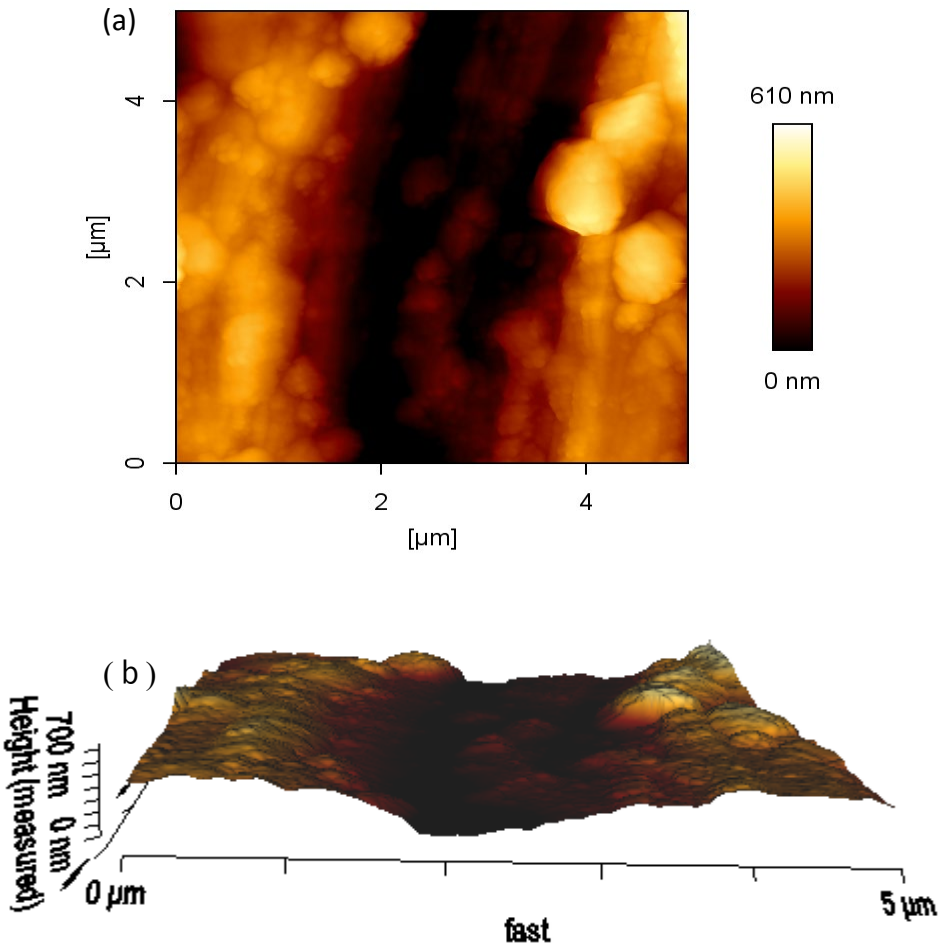

Figure 3.11: Oxide surface roughness for 400°C annealed pure aluminum (a) 2D (b) 3D.

Table 3.2: Oxide surface roughness analysis for 400°C annealed pure aluminum.

Physical size (µm)	5.000 x 5.000
Average value	-1.561×10^{-16}
Average roughness Ra (nm)	121.9
RMS roughness Rq (nm)	138.7

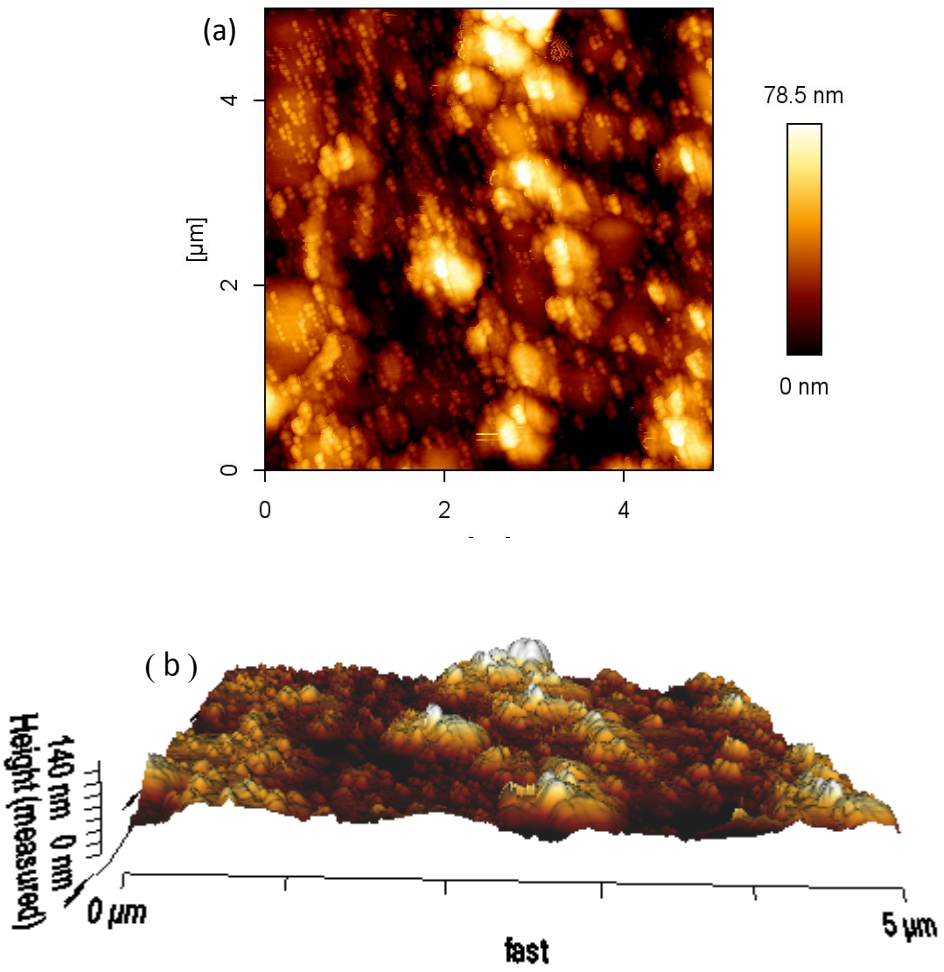

Figure 3.12: Oxide surface roughness for room temperature pure copper (a) 2D (b) 3D.

Table 3.3: Oxide surface roughness analysis for room temperature pure copper.

Physical size (µm)	5.000 x 5.000
Average value	-5.378×10^{-17}
Average roughness Ra (nm)	13.89
RMS roughness Rq (nm)	17.85

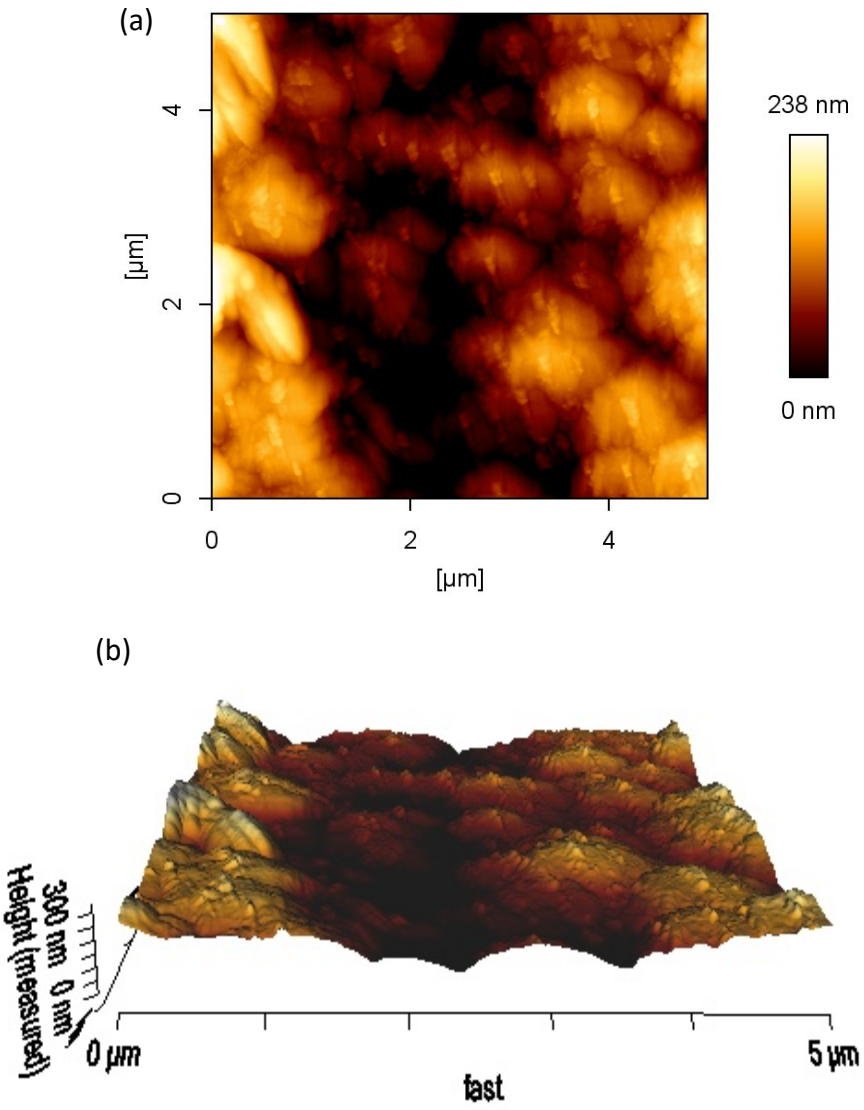

Figure 3.13: Oxide surface roughness for 400°C annealed pure copper (a) 2D (b) 3D.

Table 3.4: Oxide surface roughness analysis for 400°C annealed pure copper.

Physical size (µm)	5.000 x 5.000
Average value	-1.561×10^{-16}
Average roughness Ra (nm)	45.02
RMS roughness Rq (nm)	54.03

3.3.4 Substrate hardness testing on annealed substrates

Figure 3.14 shows annealed substrate hardness of AA1050 and C1020 from room temperature to 400˚C. AA1050 also shown a decreased trend from 45.36 Hv (RT) to 27.7 Hv (400˚C) and 103.2 Hv (RT) to 45.96 Hv (400˚C) for C1020. The optimal recrystallization regime for AA1050 is given by a temperature between 390°C and 410°C and the holding time at this temperature range is 15-20 min [153]. AA1050 experienced recrystallization process at starting at 390 to 400˚C and slow cooling in the electric furnace with air as a medium; allow the grains to growth larger and reduce the substrate hardness and become softer. The kinetic evolution of the microhardness of the pure copper obtained after isothermal recrystallization treatments carried out at 250, 300 and 380°C. During the incubation time as light decrease of the microhardness is observed due to the recovery process. Then, a large drop from Hv= 100 (at the initial cold rolled state) to Hv= 50 (at the completely recrystallized state) indicates the 399ºC occurrences of the recrystallization [153]. Our annealed substrate hardness result are good agreement with research report above.

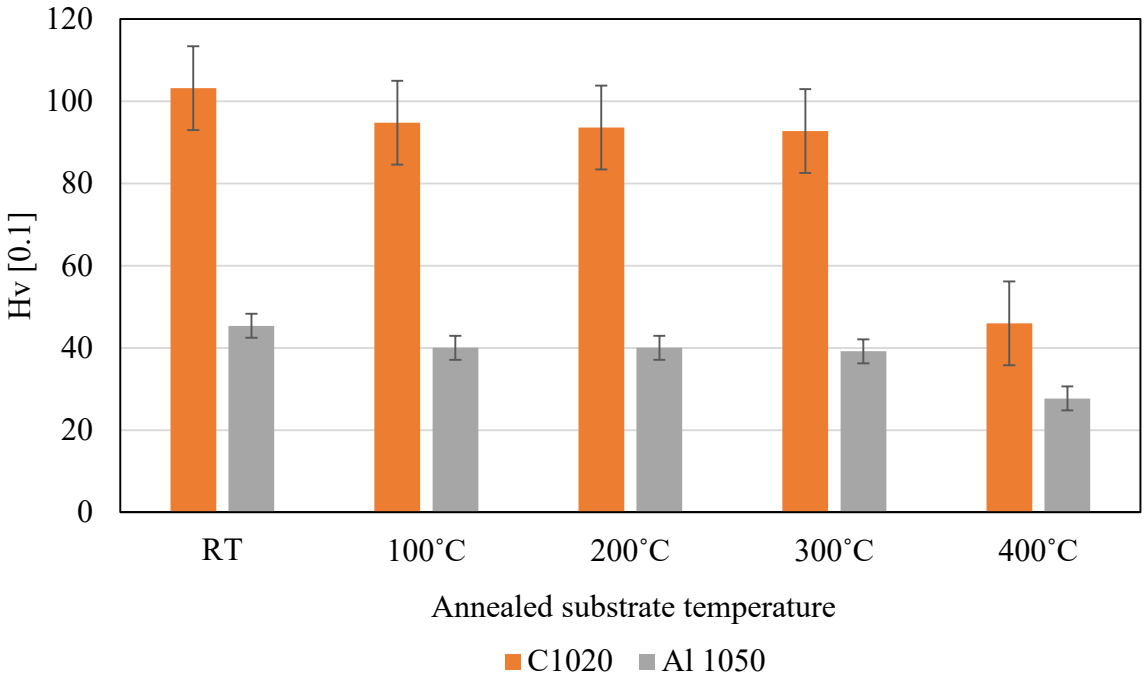

Figure 3.14: Annealed substrate hardness of AA1050 and C1020 from room temperature to 400˚C.

3.3.5 Substrate depth profile of oxide layer by XPS on annealed substrates

The results of the depth analysis of room temperature substrate and 400˚C annealed by X-ray photoelectron spectroscopy for AA1050 and C1020 substrates is shows accordingly in figure 3.15 and 3.16, respectively. The composition as a function of depth can be analyzed by in-situ argon ion beam sputtering, found on most surface analytical equipment. In depth profiling measurement with XPS, the sputtering etching rate of SiO_2 used to estimate a sputtered depth from an elemental depth profile.

Figure 3.15 (a) to (e) and figure 3.16 (a) to (e), shown that the atomic composition of oxygen in the deepest part of the oxide layer increases as the annealing substrate temperature increases from room temperature to 400˚C. This indicate that the oxide layer of pure aluminum and pure copper grows thicker as the annealing substrate temperature is increased.

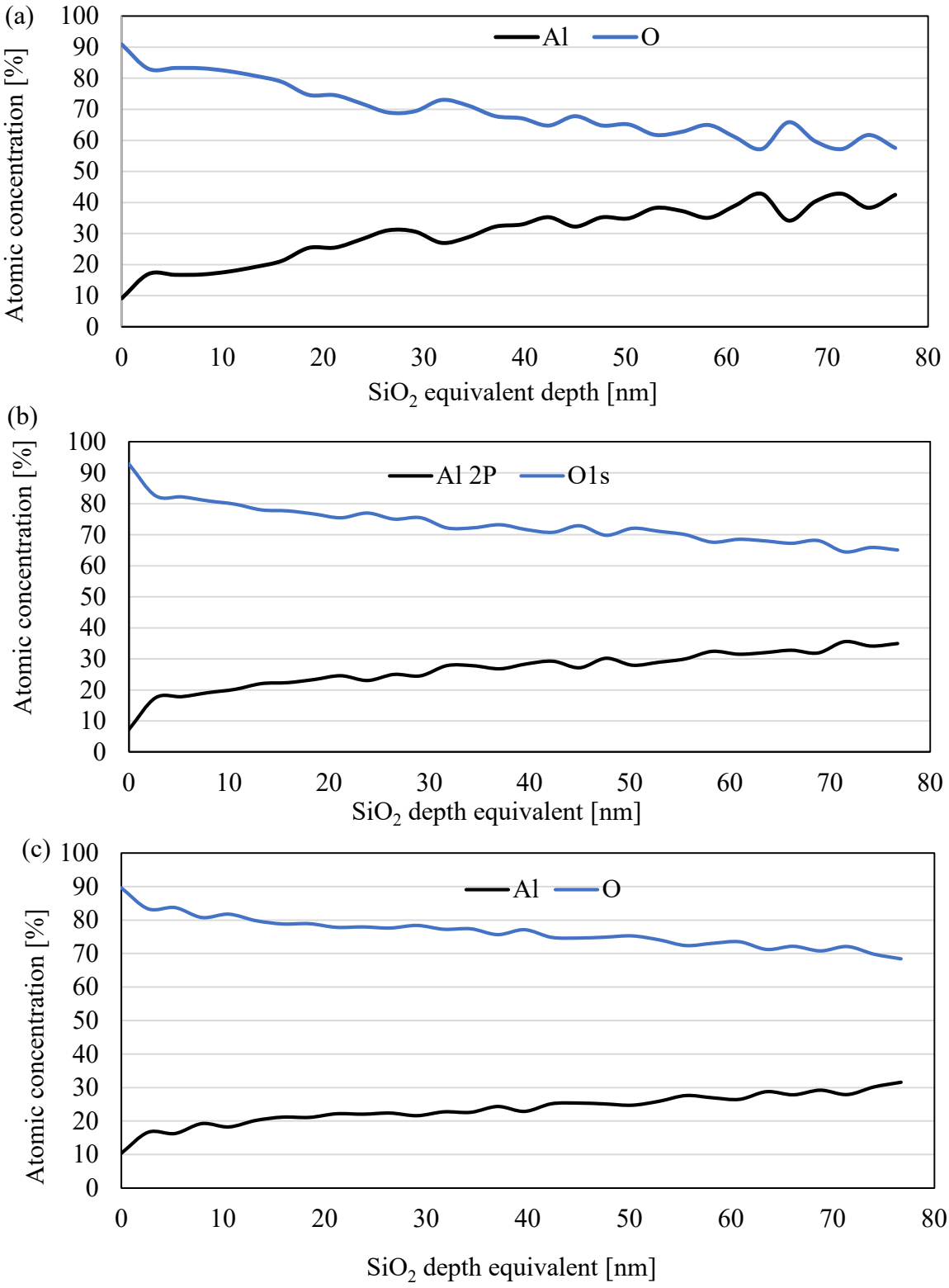

Figure 3.15: Depth profile analysis of AA1050 (a) room temperature (b) 100˚C annealed (c) 200˚C annealed.

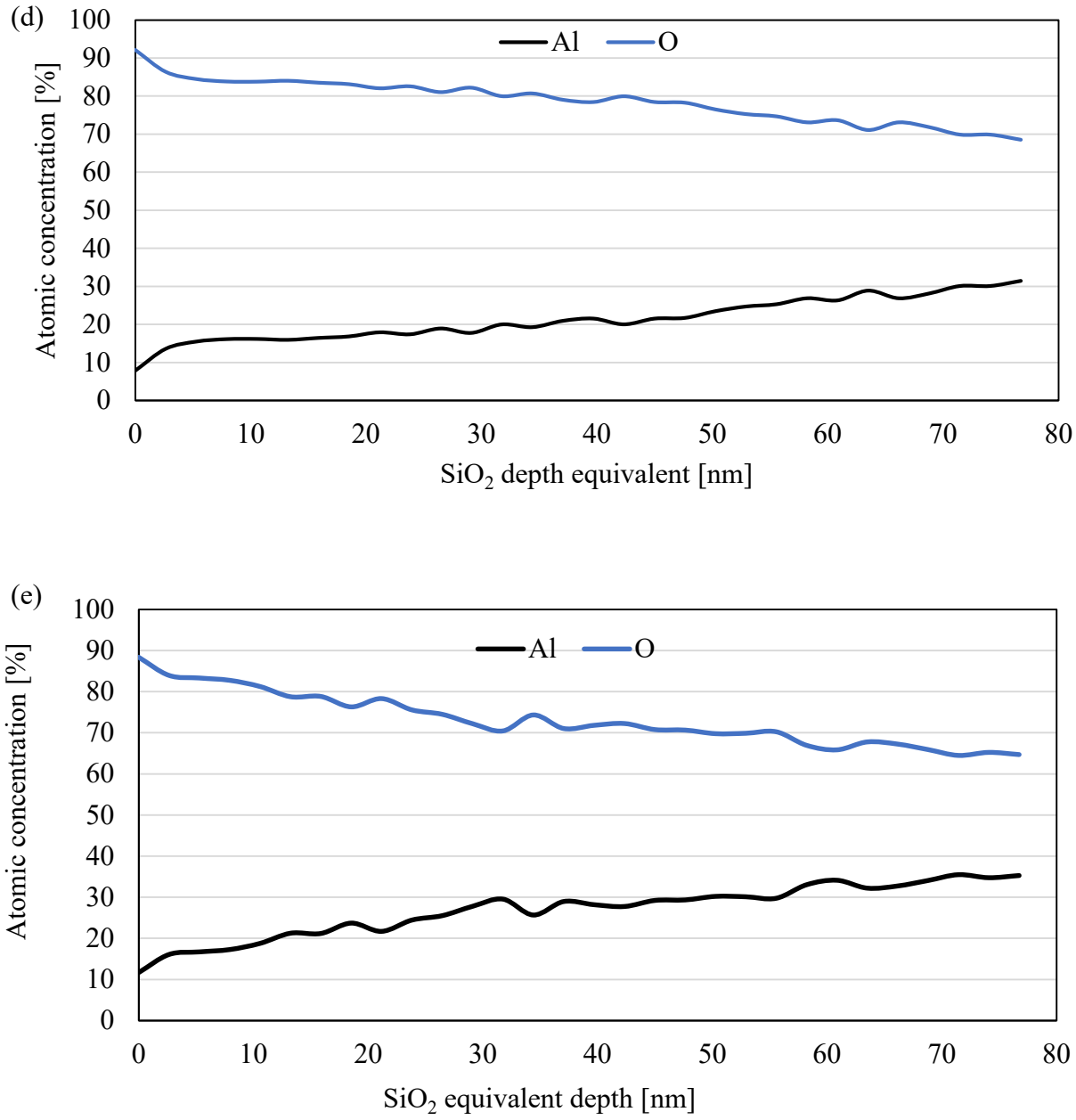

Figure 3.15: Depth profile analysis of AA1050 (d) 300˚C annealed and (e) 400˚C annealed.

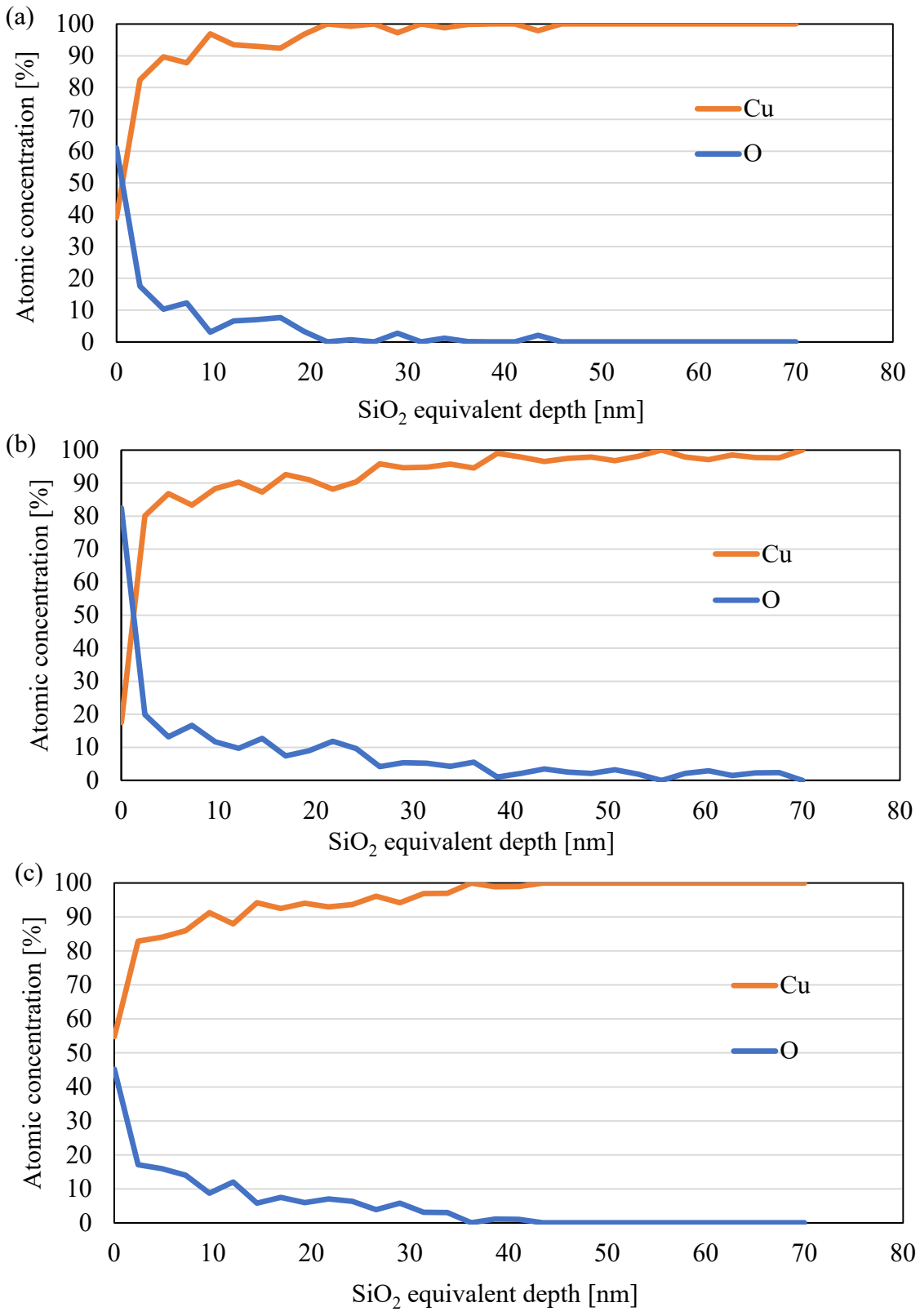

Figure 3.16: Depth profile analysis of C1020 (a) room temperature (b) 100˚C annealed (c) 200˚C annealed.

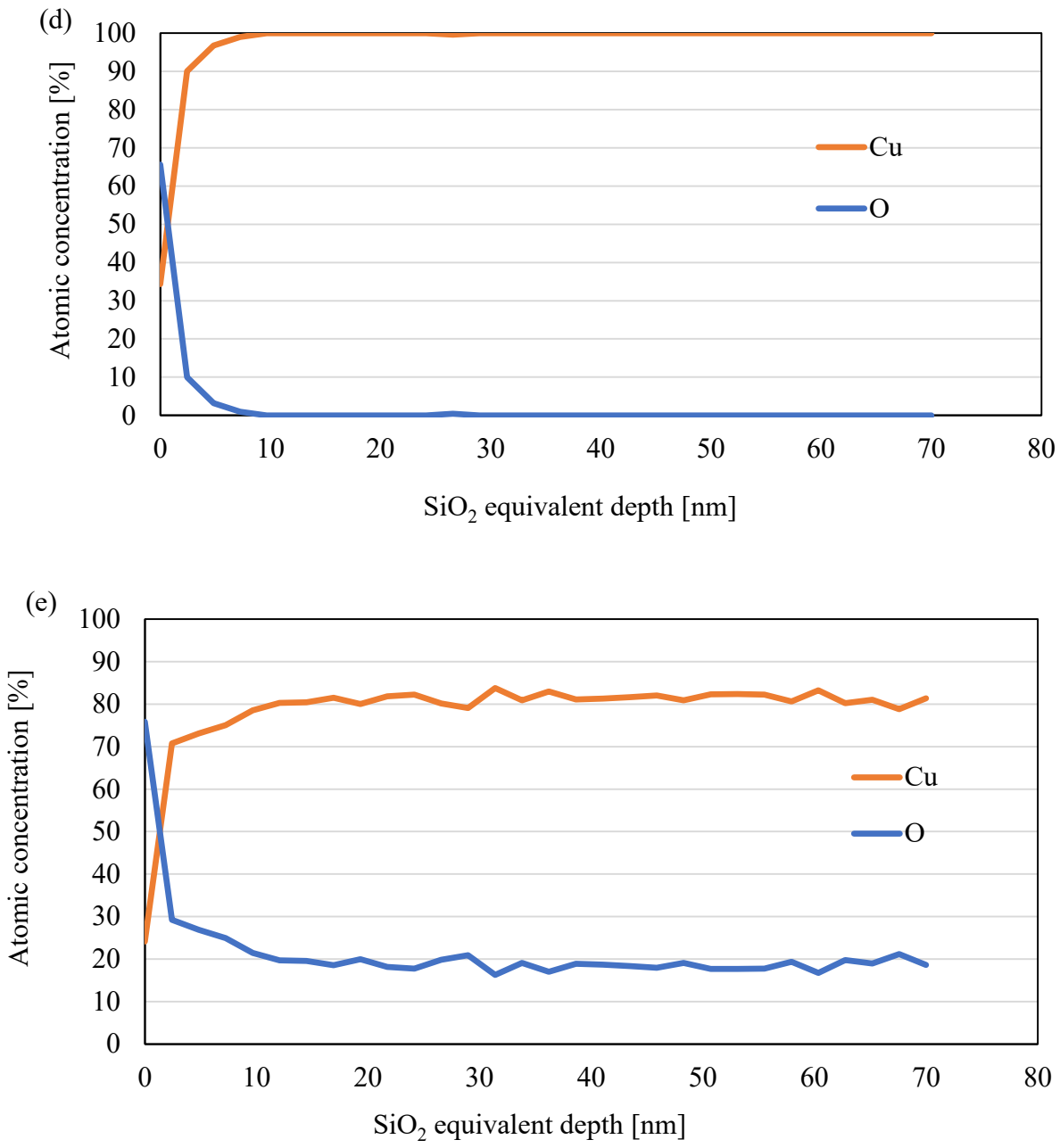

Figure 3.16: Depth profile analysis of C1020 (d) 300˚C annealed and (e) 400˚C annealed.

3.3.6 Substrate chemical composition of oxide layer by XPS

X-Ray photoelectron spectroscopy (XPS) is a versatile surface analysis technique that can be used for compositional and chemical state analysis. Outermost surface oxide composition changes are plotted in Figure 3.17 (a) to (c) and 3.18 (a) to (c) for AA1050 and C1020, respectively. In this experiment, total of 30 cycles is involved and to plot binding energy graph versus intensity to study the chemical state changes, outermost surface referring to the 1st cycle data, mid-layer referring to the 15th cycle data and deepest part referring to the 30th cycle data for each substrate conditions as indicate by figure 3.17 (b) and (c) for AA1050 and figure 3.18 (c) for C1020.

The peak position of the aluminum oxide layer, Al_2O_3 on room temperature, 100 and 200ºC annealed AA1050 indicate at 74.8 eV [155] shown by Figure 13.7 (a). The peak position of the O1s shown by Figure 13.7 (b) also support the present of aluminum oxide layer, Al_2O_3 on outermost surface at 531.3 eV [155] and slightly presented of aluminum in hydroxide on mid-layer and deepest part given by 532.4 eV [155], supported that substrate mostly Al metal state for mid layer and deepest part at room temperature substrate. Meanwhile, at the annealing temperature of 400°C for AA 1050 substrate, figure 13.7 (c**)**, the peak position of aluminum oxide layer, which was at approximately 74.8 eV [155], was detected at the outermost surface, mid-layer, and deepest part of the substrates. This indicate AA 1050 substrate experienced chemical composition changes from Al metal state in room temperature substrate to aluminum in hydroxide condition in 400°C annealed.

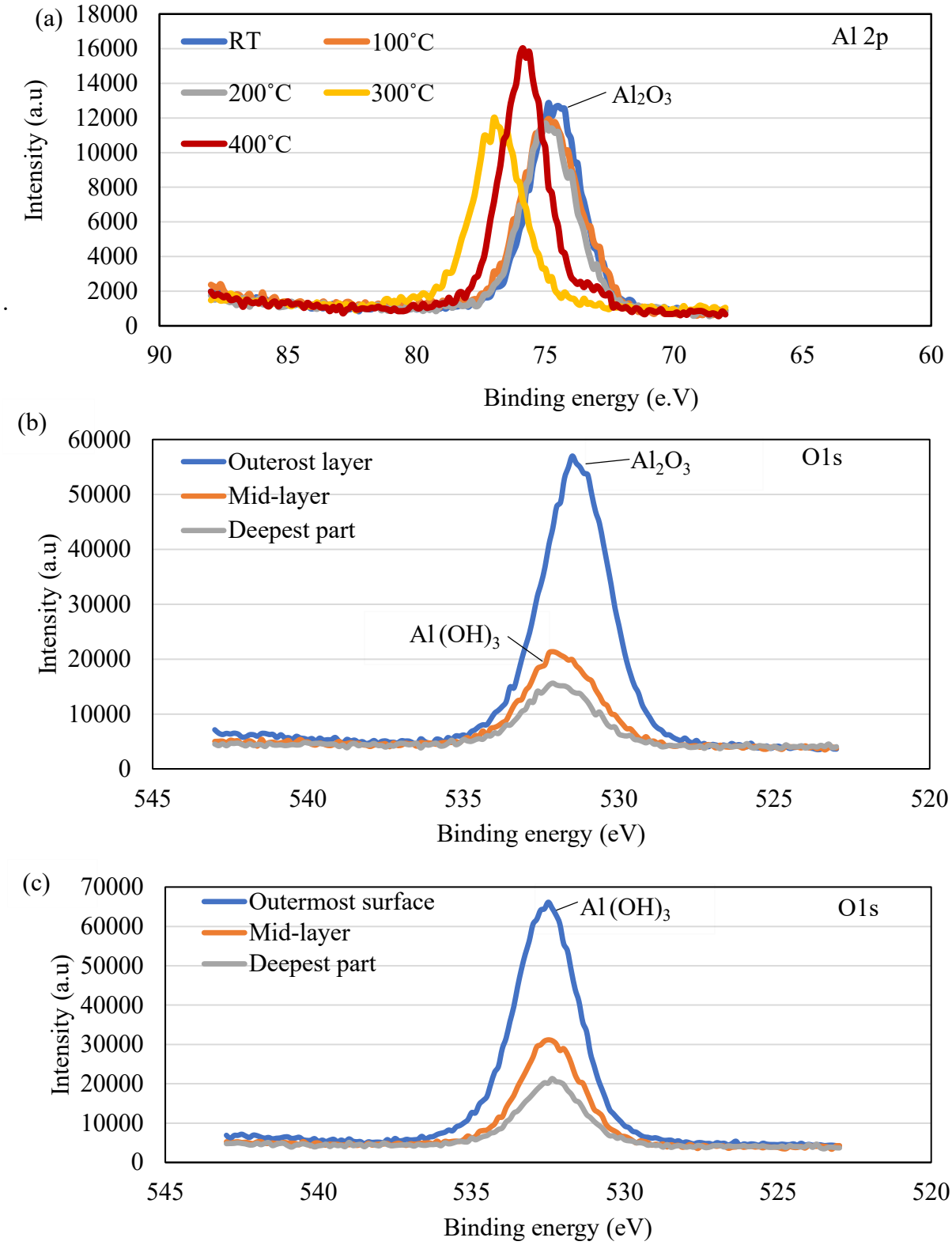

Figure 3.17: XPS spectra for (a) Al 2p AA1050 (b) O1s room temperature AA1050 (c) O1s 400ºC annealed AA1050.

Figure 3.18 (a) show XPS spectra of Cu $2p_{3/2}$ for C1020 for room temperature substrate to 400˚C annealed. The Cu $2P_{3/2}$ atomic orbital satellite peak was used to evaluate the chemical state for copper. The peak position of the copper metal for pure copper at approximately 932.5 eV [156] was prominently present in the outermost surface in the room-temperature substrate and all annealing substrate temperature. The O1s peaks shown in figure 3.18 (b) are 530.3,531.3 eV indicated the presence of Cu_2O and CuO and hydroxide species physically adsorbed on the Cu surface [157]. The peak at 529.3eV was the CuO sub-peak, when the Cu substrate contained two oxidized states, each Cu peak and corresponding O peak were detected. Figure 3.17 (c) to confirm the oxide present and the shake-up satellite peak position of CuO [157], which was at approximately 944 to 940 eV, was detected at the outermost surface, mid-layer, and deepest part of the substrates. This indicate C1020 experienced chemical composition changes from Cu metal state in room temperature substrate to cupric oxide, CuO condition in 400˚C annealed.

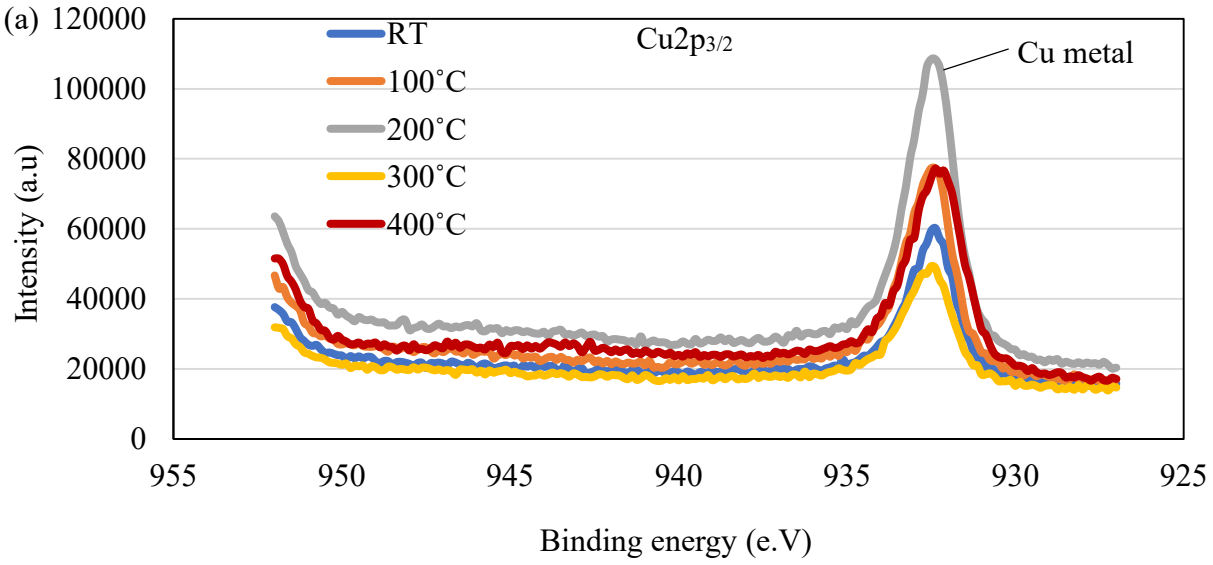

Figure 3.18: XPS spectra for: (a) $Cu2p_{3/2}$ C1020

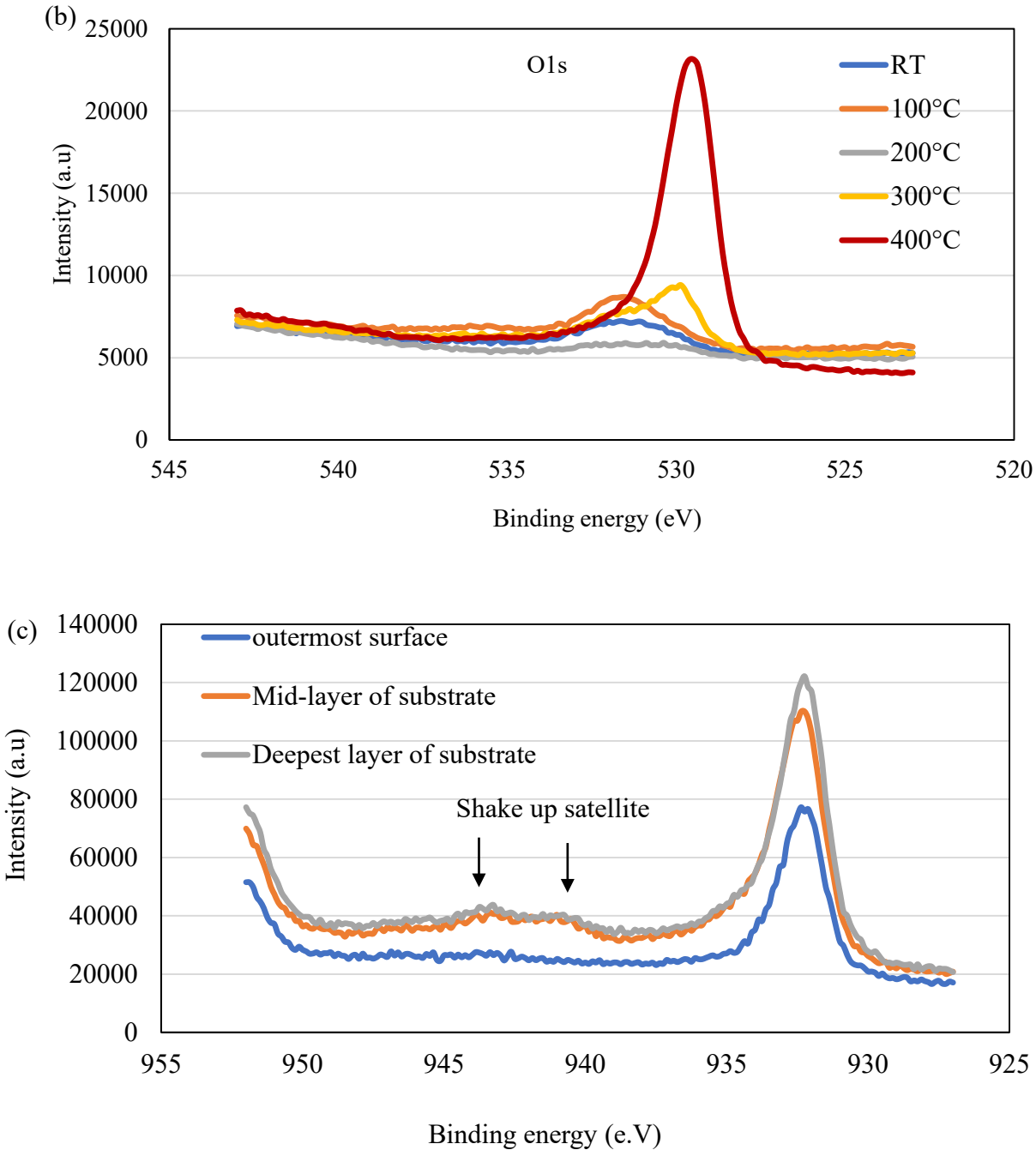

Figure 3.18: XPS spectra for: (b) O1s for C1020 (c) 400°C annealed C1020.

3.4 TiO_2 single particle deposition on annealed substrates

3.4.1 FIB splat TiO_2 particle on 400°C annealed soft metal substrates

Single particle impact morphology, which is also known as the wipe test, was conducted to study the bonding mechanism of TiO_2 powders on mirror polish of different types of substrates. Figure 3.19 (a) and (b) shown result of the TiO_2 particle impacting on 400˚C annealed AA1050 and figure 3.20 (a) and (b) for annealed C1020. Trompetter et al [158] demonstrated that for solid particles impacting on a substrate, the substrate hardness played a significant role in the as-produced solid particles. Soft substrate such as aluminium and copper, the TiO_2 particles were impacting the surface with minimal deformation, and the particles rebounded after the impact, leaving craters on the surface of the substrate [159]. Since aluminium has lower hardness in comparison with copper, the depth of the craters were deeper and experienced heavy damage as seen in the figure 3.19 (a). K.-R.Ernst et al [160] also mentioned that for soft substrate, the impact energy that was generated during the spraying process was also used for deformation of the substrate as shown by red-dotted line in figure 3.19 (b) and 3.20 (b).

The adhesion strength of the TiO_2 coating on annealed soft metals showed a decreased trend as the annealed substrate temperature is increased. This indicates that substrate deformation or mechanical anchoring is not the factors that influence the adhesion bonding of the 400˚C annealed soft metals with TiO_2 coating.

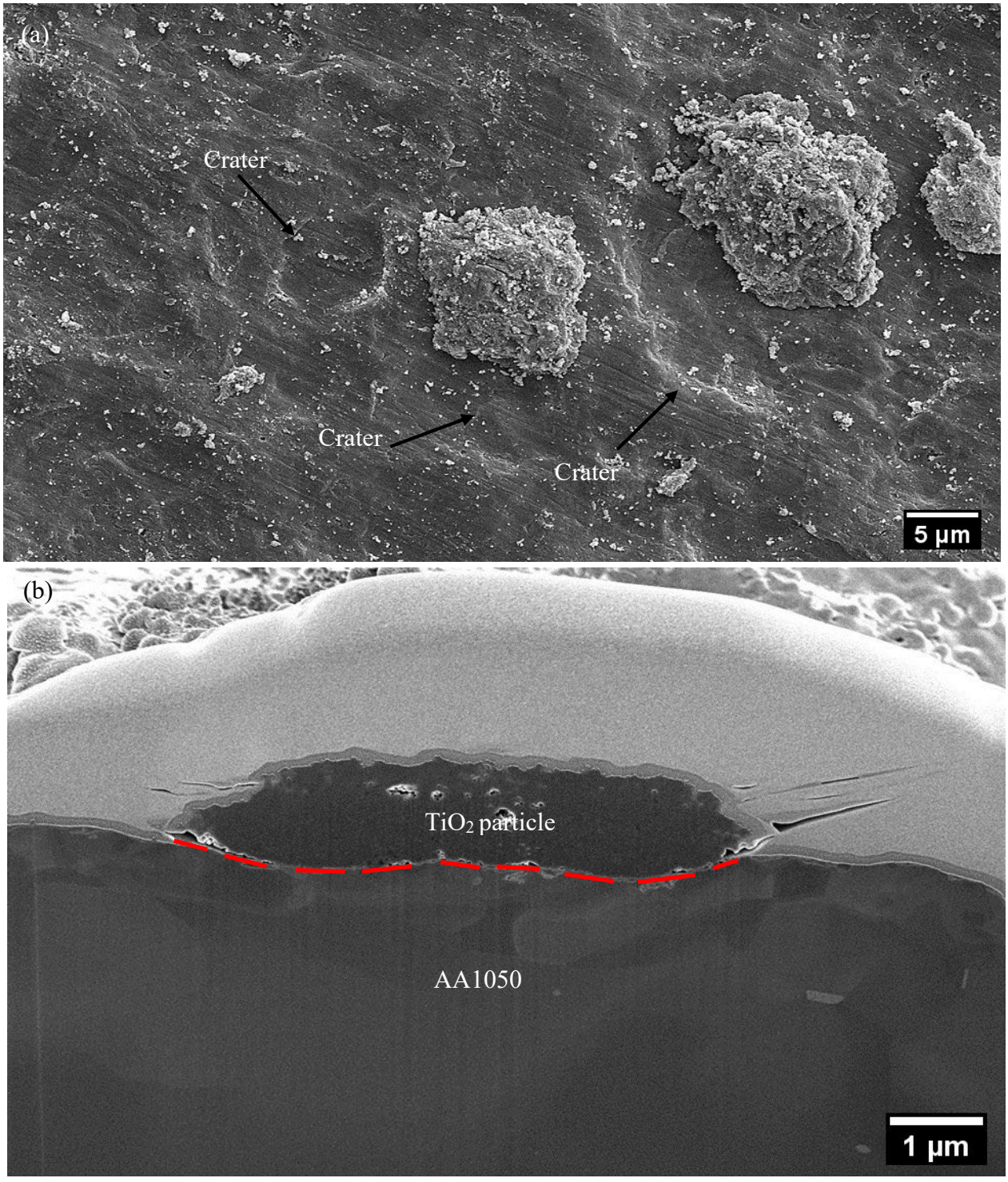

Figure 3.19: TiO_2 particle on 400˚C annealed AA1050 (a) top view (b) cross-sectional.

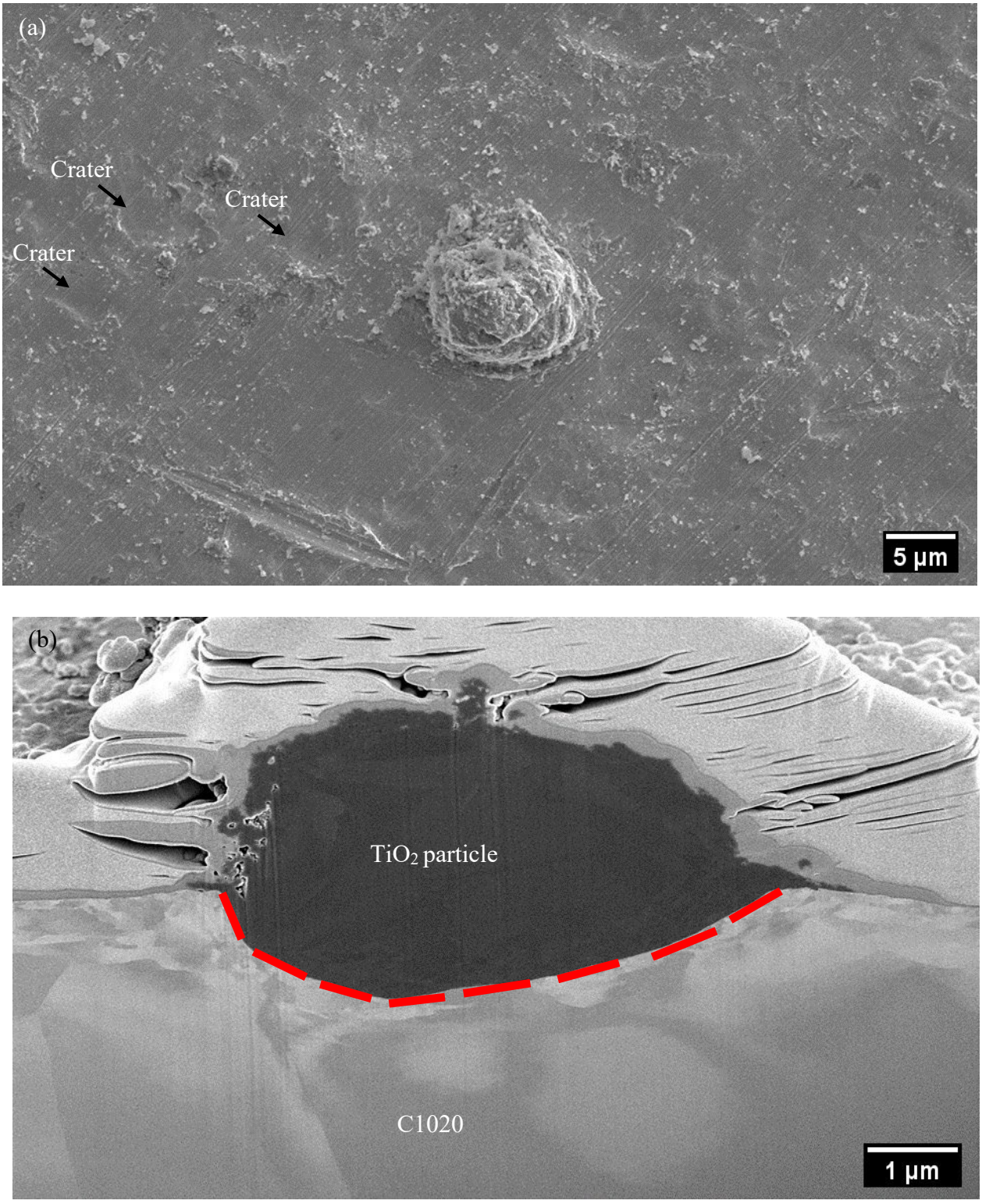

Figure 3.20: TiO_2 particle on 400˚C annealed C1020 (a) top view (b) cross-sectional.

3.4.2 TEM analysis on interface oxide layer between TiO_2 particle on 400°C soft metal substrates

Figure 3.21,3.22,3.23 and 3.24 are the STEM and TEM result at interface between single TiO_2 particle and 400˚C annealed AA1050 and C1020. Referring to FFT pattern that confirming the amorphous region occur at interlayer, it represent the existences of the remaining oxide layer with a thickness of less than 10nm for AA1050 and approximately 10 nm for C1020, after the high velocity of cold-sprayed TiO_2 impacted the substrates. Ko et al reported that the formation of a 10nm thick amorphous layer at the cold sprayed Cu/AIN interface was confirmed using the corresponding fast Fourier transform (FFT) pattern [146].

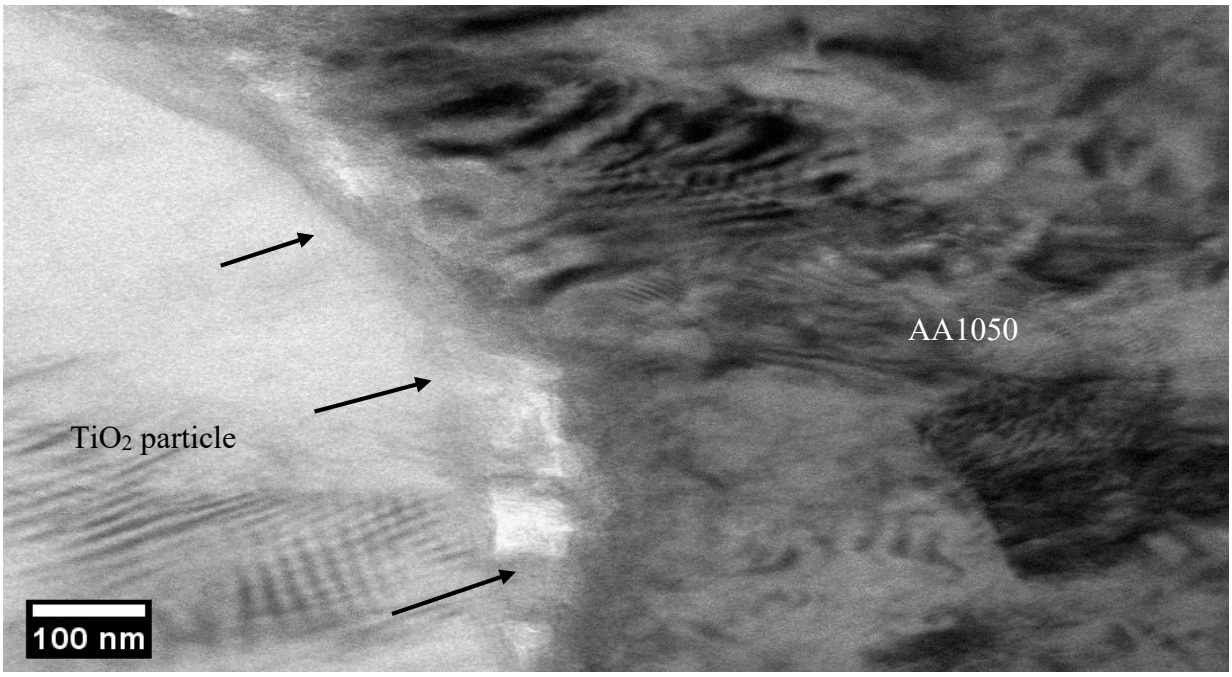

Figure 3.21: STEM of the TiO_2 / 400ºC annealed AA1050 at the interlayer area.

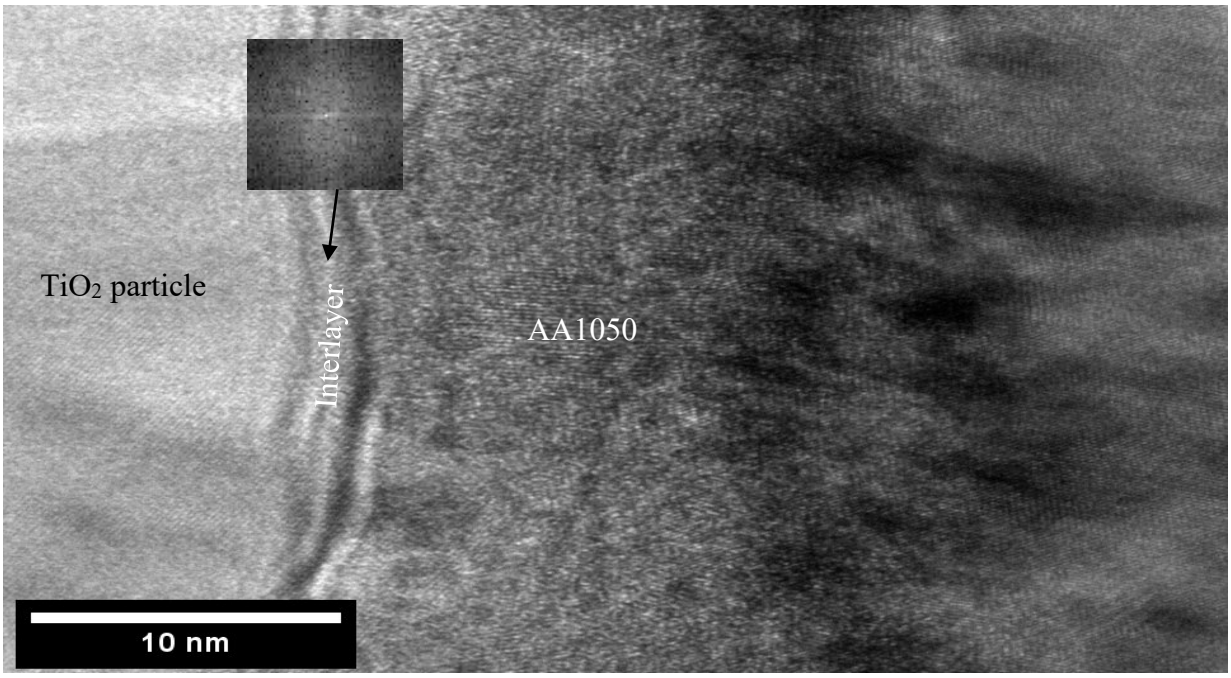

Figure 3.22: High-magnification images of the TiO_2 / 400 ºC annealed AA1050 at the interlayer area and a FFT image on the oxide interlayer.

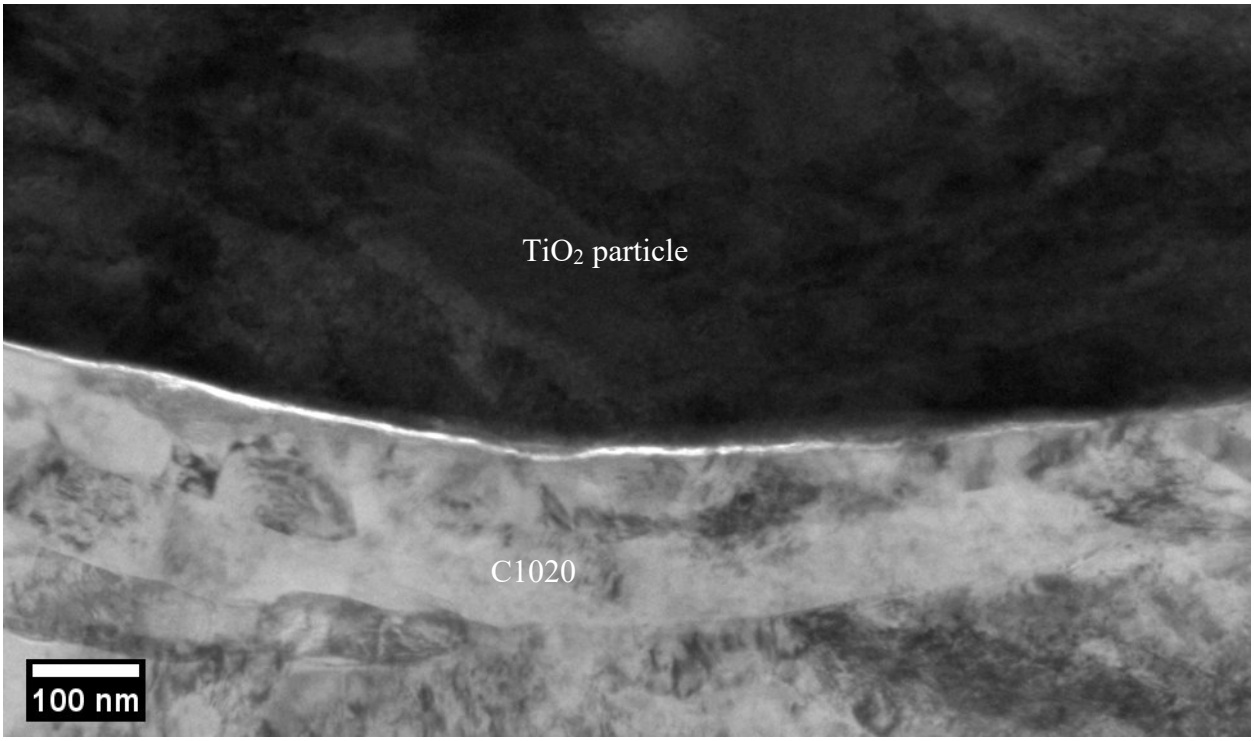

Figure 3.23: STEM of the TiO_2 / 400ºC annealed C1020 at the interlayer area.

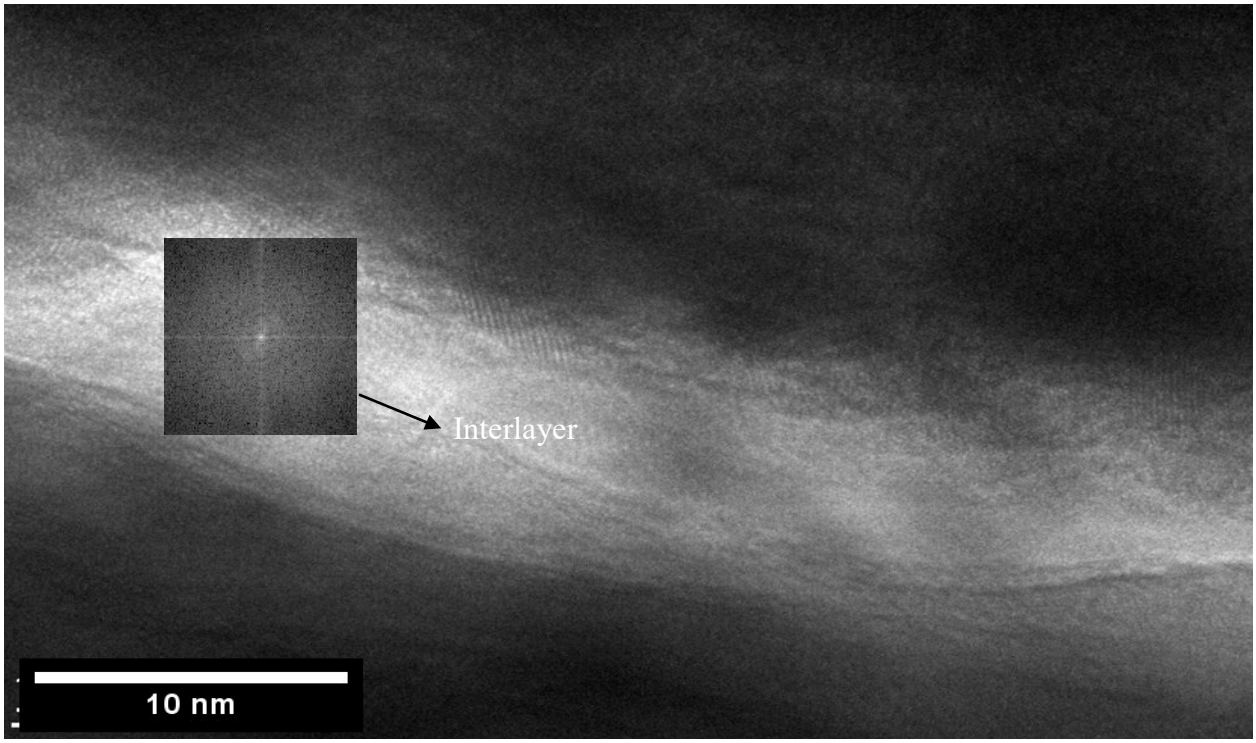

Figure 3.24: High magnification images of the TiO_2 / 400ºC annealed C1020 at the interlayer area and a FFT image on the oxide interlayer.

3.4.3 TEM line analysis on TiO_2 particle on room temperature and 400˚C annealed soft metal substrates

Figure 3.25 and 3.26 are the TEM line analysis result of single particle TiO_2 on room temperature and 400˚C annealed AA1050. It confirms the existence of Ti and O intermixing atomic on the room temperature of AA1050. On the other hand, 400°C annealed AA1050 has a higher atomic percent of O due to the remaining oxide layer as shown by figure 3.22. Assadi et al. [161] and Balíc et al. [162] reported that the interfacial bonding mechanism is an atomic length scale phenomenon and its occurrence is controlled by the presence of clean surfaces and high contact pressures to make the two surfaces mutually conforming. It could explain the decreased trend of adhesion strength of annealed substrate of soft metals from room temperature to 400°C, because the present of remaining oxide interlayer between TiO_2/Al.

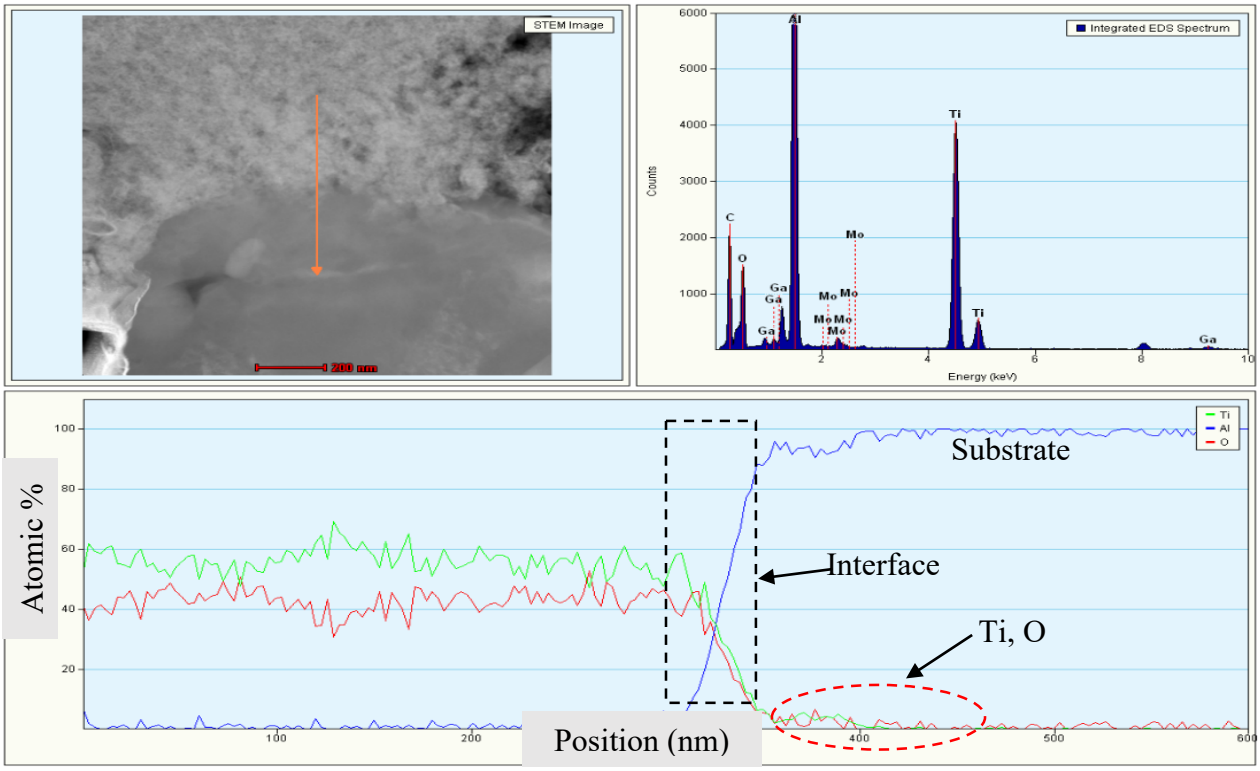

Figure 3.25: TEM line analysis of the TiO_2 on room temperature AA1050.

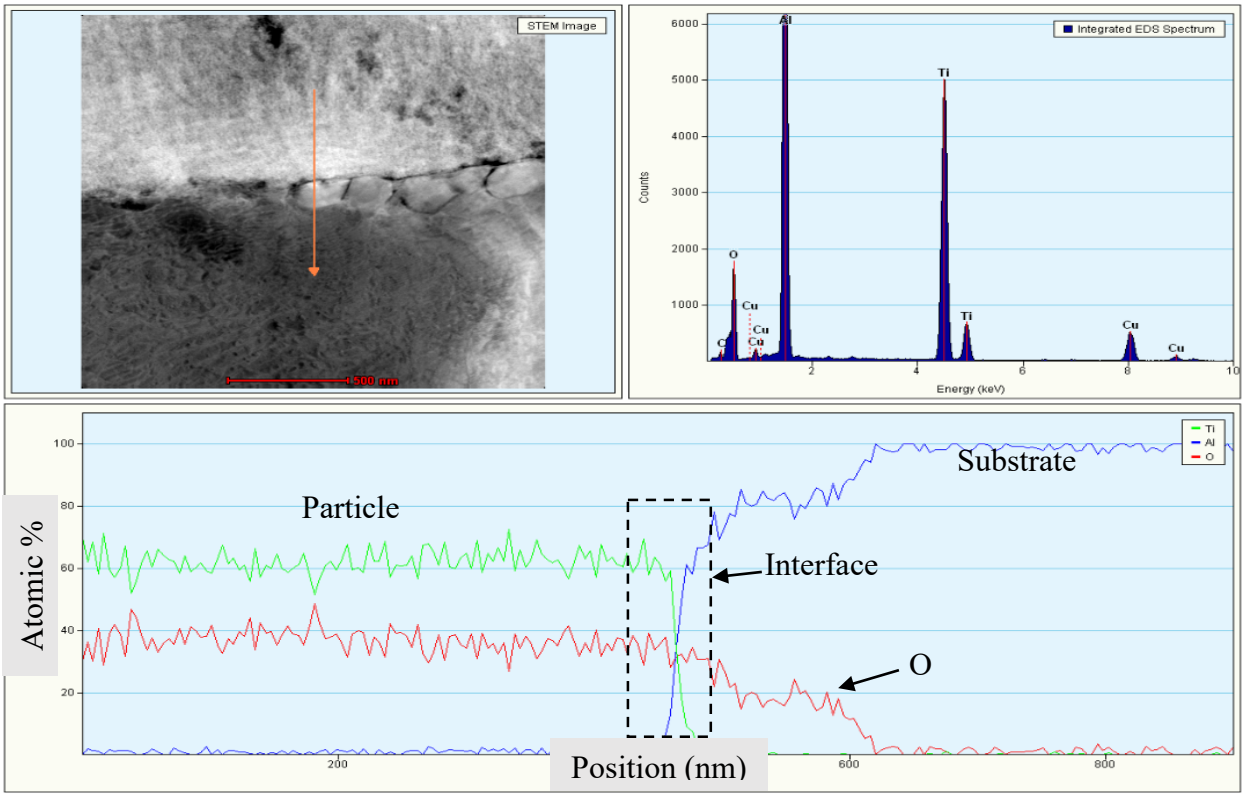

Figure 3.26: TEM line analysis of the TiO_2 on 400ºC annealed AA1050.

Figure 3.27 and 3.28 are the TEM line analysis result of single particle TiO_2 on room temperature and 400˚C annealed C1020. It confirms the existences of the atomic of Ti on room temperature of C1020. On the other hands, 400ºC annealed C1020, intermixing of Cu, Ti and O is present on particle area and no trace of Ti atomic on substrate surface. Ko et al. reported that the increasing of quantity of high oxidation state in copper feedstock can produce large amounts of rebounding particles which do not accumulate but tamping of the surface of the coating [156]. This explain why intermixing of Cu,Ti and O is present on particle area for 400°C annealed C1020 as shown in figure 3.28.

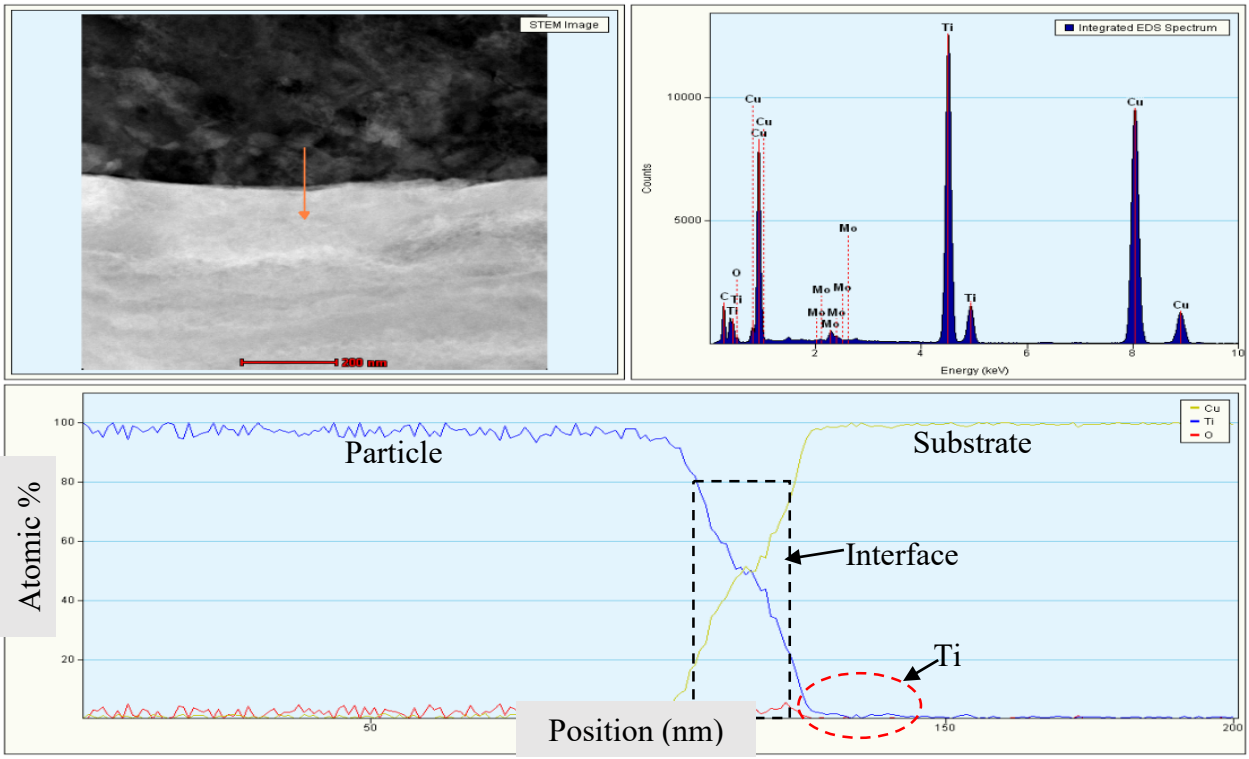

Figure 3.27: TEM line analysis of the TiO_2 on room temperature C1020.

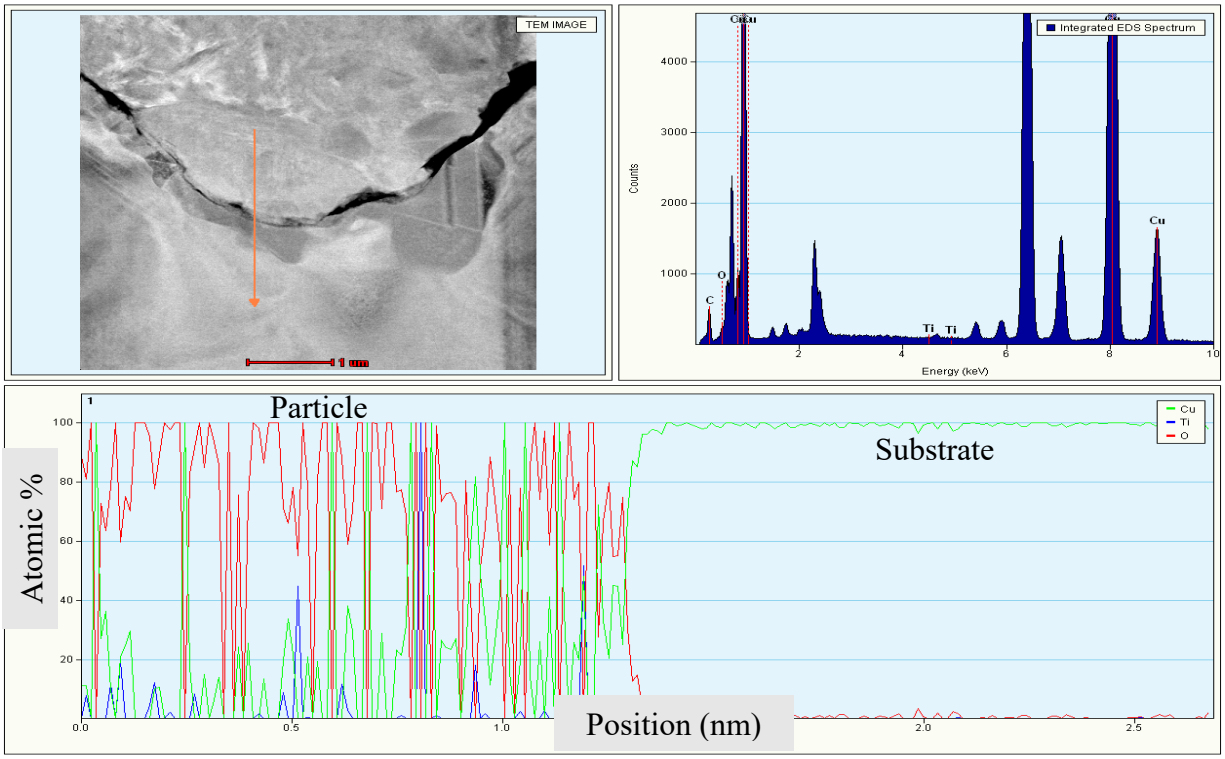

Figure 3.28: TEM line analysis of the TiO_2 on 400ºC annealed C1020.

3.5 Coating adhesion strength on oxide free 400°C annealed soft metal substrates

Figure 3.29 shown the adhesion strength of the cold-sprayed TiO_2 coating on 400˚C annealed AA 1050 and C1020 substrate with and without oxide on the substrate surface. No oxide here means, the AA1050 and C1020 were subjected to annealing in electric furnace then grit-blasted before cold spraying process. The grit-blasted is surface treatment for surface cleaning or roughening. Both soft- 400˚C annealed substrates on no oxide condition showed an increase trend of the adhesion strength cold-sprayed TiO_2 coatings compared to oxide substrate, which is 2.61 to 4.93 MPa for AA1050 and N/A to 1.44 MPa for C1020. From this result, it clearly indicates that main factor that influence the adhesion strength of the cold-sprayed TiO_2 coating on soft metals is remaining substrate oxidation that not fully removed after high impacted by cold sprayed TiO_2.

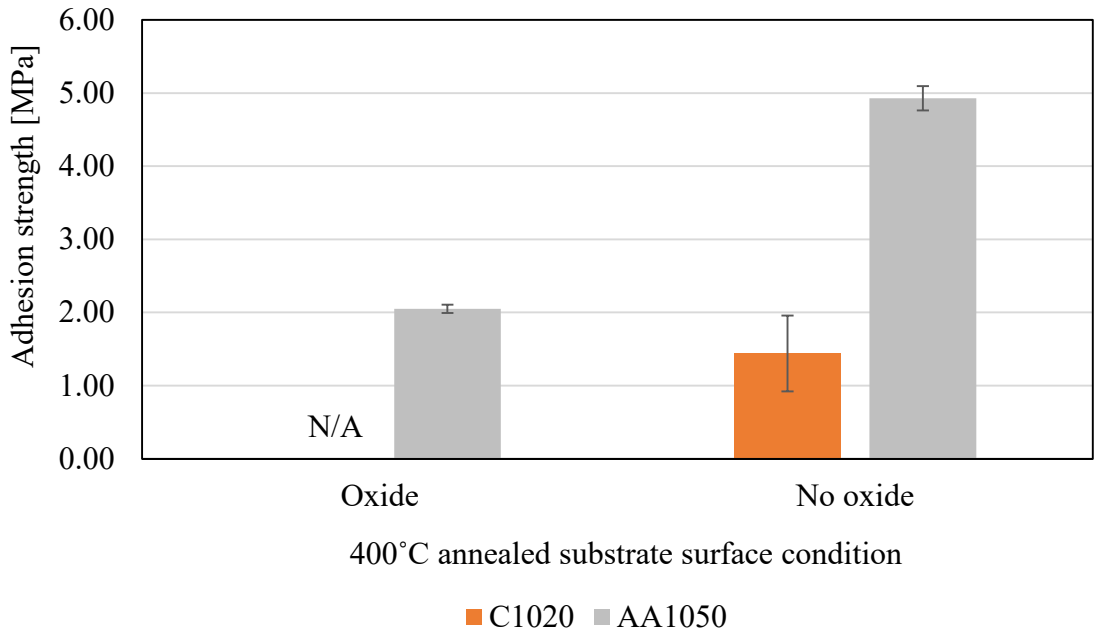

Figure 3.29: Coating adhesion strength on 400ºC annealed AA1050 and C1020.

3.6 Discussion

Cold sprayed TiO_2 coatings on the soft metals substrates revealed a decreased trend in coating adhesion strength with the increasing annealing temperature. Furthermore, the coating adhesion strength of the AA1050 substrate was higher than the C1020 substrate for all annealing conditions as shown in figure 3.3. Figure 3.4 and 3.5 shows the image of the fractured surface of substrate and TiO_2 coating after tensile strength test was conducted on AA1050 and C1020. This image confirms that the fracture was interfacial fracture of substrate and coating, thus, proving that strong cohesive bond between TiO_2 particles had been achieved during the coating formation process. EDS mapping on fracture coating on annealed AA1050 and C1020 showed that a small part of the aluminum is embedded on the TiO_2 coating and it same goes with C1020.

In order to further understand coating adhesion strength trend on soft metals substrate, microstructure investigation is conducted via SEM analysis as shown by figure 3.8 and 3.9. The images show that dense coatings with a thickness around 300µm could be obtained on a room temperature substrate of AA1050 and C1020, meaning that a critical velocity was achieved for these materials. This explans that TiO_2 coating attached to the soft metals room temperature are better than the annealed substrates. Large cracks between the coating and the annealed substrate were observed and it can be considered that the substrate annealing prior to the spraying reduces the adhesion by the titanium dioxide coating. The spraying parameters were constant for all experiments. Therefore, the substrate material and annealing did not strongly affect the deposition efficiency of the titanium dioxide cold-spraying coating method. The cold-spraying process is divided into two phases, adhesion and cohesion bonding. The first stage is the deposition of an interlayer between the substrate and the particle. This can affect the deposition behavior of the first

layer, although the deposition efficiency of the coating is mainly affected by cohesion between the particles. The effect of the substrate conditions can be ignored [78].

The adhesion strength value represent the adhesion bonding occuring between the first layer of TiO_2 coating and the surface of soft metals substrate. Therefore, analysis of substrate properties were conducted to further understand the bonding mechanism involved. The substrate conditions significantly affect the bonding features and properties of the cold-sprayed coatings[163-164].

The oxide surface roughness of the annealed soft metals showed an increased trend from room temperature to annealed at 400°C, by 20.56 to 121.9nm for AA1050 and 13.89 to 45.02nm for C1020, respectively. Singh et al. reported that substrate roughness significantly affects the deformation behavior of particle interaction with substrate surfaces, showing reduced localized plastic deformation and interfacial mixing of material for substrates of lower roughness for cold-sprayed Inconel 718. They suggested a minimum substrate roughness requirement for improved bonding prior to deposition by plastic deformation, and that the interfacial mixing of material is prominent if the powder particle interacts with the rougher substrate surface, which enhances the mechanical bonding between the powder particles and the substrate [165]. Richer et al. studied the effect of different grit size silica particles, where they found that the substrate preparation can only influence the deposition efficiency of the first few layers, and that later it is independent of the surface preparation [152]. Ziemian et al. also found that a substrate with higher surface roughness shows excellent coating adhesion when compared to a less rough surface in the case of cold-sprayed pure-Al coating [166]. Our findings showed a reversed trend as oxide surface roughness is increased, coating adhesion strength is decreased with the increasing annealing temperature. One of the reason to explain this situation is our feedstock powder, agglomerated TiO_2 powder

containing pure anatase crystalline structure with an average particle size of about 7.55 μm, is impacted on annealed soft metals substrate covered with oxide surface roughness in nanoscale. The large different between TiO_2 particle and oxide surface roughness on soft metals substrate, made the effect of oxide surface roughness is negligible. Therefore, mechanical interlocking that contributed from surface roughness factor is not the main bonding mechanism here.

Figure 3.14 shows the heat-treated soft metals value of AA1050 and C1020 from room temperature to 400°C. AA1050 and C1020 showed a declining tendency from 45.35 Hv (room temperature) to 27.7 Hv (400°C) for AA1050 and 103.2 Hv (room temperature) to 45.96 Hv (400°C) for C1020, respectively. Annealing heat treatments alter the characteristics of materials. The primary goal of annealing is to increase the ductility of a metal while decreasing its hardness [167]. The kinetic progression of pure copper micro-hardness after isothermal recrystallization proceeds at 250,300 and 380°C. The recovery process causes a modest decrease in microhardness during the incubation period. Then, a large fall in Hv from Hv = 100, at the initial cold-rolled phase to Hv = 50, at the fully recrystallized phase, confirms recrystallization [153]. AA1050 and C1020 recrystallization at 400°C [153,157] and prolonged cooling in an electric furnace with air as a medium allows grains to grow bigger and reduces substrate hardness, leading to softer pure materials. Annealed soft metals become softer at 400°C due to the recrystallization process, therefore when high velocity cold sprayed TiO_2 impacts the soft metals surface, it easier to deform due to kinetic impact energy of the sprayed particles. If the main deposition factor is the mechanical anchoring, softer substrate should have an advantage for the coating adhesion strength [150]. Nevertheless, the adhesion strength was decreased at higher annealed temperature. It means that the substrate deformation

(mechanical anchoring) is not the main bonding mechanism between the cold sprayed TiO_2 coating and the soft metals substrate.

Figures 3.15 and 3.16 show the XPS evaluations of the in-depth room temperature substrates to substrates annealed at 400°C for AA1050 and C1020 substrates, respectively. In situ argon ion beam sputtering can be used to analyze the distribution as a function of depth. Figure 3.15 a–e and 3.16 a-e shows that the atomic concentration of oxygen in the innermost part of the oxide film was raised significantly as the temperature of the annealing material rose from room temperature to 400°C. This indicates that as the annealing temperature rises, the oxide layer of soft metals substrate is thickens. According to Li et.al stated that the increasing of oxide film thickness, it will need more kinetic energy to break up and extrude the oxide film, thus a higher particle velocity is needed for bonding. In other words, the effective bonding area is decreased under the same particle impact conditions [168]. Yin et al. claimed that, in addition to the substrate hardness, also the particle velocity and the spray angle can influence the deformation behavior and final state of the oxide film. Moreover, the results indicate that the formation of a fresh metal surface followed by an immediate contact with the mating material, which can be a metal or oxide, is a necessary condition to form intimate bonding in a kinetic spraying process [169]. Since the particle velocity was constant across all experiment conditions, and with a thicker oxide layer on the substrate surface as annealing temperature is increased on soft metals substrates, this creates more inactive area to perform a bonding with TiO_2 particles, contributing to a decreasing trend in coating adhesion strength.

The composition of aluminum oxide exists at 400°C annealed is aluminum in hydroxide that represent by 74.8 eV as shown by figure 13.7 (c). This indicate AA1050 substrate experienced chemical composition changes from Al metal state in room temperature substrate to aluminum in hydroxide in 400°C annealed. Meanwhile for the composition of copper oxide films that coexist two phases, cuprous oxide, Cu_2O and cupric oxide, CuO. According to Papadimitropoulos et al claim that at temperature up to 225°C, Cu and Cu_2O is formed while above this temperature only CuO forms [157]. Both Cu_2O and CuO phases existed on our substrate and it has been supported by figure 3.17 (c) to confirm the oxide present and the shake-up satellite peak position of CuO [157], which was at approximately 944 to 940 eV, was detected at the outermost surface, mid-layer, and deepest part of the 400°C annealed C1020. Solid state reaction for Al_2O_3-TiO_2 is in the range of 1200 to 1796°C [170] and Lu et al. stated for solid state reaction between CuO-TiO_2, phase diagram of the CuO-TiO_2 system, the eutectic temperature is 900ºC in air, therefore the sample will react each other due to eutectic reaction [170]. Referring to our spray conditions that involved gas temperature of 500ºC and pressure at 3MPa, this condition is not reached up to eutectic temperature. Therefore, the chemical bonding that contributed from oxide composition factor may not be the main factor that influences the adhesion strength in cold sprayed TiO_2 onto soft metals substrate.

The objective of the wipe test was to study more about how TiO_2 particles adhere to annealed soft metals substrate. Only 400°C annealed were selected because they had the thickest oxide film. As demonstrated in Figures 3.19 and 3.20, the TiO_2 particle remained intact following the collision, whereas the base surface of the soft metals annealed at 400°C deformed due to impacting during the cold-spraying process. Trompetter et al [158] demonstrated that for solid particles impacting on a substrate, the substrate hardness played a significant role in the as-produced solid particles. Soft substrate such as aluminium and copper, the TiO_2 particles were impacting the surface with minimal deformation, and the particles rebounded after the impact, leaving craters on the surface of the substrate [159]. Since aluminium has lower hardness in comparison with copper, the depth of the craters were deeper and experienced heavy damage as seen in the figure 3.19 (a). K.-R.Ernst et al [160] also mentioned that for soft substrate, the impact energy that was generated during the spraying process was also used for deformation of the substrate as shown by red-dotted line in figure 3.19 (b) and 3.20 (b). Soft metals substrates underwent substrate deformation after being impacting by high-velocity cold-sprayed TiO_2 particles but the adhesion strength of the coatings showed a decreasing tendency as the temperature of the heat-treated base material was increased. This implies that substrate deformation or mechanical anchoring are not factors influencing the adhesion bonding of AA1050 and C1020 annealed at 400°C with a TiO_2 coating.

Bonding in cold sprayed is governed by mechanical interlocking and metallurgical bonding. Severe plastic deformation at the interface, owing to the high energy impacts of the particles, break the native oxide layers of the interacting surfaces. The disruption of oxide layers facilitates the penetration of particles into the substrate, which leads to jet formation and mechanical interlocking. Metallurgical bonding is manifested due to chemical interchange at the interface that is attributed to thermal softening caused by ASI [171]. Additionally, the formation of jets cleans the broken

oxides and instigates direct contact of particles against the substrate, which facilitates metallurgical bonding. The critical velocity required to break the oxide layer increases with the thickness of the oxide layer. Ichikawa and Ogawa [172] investigated that an increase in oxide layer thickness from 0 to 0.35 μm decreased the deposition efficiency from 55% to 0.03%. Christoulis et al. [173] demonstrated that either removal of the native oxide layer or transformation of it into an amorphous oxide layer is required to achieve effective bonding at the interface. Hassani-Gangaraj et al. [174] also reported that the native oxide layer breakage facilitates metallurgical bonding. As well, unstable jets form on impact and fragment surface asperities which is favorable for metallurgical bonding. Ichikawa et al. [175] used auger spectroscopy to determine the presence of oxides at the fractured surfaces of a Cu splat onto an Al substrate after adhesion testing. A pictorial view of the study is presented in Figure 3.21. Adhesion strength was predicted to be lesser at the center and stronger near the edges of the splats owing to the presence of an unbroken oxide layer near the center of the splats. Similar outcomes were found by Rahmati et al. [176] by employing a numerical approach to explore the effect of oxide layer on adhesion strength of CS Cu on Cu. It was demonstrated [177] that breakage of the native oxide layer from the particle and substrate allowed direct elemental contact between the particle and substrate; hence resulting in metallurgical bonding. It was also validated that a higher critical velocity was required for a thicker oxide layer.

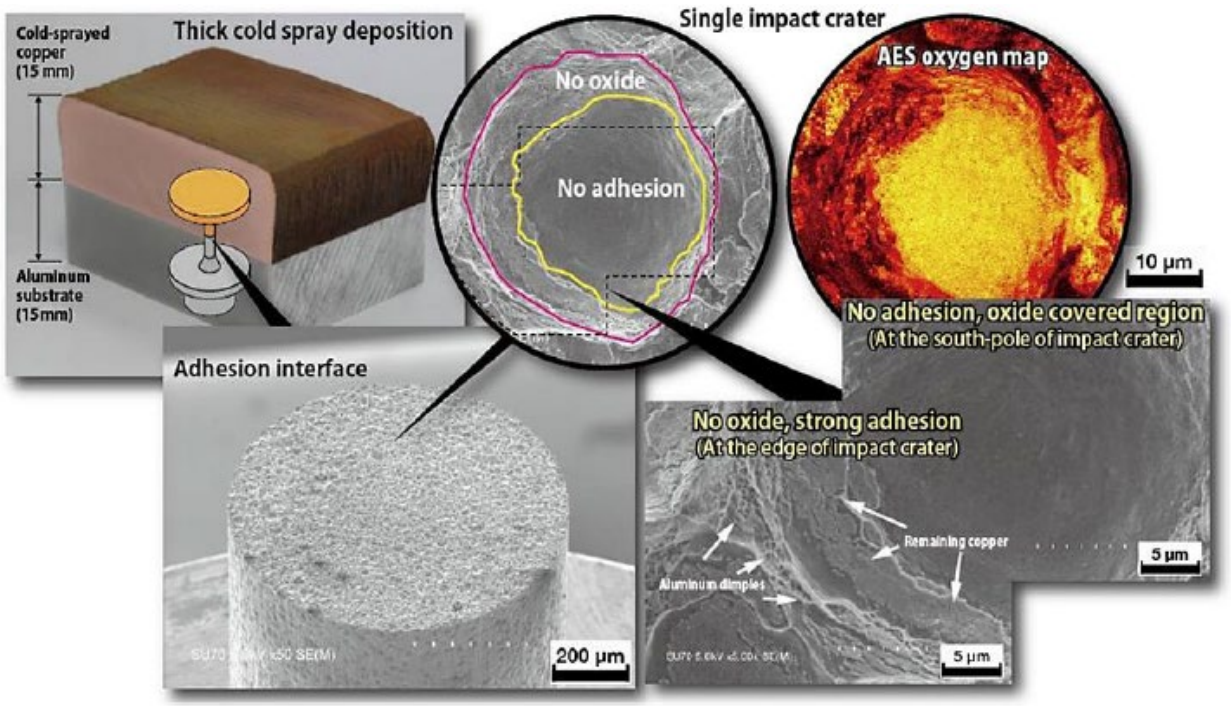

Figure 3.30: A pictorial view representing fractographs of cold sprayed Cu on Al exposed after adhesion testing showing bonded zone and auger electron spectroscopic (AES) maps representing oxide layer zone [175].

Our experiment is consistent with the results of Ichikawa et al., where substrate deformation existed on both soft metals annealed at 400°C, but the adhesion strength was lowest at this annealing temperature due to the oxide film remaining on the substrate surface after impact from cold-sprayed TiO_2 particles.

In order to further investigated the role of remaining oxide layer occurred at interlayer TiO_2/annealed soft metals substrate toward bonding mechanism involved, TEM images and line analysis on room temperature and 400°C annealed soft metals substrate were conducted.

Figure 3.21 to 3.24 is TEM images of the interface between a single TiO_2 particle and AA1050 and C1020 annealed at 400°C. The remaining oxide layer at interface between TiO_2/soft metals

substrate were confirm using FFT pattern that showed an amorphous phase present by figure 3.22 for AA1050 and 3.24 for C1020. These confirm the existences of a remaining interlayer oxide with a thickness of approximately less than 10 nm for AA1050 and 10nm for C1020, after the high-velocity cold-sprayed TiO_2 impacted the substrates. To discover more about atomic concentration changes toward the bonding mechanism between TiO_2 particles and soft metals substrates, TEM line analysis was performed on a single TiO_2 particle on soft metals substrate at room temperature and annealed at 400°C as showed by figure 3.25 to 3.28.

The TEM line analysis results of a single TiO_2 particle on AA1050 at room temperature and 400°C annealed are shown in Figures 3.25 and 3.26. These results confirm the presence of atomic Ti and O intermixing on room-temperature AA1050, as shown in figure 3.25. AA1050 annealed at 400°C, on the other hand, only had a higher atomic percentage of O due to the remaining oxide layer.

Figure 3.27 to 3.28 shows the TEM line analysis results of a single TiO_2 particle on C1020 at room temperature and after 400°C annealed. These results confirm the presence of atomic Ti on room-temperature C1020. On the other hand, for C1020 annealed at 400°C, there is intermixing of Cu, Ti, and O in the particle area, but no trace of atomic Ti on the substrate surface. Ko et al. reported that the increasing of quantity of high oxidation state in copper feedstock can produce large amounts of rebounding particles which do not accumulate but tamping of the surface of the coating [146]. This may explain the situation since 400°C annealed C1020 have thicker oxide layer compared to room temperature substrate of C1020. Coating adhesion strength testing on no oxide soft metals substrate 400°C annealed were performed to confirm the role of oxide layer on soft metals surface, as shown in figure 3.29. 400°C annealed soft metals substrate were chosen because it has thicker oxide layer and lowest coating adhesion strength for cold spray with oxide substrate conditions. No oxide here means, the AA1050 and C1020 were subjected to annealing in electric

furnace then grit-blasted before cold spraying process. The grit-blasted is surface treatment for surface cleaning or roughening. Coating adhesion strength on no oxide soft metals 400°C annealed substrates showed an increase trend which is 2.61(oxide) to 4.93 MPa (no oxide) for AA1050 and N/A (oxide) to 1.44 MPa (no oxide) for C1020. From this result, it clearly indicates that main factor that influence the adhesion strength of the cold-sprayed TiO_2 coating on soft metals substrate is remaining substrate oxidation that not fully removed after high impacted by cold sprayed TiO_2. The strength of the particle-substrate adhesion also depends on the deposition velocity [178], gas temperature [179], substrate type as well as temperature, size and type of the powders [180-181]. Assadi et al. [161] and Balíc et al. [162] reported that the interfacial bonding mechanism is an atomic length scale phenomenon and its occurrence is controlled by the presence of clean surfaces and high contact pressures to make the two surfaces mutually conforming. To date, the most dominant hypothesis on the metallurgical bonding mechanism suggests that the outward metal jet induced by the adiabatic shear instability extrudes the cracked oxide film, which initially covers particle and substrate surfaces, from the centre to the rims of the interaction area. The plastic flow exposes the fresh surfaces leading to a metal-to-metal contact that promotes the particle–substrate and the inter-particle metallurgical bonding [182]. The deposition process, involving the destruction phases of the oxide film, can be summarised in four stages represented in figure 3.30.

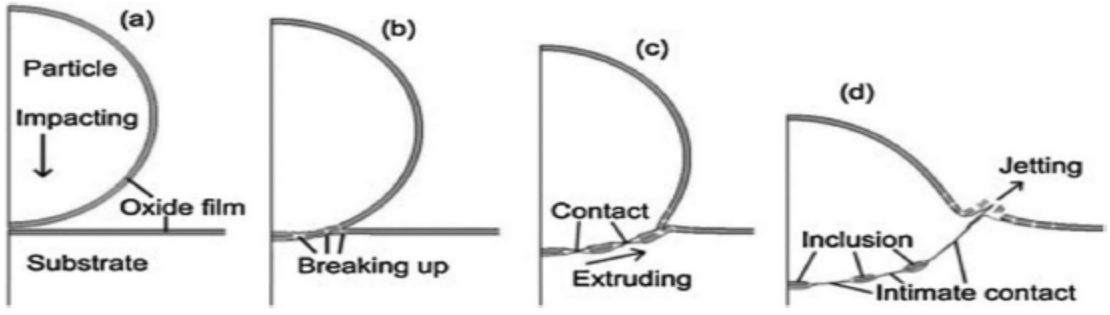

Figure 3.31: Destruction phase of the oxide film [168].

The metallurgical bonding, one the other hand, results from the chemical reactions occurring at the particle-to-particle and particle-to-substrate interfaces, which requires oxide-free interface and metal-to-metal contact. The metallurgical bonding is considered a consequence from chemical reaction at the oxide-free interface between particles or particle/substrate [57-60]. According to the results we obtained in this study, chemical reaction between cold-sprayed TiO_2 particle and newly formed soft metals substrate is considered be the main factor that contributed to metallurgical bonding. 400ºC annealed soft metals substrate decreased the hardness due to the recrystallization, however, thick oxide layer which prevent the bonding was formed and reduced the adhesion strength. Hence the bonding mechanism between cold-sprayed TiO_2 onto soft metals substrate can be explain with the chemical reaction which is similar with the cold spraying of metallic materials. Figure 3.31 shown a schematic image of cold-sprayed TiO_2 deposition onto soft metals substrate materials, having thin oxide at room temperature and thick oxide after annealing.

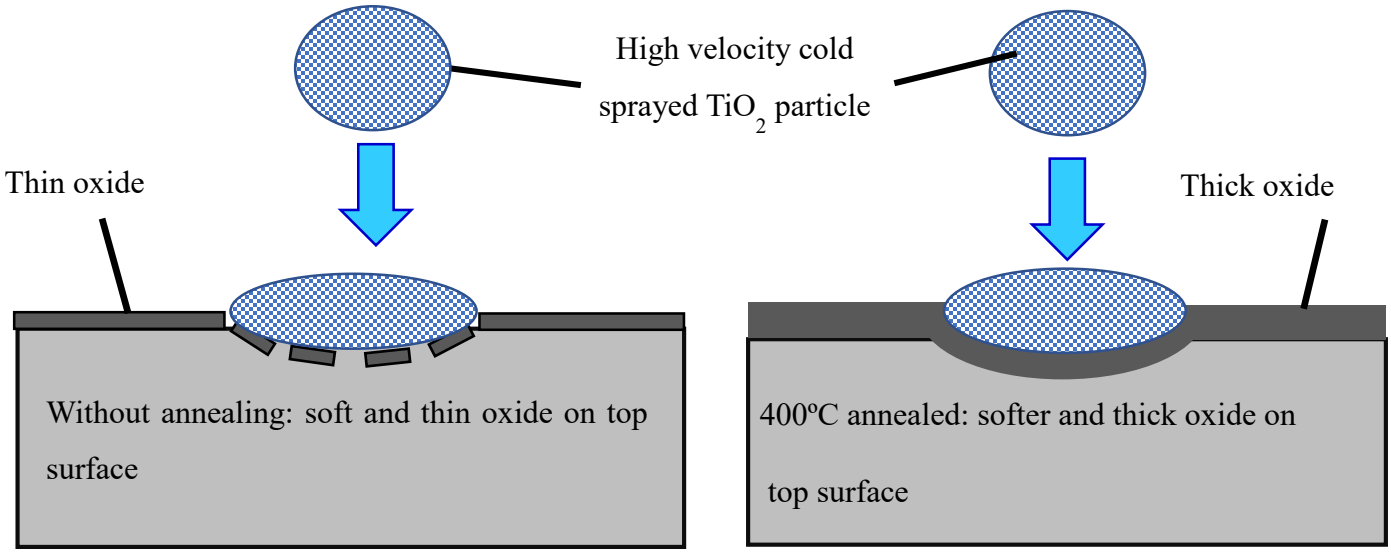

Figure 3.32: Schematic image of cold-sprayed TiO_2 deposition onto soft metals substrate materials, having thin oxide at room temperature and thick oxide after annealing.

3.7 Conclusions

Herein, we investigated the bonding mechanism of cold sprayed pure ceramic, titanium dioxide on soft metals substrate through substrate properties that are annealed in an electrical furnace temperature range from ambient temperature to 400°C. The summary of the study's finding are

1. The annealing process contributed to the induced ductility of soft metals substrate especially when annealed at a recrystallization temperature of 400°C. The soft metals substrate hardness was reduced as a result, and it became softer. When the high-velocity cold sprayed TiO_2 particle impacted the soft metals substrate surface with thick oxide film, plastic deformation of the substrate is present but some of the oxide layer remained as shown by the TEM results, which prevented metallurgical bonding from occurring in between the TiO_2 coating and soft metals substrate.
2. The primary bonding mechanism of TiO_2 particle and soft metal substrate is metallurgical bonding which required free oxide surface.

4 Bonding mechanism of cold sprayed TiO_2 coating on hard metal substrates

4.1 Introduction

Cold spray is a solid-state deposition process since the feedstock is not melted; however, the kinetic energy of the high velocity particles leads to interfacial deformation as well as localized heat at the location of impact [46,183-184]. The conversion of kinetic energy into deformation and heat results in mechanical interlocking as well as metallurgical bonding at the interface [185]. The bonding at the interface in cold spray is still mysterious to some degree since there is no exact theory that explains the bonding mechanism at the interface. However, the literature mentions that the spray particles require a certain amount of energy in combination with a critical velocity at an optimum temperature, for effective bonding to occur [161,118]. High strain rate deformation is observed around the particle-substrate interface, which produces a microscopic protrusion of material with localized heating. The combination of material deformation at the atomic level and localized heat may lead to metallurgical bonding [165,186].

Bonding at the interface is governed by the severe plastic deformation of the materials; which, with associated adiabatic shear instability (ASI) at the interface, leads to the metal-jet formation [57-60]. The high velocity particle impacts cause breakage of the native oxide layer at the surfaces, providing a particle-to-substrate contact. This true contact of the particles with the substrate may lead to the jet formation that is governed by ASI [187-189]. However, Hassani-Gangaraj et al. [190] contradicted the work of Assadi et al. [161] and Grujicic et al. [14] by reporting that ASI is not necessary for bonding in cold spray. Responding to the comments of Assadi et al. [191], Hassani-Gangaraj et al. [192] defended their simulation based research that supported ASI was not

required for bonding. These, and other scientific contradictions highlight that adhesion mechanism(s) of cold spray coatings is an unresolved topic that requires further investigation.

Delamination and poor adhesion strength of soft-on-hard and hard-on-hard interfaces are of great concern for industries such as the marine, nuclear, aerospace, automotive and electronics. Thus, understanding the mechanism of bonding can address the issue of poor adhesion and delamination, which would assist the advanced manufacturing sector. For instance, thick copper coatings on steel (SS316L) plates that would exhibit properties comparable to that of bulk Cu, along with good adhesion, are in high demand for the vacuum vessel of Tokamaks [193-194]. In this regard, Singh et al. [165] investigated the bonding mechanism of Cu particles on steel substrates (soft-on-hard interface) by altering the cold spray parameters and the substrate conditions. Drehmann et al. [148], Wustefled et al. [147] and Dietrich et al. [195] investigated the bonding mechanism for cold sprayed Al on an Al_2O_3 substrate (soft-on-hard). Their results revealed that bonding of Al particles on super-finished monocrystalline sapphire substrate occurred due to deformation-induced recrystallization in the vicinity of the particle-substrate interface. The formation of nano-sized grains at the vicinity of the interface assists metallurgical bonding, which results in improved adhesion strength between ductile Al particles and the Al_2O_3 monocrystalline ceramic substrate. Therefore, there are many factors that influence the adhesion strength, and this need optimization to achieve the best adhesion strength of the cold spray coating. Objective of this chapter to shed a light on bonding mechanism of cold sprayed pure TiO_2 on hard metals substrate (soft/hard).

4.2 Substrate and titanium dioxide coating characterization on annealed substrates

4.2.1 Adhesion strength testing and fracture surface analysis on annealed hard metal substrates

Figure 4.1 depicts the adhesion strength of a cold-sprayed TiO_2 coating on annealed hard metals represented by SUS304 stainless steel and SS400 structural steel. The TiO_2 coating on annealed SUS304 showed an increased trend of adhesion strength from room temperature to 1000°C, with values ranging from 0.51 to 2.55 MPa for SUS304 and 1.07 to 1.65 MPa for SS400 from room temperature to 400°C annealed, with no successful coating on 700 and 1000°C annealed. Coating adhesion strength on annealed SUS304 and SS400 showed a different trend, and further investigations, as discussed below, are being carried out to better understand this trend and relate it to the bonding mechanism involved.

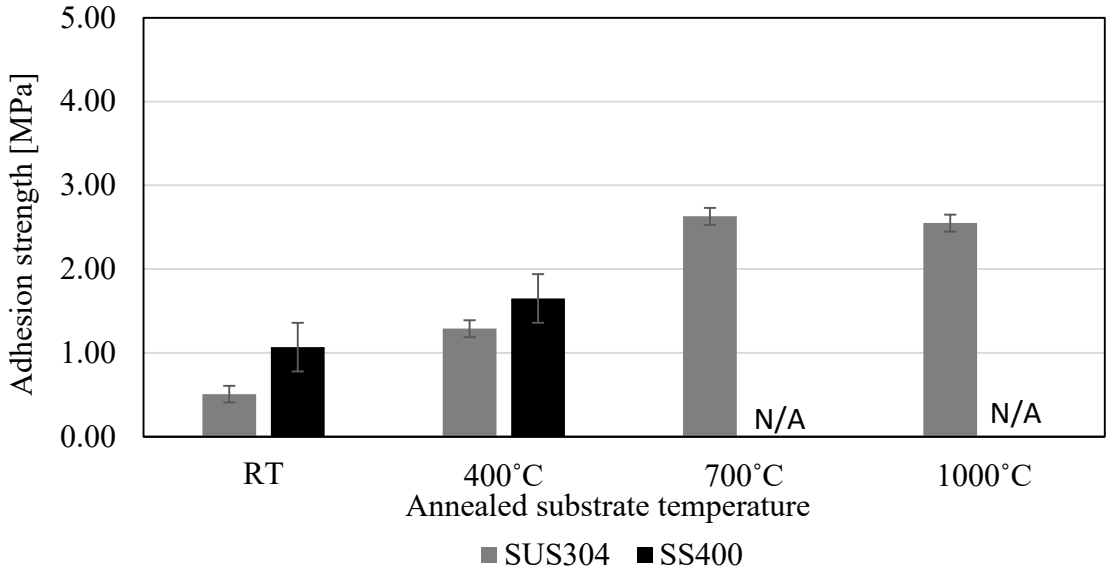

Figure 4.1: Adhesion strength of the TiO_2 coating on SUS304 and SS400 from room temperature to 1000˚C annealed.

Figure 4.2 and 4.3 shows the image of the fractured surface of substrate and TiO_2 coating after tensile strength test was conducted. This image confirms that the fracture was interfacial fracture of substrate and coating, thus, proving that strong cohesive bond between TiO_2 particles had been achieved during the coating formation process.

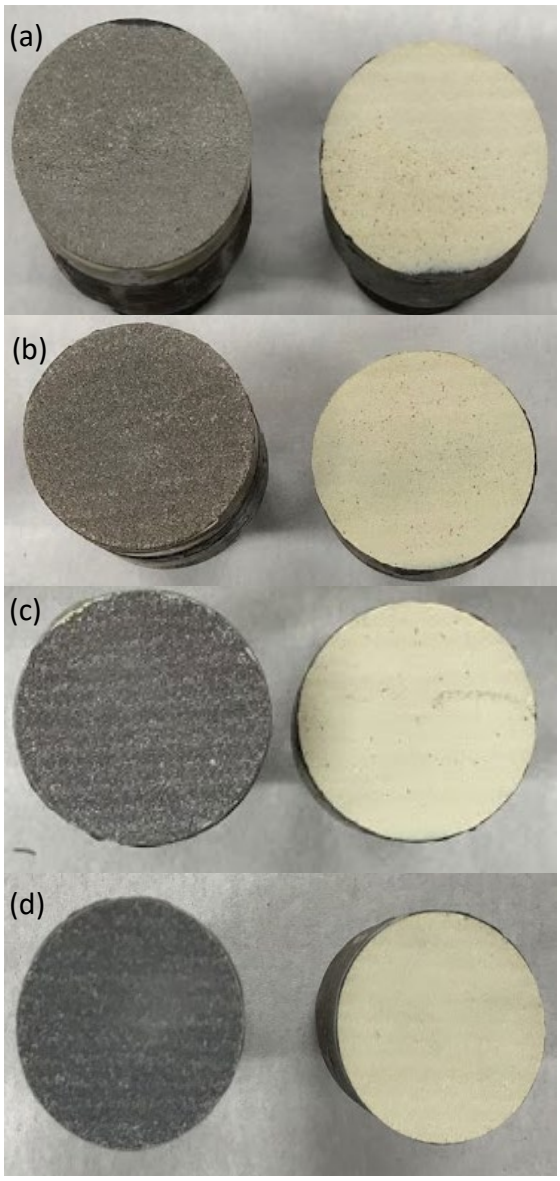

Figure 4.2: Fracture surface substrate and TiO_2 coating after tensile strength testing on SUS304. (a) Room temperature (b) annealed at 400°C (c) annealed at 700°C and (d) annealed at 1000°C.

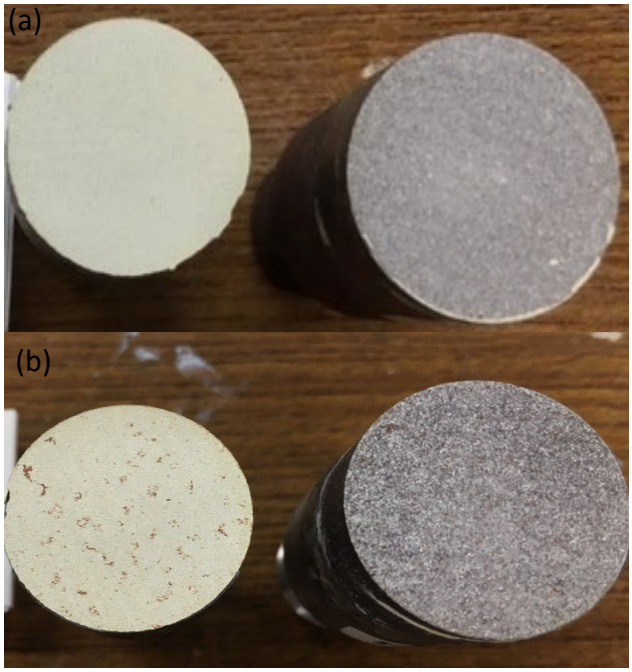

Figure 4.3: Fracture surface substrate and TiO_2 coating after tensile strength testing on SS400. (a) Room temperature and (b) annealed at 400°C.

EDS mappings, as shown in Figures 4.4 and 4.5, showed that the elements present are iron (Fe), titanium (Ti), oxygen (O), and carbon (C) for fractured titanium dioxide coating on annealed hard metals. For both hard metal substrates, only a small fraction of iron is embedded on TiO_2 coating.

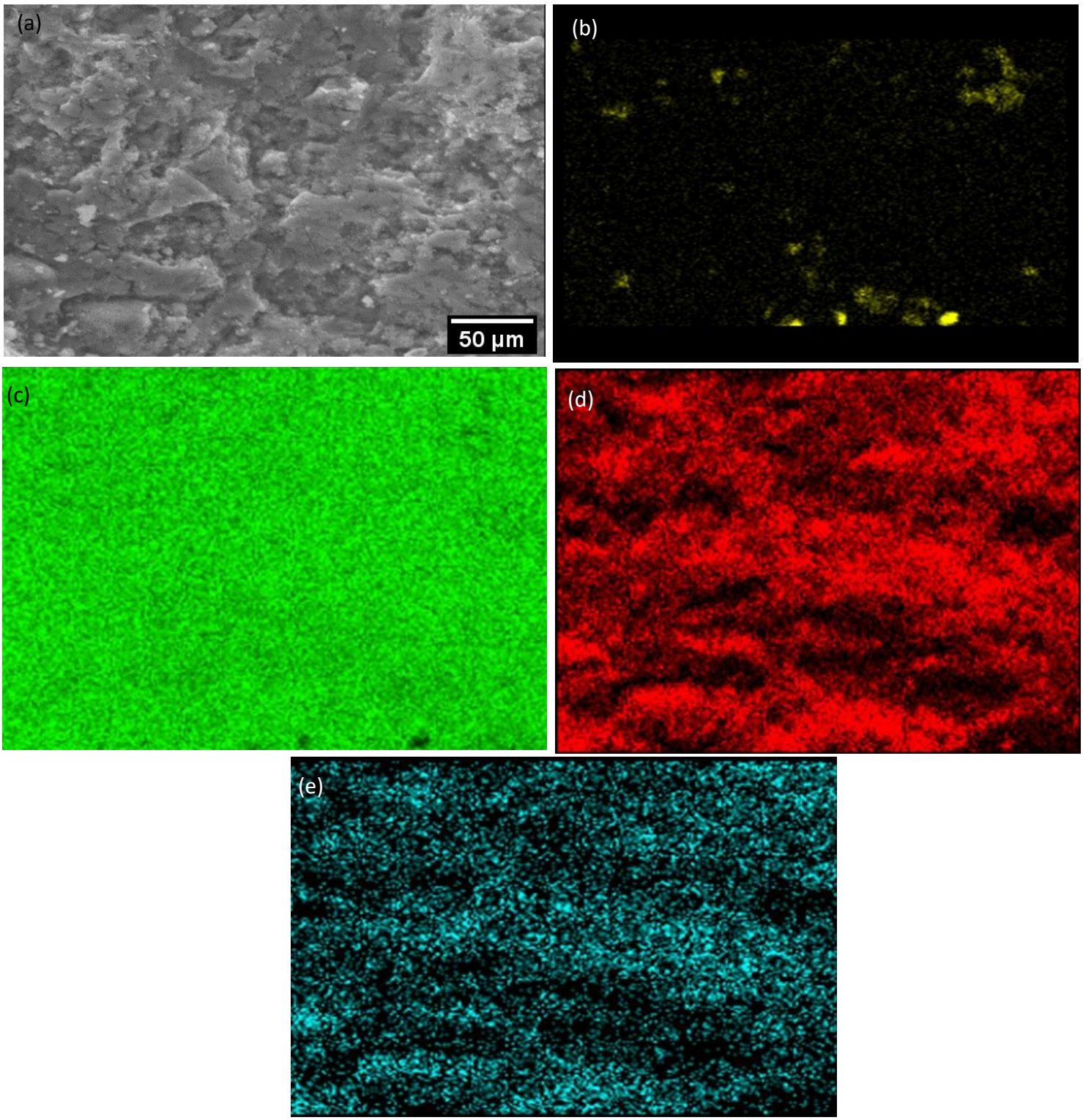

Figure 4.4: EDX on fracture coating (a) SEM image (b) Iron (c) Titanium (d) Oxygen (e) Carbon for SUS304.

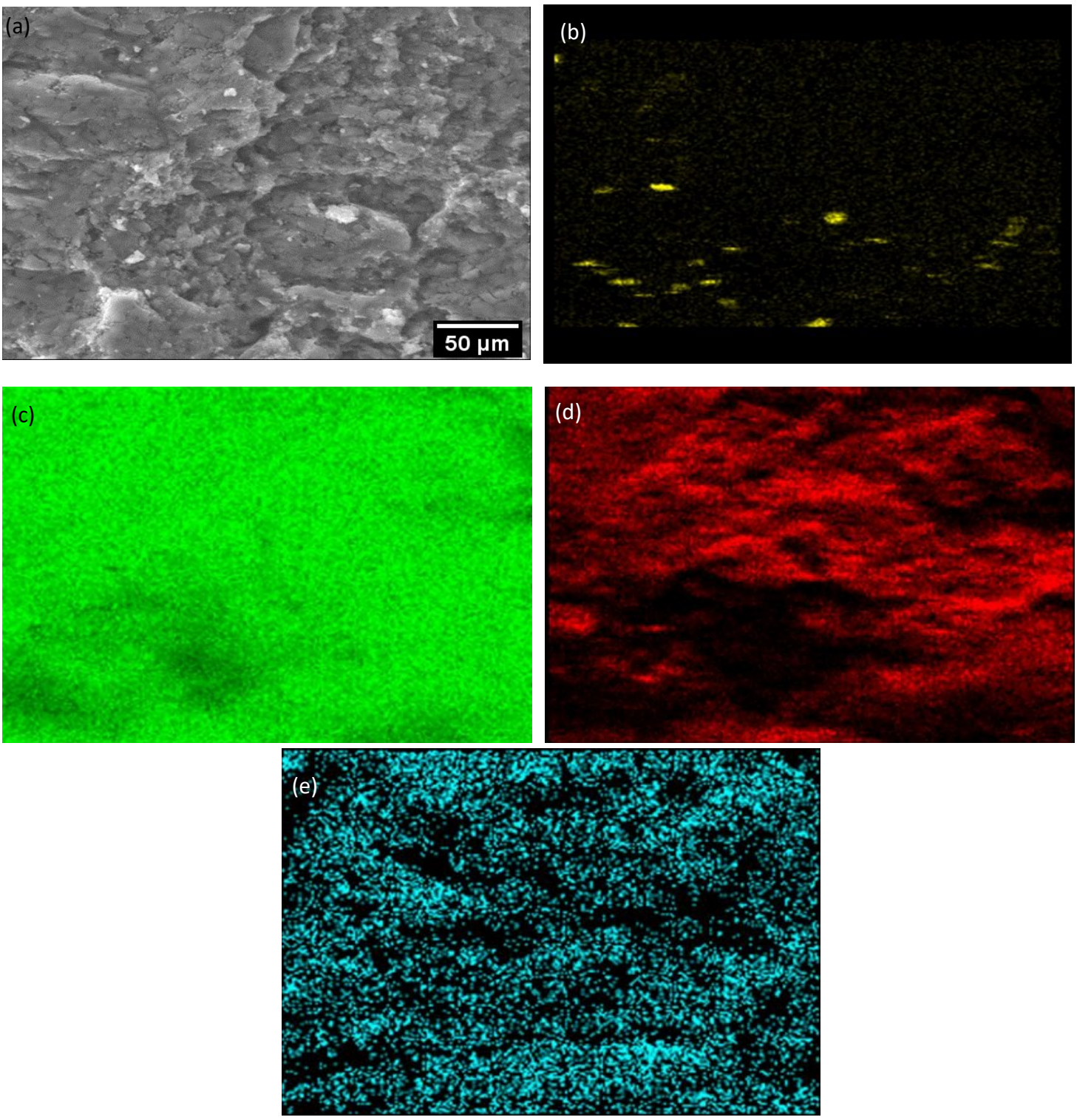

Figure 4.5: EDX on fracture coating (a) SEM image (b) Iron (c) Titanium (d) Oxygen (e) Carbon for SS400.

4.2.2 SEM microstructure cross-section on annealed substrates

Figure 4.6 and 4.7 shows the TiO_2 coating cross-sectional area on hard metals substrate for room temperature and 1000ºC annealed for SUS304 and 400°C for SS400. Substrates at room temperature and 400°C,1000°C were chosen for observation to clarify the interface adhesion between substrates which yielded the lowest and highest adhesion strength. The figures show, in all conditions, a dense coating with a thickness of 300 μm, indicating that a critical velocity of TiO_2 coating was reached for this hard metals substrate and explained an increased trend of coating adhesion strength because TiO_2 coating adhered well to the hard metals substrate from room temperature to 400°C,1000℃ annealing.

Winnicki et al. [97] sprayed three types of TiO_2 powder on a steel substrate, TiO_2 amorphous, TiO_2 anatase, and TiO_2 rutile, with coating thicknesses of 25, 30, and 9 μm, respectively. Gardon et al. [85] sprayed TiO_2 powder on a stainless steel substrate with sub-oxide preparations on the stainless steel substrate surface, with a coating thickness of 5 μm. It demonstrated that forming a thick coating of pure TiO_2 powder on a steel substrate using a cold spray process was difficult because the cold spray process required plastic deformation of the powder feedstock in order to form a coating on the substrate surface and to deposited onto a hard metals substrate is another challenge. Studies have been made to attain good adhesion strength for hard substrates, out of which, substrate pre-heating is the most common strategy. However, Singh et al. [89,194] found that electroplating of the SS 316 substrate with a softer material such as Ni improved the adhesion strength of CS Cu coatings. Furthermore, Perton et al. [91] applied laser heat treatment prior to CS to improve the adhesion strength by reducing the substrate hardness. Wang et al. [92] found that a hard steel substrate induced high deformation onto the striking Al particles, which improved the cohesive

strength in the coating nearer to the substrate. However, hard particles (Al_2O_3) were embedded inside the soft Al substrate, which led to strong interfacial bonding. Therefore, it can be concluded that the substrate hardness influences the coating properties significantly in the vicinity of the interface.

Our findings revealed a thick coating of TiO_2 on a hard metals substrate, and adhesion bonding is determined by first layer of TiO_2 coating and substrate surface. Therefore, further research is needed to better understand the bonding mechanism involved.

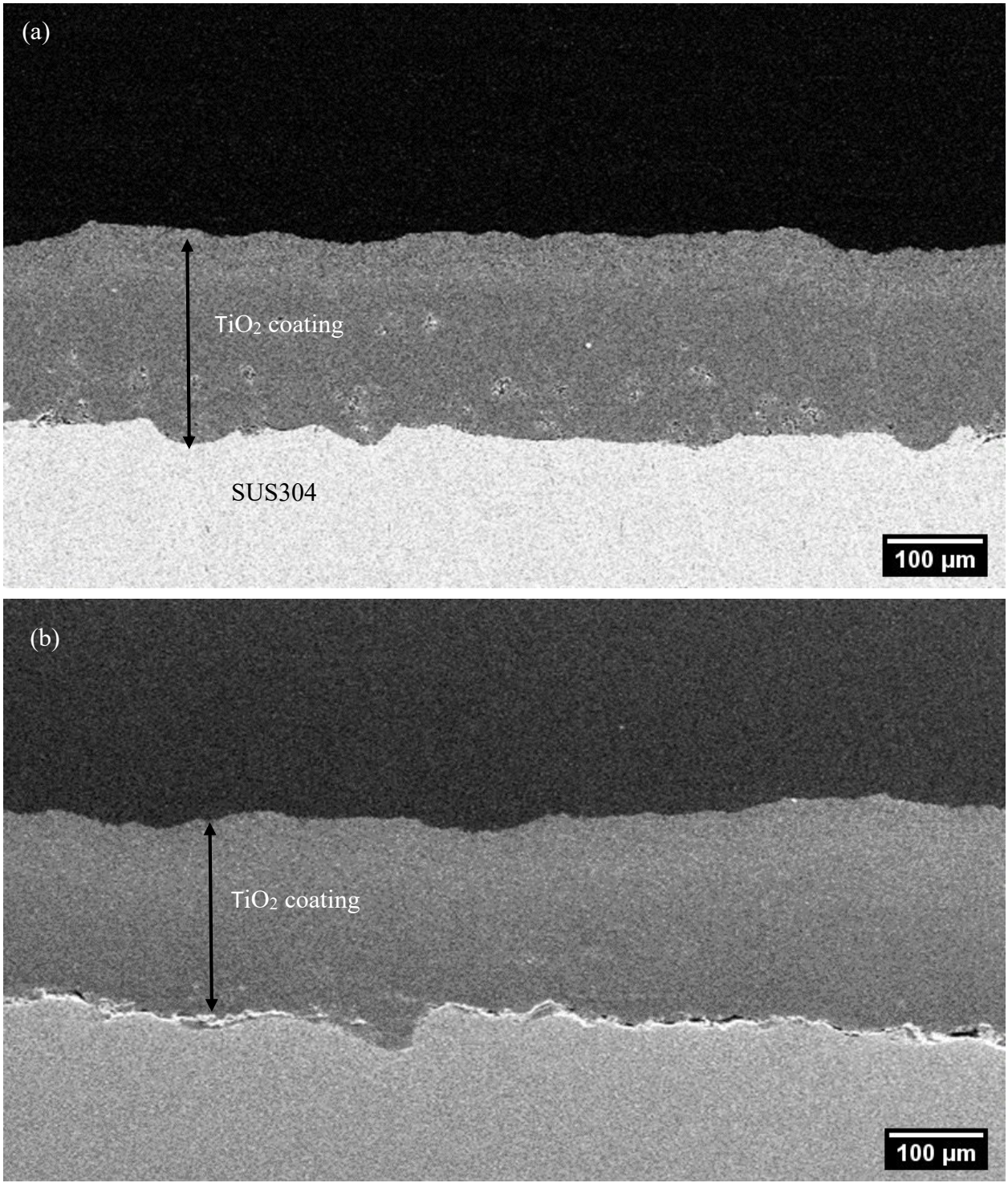

Figure 4.6: Cross-section microstructure of TiO_2 coatings on SUS304. (a) Room temperature and (b) 1000°C annealed.

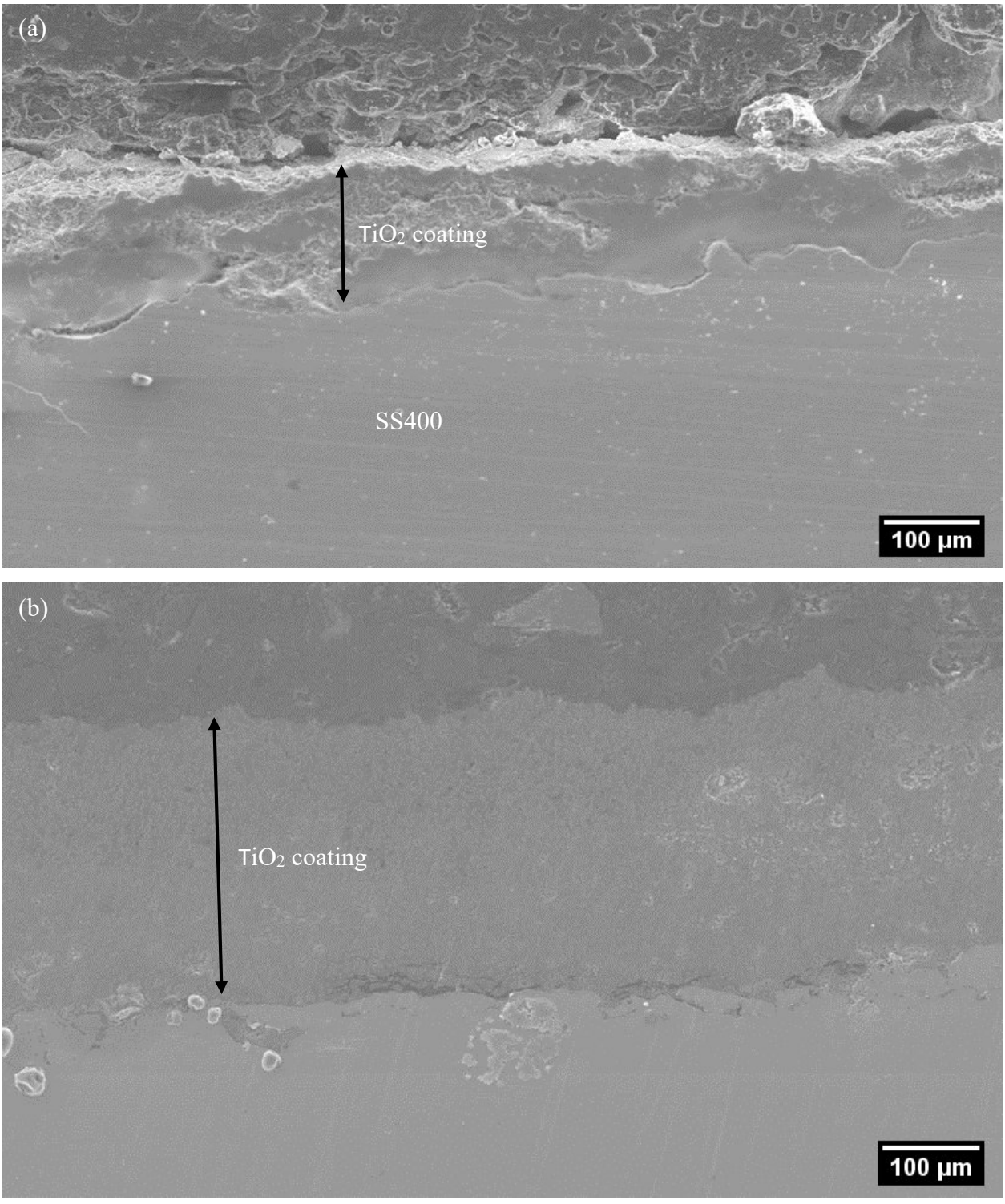

Figure 4.7: Cross-section microstructure of TiO_2 coatings on SS400. (a) Room temperature and (b) 400°C annealed.

4.2.3 Substrate surface roughness testing on annealed substrates

Figure 4.8 and 4.9 shows a AFM result of oxide surface roughness for hard metals substrate in 2D and 3D images. The result shown a decrease trend of oxide surface roughness from 87.65nm (RT) to 80.08nm (1000˚C) for SUS304 and 146.1nm(RT) to 26.45nm(400°C) for SS400, respectively as indicated by table 4.1 to 4.4.

The surface roughness of the substrate plays a prominent role in the bonding mechanism at the interface. Kumar et al. [186] found that semi-polished substrates were ideal for achieving the best adhesion for a Cu on steel combination (soft and hard). Singh et al. [165] obtained better adhesion for mirror-finished substrates than semi polished and as-received substrates for the same material combinations (soft and hard). The surface roughness were Ra 6 μm for as-received, Ra 0.5 μm for semi-polished, and Ra 0.06 μm for mirror-finished. The authors found that surface asperities and waviness of the as received substrate caused gap at the interface as shown in figure 4.8(a), resulting in poor adhesion. Furthermore, the energy of the particles was dissipated in deforming the sharper peaks of the semi-polished surface, which hindered particle penetration into the substrate and induced a gap at the interface; hence resulting in poor adhesion figure 4.8 (b). No similar surface asperities and peak hindrances were observed in the case of mirror-finished substrates, and the particles intruded into the substrate, which resulted in the highest adhesion strength as shown in figure 4.8 (c) and (d). Similar trends in adhesion strength were observed by Theimer et al. [113] for brass on steel (soft and hard) combinations.

Our findings show that while the oxide surface roughness of SUS304 decreases slightly, the coating adhesion strength increases steadily as the annealing substrate temperature rises.

Meanwhile, for SS400, an increase in annealing substrate temperature results in a significant reduction in oxide surface roughness, but coating adhesion strength is only successful up to 400°C annealed substrate. It clearly showed that, oxide surface roughness did not play any significant role toward bonding mechanism involved for TiO_2 powders on hard metals substrate. One of the reason to explain this situation is when our feedstock powder, agglomerated TiO_2 powder containing pure anatase crystalline structure with an average particle size of about 7.55 μm, is impacted on annealed hard metals substrate covered with oxide surface roughness in nanoscale, due to large different size, it has negligible impact on adhesion bonding involved.

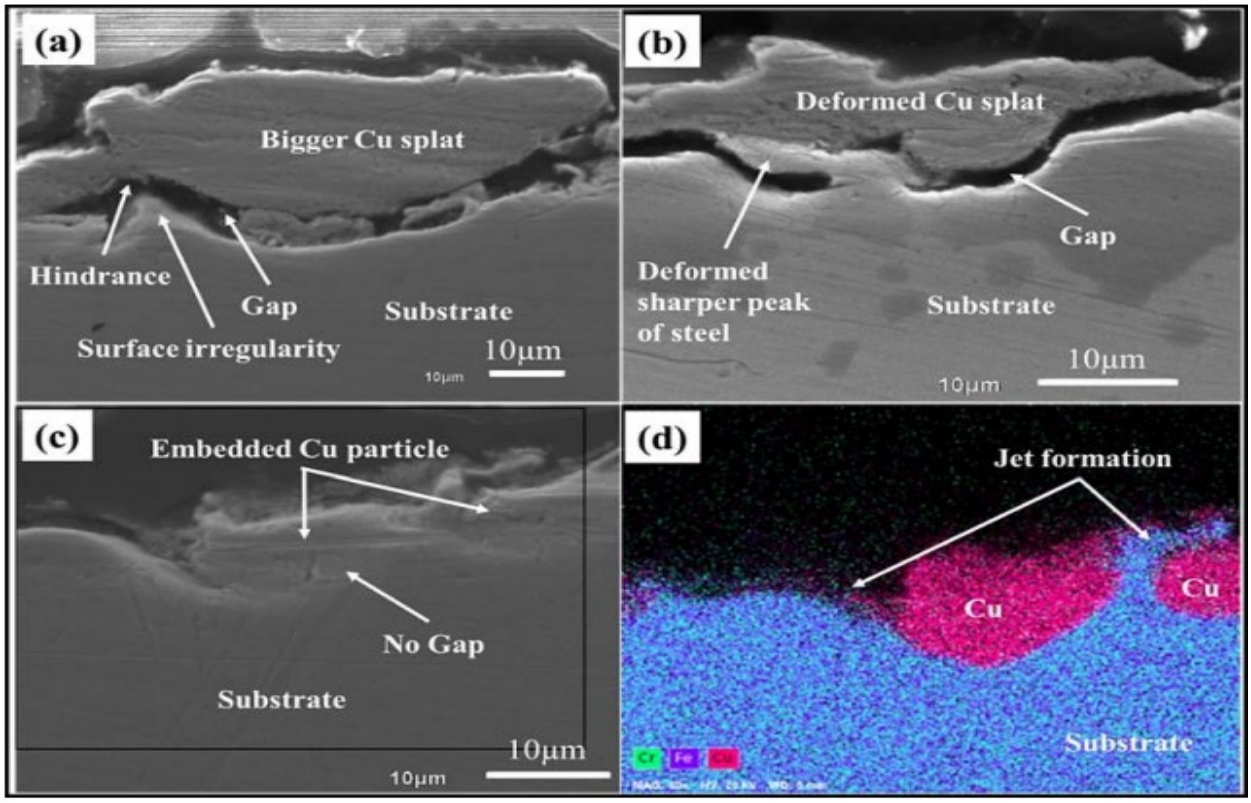

Figure 4.8: Cross-sectional SEM analysis of the high pressure cold sprayed single copper particles deposited on (a) as-received, (b) semi-polished, and (c) mirror-finished SS316L steel substrates, (d) EDS analysis of (c) [165].

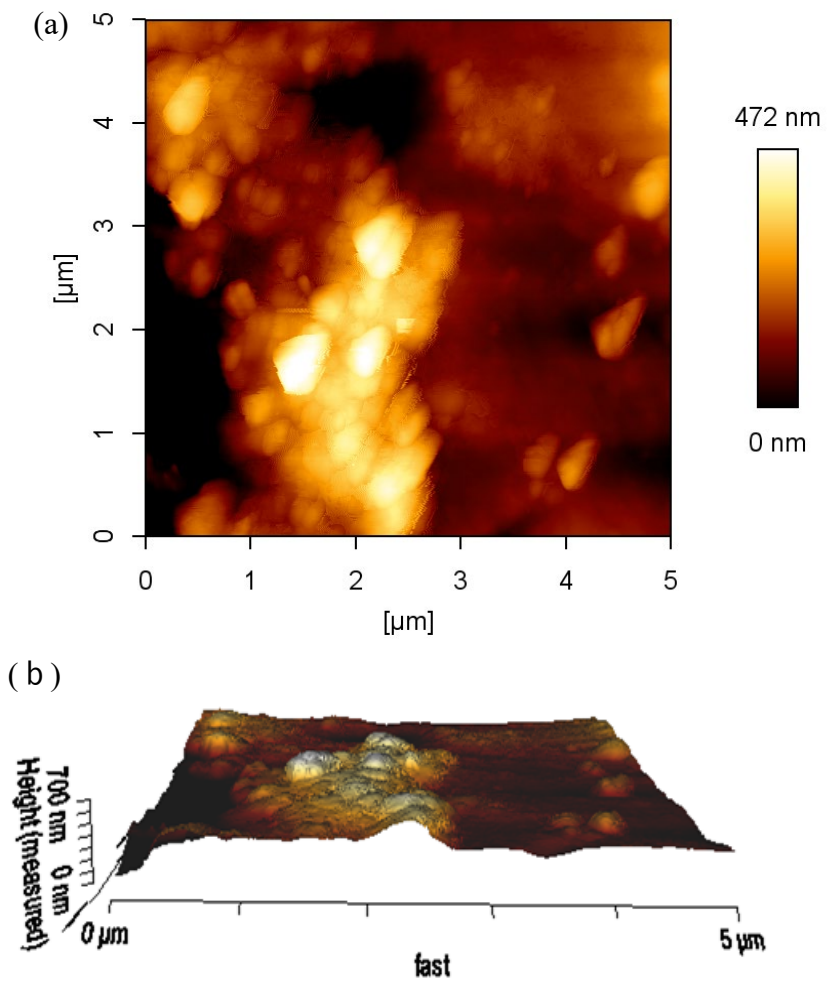

Figure 4.9: Oxide surface roughness for room temperature stainless steel (a) 2D (b) 3D.

Table 4.1: Oxide surface roughness analysis for room temperature stainless steel.

Physical size (µm)	5.000 x 5.000
Average value	1.248×10^{-16}
Average roughness Ra (nm)	87.65
RMS roughness Rq (nm)	115.60

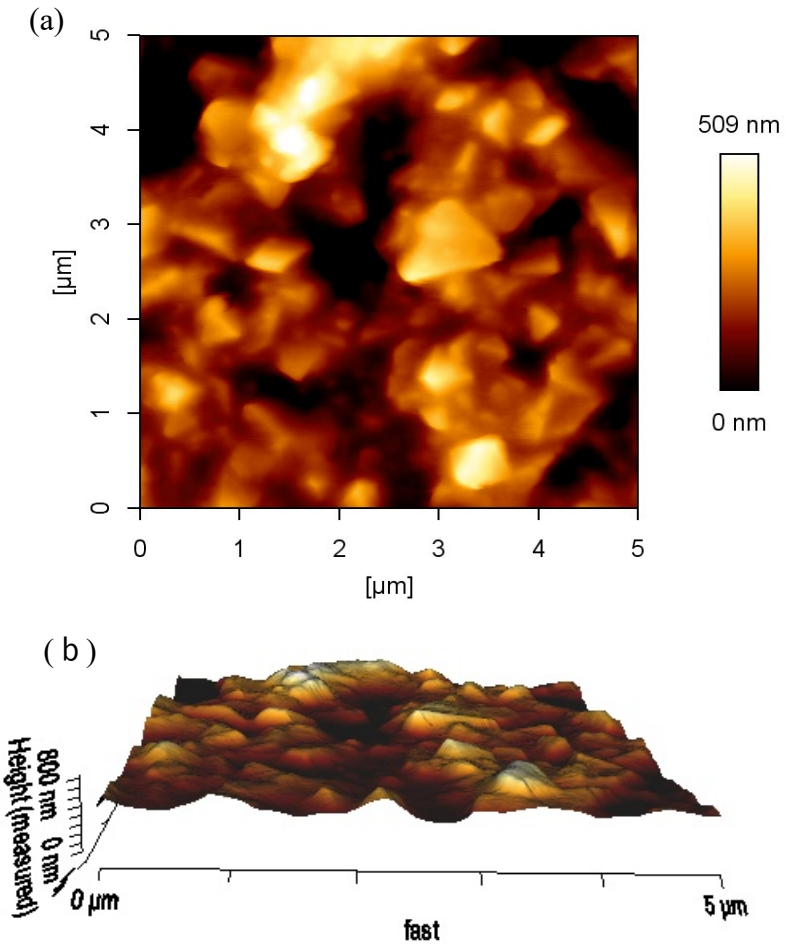

Figure 4.10: Oxide surface roughness for 1000°C annealed stainless steel (a) 2D (b) 3D.

Table 4.2: Oxide surface roughness analysis for 1000°C annealed stainless steel.

Physical size (µm)	5.000 x 5.000
Average value	-4.510×10^{-16}
Average roughness Ra (nm)	80.08
RMS roughness Rq (nm)	107.20

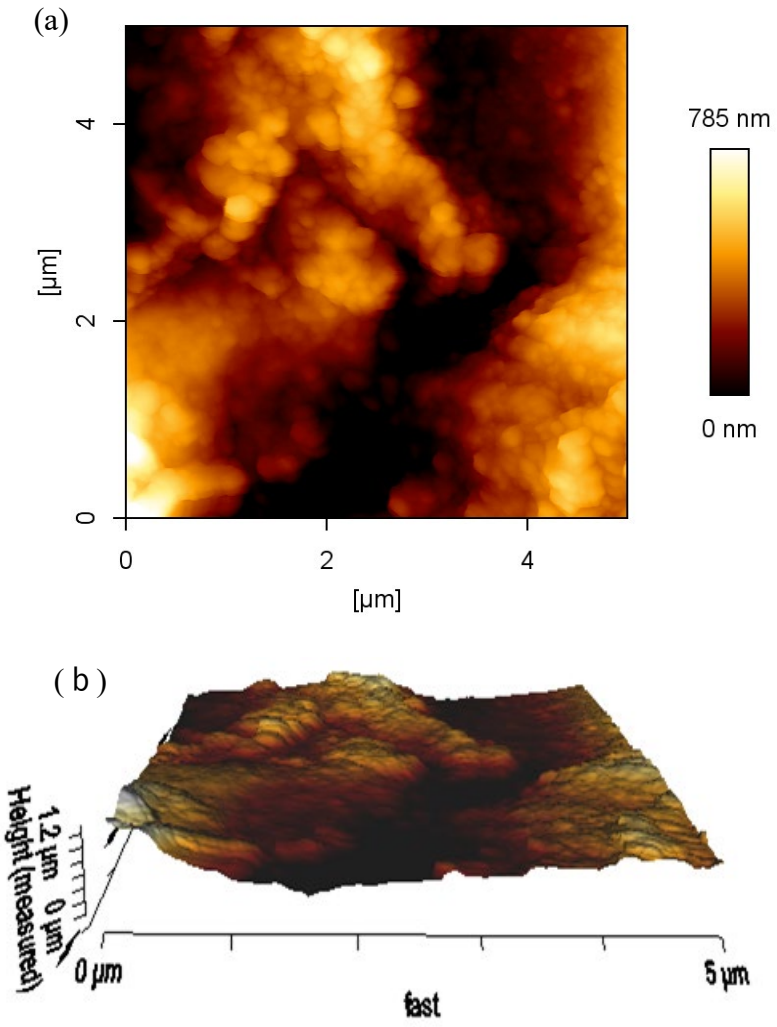

Figure 4.11: Oxide surface roughness for room temperature structural steel (a) 2D (b) 3D.

Table 4.3: Oxide surface roughness analysis for room temperature structural steel.

Physical size (µm)	5.000 x 5.000
Average value	3.600×10^{-17}
Average roughness Ra (nm)	146.1
RMS roughness Rq (nm)	178.3

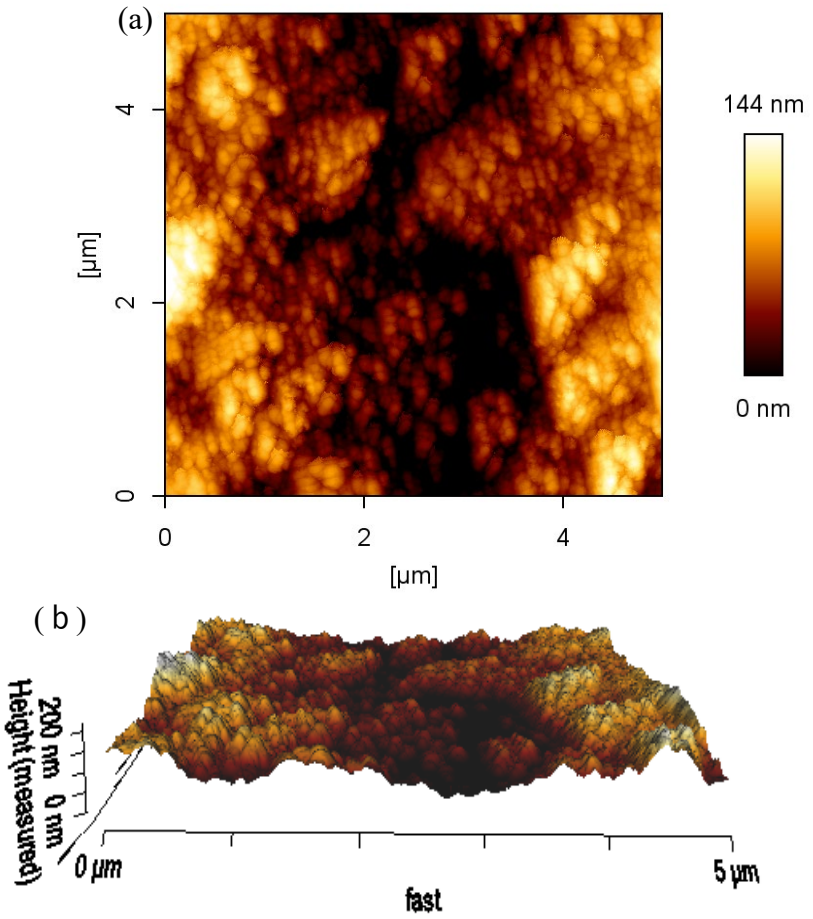

Figure 4.12: Oxide surface roughness for 400°C annealed structural steel (a) 2D (b) 3D.

Table 4.4: Oxide surface roughness analysis for 400°C annealed structural steel.

Physical size (µm)	5.000 x 5.000
Average value	1.440×10^{-16}
Average roughness Ra (nm)	26.45
RMS roughness Rq (nm)	32.68

4.2.4 Substrate hardness testing on annealed substrates

Figure 4.13 demonstrates the hardness of a hard metals substrate. Both steels showed a decreasing trend in substrate hardness as the annealing temperature was increased from room temperature to 1000°C annealed, 345.9 to 173.0 Hv for SUS304 and 170 to 114.8 Hv for SS400, respectively.

Based on the iron-carbon phase diagram, when the austenite steel is annealed at 1000ºC, which is above the eutectoid temperature of 727°C and slow cooled in the furnace using air medium, the phase transformation involved is austenite to pearlite (ferrite + cementite) [167]. This microstructure transformation is associated with a reduction of substrate hardness for 1000ºC annealed hard metals substrate and it becomes softer.

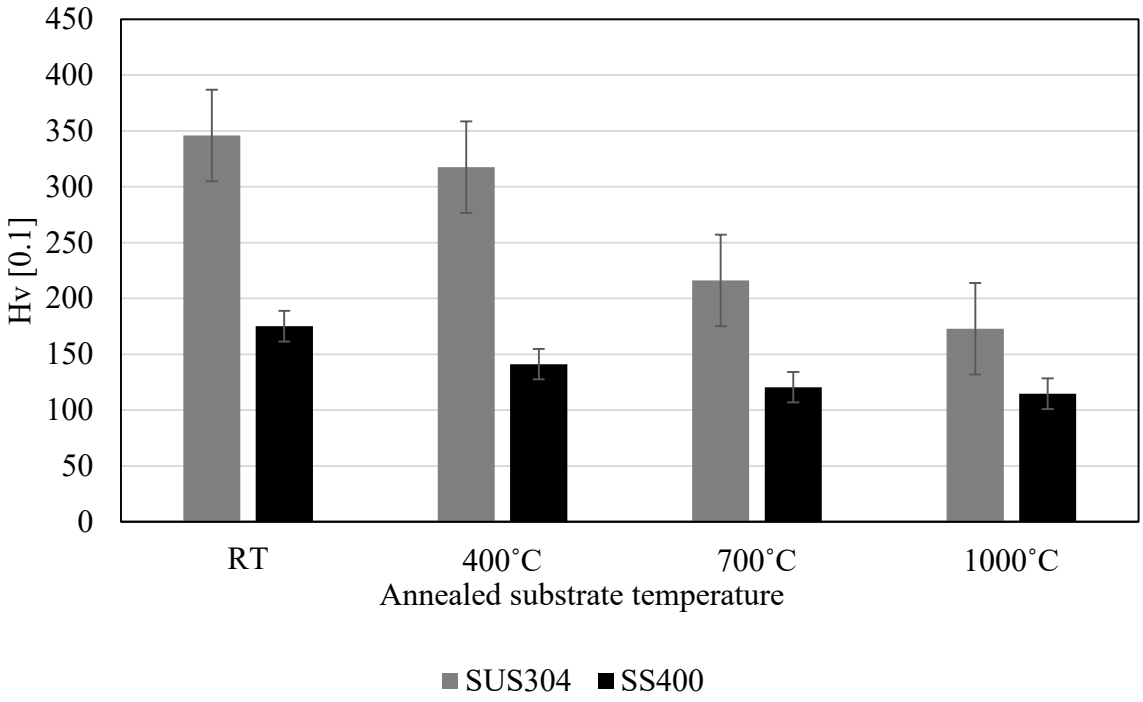

Figure 4.13: Annealed substrate hardness of SUS304 and SS400 from room temperature to 1000ºC annealed.

In cold spray, deformation of the substrate facilitates adiabatic shear instability, ASI and jet formation [140]. The formation of jets results in mechanical and metallurgical bonding at the interface [106]. Soft substrates (e.g., Al, Cu) are susceptible to higher deformation than hard substrates (e.g., ceramics, steels), hence, results in a better adhesion strength [89,166]. Studies have been made to attain good adhesion strength for hard substrates, out of which, substrate pre-heating is the most common strategy. However, Singh et al. [89] found that electroplating of the SS 316 substrate with a softer material such as Ni improved the adhesion strength of cold sprayed Cu coatings. Furthermore, Perton et al. [91] applied laser heat treatment prior to cold spray to improve the adhesion strength by reducing the substrate hardness. Wang et al. [92] found that a hard steel substrate induced high deformation onto the striking Al particles, which improved the cohesive strength in the coating nearer to the substrate. However, hard particles (Al_2O_3) were embedded inside the soft Al substrate, which led to strong interfacial bonding. Therefore, it can be concluded that the substrate hardness influences the coating properties significantly in the vicinity of the interface.

Our findings revealed that the TiO_2 coating on annealed SUS304 and SS400 increased as the annealing substrate temperature increased from room temperature to 1000°C for SUS304 and 400°C for SS400. This trend must be associated with substrate deformation in order to be related to mechanical or metallurgical bonding at the interface [106]. In our case, no substrate deformation occurred on hard metals substrate, so there was no possibility of mechanical anchoring factor that contributed from substrate hardness in hard metals substrate bonding mechanism. Another set of substrate properties, such as oxide thickness and oxide composition, must be defined.

4.2.5 Substrate depth profile of oxide layer by XPS on annealed substrates

The depth analysis of the oxide layer by X-ray photoelectron spectroscope for hard metals substrate is shown in figures 4.14 to 4.15 for SUS304 from room temperature to 700° C annealed and SS400 from room temperature to 400° C annealed. This shows that the stainless steel oxide layer thickens as the substrate's annealing temperature rises.

Kim et al. used kinetic spraying of single titanium particles on mirrored steel substrates. They showed that some portion of a thin amorphous oxide remained between the particle–substrate interface, and even a severe plastic deformation was associated with the impacts of the particles onto the substrate. The remaining oxide provided a bond between a particle or particle–substrate [196]. Ko et al. [146] reported the amorphization of oxide layer and atomic intermixing phenomena at the interface of Cu/AlN and Al/ZrO_2 bonding couples. The authors attributed bonding between metal and ceramic to chemical adhesion.

Our findings show that as the oxide thickness on the substrate surface increases, so does the coating adhesion strength of TiO_2 on hard metals (annealing substrate temperature increasing). Substrate chemical composition was performed to better understand how substrate oxide influences the bonding mechanism involved.

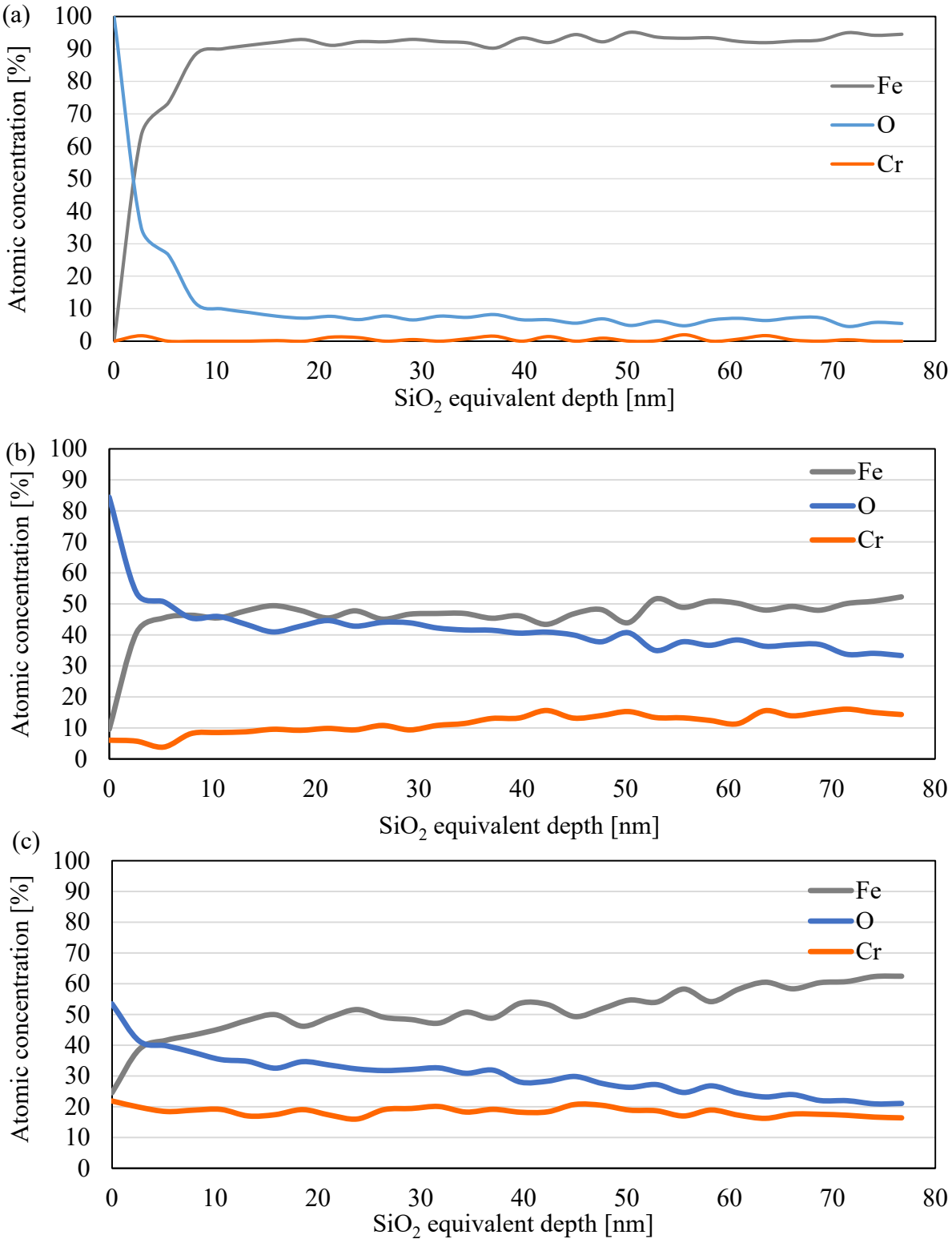

Figure 4.14: Depth profile analysis of SUS304 (a) room temperature (b) 400˚C annealed and (c) 700˚C annealed.

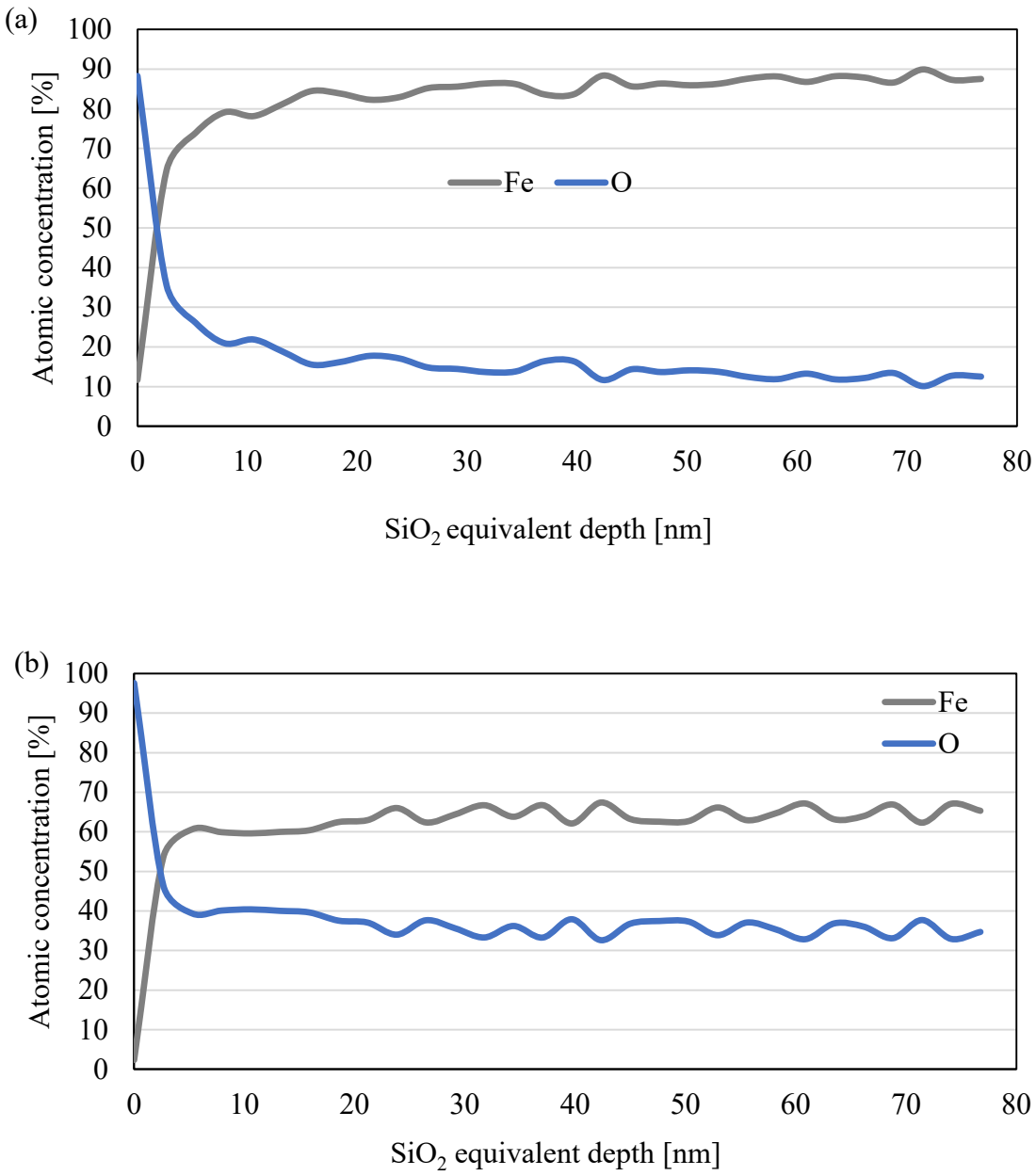

Figure 4.15: Depth profile analysis of SS400 (a) room temperature and (b) 400˚C annealed.

4.2.6 Substrate chemical composition of oxide layer by XPS

The chemical composition of the oxide layer for hard metals substrate is depicted in Figures 4.16 and 4.17. The $2P_{3/2}$ atomic orbital satellite peak was used to determine the chemical state of ferum and chromium in SUS304, as shown in figures 4.16 (a) to (c) (c). Figure 4.16 depicts the peak position of the iron metal for stainless steel at approximately 706.7eV [197] in the outermost surface of the room-temperature substrate SUS304 (a). In the meantime, at annealing temperatures of 400 and 700°C for SUS304 substrate, the peak position of hematite Fe_2O_3 (Fe^{2+}) was detected at the outermost surface of the substrates, at approximately 709.3 eV [197]. This indicates that the chemical composition of SUS304 substrate changed from Fe metal state in room temperature substrate to hematite condition in 400 and 700˚C annealed.

Figures 4.16 (b) show that the peak position of chromium metal at 574.0 eV [198] was prominent in the oxide layer of SUS304 room-temperature substrates. However, the peak position of Cr_2O_3 at 576.0 eV was present throughout the outermost surface of the oxide layer for the SUS 304 substrate at annealing temperatures of 400 and 700°C [198]. This indicates that the chemical composition of the SUS304 substrate changed from Cr metal state at room temperature to chromium oxide condition when annealed at 400 and 700°C.

Figure 4.16 (c) the peak position of the hydroxide, OH^- is indicated between 531-532 eV as indicated by red-dotted line [198]. This result indicates that one of the major components of the oxide layer at 400 and 700°C for SUS304 is mixture of Fe_2O_3 and Cr_2O_3 and hydroxide.

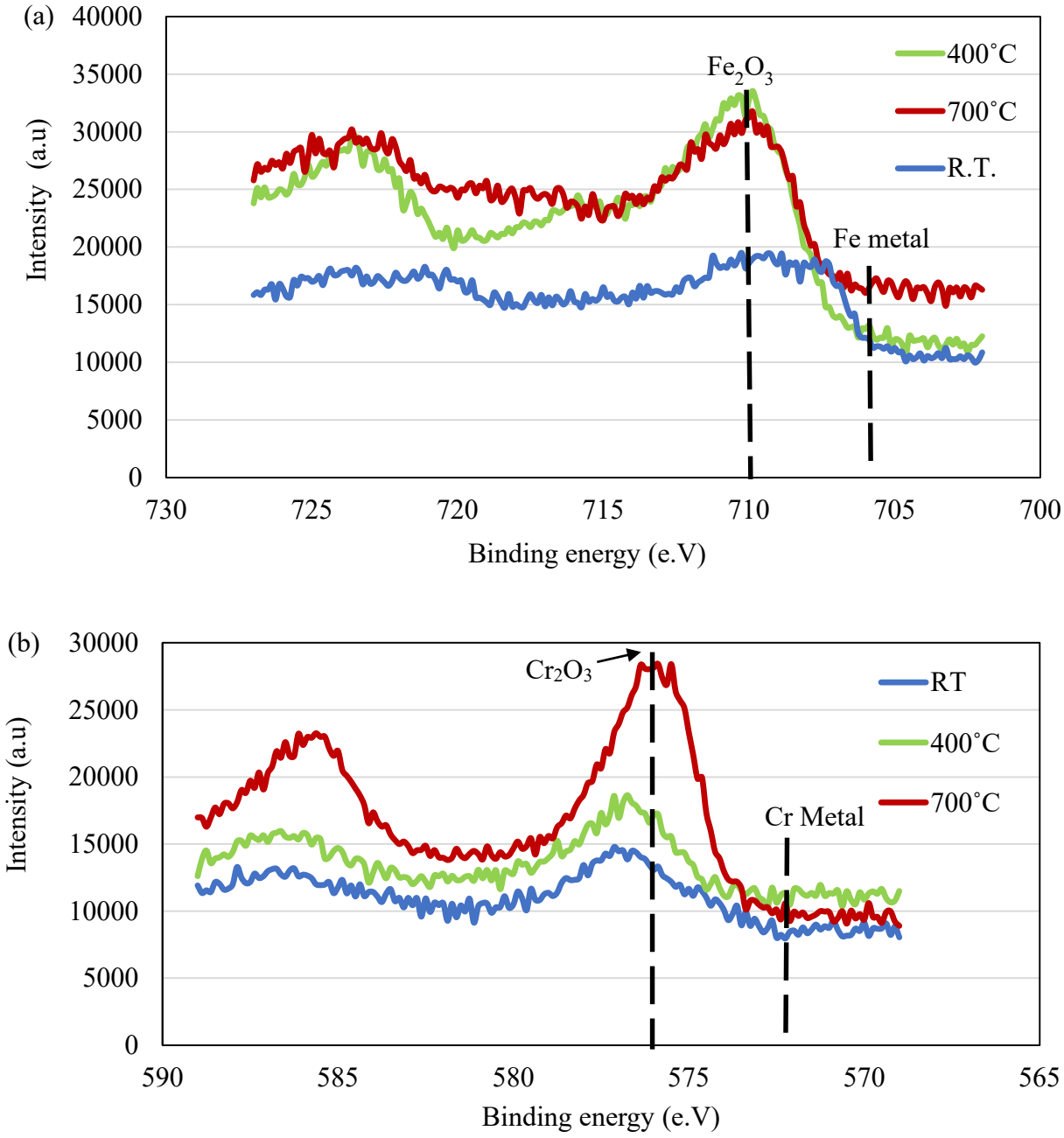

Figure 4.16: XPS spectra for SUS304: (a) Iron and (b) Chromium.

(c)

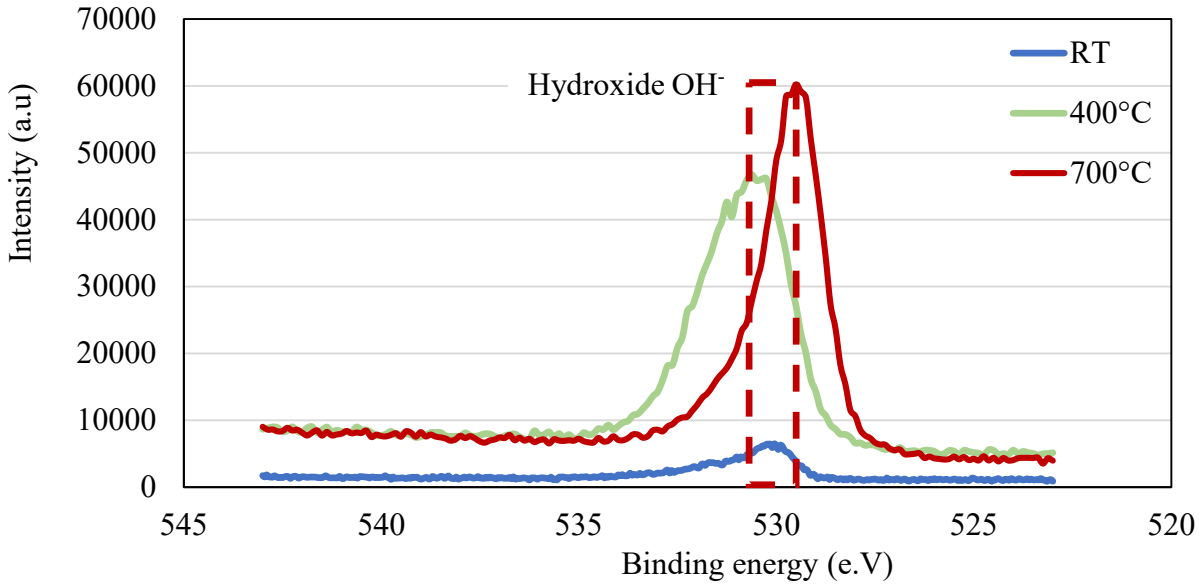

Figure 4.16: XPS spectra for SUS304: (c) O1s.

Figure 4.17 (a) depicts the peak position of the iron metal for structural steel at approximately 706.7eV [197] in the outermost surface of the room-temperature substrate SS400. In the meantime, at annealing temperatures of 400°C for SS400 substrate, the peak position of hematite Fe_2O_3 (Fe^{2+}) was detected at the outermost surface of the substrates, at approximately 709.3 eV [197]. This indicates that the chemical composition of SS400 substrate changed from Fe metal state in room temperature substrate to hematite condition in 400˚C annealed. Figure 4.17 (b) the peak position of the hydroxide, OH^- is indicated between 531-532 eV as indicated by red-dotted line [198]. This result indicates that one of the major components of the oxide layer at 400°C for SS400 is mixture of Fe_2O_3 and hydroxide.

The mechanisms of cold sprayed of metal particles on ceramics or glass involve more factors such as chemical properties of the impact particles and substrates. Song et al [199] cold sprayed Al particle on glass substrate. The interlayer with thickness of 80nm between impacted Al particle and glass substrate was composed of an amorphous phase and nano-crystalline grains with significant Na enrichment. The layer is considered to form as a result of the reaction between the impacted Al and the glass substrate, which took place due to the temporal high temperature during impact, which produced liquid phases at the interface. It is believed that the high affinity of Al with oxygen in the glass substrate enabled the relatively strong adhesion observed.

Our coating adhesion strength on hard metals substrate have a good agreement with Song et al. report. In order to further clarify how chemical composition of oxide layer on substrate surface influence toward bonding mechanism involved, single particle study or wipe test was conducted.

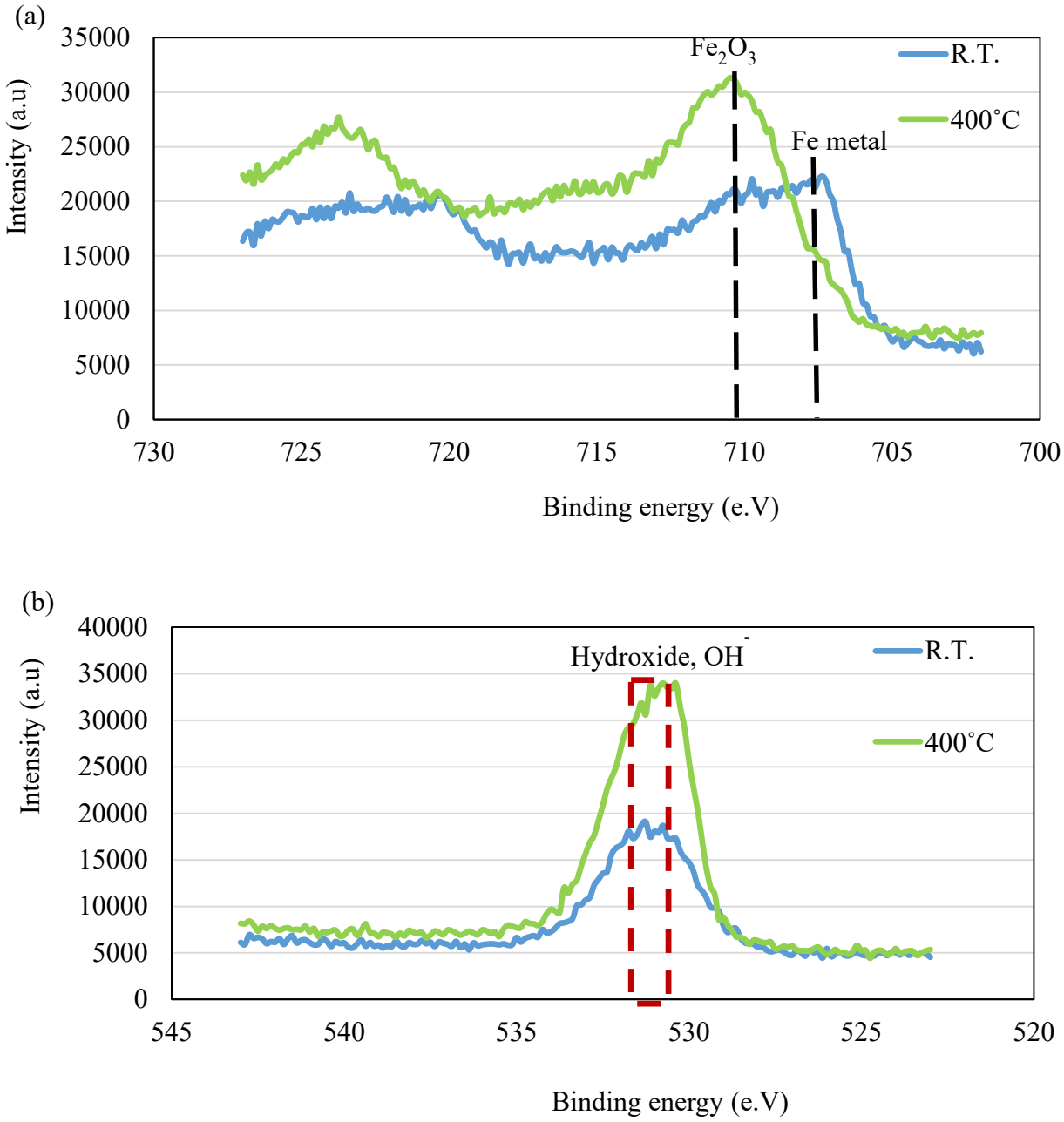

Figure 4.17 : XPS spectra for SS400 : (a) Iron and (b) O 1s.

4.3 TiO_2 single particle deposition on annealed substrates

4.3.1 FIB splat TiO_2 particle on 400°C and 1000°C annealed hard metal substrates

Figures 4.18 and 4.19 show the FIB results of TiO_2 particles on an annealed hard metals substrate. Figure 4.18 (a) depicts a top view of a TiO_2 particle impacted on annealed SUS304 at 1000°C with no crater formation on the substrate surface. As shown in Figure 4.18, the TiO_2 particle remained unchanged after the collision, and the substrate surface of the 1000°C annealed SUS304 showed little to almost no deformation due to impacting during the cold-spraying process (b). Figures 4.19 (a) and (b) show that when TiO_2 particles are impacted on 400°C annealed SS400, there is no crater formation or deformation of the annealed substrate.

A previous study undertaken by Trompetter et al. demonstrated that for a solid particle impacting on a substrate, the substrate hardness played a significant role in the as-produced solid particles [158]. Bae et al. [115-116] analysed four representative particle/substrate combinations, namely Al/Al (soft/soft), Ti/Ti (hard/hard), Al/mild steel (soft/hard), and Ti/Al (hard/soft). As for the impact cases of dissimilar materials Al/mild steel as shown by figure 4.20. In particular, the initial kinetic energy of the particle is mostly dissipated into plastic deformation of the softer counterpart; therefore, a much higher temperature on the soft side is achieved.

TiO_2 particle has less hardness [159] compared to hard metals substrate. When cold sprayed TiO_2 particle impacted on hard metals substrate, the kinetic energy of the particle is mostly converted into plastic deformation[116] and it result of no substrate deformation occur. In cold spray, deformation of the substrate facilitates adiabatic shear instability, ASI and jet formation [140]. Mechanical and metallurgical bonding occurs at the interface as a result of jet formation [106].

Our findings show that there is no substrate deformation, but coating adhesion strength increases as the annealing substrate temperature rises. It is obvious that mechanical or metallurgical bonding is not the bonding factor in play. TEM analysis and line analysis were performed to further investigate factors related to the bonding mechanism of TiO_2 coating on hard metals substrate.

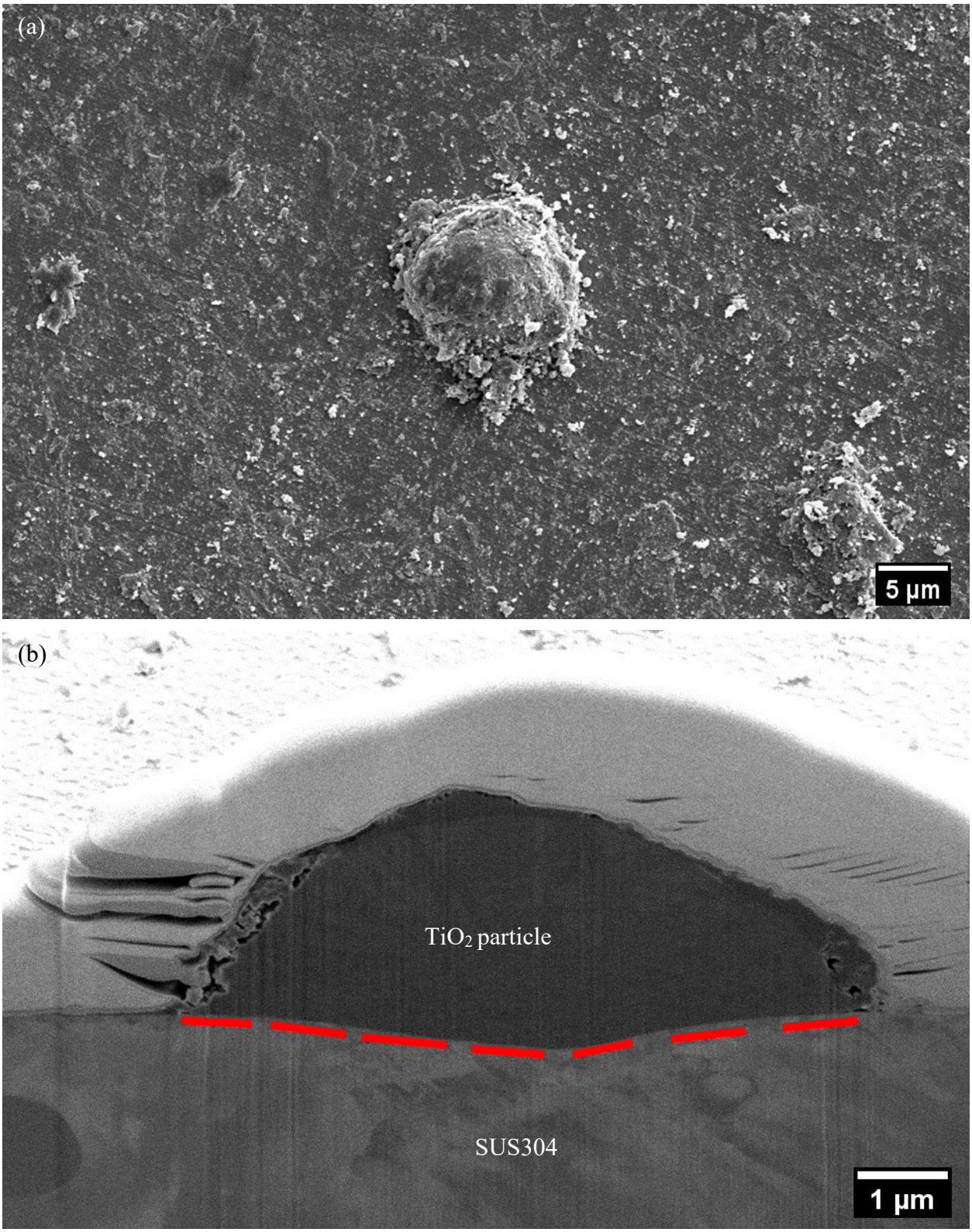

Figure 4.18: TiO_2 particle on 1000˚C annealed SUS304 (a) top view (b) cross-sectional

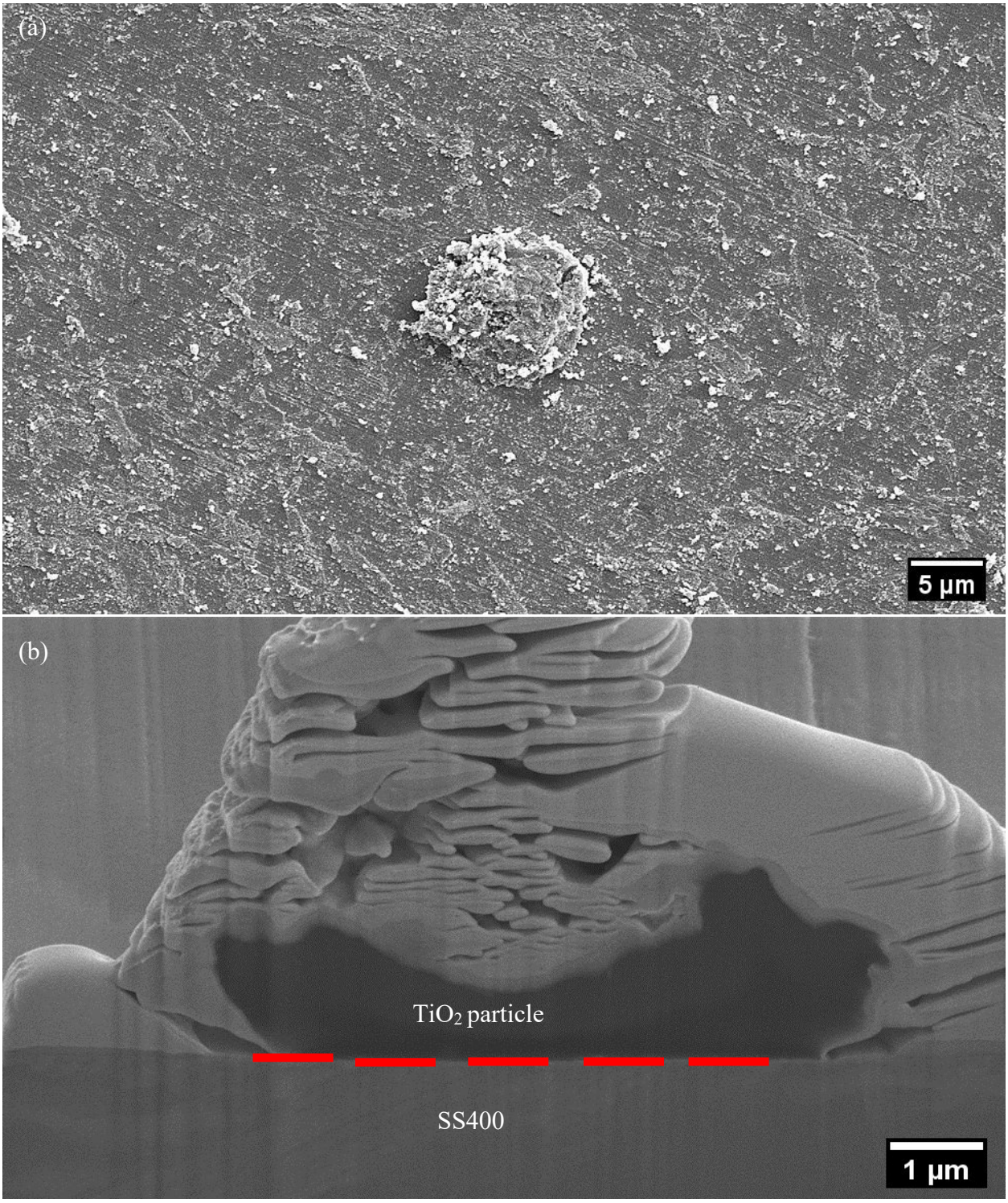

Figure 4.19: TiO_2 particle on 400˚C annealed SS400 (a) top view (b) cross-sectional.

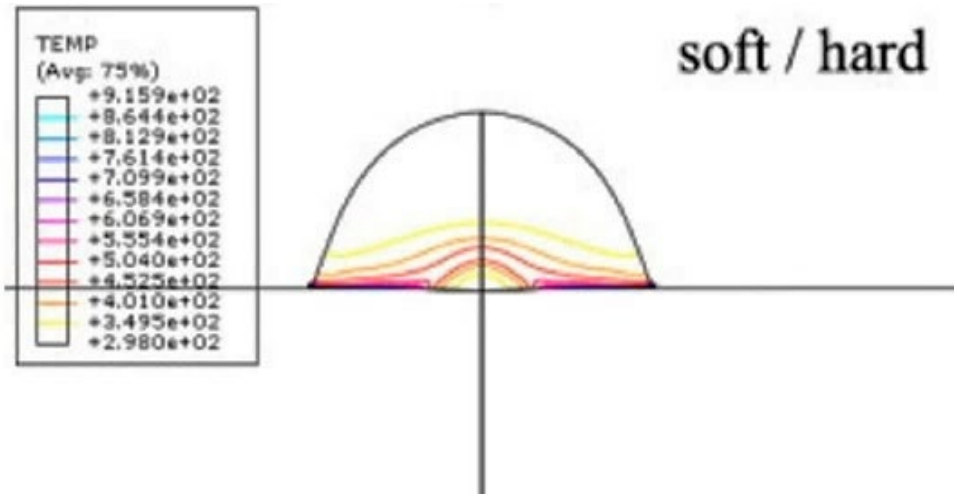

Figure 4.20: Impact process simulation for different material combination: Al/mild steel (soft/hard) [96,115-116].

4.3.2 TEM analysis on interface oxide layer between TiO_2 particle on 400°C and 1000°C hard metal substrates

Figure 4.21 to 4.24 shown as the STEM and high magnification images of the interlayer region between single-particle TiO_2 and annealed hard metals substrate. It confirms the existence of the remaining interface oxide layer after the cold-sprayed TiO_2 impacted on hard metals substrate by FFT pattern that showed an amorphous phase at interlayer, with a thickness of approximately 10nm for SUS304 and SS400 as shown by figure 4.22 and 4.24, respectively.

Kim et al. used kinetic spraying of single titanium particles on mirrored steel substrates. They showed that some portion of a thin amorphous oxide remained between the particle–substrate interface, and even a severe plastic deformation was associated with the impacts of the particles onto the substrate. The remaining oxide provided a bond between a particle or particle–substrate [196].

In order to further understand the bonding mechanism involved, TEM line analysis was conducted on room temperature and 400 and 1000°C hard metals substrate.

Figure 4.21: STEM of the TiO_2 / 1000°C annealed SUS304 at the interlayer area.

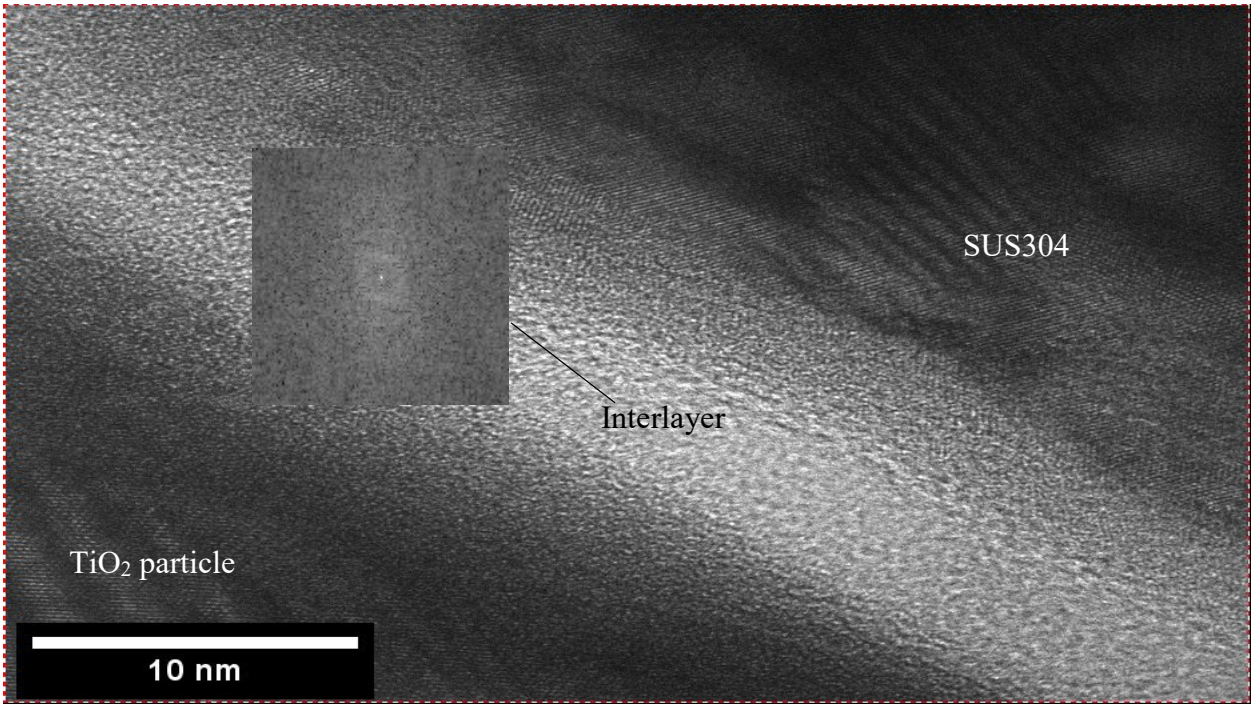

Figure 4.22: High-magnification images of the TiO_2 / 1000°C annealed SUS304 at the interlayer area and a FTT image on the oxide layer.

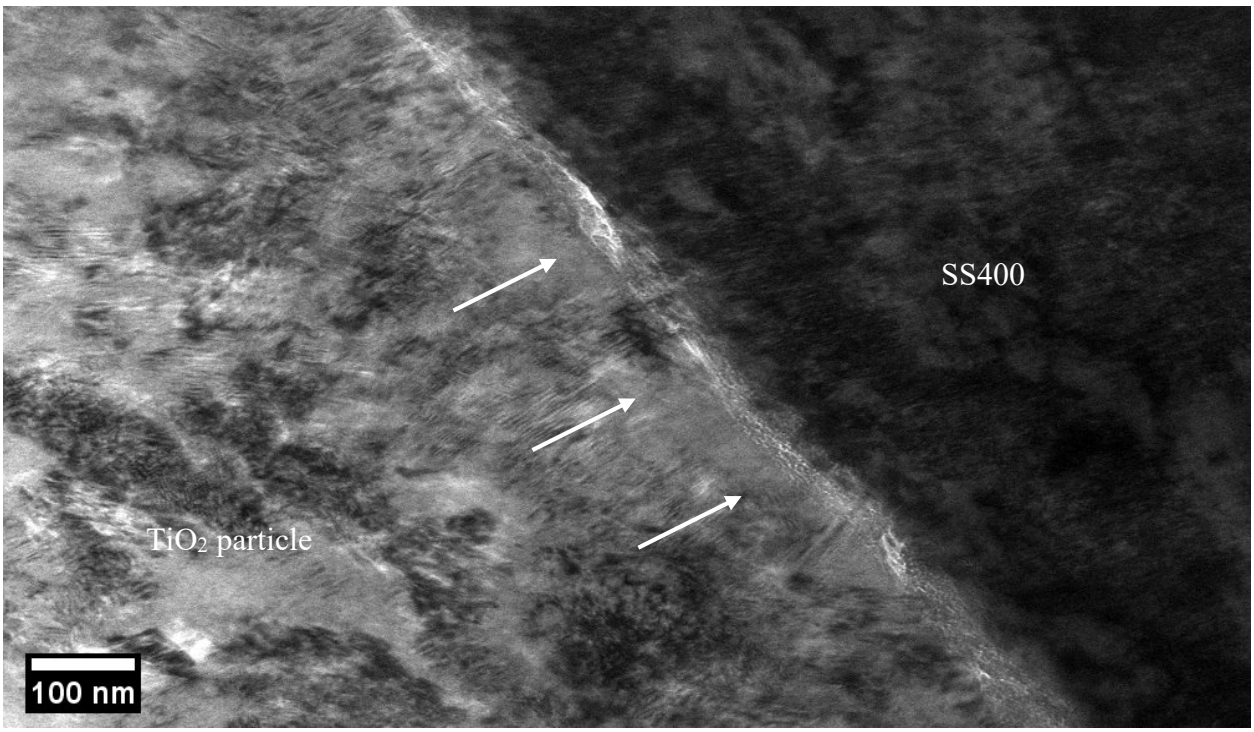

Figure 4.23: STEM of the TiO_2 / 400ºC annealed SS400 at the interlayer area.

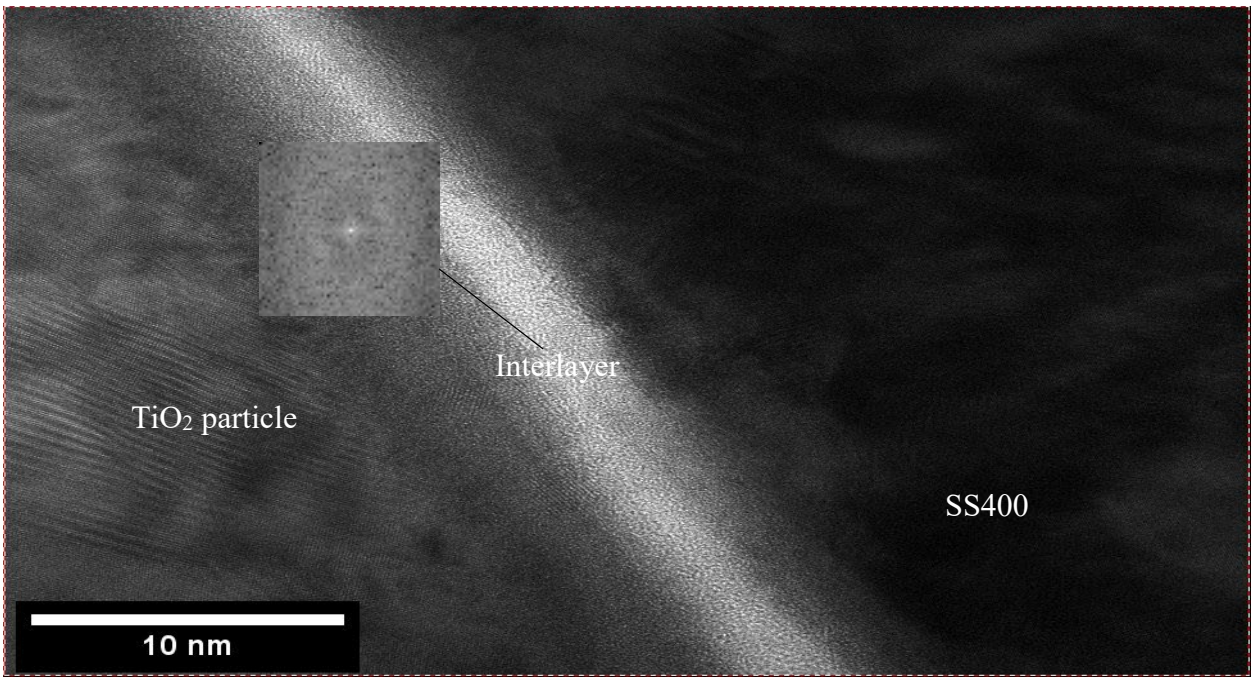

Figure 4.24: High-magnification images of the TiO_2 / 400ºC annealed SS400 at the interlayer area and a FTT image on the oxide layer.

4.3.3 TEM line analysis on TiO_2 particle on room temperature and annealed hard metal substrates

Figure 4.25 to 4.27 are the TEM line analysis result of single particle TiO_2 on room temperature and 1000˚C annealed SUS304 and 400°C annealed SS400, respectively. It confirms the existences of the atomic of Ti,O and Cr on room temperature and 1000°C annealed SUS304. On the other hands, 400ºC annealed SS400, the existences of Ti and O are presented on substrate surface. Ti and O atomic on the hard metals substrate area are contributed by TiO_2 coating and hydroxide on the substrate surface. Chromium, Cr atomic on SUS304 contributed from oxide layer on substrate surface that Cr metal on room temperature substrate and mixture of Fe_2O_3+ Cr_2O_3 and OH^- annealed at 1000°C. SUS304 had the highest trend in coating adhesion strength when annealed at 1000°C. Cr_2O_3 oxide may play an important role in the bonding mechanism. According to Song et al [199], the mechanisms of cold sprayed metal particles on ceramics or glass involve additional factors such as chemical properties of the impact particles and substrates. Drehmann et al. [200] investigated the effect of substrate pre-heating on the adhesion strength of Al particles on an AlN substrate (soft and hard). As-sprayed specimens were subsequently annealed to further enhance the adhesion strength. Adhesion strength increased with an increase in the temperature of the AlN substrate prior to spray. An additional thermal energy input due to pre and post-spray heating induced atomic mobility at the Al-AlN interface. Additionally, deformation-induced recrystallization (Figure 4.28) near the interface facilitated atomic mobility. Atomic mobility at the interface minimized the grain orientation misfit of the coating material with the substrate; hence resulting in better adhesion strength.

Pure chromium was chosen as a substrate to further investigate the role of Cr_2O_3 oxide toward bonding mechanism involved in hard metals substrate.

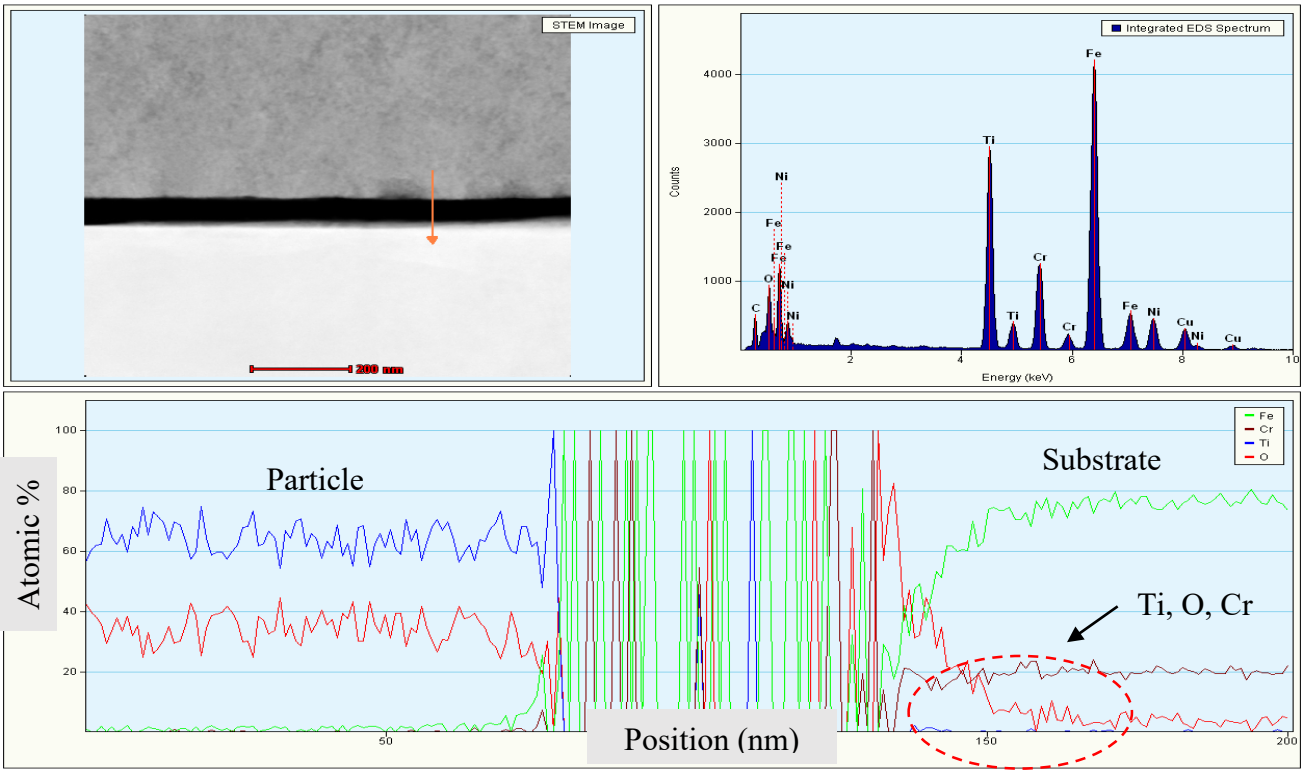

Figure 4.25: TEM line analysis of the TiO_2 on room temperature SUS304.

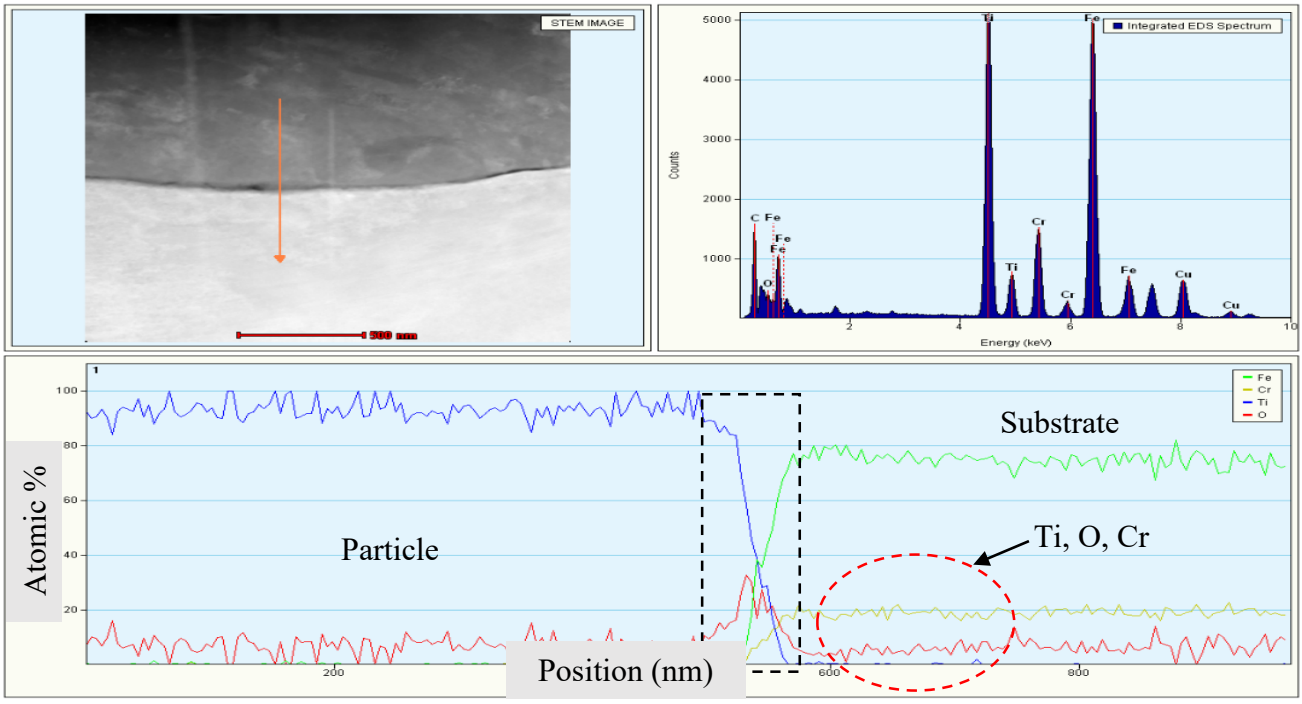

Figure 4.26: TEM line analysis of the TiO_2 on 1000ºC annealed SUS304.

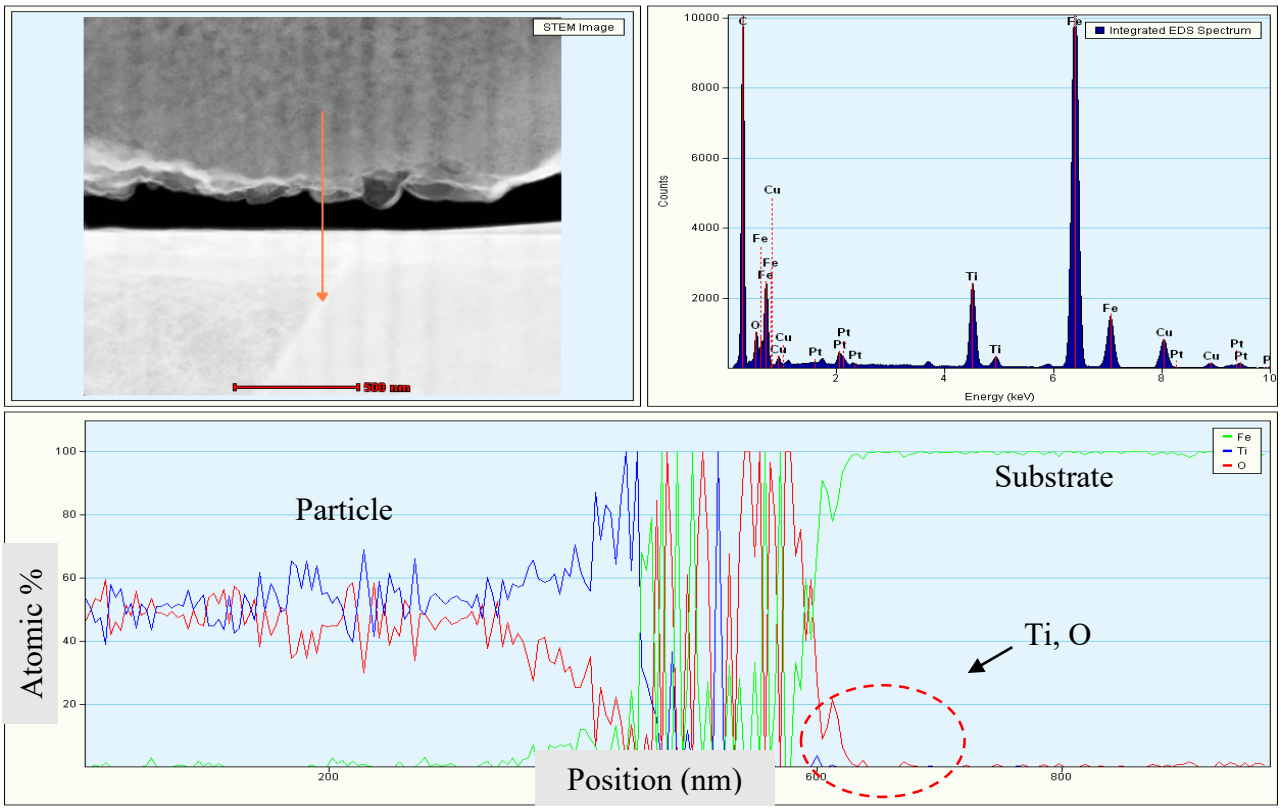

Figure 4.27: TEM line analysis of the TiO_2 on 400ºC annealed SS400.

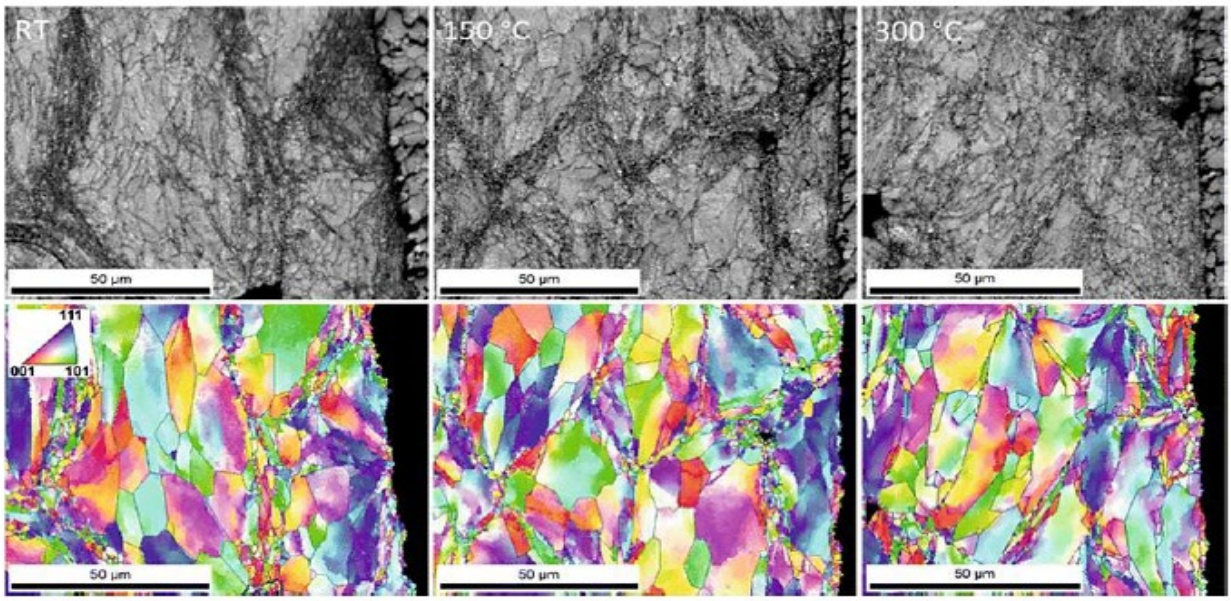

Figure 4.28: SEM and EBSD images of cold sprayed Al on AlN substrate representing recrystallization at the particle-particle and particle substrate interface in relation to substrate pre-heating temperature [200].

4.4 Influence of annealed pure chromium on bonding mechanism of hard metal substrates

4.4.1 Introduction

Chromium coatings have been used for decorative and functional purposes in a wide range of industrial applications that include automotive, aerospace, energy, and manufacturing industries. Traditional chromium coatings have been prepared by commercial electroplating technique which show excellent properties including resistance to wear and corrosion, a low friction coefficient, high hardness, and lustrous surface appearance [201]. Recently, the development of thin chromium (Cr) coatings for the zirconium-alloy fuel cladding material in light water reactors (LWRs) has drawn considerable attention in nuclear industries and research institutions. Cr has been investigated as coating material for accident-tolerant fuel cladding by improving high-temperature air and steam oxidation resistance in accident conditions without significant modifications of the current LWR design. Given the critical requirements for the nuclear reactor application, several methods have been investigated to deposit Cr coatings on Zr-alloys [201-203].

One promising coating technology for depositing Cr on Zr alloys for LWR fuel cladding with demonstrated success is the cold spray process [204]. In the cold spray process, microns sized feedstock powder is propelled at supersonic velocities (Mach 2–3) on to the surface of a substrate using pressurized gas flowing through a converging/diverging nozzle system. The particle temperature is low and the deposition occurs in solid state. Above a certain particle velocity (i.e., critical velocity), a dense and adherent coating/deposit can potentially form on the substrate due to high-strain-rate plastic deformation of particles and an associated adiabatic shear mechanism [118]. Since the particle temperature is low and the particles have a very short residence time in

the carrier gas stream, the deposits are relatively free of secondary phases and oxide inclusions, and are strongly adhered to the substrate [204].

Substrate properties such as material characteristics, hardness, temperature, and degree of oxidation play a major role during the bonding between particles and substrate. The pure chromium substrate was chosen for this chapter to clarify its role in the TiO_2/ stainless steel bonding mechanism.

4.4.2 Adhesion strength testing and fracture surface analysis on annealed substrates

Figure 4.29 depicts the adhesion strength of a cold-sprayed TiO_2 coating on annealed pure chromium. The TiO_2 coating on the annealed Cr substrates demonstrated an increased trend in adhesion strength from room temperature to 700°C, with values ranging from 0.71 to 1.44 MPa, and then decreased to 0.48 MPa when annealed at 1000°C.

The EDS analysis and spectrum on fracture coating of TiO_2 at room temperature and 700°C annealed pure chromium are shown in Figures 4.30 to 4.33. In comparison to room temperature pure chromium, a large portion of pure chromium 700°C annealed embedded on fracture coating of TiO_2. Further investigations on pure chromium substrates was carried out to better understand the role of Cr_2O_3 in the stainless steel bonding mechanism.

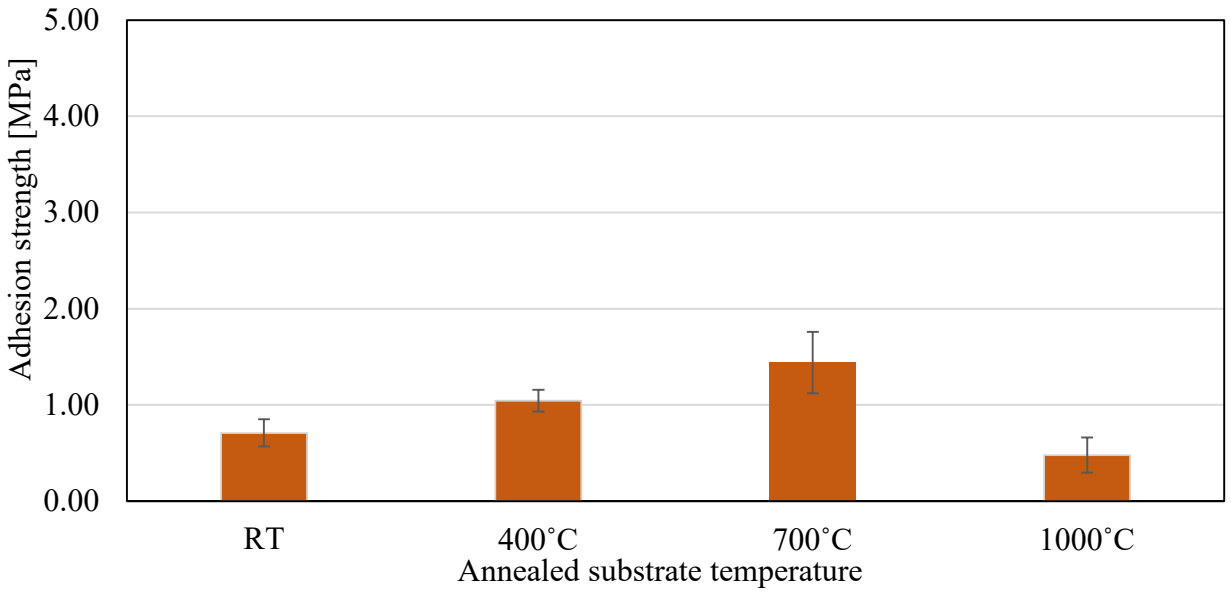

Figure 4.29: Adhesion strength of the TiO_2 coating on pure chromium from room temperature to 1000˚C annealed.

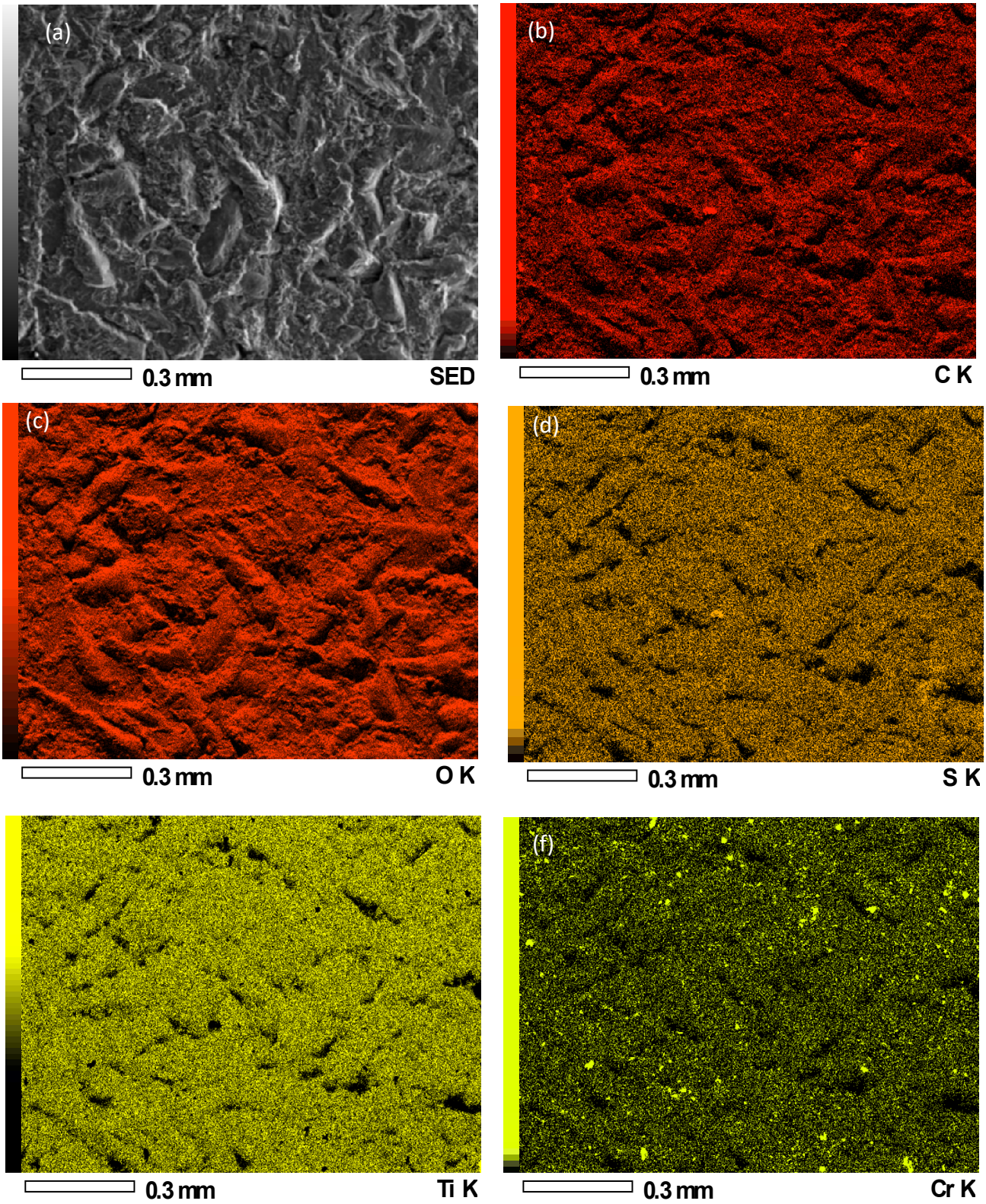

Figure 4.30: EDX on fracture coating (a) SEM image (b) Carbon (c) Oxygen (d) Sulfur (e) Titanium (f) Chromium for room temperature pure chromium substrate.

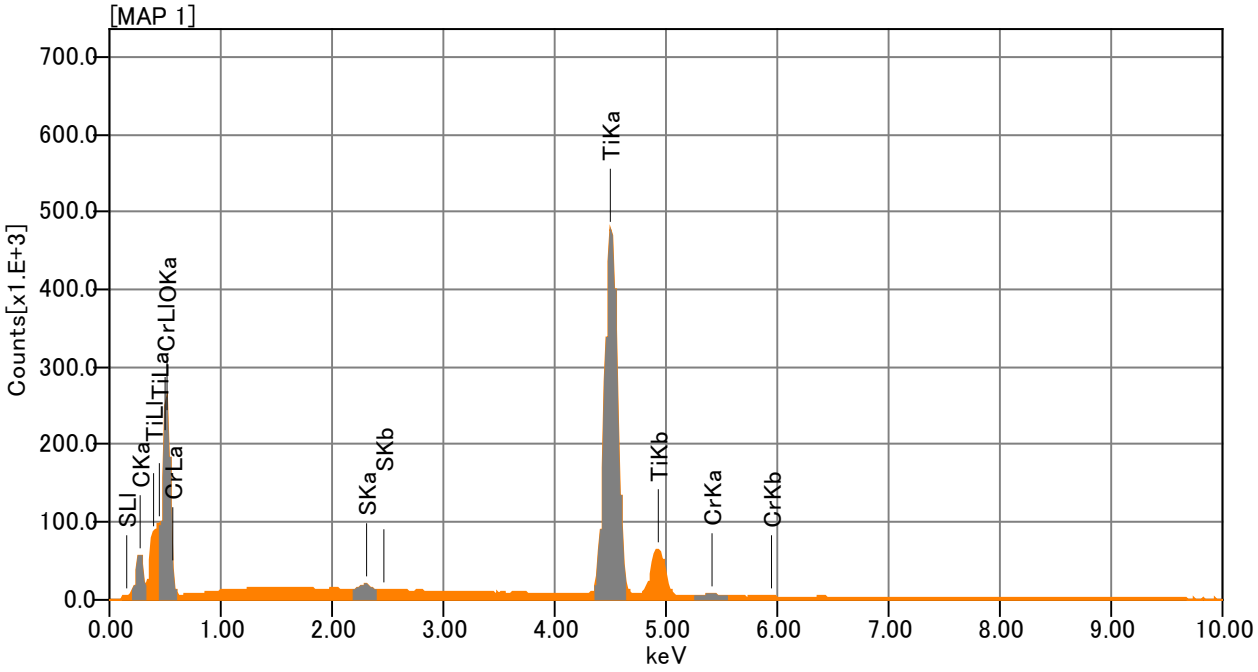

Figure 4.31: EDX spectrum on fracture coating of room temperature pure chromium substrate.

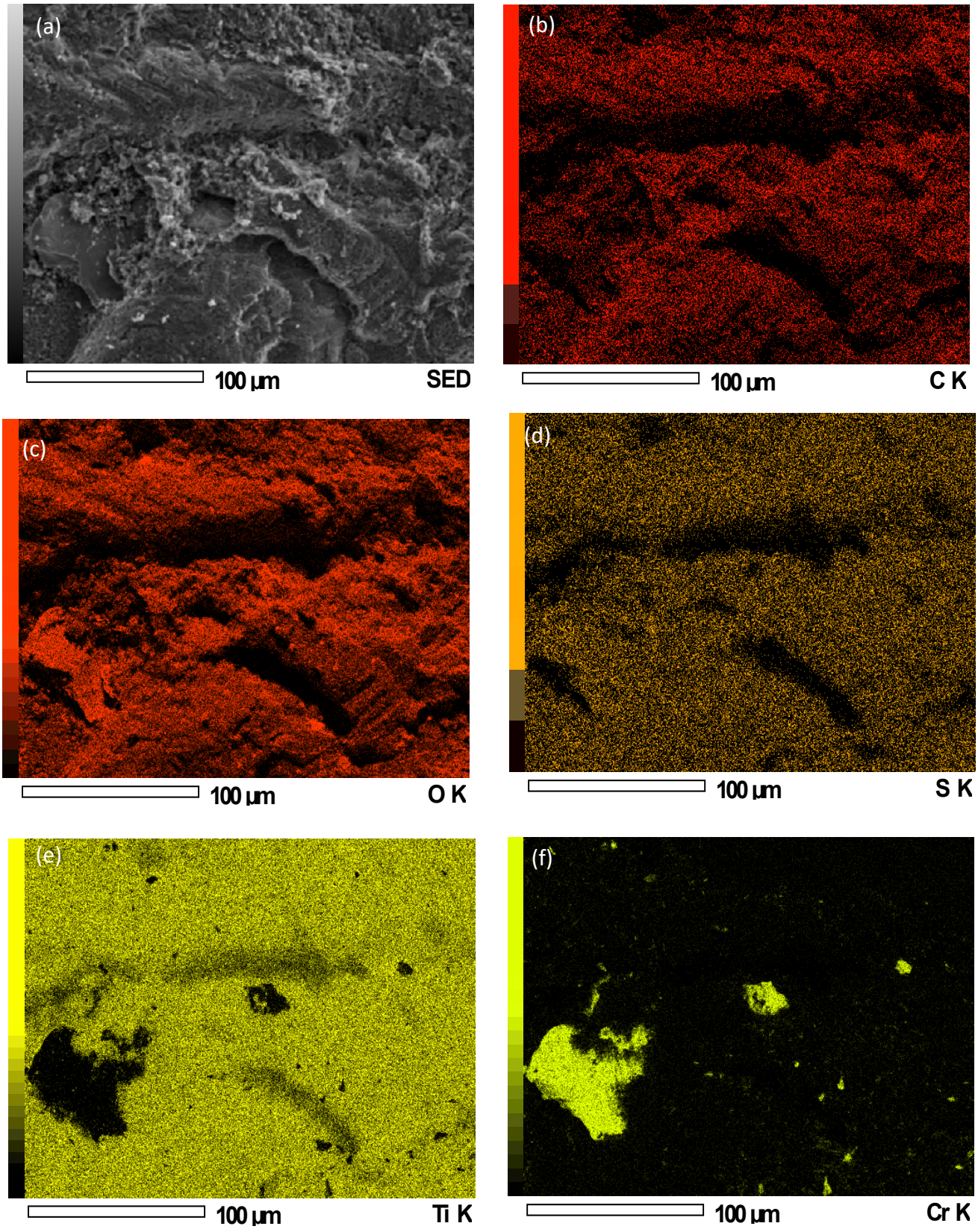

Figure 4.32: EDX on fracture coating (a) SEM image (b) Carbon (c) Oxygen (d) Sulfur (e) Titanium (f) Chromium for 700°C annealed pure chromium substrate.

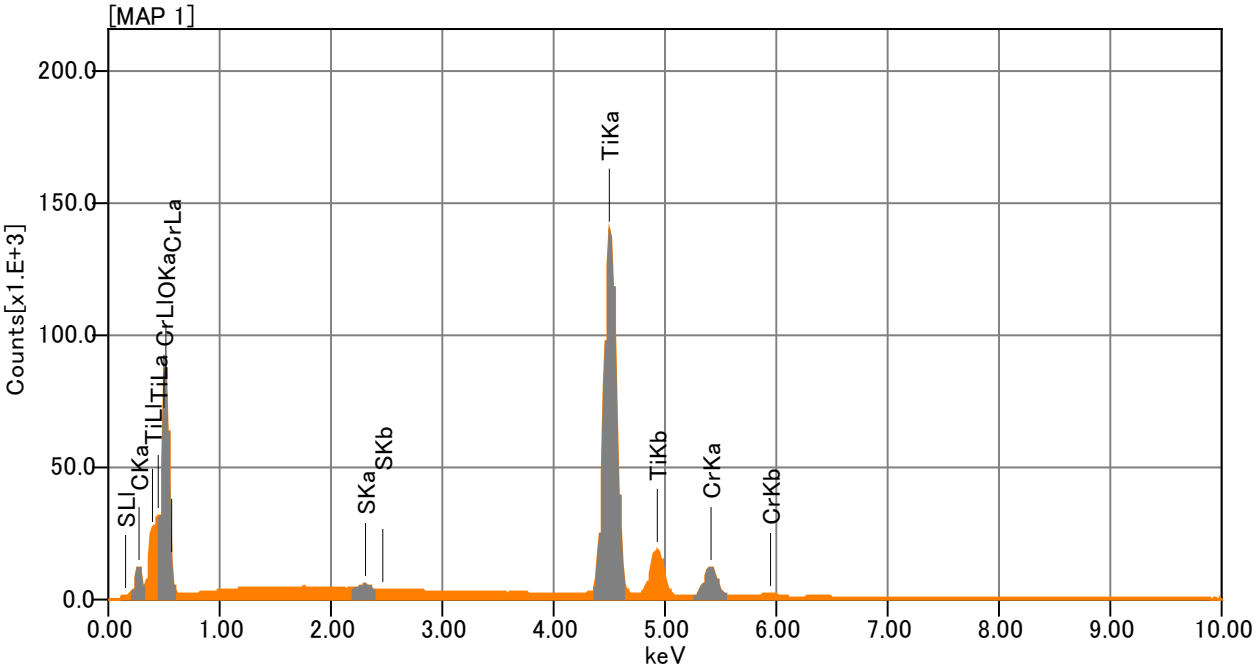

Figure 4.33: EDX spectrum on fracture coating of 700°C annealed pure chromium substrate.

4.4.3 Substrate hardness testing on annealed substrates

Figure 4.34 shows the substrate hardness of pure chromium from room temperature to 1000°C annealed. This figure showed a decrease trend of annealed substrate hardness from 265 Hv to 179.7 Hv at 700°C annealed and increased back to 192.1 Hv at 1000°C annealed. Pure chromium is a bcc metal that inherently brittle at room temperature due to the limited number of primary dislocation slip systems in the crystal structures [205-206]. When exposed to high temperature (T > 1000°C), embrittlement can also be induced via formation of brittle subnitride underneath the oxide scale [207-208]. This explains why pure chromium annealed substrate hardness at 1000ºC showed a little increased trend. To relate annealed pure chromium hardness with coating adhesion strength trend on SUS304 from room temperature to 1000°C annealed, no correlation can be made. Therefore, investigations of oxide properties in term of oxide thickness and chemical composition were carried out.

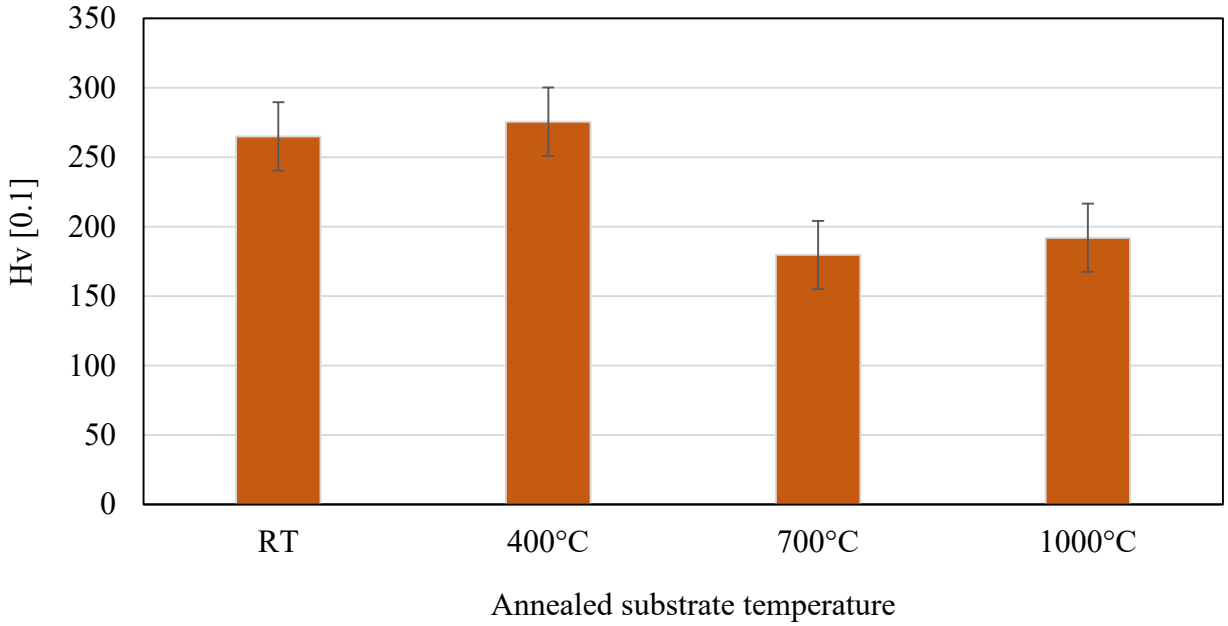

Figure 4.34: Annealed substrate hardness of pure chromium from room temperature to 1000˚C.

4.4.4 Substrate depth profile of oxide layer by XPS on annealed substrates

Figure 4.35 (a) to (d) depicts the concentration of oxygen and chromium in the substrates as a function of depth. The data show that the concentration of oxygen in the near-surface region increases with annealed temperature. This indicates that the pure chromium oxide layer thickens as the annealing substrate temperature rises. Coating adhesion strength increased from room temperature to 700°C annealed and decreased back to 1000°C annealed as oxide thickness increased on pure chromium annealed substrate. It was discovered that the oxide properties of Cr_2O_3 from room temperature to 700°C have an effect on the bonding mechanism involved. As a result, the chemical composition of the oxide was studied further.

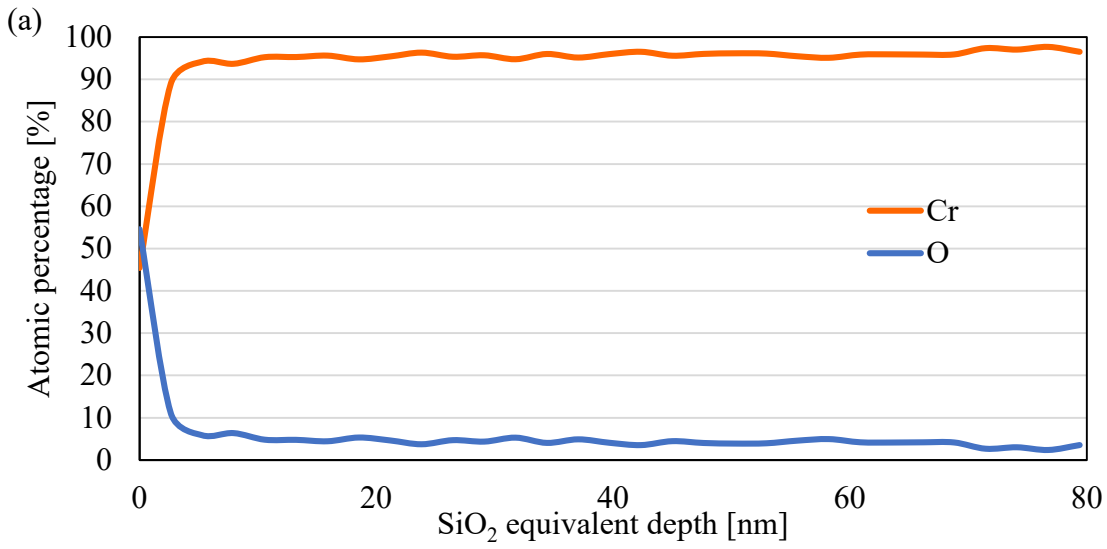

Figure 4.35: Depth profile analysis of pure chromium (a) room temperature.

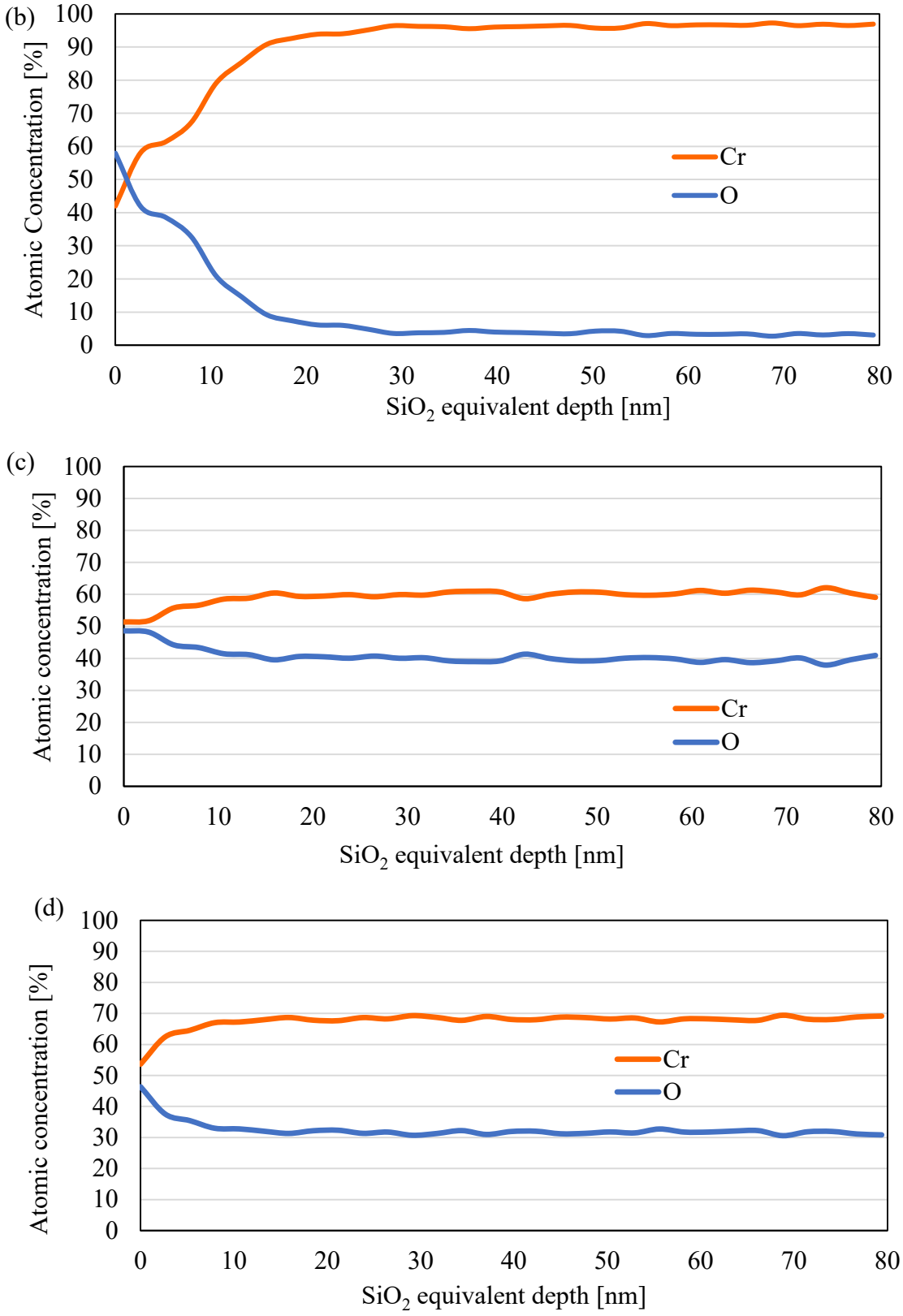

Figure 4.35: Depth profile analysis of pure chromium (b) 400°C annealed (c) 700˚C annealed and (d) 1000˚C annealed.

4.4.5 Substrate chemical composition of oxide layer by XPS

Figures 4.36 (a) and (b) show that the chemical state of chromium and oxygen for pure chromium.

The position of chromium metal at 574.0 eV was prominently present in the oxide layer for the room-temperature substrates for pure chromium. However, at the annealing temperature of 400, 700 and 1000°C substrate, the peak position of Cr_2O_3 at 576.0 eV [209] was present throughout the outermost surface of the oxide layer for the pure chromium substrate as shown by Figure 4.35 (a). This result indicates that the major components of the oxide layer at 400, 700 and 1000 °C for pure chromium is Cr_2O_3. Figure 4.36 (b) showed that hydroxide also present on outermost surface on room temperature to 700°C annealed, where the peak position is 531-532 eV[209] as indicated by red-dotted line. Metal oxide is present on outermost surface on 1000°C annealed where the peak is 530 eV [209].

Based on our findings, hydroxide, OH^- that exist at room temperature to 700°C annealed pure chromium play a significant role in the increased trend of coating adhesion strength as annealing temperature increases. Pure chromium, Cr_2O_3, and metal oxide are present on the substrate surface after 1000°C annealing. This could account for the decreasing trend in coating adhesion strength on 1000°C pure chromium.

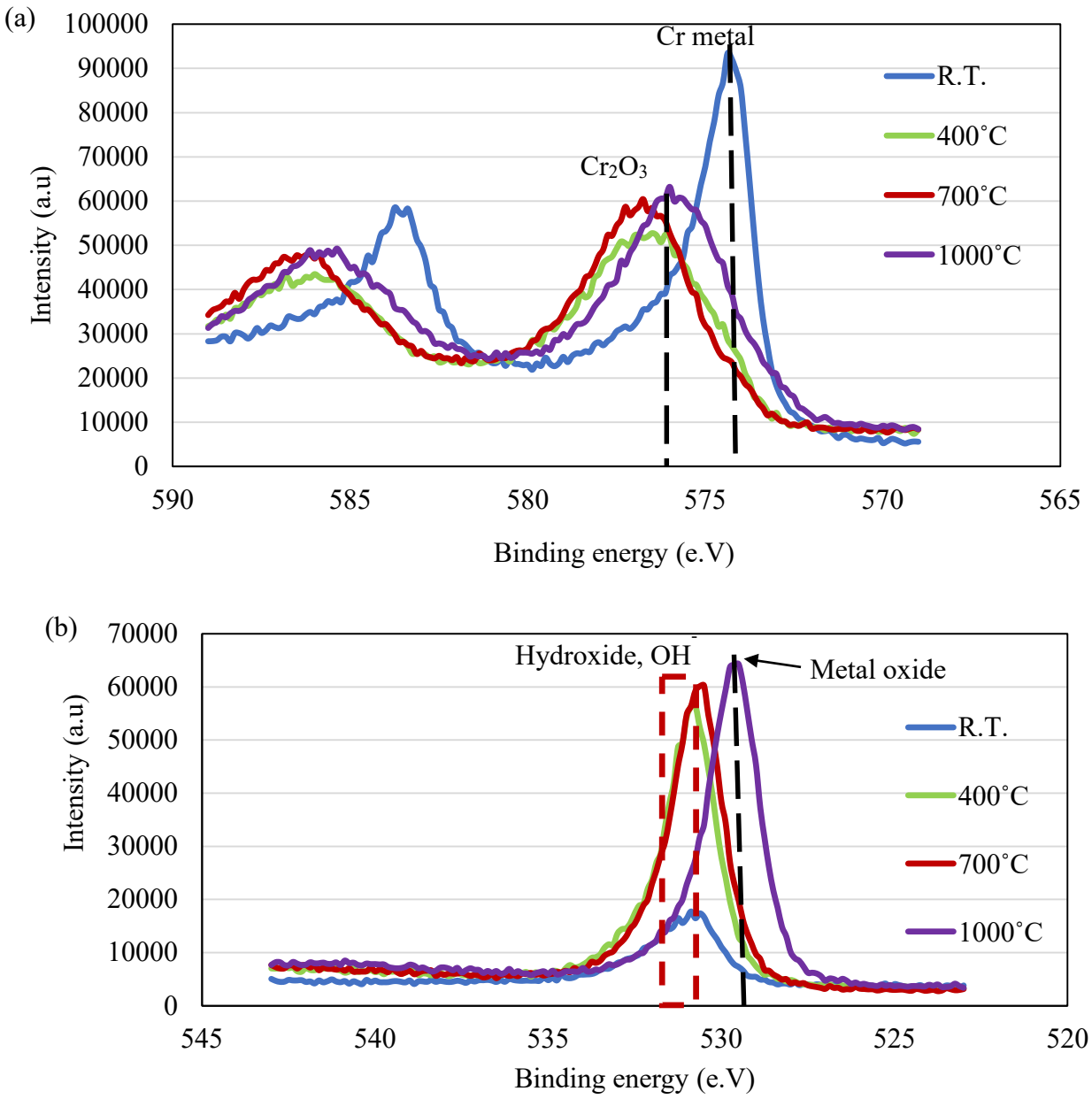

Figure 4.36: XPS spectra for pure chromium: (a) Chromium and (b) O1s.

4.5 Discussion

Coating adhesion strength of TiO_2 onto hard metals substrate showed an increased trend as annealing substrate temperature is increased as shown by figure 4.1. Figure 4.2 and 4.3 shows the image of the fractured surface of substrate and TiO_2 coating after tensile strength test was conducted on SUS304 and SS400. This image confirms that the fracture was interfacial fracture of substrate and coating, thus, proving that strong cohesive bond between TiO_2 particles had been achieved during the coating formation process. EDS mapping on fracture coating on annealed SUS304 showed that a small part of the ferum is embedded on the TiO_2 coating and it same goes with SS400 as shown by figure 4.4 and 4.5,respectively.

In order to further understand coating adhesion strength trend on hard metals substrate, microstructure investigation is conducted via SEM analysis as shown by figure 4.6 and 4.7. The images show that dense coatings with a thickness around 300 μm could be obtained on all substrate conditions of hard metals substrate, meaning that a critical velocity was achieved for these materials. The spray particles require a certain amount of energy in combination with a critical velocity at an optimum temperature, for effective bonding to occur [118,138,161]. Coating of brittle materials (ceramic powder) on hard-interfaces (a hard-on-hard interface), the effect of residual stresses on the coating properties, and delamination of thick coatings remain technical challenges [149,210-211].

Delamination and poor adhesion strength of soft-on-hard (TiO_2/steel) and hard-on-hard (Titanium/steel) interfaces are of great concern for industries such as the marine, nuclear, aerospace, automotive and electronics. Thus, understanding the mechanism of bonding can address the issue of poor adhesion and delamination, which would assist the advanced manufacturing

sector.

Our result showed a good contact between TiO_2 coating and substrate surface in room temperature and annealed substrate. The adhesion strength of cold spray coatings with the substrate is not only based on mechanical interlocking. It is determined also by adiabatic shear instability, plastic deformation of the colliding materials and static recrystallization [173,106,172,108-109]. All these factors are attributable to substrate conditions such as hardness, material chemistry, surface roughness and temperature of the substrate. The substrate conditions significantly affect the bonding features and properties of the cold-sprayed coatings[50,164]. Therefore, substrate analysis were conducted to further understand bonding mechanism involved for hard metals substrate.

The roughness of the substrate's surface is important in the bonding mechanism at the interface [15]. Figures 4.9,4.10.4.11, and 4.12 show a decreasing trend in oxide surface roughness as annealed substrate temperature increases for both hard metals substrate. Tables 4.1 to 4.4 show the mean oxide surface roughness values for both hard metals substrate.

The surface roughness of the substrate plays a prominent role in the bonding mechanism at the interface. However, there are contradicting reports on the effect of substrate roughness concerning adhesion for soft-on-soft interfaces. For instance, Hussain [187] reported that smoother substrate surfaces are best for good adhesion strength, whereas, Ghelichi and Guagliano [210] had a conflicting report. Similarly, Kumar et al. [54] found that semi-polished substrates were ideal for achieving the best adhesion for a Cu on steel combination. Similar trends in adhesion strength were observed by Theimer et al. [113] for brass on steel combinations.

The mechanical interlocking and the metallurgical bonding are believed to be the main internal bonding mechanisms in cold spray [117]. The mechanical bonding consists of non-chemical interactions, in which the harder particles are mechanically trapped by the soft substrate material to form a mutual interlocking [117]. In our case, soft particle where impacted on hard substrates and our findings showed a reversed trend as oxide surface roughness is decreased, coating adhesion strength is an increased with the increasing annealing temperature. One of the reason to explain this situation is our feedstock powder, agglomerated TiO_2 powder containing pure anatase crystalline structure with an average particle size of about 7.55 μm, is impacted on annealed hard metals substrate covered with oxide surface roughness in nanoscale. The large different between TiO_2 particle and oxide surface roughness on hard metals substrate, made the effect of oxide surface roughness is negligible. Therefore, mechanical interlocking that contributed from surface roughness factor is not the main bonding mechanism here.

The substrate conditions significantly affect the bonding features and properties of the cold-sprayed coatings [50,165]. In particular, the substrate roughness and hardness are the main influencing parameters in the cold spray bonding [135]. As a result, an investigation of annealed substrate hardness properties was carried out in order to better understand the bonding mechanism involved in TiO_2 bonding on hard metals substrate. Figure 4.13 demonstrates the hardness of a hard metals substrate. Both steels showed a decreasing trend in substrate hardness as the annealing temperature was increased from room temperature to 1000°C annealed, 345.9 to 173.0 Hv for SUS304 and 170 to 114.8 Hv for SS400, respectively. Based on the iron-carbon phase diagram, when the austenite steel is annealed at 1000ºC, which is above the eutectoid temperature of 727°C and slow cooled in the furnace using air medium, the phase transformation involved is austenite

to pearlite (ferrite + cementite) [167]. This microstructure transformation is associated with a reduction of substrate hardness for 1000ºC annealed hard metals substrate and it becomes softer.

In cold spray, deformation of the substrate facilitates adiabatic shear instability, ASI and jet formation [86-87]. The formation of jets results in mechanical and metallurgical bonding at the interface. Soft substrates (e.g., Al, Cu) are susceptible to higher deformation than hard substrates (e.g., ceramics, steels), hence, results in a better adhesion strength [88-89]. Studies have been made to attain good adhesion strength for hard substrates, out of which, substrate pre-heating is the most common strategy. However, Singh et al. [89-91] found that electroplating of the SS 316 substrate with a softer material such as Ni improved the adhesion strength of cold spray Cu coatings. Furthermore, Perton et al. [91] applied laser heat treatment prior to cold spray to improve the adhesion strength by reducing the substrate hardness. Wang et al. [92] found that a hard steel substrate induced high deformation onto the striking Al particles, which improved the cohesive strength in the coating nearer to the substrate. However, hard particles (Al_2O_3) were embedded inside the soft Al substrate, which led to strong interfacial bonding. Therefore, it can be concluded that the substrate hardness influences the coating properties significantly in the vicinity of the interface.

Pre-heating of the substrate influences the bond strength of the cold spray deposits for soft on-hard (TiO_2/steels) and hard-on-hard interfaces. Pre-heating induces softness to the substrate surface, which facilitates deformation of the substrate during the impact of the particles, resulting in jet formation and better bonding strength [108-109,211-212]. Watanabe et al. [213] reported that adhesion strength of cold spray combinations of (i) Cu on A5083, (ii) Cu on Fe, and (iii) Fe on Cu improved by pre-heating the substrate since there was relief of thermal stresses. Goldbaum et al. [180] observed an increase in recrystallization at the splat boundaries and splat-substrate interface

due to substrate pre-heating, which increased both cohesion and adhesion strength of the cold spray coatings. As annealed substrate hardness decreased from room temperature to 1000°C annealed, our coating adhesion strength increased. To relate this situation to mechanical or metallurgical bonding, substrate deformation must be associated with adiabatic shear instability, ASI phenomena [86-87], but in our case, no substrate deformation occurs. As a result, mechanical anchoring, which is influenced by substrate hardness, is not the primary factor influencing bonding mechanism TiO_2/hard metals substrate.

The thickness of the oxide layer on the substrate surface increased as the temperature of the substrate increased during annealing. Oxide analysis was performed to confirm this situation. Figures 4.14 and 4.15 show the XPS evaluations of the in-depth room temperature substrates to substrates annealed from room temperature to 700°C and 400°C for SUS304 and SS400 substrates, respectively. In situ argon ion beam sputtering can be used to analyze the distribution as a function of depth. Figure 4.14 a–c and 4.15 a-b shows that the atomic concentration of oxygen in the inner most part of the oxide film was raised significantly as the temperature of the annealing material rose from room temperature to 700°C and 400°C, respectively for both hard metals substrate. This indicates that as the annealing temperature rises, the oxide layer of hard metals substrate are thicker. The literature indicates that bonding in cold spray is governed by mechanical interlocking and metallurgical bonding. Severe plastic deformation at the interface, owing to the high energy impacts of the particles, break the native oxide layers of the interacting surfaces. The disruption of oxide layers facilitates the penetration of particles into the substrate, which leads to jet formation and mechanical interlocking [171]. Ichikawa et al. [172] investigated the effect of the substrate conditions on the deposition process finding out that the initial oxide film thickness has a

substantial effect on the deposition efficiency. Yin et al. [169] claimed that, in addition to the substrate hardness, also the particle velocity and the spray angle can influence the deformation behaviour and final state of the oxide film. Moreover, the results indicate that the formation of a fresh metal surface followed by an immediate contact with the mating material, which can be a metal or oxide, is a necessary condition to form intimate bonding in a kinetic spraying process. Many researchers have observed adhesion between metal coatings and smooth ceramic substrates. This suggests that mechanical interlocking is not necessary for adhesion and a chemico-physical interaction at the metal/ ceramic interface significantly contributes to adhesion [196,199,184].

Our findings revealed that as the oxide thickness on hard metals substrate increased due to the annealing process, coating adhesion strength, particularly for SUS304, increased steadily. Meanwhile, coating on SS400 substrates showed a slight increase from room temperature to 400°C annealed, with no successful coating on 700 and 1000°C annealed substrates. This trend seems reversed from mechanical or metallurgical bonding mechanism, where it requires oxide free surface in order to form intimate contact between particle/substrate and provide good adhesion bonding. To further understand how oxide thickness plays a role towards bonding mechanism involved, chemical oxide analysis was conducted.

The chemical composition of the oxide layer for hard metals substrate is depicted in Figures 4.16 and 4.17. In this experiment, the annealed 400 and 700˚C SUS304 oxide consists of mixture of Fe_2O_3, Cr_2O_3 and OH^- in the outermost layer. Meanwhile, 400˚C annealed SS400 oxide consists of mixture Fe_2O_3 and OH^-.

The Ellingham-Richardson diagram [214] as shown by Figure 4.37 below is utilized to show the standard free energy of formation for oxides as a function of temperature and equilibrium oxygen partial pressure at 200°C as indicated by red-dotted line and blue arrow for iron, chromium, and

titanium. Our gas temperature is 500°C and referring to previous work in our lab, 200°C is the temperature on substrate when coating is form. Gibbs equation helps us to predict the spontaneity of a reactions on the basis of enthalpy and entropy values directly. Thus, when the reaction is exothermic, enthalpy of the system is negative, thus making Gibbs free energy negative. Hence, we can say that the reaction will proceed in the forward direction due to a positive value of the equilibrium constant. This law can be scaled for two different reactions taking place in a system too. The overall reaction (combination of two reactions) will occur if and only if net ΔG (sum of ΔG's of both the reactions) of the two possible reactions is negative [215].

Based on Figure 4.37, we can arrange metal oxide for substrates involved as below;

$$\xrightarrow{\text{Stable}}$$

$$Fe_2O_3 < Cr_2O_3 < TiO_2$$

Metal oxide for both hard metals that involved Fe_2O_3, Cr_2O_3 and OH^-. The oxidation process of metal generally depends on thermodynamics and kinetics. The relationship between the standard Gibbs free energy change $\triangle G^\circ$ and the temperature T [216] is presented as follows:

$$\triangle G^\circ(Fe_2O_3) = -543{,}349\ (j/mol) + 167.4\ (J/mol\ K)T$$

$$\triangle G^\circ(Cr_2O_3) = -746{,}844\ (j/mol) + 173.2\ (J/mol\ K)T$$

$\triangle G^\circ$ will be less than 0 when T changes within a certain range, indicating that the reaction favors generating the oxides. Moreover, $\triangle G^\circ$ for Cr_2O_3 is always more negative than $\triangle G^\circ$ (Fe_2O_3) at the same T, implying the greater affinity of oxygen to chromium. Therefore, the Cr_2O_3 formation is

thermodynamically preferred in SUS304 substrate. Meanwhile, for Fe atom, although the thermodynamics of its oxidation process is not dominant, it is the most mobile atom in the oxide film [217]. Therefore, the Fe_2O_3 formation is controlled more by kinetics than thermodynamics. Figure 4.38 below showed schematic diagram of oxidation process and mechanism of the stainless steel under laser irradation air [217].

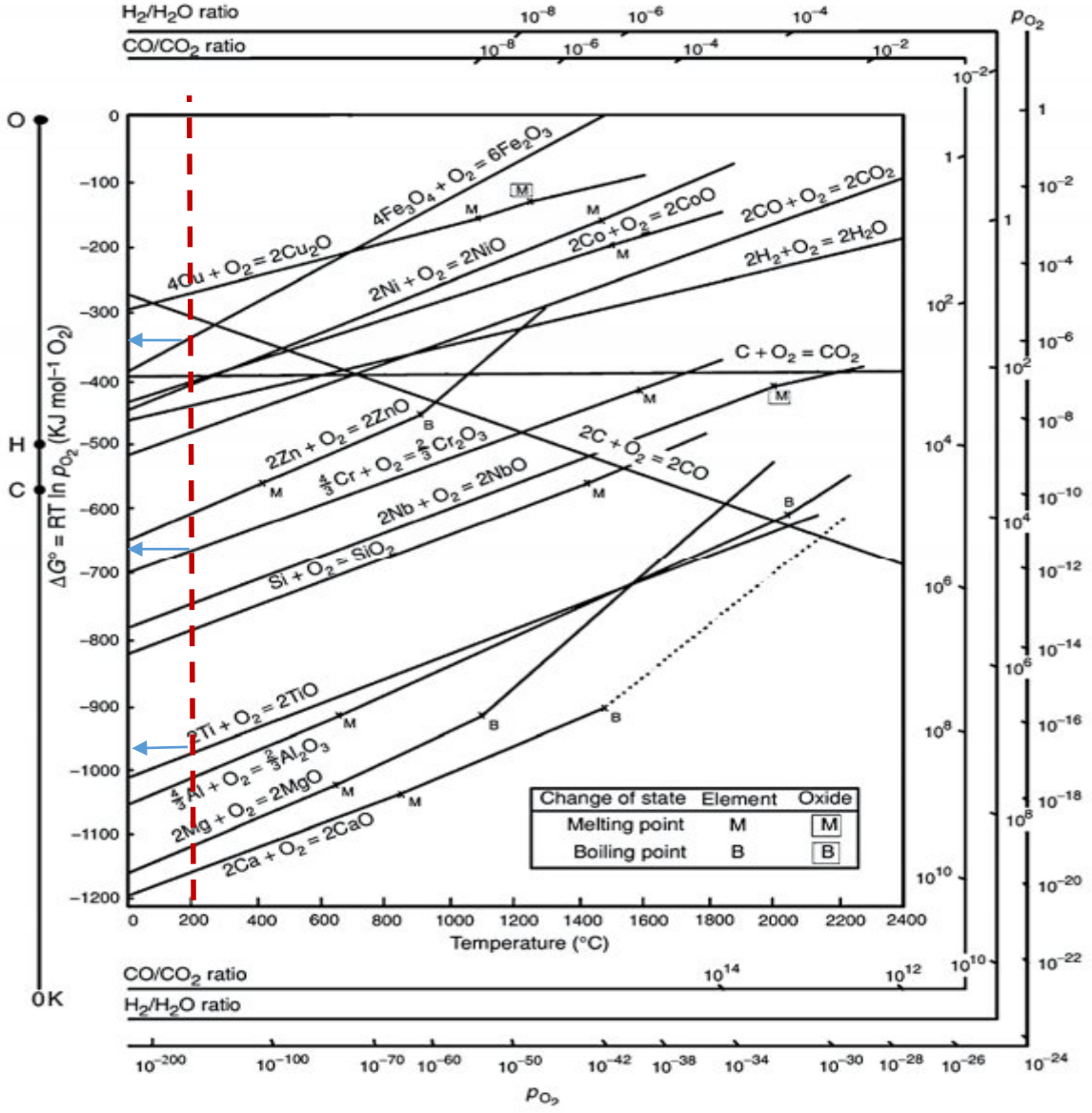

Figure 4.37: Ellingham-Richardson diagram for selected elements [214].

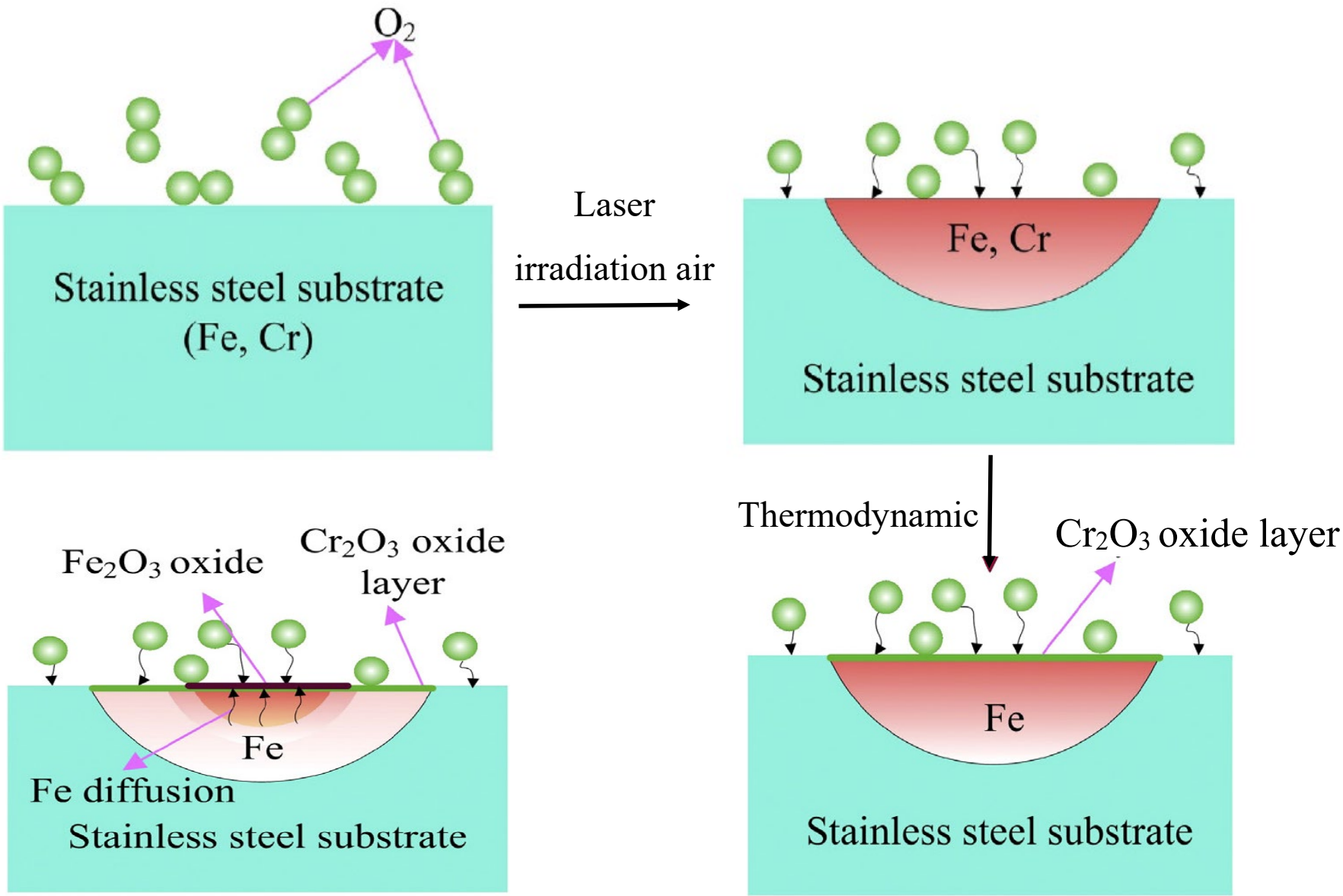

Figure 4.38: Schematic diagram of oxidation process and mechanism of the stainless steel under laser irradation air [217]

According to our findings, the annealed SUS304 oxide contains a mixture of Fe_2O_3, Cr_2O_3, and OH^- in the outermost layer, and coating adhesion strength increased steadily as the substrate annealing temperature increased. Meanwhile, SS400, an oxide composed of Fe_2O_3 and OH^-, was coated successfully at room temperature and 400°C annealed only. It is clear that chromium oxide, Cr_2O_3, plays a role in the bonding mechanism between TiO_2/SUS304. As a result, a pure chromium substrate was chosen to clarify the effect of chromium oxide, Cr_2O_3, on the bonding mechanism involved.

Coating adhesion strength on annealed pure chromium showed an increased trend from room temperature (0.709 MPa) to 700ºC (1.44 MPa) and decreased back to 1000ºC (0.479 MPa) as shown by figure 4.29. EDX analysis and spectrum for room temperature and 700°C annealed were shown by figure 4.30 to 4.33. In comparison to room temperature pure chromium, a large portion of pure chromium 700°C annealed embedded on fracture coating of TiO_2. In order to further understand this trend, substrate properties such as hardness, oxide thickness and oxide composition were conducted.

Figure 4.34 shows the substrate hardness of pure chromium from room temperature to 1000°C annealed. This figure showed a decrease trend of annealed substrate hardness from 265 Hv to 179.7 Hv at 700°C annealed and increased back to 192.1 Hv at 1000°C annealed. Pure chromium is a bcc metal that inherently brittle at room temperature due to the limited number of primary dislocation slip systems in the crystal structures [205-206]. When exposed to high temperature (T > 1000°C), embrittlement can also be induced via formation of brittle subnitride underneath the oxide scale [207-208]. This explains why pure chromium annealed substrate hardness at 1000ºC showed

a little increased trend. To relate annealed pure chromium hardness with coating adhesion strength trend on SUS304 from room temperature to 1000°C annealed, no correlation can be made. Therefore, investigations of oxide properties in term of oxide thickness and chemical composition were carried out.

Figure 4.35 (a) to (d) depicts the concentration of oxygen and chromium in the substrates as a function of depth. The data show that the concentration of oxygen in the near-surface region increases with annealed temperature. This indicates that the pure chromium oxide layer thickens as the annealing substrate temperature rises. Coating adhesion strength increased from room temperature to 700°C annealed and decreased back to 1000°C annealed as oxide thickness increased on pure chromium annealed substrate. It was discovered that the oxide properties of Cr_2O_3 from room temperature to 700°C have an effect on the bonding mechanism involved. As a result, the chemical composition of the oxide was studied further.

Figures 4.36 (a) and (b) show that the chemical state of chromium and oxygen for pure chromium.

The position of chromium metal at 574.0 eV was prominently present in the oxide layer for the room-temperature substrates for pure chromium. However, at the annealing temperature of 400, 700 and 1000°C substrate, the peak position of Cr_2O_3 at 576.0 eV [209] was present throughout the outermost surface of the oxide layer for the pure chromium substrate as shown by Figure 4.35 (a). This result indicates that the major components of the oxide layer at 400, 700 and 1000 °C for pure chromium is Cr_2O_3. Figure 4.36 (b) showed that hydroxide also present on outermost surface on room temperature to 700°C annealed, where the peak position is 531-532 eV [209] as indicated by red-dotted line. Metal oxide is present on outermost surface on 1000°C annealed where the peak is 530 eV [209].

Based on our findings, hydroxide, OH^- that exist at room temperature to 700°C annealed pure chromium play a significant role in the increased trend of coating adhesion strength as annealing temperature increases. Pure chromium, Cr_2O_3, and metal oxide are present on the substrate surface after 1000°C annealing. This could account for the decreasing trend in coating adhesion strength on 1000°C pure chromium.

TiO_2 usually has oxygen vacancies [218]. These defects are considered to be important sites for adsorption and promotion of many surface reactions. Both O_2 and H_2O can easily heal the oxygen vacancy defects through dissociation. O_2 dissociation at the oxygen vacancies of TiO_2 can heal the surface defects, restoring the stoichiometric surface. H_2O dissociation, on the other hand, leads to the formation of two OH groups on the surface. Such OH groups can considerably affect the electronic properties of TiO_2, which may lead to further adsorption, diffusion and dissociation of O_2 and H_2O.

TiO_2 has a characteristic structure of bridging oxygen atom rows along the [001] direction, six fold-coordinated (6c or 6f) Ti atoms below the bridging oxygen and five-fold-coordinated (5c or 5f) Ti atoms in troughs between bridging oxygen rows, as shown in figure 4.39. The bridging oxygen vacancy (O_{br}) is a common defect on TiO_2. Such oxygen vacancies can be created by annealing the surface at the high temperature or bombarding with electrons [219]. For each O_{br}, two excess electrons remain on the surface. Consequently, TiO_2 becomes rather reactive for the dissociation of electrophilic adsorbates such as O_2 and H_2O. Hence, it is important to understand the electronic structure of the defective TiO_2 surfaces [220].

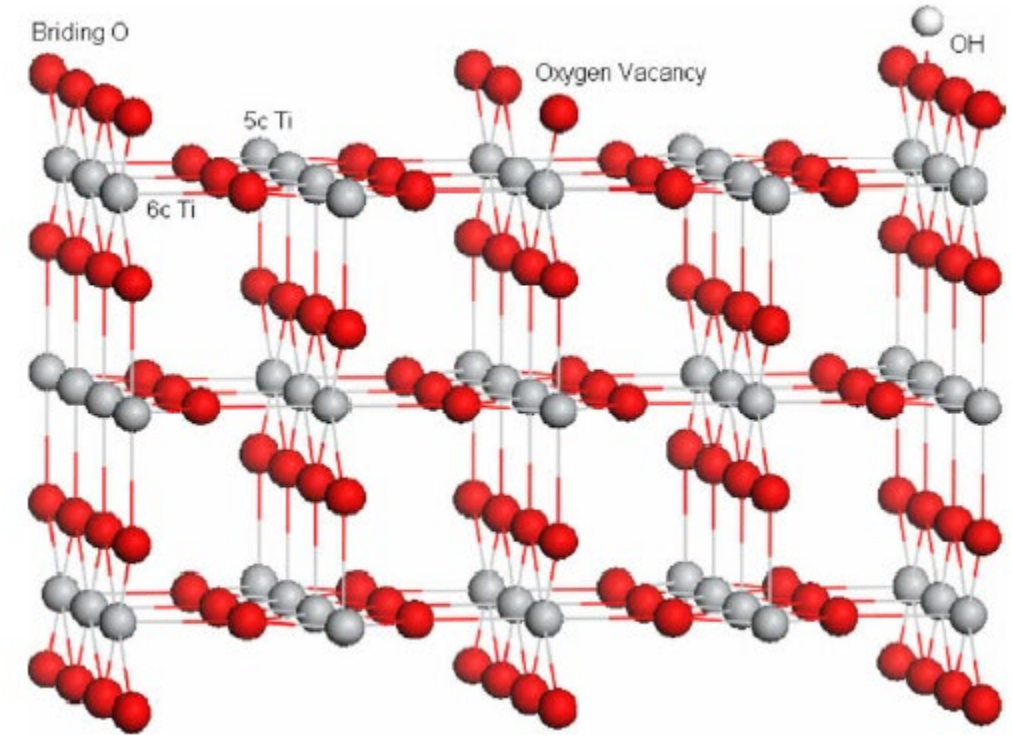

Figure 4.39: Side view of the TiO_2 surface with one oxygen vacancy and an OH group. O atoms are represented by red spheres and Ti atoms by grey spheres [218]

In order to further understand how oxide interaction plays a role in bonding mechanism of hard metals substrate, single particle study or wipe test was conducted. The objective of the wipe test was to study more about how TiO_2 particles adhere to annealed hard metals substrate. Only 1000°C and 400°C annealed were selected because they had the thickest oxide film.

As demonstrated in Figures 4.18 and 4.19, the TiO_2 particle remained intact following the collision, whereas the base surface of the hard metals annealed at 1000°C and 400°C remained unchanged after the impacting during the cold-spraying process.

In the cold spray deposition process, the particle/substrate interaction can be classified into four impact cases according to the physical and mechanical properties of the processed materials: soft/soft, hard/hard, soft/hard, and hard/soft. In order to investigate the particle impact behaviour under the mentioned different impact conditions, Bae et al. [96,115-116] analysed four representative particle/substrate combinations, namely Al/Al (soft/soft), Ti/Ti (hard/hard), Al/mild steel (soft/hard), and Ti/Al (hard/soft). In the case of Al/ Al, as shown in Figure 4.30(a), a relatively large deformation was observed as compared to the Ti/Ti case (Figure 4.30 (b)), due to the lower strength of the processed material. Moreover, the Al/Al condition shows a wider high temperature region in the substrate than that of Ti/Ti owing mainly to its relatively high ductility, high thermal softening effect, and low strain hardening. As for the impact cases of dissimilar materials Al/mild steel and Ti/Al, Figure 4.30 (c and d), a different impact behaviour was observed with respect to the previous cases. In particular, the initial kinetic energy of the particle is mostly dissipated into plastic deformation of the softer counterpart; therefore, a much higher temperature on the soft side is achieved. The simulation outcomes point out that the soft/hard case results in pronounced flattening of the softer particles with a slightly deformed substrate (Figure 4.30 (c)). On the other hand, in the hard/soft case the substrate experienced a significant deformation with a less deformed particle that deeply penetrated into the softer counterpart (Figure 4.30 (d)). In addition, relatively low critical velocities of 365m s−1 for Al/mild steel and 665m s−1 for Ti/Al were numerically found. It was also proved that at the interface between particles and substrate the temperatures can reach the melting [25,47,74,25]

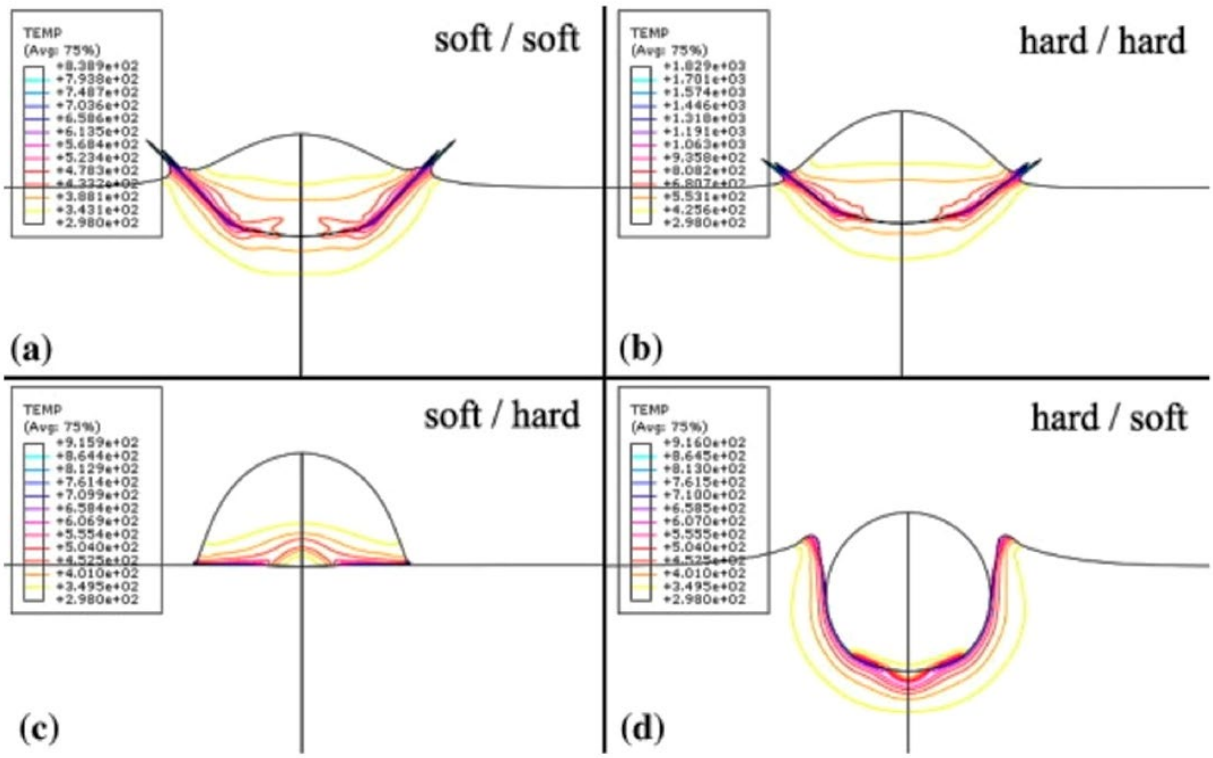

Figure 4.40: Impact process simulation for different material combination: (a) Al/Al (soft/soft), (b) Ti/Ti (hard/hard), (c) Al/mild steel (soft/hard), (d) Ti/Al (hard/Soft) [96,115-116].

Our results agreed well with 4.30 (c), in which TiO_2 particles impacted on hard metals substrates and the substrate remained unchanged after the impact. There is no correlation between the increasing trend of coating adhesion strength of hard metal substrates, particularly SUS304, and substrate deformation. As previously stated, mechanical anchoring caused by substrate hardness is not a factor in the bonding mechanism TiO_2/hard metals substrate.

According to Song et al [199], the mechanisms of cold sprayed metal particles on ceramics or glass involve additional factors such as chemical properties of the impact particles and substrates. Kim et al.[196] used kinetic spraying of single titanium particles on mirrored steel substrates. They showed that some portion of a thin amorphous oxide remained between the particle–substrate interface, and even a severe plastic deformation was associated with the impacts of the particles onto the substrate. The remaining oxide provided a bond between a particle or particle–substrate[196]. Therefore, TEM analysis was conducted on single particle TiO_2/ hard metals substrate.

Figure 4.21 to 4.24 shown as the STEM and high magnification images of the interlayer region between single-particle TiO_2 and annealed hard metals substrate. It confirms the existence of the remaining interface oxide layer after the cold-sprayed TiO_2 impacted on hard metals substrate by FFT pattern that showed an amorphous phase at interlayer, with a thickness of approximately 10nm for SUS304 and SS400 as shown by figure 4.22 and 4.24, respectively.

Salim et al [84] prepared TiO_2 coatings of 400 μm and 150 μm on metal and tile respectively. It was observed that adhesion strength changed little with the change of spraying parameters. This indicated that mechanical interlocking was not the main bonding mechanism in this case, so was the substrates' shear instability. It was discovered that both the hardness and the oxidizability of the substrates affected adhesion strength of TiO_2 coatings. The adhesion strength of TiO_2 coatings could be improved by changing the surface chemistry of the substrates. It was proposed that the chemical or physical bonding mechanism was the main bonding mechanism of ceramic coating. TEM images proved the existence of chemical bonding between TiO_2 particles. By the way, preheating could increase the oxidizability of the substrate, thus deteriorating the adhesion strength of coatings. The result seems to be in agreement with the chemical bonding mechanism.

Figure 4.25 to 4.27 are the TEM line analysis result of single particle TiO_2 on room temperature and 1000˚C annealed SUS304 and 400°C annealed SS400, respectively. It confirms the existences of the atomic of Ti,O and Cr on room temperature and 1000°C annealed SUS304. On the other hands, 400ºC annealed SS400, the existences of Ti and O are presented on substrate surface. Ti and O atomic on the hard metals substrate area are contributed by TiO_2 coating and TiO_2 usually has oxygen vacancies [218]. These defects are considered to be important sites for adsorption and promotion of many surface reactions. Our titanium dioxide powders feedstock also has unique properties that once break at collision and may bond again, it gives cohesion and adhesion bonding [100-101].

Yamada et al. reported that the agglomerated powder of TiO_2 in nano-scale primary particles, which also contained nanoporosity, was fractured, leaving an unstable surface with a dangling bond structure. The fractured particles decoupled and formed a surface with an improved stability to reobtain a stable surface, which led to bonding of newly impacting particles and coating building [100]. When high velocity cold sprayed TiO_2 particle impacted on annealed stainless steel that already consist of oxide mixture Cr_2O_3+Fe_2O_3 + OH^- on the top surface, inter oxide reaction occurs. TiO_2 particle that already have oxygen vacancy, the particle will break at collision and bond again to give cohesion and adhesion bonding by inter oxide reaction TiO_2-OH^- from chromium oxide on SUS304 that thermodynamically preferred compared to Fe_2O_3. This explain an increased trend of TiO_2 coating on annealed SUS304 substrate from room temperature to 1000°C annealed. The passivation layer; its thickness, chemistry (hydroxide) and structure, can contribute significantly to impact adhesion. While it is notionally somewhat unexpected that 3 nm of growth in a passivation layer can affect impact bonding to such a large degree, it can be rationalized on the

basis of how localized the interface deformation leading to bonding [199]. Figure 4.31 shown proposed schematic diagram on bonding mechanism of cold sprayed TiO_2 on SUS304.

Structural steel, SS400, which also contains the oxide mixture Fe_2O_3+OH^- on the outermost surface of 400°C annealed steel, only showed a slight increase in coating adhesion strength when compared to room temperature substrate and no successful coating at 700 and 1000°C. This could imply that SS400 requires a substrate surface that is free of oxide in order to form a good adhesion bond between TiO_2-SS400. Winnicki et al [12] cold sprayed TiO_2 on mild steel and the bonding mechanism proposed is mechanical interlocking.

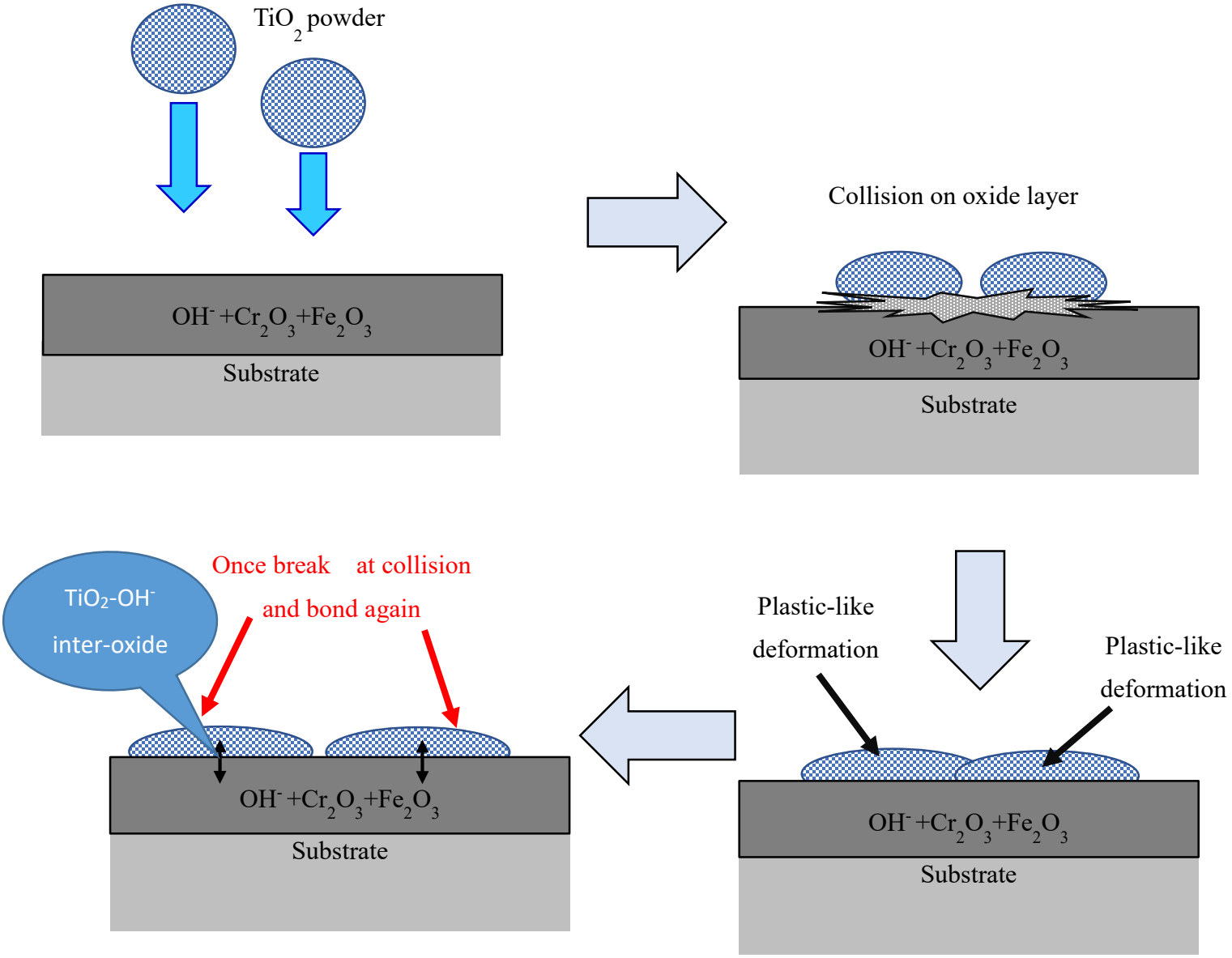

Figure 4.41: Schematic diagram on bonding mechanism of cold sprayed TiO_2 on SUS304.

4.6 Conclusions

Herein, we investigated the bonding mechanism of cold sprayed pure ceramic, titanium dioxide on hard metals substrate through substrate properties that are annealed in an electrical furnace temperature range from ambient temperature to 1000°C. The summary of the study's finding are

1. The primary bonding mechanism of TiO_2 particle and SUS304 substrate is inter-oxide bonding, which is provided by a chemical reaction of TiO_2-OH^-, where OH^- is provided by chromium oxide, Cr_2O_3, which is thermodynamically preferred in SUS304.

2. Only certain substrate oxide compositions on certain materials, such as SUS304, have chemically induced inter-oxide bonding. Other oxide compositions of the substrate, such as SS400 must be removed in order for TiO_2-substrate to form a bond.

5 Summary of bonding mechanism of cold sprayed titanium dioxide

The cold gas dynamic spray or generally referred cold spray, is a relatively new spray technology which falls under the larger family of thermal spray process [1-4]. In conventional thermal spraying processes, such as wire arc and flame spray, the sprayed particles are partially or fully molten when they deposit on the substrate [5,6]; moreover, the impacting velocity onto a target surface is usually below 200 m s−1 [7,8]. By the advent of high-velocity oxyfuel process, the particles velocity was increased and the processable materials selection was amplified [9]. On the other hand, the cold spray uses less thermal and more kinetic energy, so the powder particles remain in a solid state upon impact onto substrate [10]. Therefore, it can cope with the production of different kind of coatings, pure metals, alloys, composites, nanostructure materials as well as amorphous materials [106], on a wide variety of substrate.

In the cold spraying process, it can be divided into metallic cold spray, metallic particles on the metallic substrate, metallic particle on polymeric substrate, ceramic coatings; ceramic metallization where metal matrix composite (with binder) deposited on ceramic substrate and cold spraying of pure ceramic powder without binder (TiO_2) on metals substrate.

The most accepted theory for adhesion mechanism in metallic cold spray are mechanical interlocking and metallurgical bonding. Cold spray is a solid-state deposition process since the feedstock is not melted; however, the kinetic energy of the high velocity particles leads to interfacial deformation as well as localized heat at the location of impact [46,81]. The conversion of kinetic energy into deformation and heat results in mechanical interlocking as well as metallurgical bonding at the interface [76]. Bonding at the interface is governed by the severe plastic deformation of the materials; which, with associated adiabatic shear instability (ASI) at the

interface, leads to the metal-jet formation [45,76]. The high velocity particle impacts cause breakage of the native oxide layer at the surfaces, providing a particle-to-substrate contact. This true contact of the particles with the substrate may lead to the jet formation that is governed by ASI [15,19,27].

Drehmann et al. [148], Wustefled et al. [147] and Dietrich et al [195] bonding mechanism for cold sprayed Al on an Al_2O_3 substrate (soft on hard). Their results revealed that bonding of Al particles on super-finished monocrystalline sapphire substrate occurred due to deformation-induced recrystallization in the vicinity of the particle-substrate interface. The formation of nano-sized grains at the vicinity of the interface assists metallurgical bonding, which results in improved adhesion strength between ductile Al particles and the Al_2O_3 monocrystalline ceramic substrate.

The annealing process contributed to the induced ductility of soft metals substrate especially when annealed at a recrystallization temperature of 400°C. The soft metals substrate hardness was reduced as a result, and it became softer. When the high-velocity cold sprayed TiO_2 particle impacted the soft metals substrate surface with thick oxide film, plastic deformation of the substrate is present but some of the oxide layer remained as shown by the TEM results, which prevented metallurgical bonding from occurring in between the TiO_2 coating and soft metals substrate. The metallurgical bonding, one the other hand, results from the chemical reactions occurring at the particle-to-particle and particle-to-substrate interfaces, which requires oxide-free interface and metal-to-metal contact. The metallurgical bonding is considered a consequence from chemical reaction at the oxide-free interface between particles or particle/substrate [58-61]. Bonding mechanism cold sprayed TiO_2 on soft metals showed a similar trend like metallic cold spray, metallurgical bonding which required free oxide surface.

On the other hands, bonding mechanism cold sprayed TiO_2 on hard metals especially stainless steel, SUS304 showed a reversed trend from adhesion mechanism in metallic cold spray. The annealing process contributed to the induced ductility of hard metals substrate and also thicker substrate oxide. Coating adhesion strength on stainless steel showed an increased trend as substrate annealed temperature is increased (thicker oxide). The primary bonding mechanism of TiO_2 particle and SUS304 substrate is chemical bonding by inter-oxide bonding, which is provided by a chemical reaction of TiO_2-OH^-, where OH^- is provided by chromium oxide, Cr_2O_3, which is thermodynamically preferred in SUS304. Only certain substrate oxide compositions on certain materials, such as SUS304, have chemically induced inter-oxide bonding. Other oxide compositions of the substrate, such as SS400 must be removed in order for TiO_2-substrate to form a bond.

6 General Conclusions

The conventional method used to make the TiO_2 coating is by plasma sprayed and has an average coating adhesion strength of 25 MPa, but the drawback of the conventional thermal spraying process for the preparation of the TiO_2 coating is the irreversible phase transformation of TiO_2 structure from anatase to a less photocatalytic rutile phase at 500-600°C under normal conditions.

The cold spray process is therefore the most appropriate process since it uses low processing temperature during the process and is based on the kinetic energy of the deposition particle. The main interest of this study is to understand the bonding mechanism involved between TiO_2 and metals substrate, in order to increased coating adhesion strength.

This research work focus on two different cluster of substrate materials, soft metals (aluminum and copper) and hard metals (stainless steel and structural steel) to clarify bonding mechanism involved. The adhesion strength of cold coatings with the substrate is not only based on mechanical interlocking. It is determined also by adiabatic shear instability, plastic deformation of the colliding materials and static recrystallization [173,106,172,108-109]. All these factors are attributable to substrate conditions such as hardness, material chemistry, surface roughness and temperature of the substrate.

(1) Soft metal substrates

The annealing process contributed to the induced ductility of pure aluminum and pure copper especially when annealed at a recrystallization temperature of 400˚C. The substrate's hardness was reduced as a result, and it became softer. When the high-velocity cold sprayed TiO_2 particle impacted the soft metal substrates annealed at 400°C with an oxide film, hence the energy dissipating into the substrate is even more, naturally resulting in the relatively large deformation in the substrate and small in the particle. This plastic deformation will break the thin oxide and expose a new substrate surface, promoting intimate particle/substrate bonding where atomic reaction between cold-sprayed TiO_2 particle and newly formed pure metals substrate that is oxide free via metallurgical bonding.

Coating adhesion strength on 400°C annealed soft metal substrates decreased even plastic deformation of the substrate present because some of the oxide layer remained as shown by TEM results, preventing metallurgical bonding between the TiO_2 coating and soft metal substrates.

Some recommendation can be made from the results obtained and observations made during the studies, such as prepared the oxide-free surface of the soft metal substrates from room temperature to 300°C annealed to confirm the bonding mechanism involved.

(2) Hard metal substrates

When a high velocity cold sprayed TiO_2 particle impacts on the surface of annealed hard metal substrate, such as SUS304 or SS400, there is little to almost no plastic deformation of the substrate. As a result, metallurgical bonding, which requires plastic deformation and oxide-free metal, is not present here to explain the increase in coating adhesion strength as the annealed substrate temperature rises. When metal is used as a substrate, the surface of the substrate will naturally contain oxide.

As a result, increasing the annealed substrate temperature resulted in thicker substrate oxide on the top. SUS304 has an oxide layer composed of Fe_2O_3, Cr_2O_3, and OH^-. The contribution of OH^- by Cr_2O_3, which is thermodynamically preferred in SUS304, has a dominant effect on the bonding mechanism involved. This trend has been confirmed by pure chromium substrates, where hydroxide (OH^-) on the surface of pure chromium causes an increase in coating adhesion strength from room temperature to 700°C. However, because hydroxide is removed from the surface during 1000°C annealing, coating adhesion strength at this temperature is reduced.

TiO_2 contributes Ti and O atomic on the hard metals substrate area, which usually has oxygen vacancies. These defects are thought to be important sites for adsorption and the promotion of a variety of surface reactions. According to the Ellingham diagram, TiO_2 has a high affinity for oxygen. Furthermore, our titanium dioxide powders have the unique property of breaking at collision and bonding again, which provides cohesion and adhesion bonding.

Chemical bonding by inter-oxide bonding is the primary bonding mechanism of TiO_2 particle and SUS304 substrate, which is provided by a chemical reaction of TiO_2-OH^-, where OH^- is provided by chromium oxide, Cr_2O_3, which is thermodynamically preferred in SUS304.

Only certain substrate oxide compositions on certain materials, such as SUS304, have chemically induced inter-oxide bonding. Other oxide compositions of the substrate such as SS400, must be removed in order for TiO_2-substrate to form a bond.

Some recommendations can be made from the results obtained and observations made during the studies by prepared the oxide-free surface of the structural steel substrate to confirm the bonding mechanism involved. On top of that, to improve coating adhesion, prepare a Cr_2O_3 sub oxide on a SUS304 substrate prior to the cold spray process.

Schematic images for general conclusion the bonding mechanism of cold sprayed TiO_2 on metal substrates shown in Figure 6.1 below;

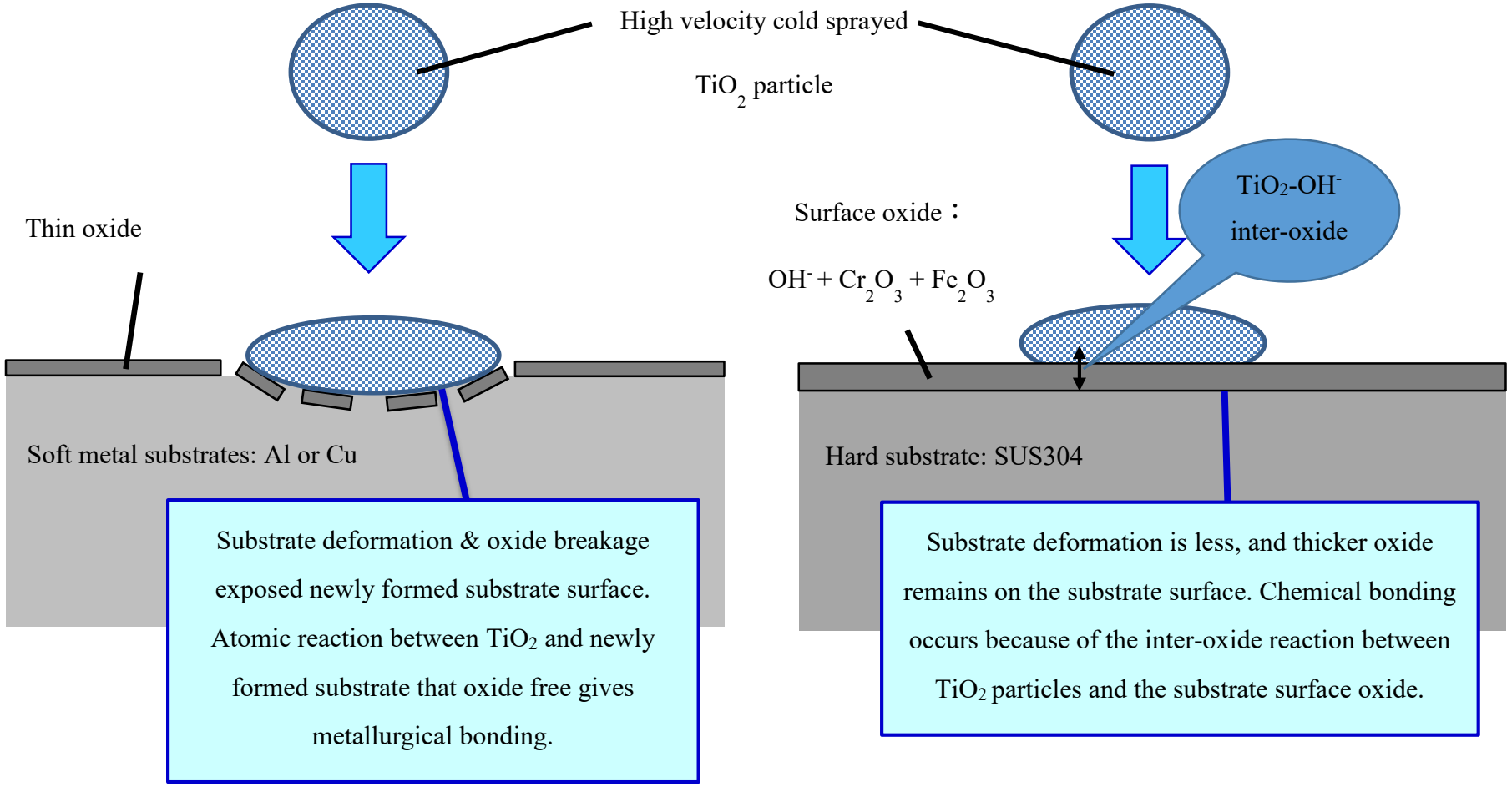

Figure 6.1: Schematic images of general conclusions the bonding mechanism of cold sprayed TiO_2 on metal substrates

(3) Contribution of this study to the research/academic field

1. Understanding the bonding mechanism of cold sprayed pure ceramic powder, TiO_2, on soft and hard metals substrates provides new opportunities to prepare the substrates for cold spray process to increase coating adhesion strength in the future, particularly for ceramic cold spray, which already has its own challenges due to brittle properties because cold spray process required plastic deformation of powder feedstock to form a coating on substrate surface. The highest coating adhesion strength we were able to attain is 4.93 MPa on 400°C annealed pure aluminum with no oxide condition.
2. In addition, clarifying the role of OH^- developed from Cr_2O_3, which is thermodynamically preferred in SUS304, opened up a new pathway for preparing cold spray coatings on stainless steel. Preparing a cold sprayed coating on hard metals such as stainless steel is already difficult in the cold spray process; thus, this opportunity will improve adhesion bonding involving stainless steel material.
3. This study is only the beginning of future research into ceramic coating using the cold spray process. The findings of this study indicate that it is possible to deposit ceramic materials, which were previously thought to be difficult to deposit using this coating process due to the brittle nature of the powders. Understanding the bonding mechanism between pure TiO_2 powder and soft and hard metal substrates can lead to improved coating adhesion strength in ceramic cold spray. This finding opens up new possibilities for the potential application of thick and large areas for the preparation of ceramic coatings.

(4) Contributions of this study to the industrial field

1. Promising results that reveal in this study shows that cold spray can be a good alternative to prepare cold sprayed pure TiO_2 coating with good adhesion strength on ceramic tiles. On top of that, this technology not only applicable for outdoor applications such as for the wall of building but also for indoor application to preserve the indoor quality such as in gymnasium, hospitals.
2. Delamination and poor adhesion strength of soft-on-hard (TiO_2 / steels) and hard-on-hard (Ti/Ti) interfaces are of great concern for industries such as the marine, nuclear, aerospace, automotive and electronics. Thus, understanding the mechanism of bonding can address the issue of poor adhesion and delamination, which would assist the advanced manufacturing sector. The understanding of bonding mechanism of TiO_2/steel will contribute to good adhesion bonding and can be applied as TiO_2-based implants for bone and dental.

Publications List and Oral Presentations

List of Journals

1. **Noor irinah Omar**, Santirraprahkash Selvami, Makoto Kaisho, Motohiro Yamada, Toshiaki Yasui and Masahiro Fukumoto, "Deposition of titanium dioxide coating by the cold-spray process on annealed stainless-steel substrate," *Coatings* **2020**. Doi: 10.3390/coatings10100991.

2. **Noor irinah Omar**, Motohiro Yamada, Toshiaki Yasui and Masahiro Fukumoto, "Bonding mechanism of cold-sprayed TiO_2 coatings on copper and aluminum substrates," *Coatings* **2021**. Doi:10.3390/coatings11111349.

List of Proceedings

1. **Noor irinah omar**, Motohiro Yamada, Toshiaki Yasui and Masahiro Fukumoto, "On the role of substrate properties into bonding mechanism of cold sprayed Titanium Dioxide, TiO_2" IOP conference series: Material Science and Engineering **920** (2020) 012009. Doi: 10.1088/1757-899X/920/1/012009.

List of Oral Presentations

1. **Noor irinah binti Omar**, Kondai Ogasawara, Motohiro Yamada, Toshiaki Yasui and Masahiro Fukumoto, "Effect of Substrate Properties on Adhesion Strength of Cold Sprayed TiO_2," International Thermal Spray Conference, ITSC 2019, Yokohama, Japan, 26-29 May 2019.

2. **Noor irinah Omar**, Motohiro Yamada, Toshiaki Yasui and Masahiro Fukumoto, "On the role of substrate properties into bonding mechanism of cold sprayed Titanium Dioxide, TiO_2," 6th International Conference of Global Network for Innovative Technology, IGNITE 2019, Park Royal Resort, Penang, Malaysia, 2nd-3rd December 2019.

3. **Noor irinah Omar**, Santirraprahkash Selvamani, Motohiro Yamada, Toshiaki Yasui and Masahiro Fukumoto, "Influenced of substrate oxidation on adhesion strength of cold-sprayed titanium dioxide coating," Japan Thermal Spray Society, 2020 JTSS Fall Meeting, Zoom meeting, 27-28 October 2020.

Acknowledgements

I would like to express the deepest appreciation to my supervisors, Associate Prof. Dr.Toshiaki Yasui, Assistant Prof. Dr. Motohiro Yamada and Prof. Dr. Masahiro Fukumoto, whose expertise, generous guidance and full support, understanding and encouragement throughout my three years of study and research. Without their guidance and persistent help, this thesis would not have been possible. I am also largely indebted to their kindness and help during my living in Toyohashi, Japan.

My sincere appreciation also goes to all members of the Interface and surface Fabrication laboratory, Department of Mechanical Engineering, Toyohashi University of Technology, for their help and cooperation during my study. I am highly indebted and grateful to all the cold spray group members for their valuable discussion and help during my experimental works. I also wish to acknowledge the support received from the administration and technical staff of Toyohashi University of Technology during my PhD journey.

I would like to express sincere gratitude to my sponsors; Interface and surface Fabrication laboratory, Majlis Amanah Rakyat, MARA and Universiti Teknikal Malaysia Melaka, UTeM for their financial support and giving me the opportunity to do the PhD.

It is my privilege to thank my dear husband, Mr.Mohd Khusairey bin Khalid, my son; Muhammad Abdul Hakim bin Mohd Khusairey and my mother; Mrs.Hajjah Masnah binti Talib, for their constant encouragement, love and understanding throughout this PhD journey. Also, to all my family members and friends for all the motivation words and supports which help me to survive, not letting me give up and keep me going to achieve my dreams.

References

[1] J.R.Davis: Handbook of Thermal Spray Technology (2004) TSS/ASM International.

[2] H.Assadi , F.Gartner , H.Stoltenhoff, H.Kreye: Acta Mater. 51 (2003) 4379-4394.

[3] M.Grujicic, C.L. Zhao, W.S. DeRosset, D. Helfritch: Mater. Des. 25 (2004) 681- 688.

[4] T. Schmidt, F.Gaertner , H.Kreye: J. Therm. Spray Technol.15 (2006) 488-494.

[5] T.Schmidt , F.Gartner , H. Assadi, H. Kreye: Acta Mater. 54 (2006) 729-742.

[6] J.Karthikeyan: The Advantages and Disadvantages of the Cold Spray Coating Process, in The Cold Spray Materials Deposition Process: Fundamentals and Applications Victor K. Champagne, Editor. (2007) Woodhead; CRC Press. p. 62-71.

[7] W.Wong, E.Irissou , J. -G.Legoux, S.Yue: Therm. Spray Glob. Solut. Futur. Appl. Eds., Singapore, (2010).

[8] C.Borchers, F.Gartner, T.Stoltenhoff, H.Assadi, H.Kreye: J. of Appl. Phys. 93 (2003) 10064-10070.

[9] J.Haynes, A.Pandey, J.Karthikeyan, A.Kay: (2006) ASM International: Seattle, WA.

[10] R.C.Dykhuizen, M.F.Smith: J. Therm. Spray Technol. 7 (1998)205-212.

[11] A. Alkhimov, V.Kosarev, S.Klinkov: J. Therm. Spray Technol. 10 (2001)375-381.

[12] T.S.Price: Cold Gas Dynamic Spraying of Titanium Coating, PhD Thesis, University of Nottingham, (2008).

[13] P.H.Oosthuizen, W.E.Carscallen: Compressible Fluid Flow Mcgraw-Hill Series in Aeronautical and Aerospace Engineering. (1997): McGraw-Hill.

[14] M.Grujicic, C.L. Zhao, C.Tong, W.S.DeRosset, D.Helfritch: Mater Sci and Eng A, 368 (2004)222-230.

[15] M. Grujicic, C.Tong, W. DeRosset, D. Helfritch: J. Eng. Manufact. 217 (2003) 1603-1613.

[16] J.Lee, S.Shin, H.Kim, C.Lee: Appl. Surf. Sci. 253 (2007) 3512-3520.

[17] W.Y.Li, C.Zhang, X.P.Guo, G.Zhang, H.L.Liao, C.J.Li C.Coddet: Mater. Des. 29 (2008) 297-304.

[18] F.Gartner, T.Stoltenhoff, T.Schmidt, H.Kreye: J. Therm. Spray Technol. 15 (2006):223-232.

[19] T.Van Steenkiste, J.R.Smith: J. Therm. Spray Technol.13 (2004)274-282.

[20] D.L.Gilmore, R.C.DyKhuizen, R.A.Neiser, T.J.Roemer, M.F.Smith: J. Therm. Spray Technol. 8 (1999)576-582.

[21] J.Pattison, S.Celotto, A.Khan, W.O'Neill : Surf. Coatings Technol. 202 (2008)1443- 1454.

[22] B.Samareh, O.Stier, V.Luthen, A.Dolatabadi : J. Therm. Spray Technol.18 (2009) 934-943.

[23] T.Stoltenhoff, H.Kreye, H.J.Richter : J. Therm. Spray Technol.11 (2002)542-550.

[24] S.Yin, Wang, X.-f., Li, W.-y., and Xu, B.-p: J. Therm. Spray Technol. 12 (2014)354-360.

[25] R.Morgan, P.Fox, J.Pattison, C.Sutcliffe, W. O'Neill: Mater Letters. 58 (2004) 1317-1320.

[26] A.N.Papyrin : Cold Spray Technology (2007): Elsevier.

[27] T.H.Van Steenkiste, J.R.Smith, R.E.Teets: Surf. Coatings Technol. 154 (2002) 273-252.

[28] A.N.Papyrin, S.V.Klinkov, V.F.Kosarev: Effect of Substrate Activation on the Process of Cold Spray Coating Formation, (2005) ASM International: Basel, Switzerland.

[29] R.C.Dykhuizen, M.F.Smith, D.L.Gilmore, R.A.Neiser, X.Jiang, S.Sampath: J. Therm. Spray Technol. 8 (1999) 559-564.

[30] K.Kang, S.Yoon, Y.Ji, C.Lee: Mater. Sci. Eng. A. 486 (2008) 300-307.

[31] C.J.Li, H.T.Wang, Q.Zhang, G.J.Yang, W.Y.Li, H.Liao: J. Therm. Spray Technol. 19 (2010) 95-101.

[32] S.Guetta, M.Berger, F.Borit, V.Guipont, M.Jeandin, M.Boustie ,Y. Ichikawa, K.Sakaguchi, K.Ogawa: J. Therm. Spray Technol.18 (2009) 331-342.

[33] S.Barradas, V.Guipont, R. Molins, M. Jeandin, M. Arrigoni, M. Boustie, C.Bolis, L.Berthe, M.Ducos: J. Therm. Spray Technol. 16 (2007) 548-556.

[34] S.Barradas, R.Molins, M. Jeandin, M. Arrigoni, M.Boustie, C.Bolis, L.Berthe, M.Ducos: Surf. and Coatings Technol.197 (2005) 18-27.

[35] P.King, S.Zahiri, , M.Jahedi: Copper Particle Impact onto Aluminium By Cold Spray, in Thermal Spray: Global Coating Solutions, (2008) ASM International: Maastricht, The Netherlands.

[36] T.S.Price, P.H.Shipway, D.G.McCartney, E.Calla, D.Zhang: J. Therm. Spray Technol.16 (2007) 566-570.

[37] M.Grujicic, J.R.Saylor, D.E.Beasley, W.S. DeRossee, D.Helfritch: Appl. Surf. Sci. 219 (2003) 211-227.

[38] S.V.Klinkov, V.F. Kosarev, M.Rein: Aero. Sci. Technol. 9 (2005)582-591.

[39] V.K.Champagne, D.Helfritch, P.Leyman, S.G.Ahl, B. Klotz: J. Therm. Spray Technol. 14 (2005) 330-334.

[40] K.Balani, A.Agarwal, S.Seal, J.Karthikeyan: Script Mater. 53 (2005)845-850.

[41] T.Marrocco, D.G.McCartney, P.H.Shipway, A.J.Sturgeon: J. Therm. Spray Technol. 15 (2006) 263-272.

[42] J.W.Wu, J.G.Yang, H.Y.Fang, , S.Yoon, C. Lee: Appl. Surf. Sci. 252 (2006) 7809-7814.

[43] H. Makinen, J. Lagerbom, and P. Vuoristo: Adhesion of Cold Sprayed Coatings: Effect of powder, Substrate, and Heat Treatment, in Thermal Spray: Global Coating Solutions, B.R. Marple, M.M. Hyland, Y. Lau, C. Li, R.S. Lima, and G. Montavon, Editors. (2007) ASM International: Beijing, People's Republic of China. P. 31-36.

[44] K. Sakaki, T. Tajima, H. Li, S. Shinkai, Y. Shimizu: Influence of Substrate Conditions and Traverse Speed on Cold Sprayed Coatings, in Thermal Spray: Advances in Technology and Application (2004) ASM International: Osaka, Japan. p. 358-362.

[45] P. Richer, B. Jodoin, K. Taylor, E. Sansoucy, M. Johnson, and L. Ajdelsztajn: Effect of Particle Geometry and Substrate Preparation in Cold Spray, in Thermal spray: Exploring its surfacing potential, E. Lugscheider, Editor (2005) ASM International: Basel, Switzerland.

[46] T.Schmidt T, H. Assadi , F.G¨artner F, H.Richter , T. Stoltenhoff , H.Kreye: J. Therm. Spray Technol. 18 (2009) 794–808.

[47] T. Schmidt, H. Assadi H, F. Gärtner: J. Therm. Spray Technol.18 (2009) 794–808.

[48] J. Wu J, H.Fang , S.Yoon, et al: Scr Mater. 54 (2006) 665–669.

[49] M. Winnicki M, A. Małachowska, M.Korzeniowski: Surf Eng. 34 (2018) 235–242.

[50] A.Viscusi , A.Astarita , R.Della Gatta , F.Rubino: Surf Eng. 35 (2019) 743–71.

[51] King P, Yandouzi M, Jodoin B. The physics of cold spray. Mod Cold Spray Mater Process Appl 2015:31–72

[52] Y. Xie , S.Yin , C.Chen C, MP.Planche, H.Liao H, R.Lupoi: Scr Mater.125 (2016) 1-4.

[53] S.Kumar, G.Bae, C.Lee: Surf.Coatings Technol. 304 (2016) 592-605.

[54] F.Meng, D.Hu, Y.Gao , S.Yue, J.Song: Mater Des. 109 (2016) 503–10.

[55] T.Hussain, DG.McCartney, PH.Shipway: Surf. Coatings Technol. 205 (2011) 5021–7.

[56] Y. Ichikawa, R.Tokoro , M.Tanno, K. Ogawa: Acta Mater. 164 (2019) 39–49.

[57] Alkhimov AP, Papyrin AN, Vyazemskogo U, Kosarev VF, Nesterovich NI, Shushpanov MM. Gas-dynamic spraying method for applying a coating. United States Patent. US 5302414; 1994.

[58] E.Irissou, JG.Legoux, AN.Ryabinin, B. Jodoin, C,Moreau: J. Therm. Spray Technol. 17 (2008) 495–516.

[59] D.Goldbaum, D.Poirier, E. Irissou, JG. Legoux, C.Moreau C: Mater Process Appl. (2015) 403–29.

[60] A.Moridi, SM. Hassani-Gangaraj, M.Guagliano, M.Dao: Surf. Eng. 30 (2014) 369–95.

[61] S.Grigoriev, A.Okunkova, A.Sova, P.Bertrand, I.Smurov: Surf.Coatings Technol. 268 (2015) 77–84.

[62] RR.Chromik, SA. Alidokht, JM.Shockley, Y.Zhang: Cold-Spray Coat. (2018) 321–48.

[63] SM. Hassani-Gangaraj, A.Moridi, M.Guagliano M: Surf Eng. 31 (2015) 803–15.

[64] A.O. Tokarev: Met. Sci. Heat Treat. 35 (1996) 136-145.

[65] V.K. Champagne, D. Helfritch, P. Leyman, S. Grendahl, B. Klotz: J. Therm. Spray Technol. 14 (2005) 330–334.

[66] K.H. Ko, J.O. Choi, H. Lee: Mater. Lett. 136 (2014) 45–47.

[67] A. Ganesan, M. Yamada, M. Fukumoto: J. Therm. Spray Technol. 22 (2013) 1275–1282.

[68] R. Lupoi, W. O'Neill: Surf. Coatings Technol. 205 (2010) 2167–2173.

[69] D. Seo, M. Sayar, K. Ogawa: Surf. Coatings Technol. 206 (2012) 2851–2858.

[70] T. Hussain, D.G. McCartney, P.H. Shipway: Mater. Sci. Technol. 28 (2012) 1371–1378.

[71] D.-Y. Kim, J.-J. Park, J.-G. Lee, D. Kim, S.J. Tark, S. Ahn et al.: J. Therm. Spray Technol. 22 (2013) 1092–1102.

[72] M.R. Rokni, C.A. Widener, G.A. Crawford, M.K. West: Mater. Sci. Eng. A. 625 (2015) 19–27.

[73] H.Y. Lee, Y.H. Yu, Y.C. Lee, Y.P. Hong, K.H. Ko: Appl. Surf. Sci. 227 (2004)244–249.

[74] I. Burlacov, J. Jirkovský, L. Kavan, R. Ballhorn, R.B. Heimann : J. Photochem. Photobiol. A: Chem. 187 (2007) 285–292.

[75] D. Zhang, P.H. Shipway, D.G. McCartney: J. Therm. Spray Technol. 14 (2005) 109–116.

[76] X.. L. Zhou, A.F. Chen, J.C. Liu, X.K. Wu: Surf. Coatings Technol. 206 (2011) 132–136.

[77] Y. Zou, W. Qin, E. Irissou, J.-G. Legoux, S. Yue, J.A. Szpunar: Scr. Mater. 61 (2009) 899–902.

[78] P.C. King, S. Zahiri, M. Jahedi, J. Friend: Surf. Coatings Technol. 205 (2010) 2016–2222.

[79] P.C. King, A.J. Poole, S. Horne, R. de Nys, S. Gulizia, M.Z. Jahedi: Surf. Coatings Technol. 216 (2013) 60–67.

[80] A.S. Alhulaifi, G.A. Buck, W.J. Arbegast: J. Therm. Spray Technol. 21 (2012) 852–862.

[81] Y. Xu, I.M. Hutchings: Surf. Coatings Technol. 201 (2006) 3044–3050.

[82] L. Zhu, T.-C. Jen, Y.-T. Pan, H.-S. Chen: J. Therm. Spray Technol. 26 (2017)1859–1873.

[83] M. Yamada, H. Isago, H. Nakano, M. Fukumoto: J. Therm. Spray Technol. 19 (2010) 1218–1223.

[84] N.T.Salim, M.Yamada, H.Nakano, K.Shima, H.Isago, M.Fukumoto: Surf.Coat.Tech. 206 (2011) 366-371.

[85] M.Gardon, C.Fernández-Rodíguez, D.Garzón Sousa, J.M. Doña-RodRíguez, S.Dosta, I.G.Cano, J.M. Guilemany: J. Therm. Spray Technol. 23 (2014) 1135–1140.

[86] C.Cao,W.Li, K.Yang, C.Li, G.Ji: Mater.rev.33 (2019) 277-282.

[87] S.Yin,X.Suo, J.Su, Z.Guo,H.Liao,X.Wang: J.Therm.Spray Technol. 23 (2014) 76-83.

[88] C.W.Ziemian, W.J.Wright, D.E.Cipoletti: J.Therm.Spray Technol. 27 (2018) 843-856.

[89] S.Singh, S.Chaudhary, H.Singh: Surf.Coat.Technol. 375 (2019) 54-65.

[90] S.Singh, H.Singh: Vacuum.172 (2020) 109092.

[91] M.Petron, S.Costil, W.Wong, D.Poirier, E.Irissou, J.-G.Legoux, A.Blouin, S.Yue: J.Therm.Spray Technol. 21 (2012)1322-1333.

[92] L.S.Wang, H-F.Zhou, K-J.Zhang, Y-Y.Wang, C-X.Li, X.T.Luo,G-J.Yang, C- J.Li: Ceram.Int. 315(2017) 314-325.

[93] Q.Wang,N.Birbilis, M-X.Zhang: Mater.Lett.65 (2011) 1576-1578.

[94] T.Go,Y.J.Sohm,G.Mauer, R.Vaben,J.G-Julian:J.Eur.Ceram.Soc.39(2019) 860-867.

[95] M.R.Rokni, S.R.Nutt,C.A.Widener, V.K.Champagne, R.H.Hrabe: J.Therm.Spray Technol. 26 (2017) 1308-1355.

[96] G.Bae,Y.Xiong,S.Kumar: Acta Mater.56.(2008) 4858-4868.

[97] M.Winnicki, A.Baszczuk, M.Jasiorski, B.Borak, A.Małachowska: Surf. Coatings Technol. 371 (2019) 194–202.

[98] H.Hajipour, A.Abdollah-Zadeh, H.Assadi, E.Taheri-Nassaj, H.Jahed: J. Therm. Spray Technol. 27 (2018) 1542–1550.

[99] G.-J. Yang, C.-J. Li, F. Han, W.-Y. Li, A. Ohmori: Appl. Surf. Sci. 254 (2008) 3979–3982.

[100] M. Yamada, H. Isago, K. Shima, H. Nakano, M. Fukumoto: T. J, Deposition of TiO_2 Ceramic Particles on Cold Spray Process, in: and G.M. B.R. Marple, A. Agarwal, M.M. 39 Hyland, Y.-C. Lau, C.-J. Li, R.S. Lima (Ed.), Therm. Spray Glob. Solut. Futur. Appl., Eds., Singapore, 2010, (2010) pp. 172 – 176.

[101] Toibah Abd Rahim, Keisuke Takahashi, Motohiro Yamada and Masahiro Fukumoto: Mater trans. 57 (2016) 1345-1350.

[102] K.Schmidt, S.Buhl, N.Davoudi, C.Godard, R.Merz, I.Raid, E.Kerscher,; M.Kopnarski, C.M.Renno, S.Ripperger, et al. : Surf. Coatings Technol. 309 (2017) 749–758.

[103] J.-O.Kliemann, H.Gutzmann, F.Gärtner, H.Hübner, C.Borchers, T. Klassen: J. Therm. Spray Technol. 20 (2010) 292–298.

[104] H.Gutzmann, S.Freese, F.Gartner, T.Klassen : Cold gas spraying of ceramics using the example of titanium dioxide. In Proceedings of the international Thermal Spray Conference, ITSC, Hamburg, Germany, 27–29 September (2011) pp. 391–396.

[105] D.K.christoulis, S.Guetta,V.Guipont, M.Jeandin: J.Therm.Spray Technol. 20 (2011) 523-533.

[106] Z.Arabgol, M.V.Vidaller, H.Assadi, F.Gartner, T.Klassen: Acta Mater. 127 (2017) 287301.

[107] Y.Ichikawa, K.Ogawa: J.Therm.Spray Technol. 24 (2015)1269-1276.

[108] M.Fukumoto, H.Wada, K.Tanabe, M.Yamada, E.Yamaguchi, A.Niwa, M.Sugimoto, M.Izawa: J.Therm.Spray Technol. 16 (2007) 643-650.

[109] O.Noor irinah, M.Yamada, T.Yasui, M.Fukumoto: IOP Conf.Ser. 920 (2020) 012009.

[110] R.C.Dykhuizen, M.F.Smith, D.L.Gilmore, R.A.Neiser,X.Jiang and S.Sampath: J.Therm. Spray Technol. 8 (1999) 559-564.

[111] M.Grujicic, J.R.Saylor, D.E.Beasley, W.S.DeRosset and D.Helfritch: Appl.Surf.Sci. 219 (2003) 211-227.

[112] S.Barradas, R.Molins, M.Jeandin, M.Arrigoni, M.Boustie, C.bolis, L.Berthe and M.Ducos: Surf and Coat Tech. 197 (2005) 18-27.

[113] S.Theimer,M.Graunitz, M.Schulze,F.Gaertner, T.Klassen: J.Therm.Spray Technol. 28 (2019) 124-134.

[114] T.S.Prince,P.H.Shipway, D.G.McCartney, E.Calla and D.Zhang : J.Therm. Spray Technol. 16 (2007) 566-570.

[115] G.Bae, Y.Xiong, S.Kumar, K.Kang and C.Lee : Acta Mater. 56 (2008) 4858-4868.

[116] G.Bae, S.Kumar, S.Yoon, K.Kang, H.Na, H.Kim and C.Lee: Acta Mater. 57 (2009) 5654-5666.

[117] T.Hussain, D.McCartney, P.Shipway and D.Zhang: J.Therm. Spray Technol. 18 (2009) 364-379.

[118] H. Assadi, F. Gärtner, T. Stoltenhoff, H. Kreye: Acta Mater. 51 (2003) 4379–4394.

[119] K.Balani, T.Laha, A.Agarwal, J.Karthikeyan, N.Munroe: Surf.Coat.Technol. 195 (2005) 272-279.

[120] R.Morgan, P.Fox, J.Pattison, C.Sutcliffe, W.O'Neill: Mater.Lett. 58 (2004) 1317-1320.

[121] T.H.Van Stenkiste, J.R.Smith,R.E.Teets:Surf.Coat.Technol.154(2002)237-252.

[122] K.Balani,A.Agarwal,S.Seal,J.Karthikeyan: Scrip.Mater. 53 (2005) 845-850.

[123] D.Zhang, P.H.Shipway, D.G.McCartney: J.Therm.Spray Technol. 14 (2005)109-116.

[124] W.B.Choi, L.Li, V.Luzin, R.Neiser, T.Gnaupel-Herold, H.J.Prask. S.Sampath, A.Gouldstone: Acta Mater. 55 (2007) 857-866.

[125] E.Irissou, B.Arsenault:Corrosion study of Cold sprayed Aluminum coating onto Al 7075 Alloy, in Thermal Spray:Global Coating Solutions, B.R.Marple, M.M. Hyland, Y.-C.Lau,

C.-J.Li, R.S.Lima and G.Montavon, Editors. 2007, ASM International: Beijing, people's republic of china. P. 549-554.

[126] D.Zhang, P.H.Shipway, D.G.McCartney: J.Therm.Spray Technol. 14 (2005)109-116.

[127] C.Borchers, F.Gartner,T.Stoltenhoff,H.Assadi,H.Kreye: J. Appl. Physc. 93 (2003) 10064-10070.

[128] P.King, S.Zahiri, M.Jahedi: Copper Particle Impact onto Aluminum by cold spray, in Thermal Spray:Global Coating Solutions, E.Lugscheider,Editor, 2008,ASM International: Maastricht,The Netherlands.

[129] P.King,S.Zahiri and M.Jahedi: Metallur and Mater Trans A. 40 (2009) 2115-2123.

[130] R.C.Mccune, W.T.Donlon, O.O.Popoola, E.L.Cartwright: J.Therm.Spray Technol. 9 (2000) 73-82.

[131] C.Borchers, F.Gartner, T.Stoltenhoff,H.Kreye: J.Appl.Physc.96(2004) 4288-4292.

[132] H.Koivuluoto, J.Lagerbom, P.Vuoristo: J.Therm.Spray Technol.16(2007) 488-497.

[133] T.Kairet,M.DEgrez,F.Campana,J.P.Janssen: J.Therm.Spray Technol.16 (2007) 610-618.

[134] T.Stoltenhoff,C.Borchers,F.Gartner,H.Kreye: Surf.Coat.Technol. 200 (2006)4947-4960.

[135] E.Calla,D.G.McCartney,P.H.Shipway:J.Therm.Spray Technol. 15 (2006) 255-262.

[136] K.I.Triantou,C.I.Sarafoglou,D.I.Pantelis,D.K.Christoulis,V.Guipont,M.Jeandin,A.Zarouli M.Vardavoulias: A Microstructural study of cold sprayed Cu coatings on 2017 Al Alloy, , in Thermal Spray: Global Coating Solutions, E.Lugscheider,Editor, 2008,ASM International: Maastricht,The Netherlands.

[137] P.C.King, S.H.Zahiri, M.Jahedi: Acta.Mater. 56(2008)5617-5626.

[138] M.Grujicic, C.L.Zhao, W.S.DeRosset, D.Helfritch: Mater&Design. 25 (2004) 681-688.

[139] M.Grujicic, J.R.Saylor, D.E.Beasley, W.S.DeRosset, D.Helfritch: Appl.Surf.Sci. 219 (2003) 211-227.

[140] W.Y.Li, H.L.Liao,C.J.Li, H.S.Bang,C.Coddet: Appl.Surf.Sci. 253 (2007) 5084-5091.

[141] R.C.Dykhuizen, M.F.Smith, D.L.gilmore, R.A.Neiser,X.Jiang, S.Sampath: J.Therm.Spray Technol. 8 (1999) 559-564.

[142] T.S.Prince, P.H.shipway, D.G.McCartney, E.Calla, D.Zhang: J.Therm. Spray Technol. 16 (2007) 566-570.

[143] F.A.Calvo, A.urena, J.M.G.Desalazar, F.Molleda: J.Mater.Sci. 23 (1988) 2273-2280.

[144] Y.Funamizu, K.Watanabe: Trans. Japan. Institute of Metals. 12 (1971) 147-155.

[145] J.Qin, Q.Huang, X.Wang, X.Suo, J.Wang, H.Li: J.Mater.Process.Tech. 288 (2021) 116845

[146] K.H.Ko, J.O.Choi,H.Lee: Mater.Lett. 175 (2016) 13-15.

[147] C.Wustefeld, D.rafaja,M.Motylenko,C.Ullrich,R.Drehmann,T.Grund,T.Lampke,B.Wielag

e: Acta.Mater. 128 (2017) 418-427.

[148] R.Drehmann, T.Grund, T.Lampke, B.Wielage, K.Manygoats, T.Schucknecht,D.Rafaja: J.Therm.Spray Technol. 23 (2014) 68-75.

[149] R.Kromer, Y.Danlos, S.Costil: J.Therm.Spray Technol. 27 (2018) 809-817.

[150] P.C.King,S.Zahiri, M.Jahedi, J.Friend: Surf.Coat.Technol. 7 (2010) 2016-2022.

[151] Winnicki, M.; Jasiorski, M.; Baszczuk, A.; Borak, B. Preliminary studies of TiO_2 coatings by deposition onto ABS polymer substrates by low pressure cold spraying. In Proceedings of the Les Rencontres Internationalessur la Projection Thermique—RIPT 9, Jülich, Germany,11–13 December 2019.

[152] P.Richer, B.Jodoin and L.Ajdelsztajn: J. Therm. Spray Technol. 15 (2006) 246–254.

[153] G. Benchabanea, Z. Boumerzouga, Z. I. Thibonb, T. Gloriantb : Mater. Charact. 59 (2008) 1425–1428.

[154] R.Kromer, Y.Danlos, S.Costil: J.Therm.Spray Technol. 27 (2018) 809-817.

[155] N.Kumar, K.Biswas: J.Mater.Res.Technol. 8 (2019) 63-74.

[156] K.H. Ko, J.O. Choi, H. Lee and B.J. Lee: Powder Technol. 218 (2012) 119.

[157] G Papadimitropoulos, N Vourdas, V Em Vamvakas and D Davazoglou: J. Phys.: Conf. Ser.10 (2005) 182.

[158] W. Trompetter, M. Hyland, D. McGrouther, P. Munroe and A. Markwitz: J. Therm. Spray Technol., 15 (2006) 663-669.

[159] A. R. Toibah, M. Sato, M. Yamada and M. Fukumoto: Mater. Manuf. Process. 31 (2016) 1527-1534.

[160] K.-R. Ernst, J. Braeutigam, F. Gaertner and T. Klassen: J. Therm. Spray Technol., 22 (2012) 422-432.

[161] H.Assadi,H.Kreye,F.Gartner,T.Klassen: Acta.Mater. 116 (2016) 382-407.

[162] E.Balic, M.Hadad, P.P.Bandyopadhyay, J.Michler : Acta Mater. 57 (2009) 5921-5926.

[163] A.Viscusi, A.Astarita, S.Genna: Trans IMF. 96 (2018) 34-40.

[164] S.Dong, H.Liao: Surf Eng. 34 (2018) 1173-180.

[165] S.Singh,H.Singh,R.Kumar Buddu: Surf.Eng. 36 (2020) 1067-1080.

[166] C.W.Ziemian, M.Sharma, B.D.Bouffard, T.Nissley, T.Eden : Mater&Design. 54 (2014) 212-221.

[167] Clayton, C.R. Materials science and engineering: An introduction. Mater. Sci. Eng. 1987, 94, 266–267.

[168] W.Y.Li, C.-J. Li, H. Liao: Appl Surf Sci. 256 (2010) 4953–4958.

[169] S.Yin, X.Wang, W.Li: Appl Surf Sci. 259 (2012) 294-300.

[170] F-Hsing Lu, F-X Fang, Y-S.Chen : J.Eur.Ceram.Society 21 (2001) 1-10.

[171] Y.Ichikawa ,R.Tokoro, K.Ogawa: Investigation of cold spray bonding mechanism focusing on the thin oxide film present in the deposition interface. In Proceedings of the International Thermal Spray Conference, Orlando, FL, USA, 7–10 May 2018. pp. 238–241, ISBN 9781627081603.

[172] Y.Ichikawa, K.Ogawa: J.Therm. Spray Technol. 24 (2015) 1269-1276.

[173] D.K.Christoulis, S.Guetta, V.Guipont, M.Jeandin: J.Therm.Spray Technol. 20 (2011) 523-533.

[174] M.Hassan-Gangaraj, D.Veysset, K.A.Nelson, C.A.Schuh : Appl Surf Sci. 476 (2019) 528-532.

[175] Y.Ichikawa, R.Tokoro, M.Tanno, K.Ogawa: Acta Mater. 1 (2019) 39-49.

[176] S.Rahmati, A.Zuniga, B.Jodoin, R.G.A.Veiga: Comp Mater Sci. 171 (2020) 109-219.

[177] S.Rahmati, R.G.A.Veiga, A.Zuniga, B.Jodoin : J.Therm.Spray Technol. 30 (2021) 1777-1791.

[178] RR.Chromik, D.Goldbaum, JM.Shockley: Surf.Coat.Technol. 205 (2010) 1409-1414.

[179] X.Meng,J.Zhang, J.Zhao: J Mater Sci Technol. 27 (2011) 809-815.

[180] D.Goldbaum, JM.Shockley, RR.Chromik : J.Therm. Spray Technol. 21 (2012) 288-303.

[181] H.Koivuluoto, P.Vuoristo : J.Therm. Spray Technol. 19 (2010) 1081-1092.

[182] AO.Tokarev : Met Sci Heat Treat. 38 (1996) 136-139.

[183] C.W.Ziemian, W.J.Wright, D.E.Cipoletti: J.Therm.Spray Technol. 27 (2018) 843-856.

[184] M.V.Vidaller, A.List, F.Gaertner, T.Klassen: J.Therm.Spray Technol. 24 (2015) 644-658.

[185] B.A.Welk, R.E.A.Williams, G.B.Viswanathan, M.A.Gibson: Ultramicro.134 (2013) 193-199.

[186] S.Kumar, G.Bae,C.Lee: Surf.Coat.Technol. 304 (2016) 592-605.

[187] T.Hussain: KEM. 533 (2012) 53-90.

[188] C.Borchers. T.Stoltenhoff, F.Gaartner, H.kreye, H.Assadi: MRS Proc. 673 (2001) 10.1-10.6.

[189] R.Nikbakht, S.H.Seyedein, S.Kheirandish,H.Assadi, B.Jodoin: Appl.Surf.Sci. 444 (2018) 621-632.

[190] M.Hassani-Gangaraj, D.Veysset, V.K.Champagne, K.A.Nelson, C.A.Shuh: Acta Mater. 158 (2018) 430-439.

[191] H.Assadi, F.Gartner, T.Klassen, H.Kreye: Script Mater. 162 (2019) 512-514.

[192] M.Hassani-Gangaraj, D.Veysset, V.K.Champagne, K.A.Nelson, C.A.Schuh: Script Mater.162 (2019) 515-519.

[193] S.Singh, M.Kumar, G.P.S. Sodhi, R.K.Buddu, H.Singh: Fusion Eng.Des. 128 (2018) 126-137.

[194] S.Singh, H.Singh, S.Chaudhary, R.K.Buddu: Surf.Coat.Technol. 389 (2020) 125619.

[195] D.Dietrich, B.Wielage,T.Lampke,T.Grund,S.Kumme: Adv.Eng.Mater. 14 (2011) 275-278.

[196] K.H.Kim and S.Kuroda: Scr.Mater. 63 (2010) 215-218.

[197] M.C.Biesinger: Surf.Interface.Anal.49 (2017) 1325-1334.

[198] H.B.Goodwin, E.A.Gilbert, C.M.Schwartz, and C.T.Greenidge: J. Electrochem. Soc. 100(1953)152-160.

[199] M.Song, H.Araki,S.Kuroda,K.Sakaki: J.Physc.D:Appl.Physc. 46 (2013) 195301.

[200] R.Drehman,T.Grund, T.Lample, B.Wielage, C.Wustefeld, M.Motylenko,D.Rafaja: J.Therm.Spray Technol. 27 (2018) 446-455.

[201] A.Almotairi, A.Warkentin, Z.Farhat: Eng Fail Anal. 66 (2016) 130-140.

[202] HG.Kim, IH.Kim : J Nucl Mater. 465 (2015) 531-539.

[203] Y.Wang, W.Zhou, Q.Wen, X.Ruan, F.Luo, G.Bai, Y.Qing, D.Zhu: Surf.Coat.Technol. 344 (2018) 141-148.

[204] L.Ajdelsztajn, B.Jodoin, GE.Kim,JM Schoenung: Metal Mater Trans A. 36A (2005) 657-666.

[205] H.B.Goodwin, E.A.Gilbert, C.M.Schwartz, and C.T.Greenidge: J. Electrochem. Soc. 100 (1953)152-160.

[206] E.A.Brandes, H.T.Greenaway, and H.E.N.Stone: Nature. 178(1956) 587.

[207] K.Taneichi, T.Narushima, Y.Iguchi, and C.Ouchi : Mater. Transact. 47 (2006) 2540.

[208] A.U.Seybolt and D.H.Haman : Transactions of the Metallurgical Society of AIME, 230 (1964)1294.

[209] J.F.Moulder, W.F.Stickle,P.E.Sobol and K.D.Bomben and J.Chastain: Handbook of X-ray Photoelectron spectroscopy. 1993. m/s 45.

[210] R.Ghelichi, M.Guagliano: Fra.Int.Strut. 3 (2013) 30-44.

[211] Y.Xie,M.-P.Planche, R.Raoelison, H.Liao: J.Therm.Spray Technol. 25 (2016) 123-130.

[212] K.Lee, M.Lee, J.Yu, H.J.Kim: J.Korean Inst.Met.Mater. 47 (2009) 728-733.

[213] Y.Watanabe,C.Yoshida, K.Atsumi, M.Yamada, M.Fukumoto: J.Therm.Spray Technol. 24 (2014) 86-91.

[214] N.Birks, G.H.Meier, and F.S.Pettit: Cambridge University Press, 2006.

[215] P.Straton: Int.Heat treat.Surf.Eng. 7 (2013) 70-73.

[216] G.CAllen, J.M.Dyke, S.J.Harris, A.Morrist: Oxid.Met. 29 (1988) 391-408.

[217] C.Y.Cui, X.G.Cui,X.D.Ren,M.J.Qi,J.D.Hu, Y.M.Wang:Appl.Surf.Science.305 (2014) 817-824.

[218] L-Min Liu, P.Crawford, P.Hu: Prog in Surf Sci. 84 (2009) 155-176.

[219] K.Onda, B.Li, H.Petek: Phys. Rev.B. 70 (2004) 045415.

[220] M.V.Ganduglia-Pirovano, A.Hofmann, J.Sauer; Surf.Sci.Rep. 62 (2007) 219-228.